THE RELATIONSHIP BETWEEN CRUSTAL DENSITY AND VOLCANIC ROCKS IN THE WESTERN UNITED STATES INCLUDING A COMPARISON OF ISOSTATIC COMPENSATION TECHNIQUES FOR GRAVITY DATA CORRECTION

BY

Copyright 2008
Linda Pickett Garinger

Submitted to the graduate degree program in Geology and the
Faculty of the Graduate School of the University of Kansas
In partial fulfillment of the requirements for the degree of
Doctor of Philosophy

Committee:

_____
Dr. Ross A. Black (Co-chairperson)

_____
Dr. J. Douglas Walker (Co-chairperson)

_____
Dr. Gwen Macpherson

_____
Dr. Rick Devlin

_____
Dr. Johannes Feddema

Date Defended: April 11, 2008

The Dissertation Committee for Linda Pickett Garinger certifies
that this is the approved version of the following dissertation:

THE RELATIONSHIP BETWEEN CRUSTAL DENSITY AND VOLCANIC ROCKS IN THE WESTERN UNITED STATES INCLUDING A COMPARISON OF ISOSTATIC COMPENSATION TECHNIQUES FOR GRAVITY DATA CORRECTION

Committee members:

_____
Dr. Ross A. Black (Co-chairperson)

_____
Dr. J. Douglas Walker (Co-chairperson)

_____
Dr. Gwen Macpherson

_____
Dr. Rick Devlin

_____
Dr. Johannes Feddema

Date Approved: April 22, 2008

Abstract

Linda Pickett Garinger
Department of Geology
University of Kansas

Processes and properties controlling magma ascent may include magma viscosity, the stress regime in surrounding country rock, geometric relationship between the rising magma and connected source area (if any), and density contrast between the magma and country rock. The purpose of this study was to determine the role upper crustal density plays in the control of magma ascent through the use of gravity modeling to obtain estimates of crustal density and then relating that density to the type and location of late Tertiary and Quaternary volcanics. A comparison of commonly used isostatic correction techniques was conducted to assess the impact the differences in correction technique have on isostatic gravity anomaly values, and thus on the results of gravity modeling. The choice of isostatic correction method was found to change the isostatic correction value by as much as 30 mgal over 36 km in areas of rapidly changing elevation. However, in most areas the difference in isostatic correction values are long in wavelength and will not greatly impact gravity modeling. A new idea for preparing an isostatic correction is introduced in preliminary form. Models of crustal density contrasts were prepared for three study areas in California and Nevada through the use of forward gravity modeling on isostatic gravity anomaly datasets. The results of the gravity models were gridded layers of crustal density contrasts that would reproduce the value of the isostatic gravity anomaly in that area. The location, type and quantity of late Tertiary and Quaternary volcanics were evaluated with respect to the value of crustal density in the underlying "basement" (lowest layer). Approximately half of the late Tertiary and Quaternary basalt in the study areas has erupted through crust that is less dense than the magma was. It is likely that in these cases that a conduit exists connecting the erupting magma to a deep source to provide sufficient buoyancy force for eruption.

Acknowledgements

I thank the Geothermal Program Office of the Navy for financial support of this research.

I am very grateful to the Department of Geology at the University of Kansas, the Association for Women Geoscientists, The American Mineralogical Society, and the Kansas Geological Foundation for financial support of my graduate studies.

I would like to express my sincere gratitude to my advisors Ross Black and Doug Walker for their guidance throughout the entire course of my graduate studies as well as the completion of this project. Their helpful editing suggestions greatly improved the quality and clarity of the manuscript. I appreciate the patience and instruction Ross and Doug provided as co-chairs of my committee.

I also thank the other members of my committee, Gwen Macpherson, Rick Devlin, and Johan Fedemma for their support. I especially appreciate Gwen's editing comments and encouragement during my longer than expected graduate school journey at KU.

Thank you to all the staff in the KU Geology office for taking care of innumerable details and answering uncountable questions.

I learned a great deal and received tremendous support from the faculty of the KU Geology Department, especially Roger Kaesler, Tony Walton, and Geoff Abers. Roger's humor and encouragement during field camp as my then five-year-old daughter attended with me, was over and above the call of duty. I learned a great deal about geology from Tony and Geoff as I made the transition from Engineer and Atmospheric Scientist to Geologist.

I very much appreciate the support Washburn University has provided during the last year of this project.

I thank Clint for his love, patience, encouragement, and support as I finished this work.

Lastly and most importantly I want to thank my daughter, Laura. Thank you Laura for coming along on this journey with me; attending classes on occasion, going to field camp and "hanging-out" in my office while I worked. Your smile and never ending optimism are inspirational in so many ways.

Contents

List of Tables

List of Figures

Chapter 1

Introduction

1.1 Introduction

Processes and properties controlling magma ascent may include magma viscosity, the stress regime in surrounding country rock, geometric relationship between the rising magma and connected source area (if any), and density contrast between the magma and country rock. Glazner et al. (2004) present evidence that at least some large plutons formed from repeated emplacement of small magmatic intrusions, suggesting that buoyant rise of small parcels of magma is an important mechanism in pluton formation and growth. In general, there are two ways magma may rise through the crust: unconnected to a deep source, or connected to a deep source via a conduit.

If magma rises as a parcel, the buoyancy force will be proportional to the difference in density between the magma and surrounding crustal rock. In this instance, the magma will rise until it reaches neutral buoyancy or until the strength of the crust is such that the buoyancy force can no longer overcome local stress.

If magma is connected to a deeper source area via a conduit, crustal density is also important to ascent. A column of magma will rise to the level where the gravitational attraction of the column of magma is equal to that of the column of rock surrounding the conduit. The equation describing this behavior is:

$$\int_{z=0}^{z=D} \rho_{\text{magma}}\, g\, dz = \int_{z=0}^{z=S} \rho_{\text{crust}}\, g\, dz$$

where ρ = density,

g = gravitational acceleration,

D = depth from the top to the base of the magma column,

S = depth of the crustal column from the surface to the magma source level.

In either instance (magma parcel or column) the greater the density contrast between the magma and the surrounding rock, the farther the magma will rise.

Glazner and Ussler (1988) observed a correlation between the depth of inferred magma bodies and P-wave velocity (V_p) discontinuities in several areas of the Basin and Range province of the Western United States. The observed increase in P-wave velocity with depth indicates a change in the nature of the crust, generally interpreted as an increase in crustal density. Although V_p is actually inversely proportional to rock density, elastic moduli that are proportional to V_p also depend on rock density and increase rapidly with the density. The result of this trend is that V_p increases linearly with depth (Birch, 1961). Glazner and Ussler (1988) further observe that calculated crustal density profiles indicate that basaltic magma should have a greater density than the crust above the V_p discontinuity and a lesser density than the crust below, implying that mafic magma is buoyantly trapped at the discontinuity. As the magma solidifies it becomes denser, thus further defining the discontinuity.

Taking the idea a step further, Glazner and Ussler (1989) proposed that crustal density is an important control on the location and geochemical character of volcanics and that the transition from intermediate to basaltic volcanism in the Basin

and Range and Mojave Desert is due to an increase in average crustal density from crustal thinning. They observed that basaltic volcanism increased over time, and that younger basalts are less contaminated by crustal rocks. The research described in this document was based on these observations and further quantifies the role crustal density plays in magma control.

1.2 Purpose and Goals

This dissertation describes results of the project 'The Relationship of Crustal Density and Magmatism in Extensional Environments' undertaken at the University of Kansas under funding from the Geothermal Program Office of the Navy. The project was designed to test the hypothesis that crustal density, which varies laterally on the scale of tens of kilometers over the western U.S., controls the nature of magmatic activity due to buoyancy effects. Specifically, the hypothesis states that basaltic magmas will have a tendency to pond within the crust in areas with lower crustal density, while having a tendency to erupt in areas of greater crustal density due to differences in buoyancy forces. Areas in which the basaltic magmas pond within the crust should also correlate with areas where rhyolitic melts are generated and rhyolitic magmatic centers can be formed. Commercial grade geothermal resources tend to be concentrated near rhyolitic magmatic centers.

To test the hypothesis it is necessary to estimate crustal density contrasts and correlate crustal density with the character of erupted volcanics. Isostatic gravity anomaly data are used to infer upper crustal density in this study, and the method used for the isostatic correction should be considered as a possible source of error for

this as well as other applications. The isostatic gravity anomaly reflects density heterogeneities within the upper crust and is useful for interpreting structural features, tectonic evolution, and inferring the location of magma bodies and dense deposits. The long wavelength isostatic correction is meant to remove from the gravity data set the effect of rock masses supporting high topography. Errors in the isostatic correction produce errors in the isostatic anomaly and therefore in the interpretation of the crustal density. The two most commonly used methods of isostatic correction, the Airy-Heiskanen and Pratt-Hayford correction techniques, were developed in the early to mid twentieth century when the nature of the lower crust and upper mantle and the interface between the two was largely unknown. Increased understanding of the true crust and mantle boundary makes a new comparison of isostatic correction methods appropriate.

This study consists of two parts: the isostatic gravity correction method comparison and forward gravity modeling to obtain crustal density contrasts. The results are presented in the following chapters. Chapter 2 outlines the overall approach to gravity modeling used to estimate crustal density. Chapter 3 describes the comparison of the Airy-Heiskanen and Pratt-Hayford isostatic correction techniques and parameters, and introduces a different approach to calculating the isostatic correction value. Chapter 4 contains the results of gravity modeling. This chapter also includes general comments regarding the location and character of volcanic rocks in the study areas. Overall trends and conclusions are found in Chapter 5.

Chapter 2

Approach to study

2.1 Introduction

In order to evaluate whether denser magma tends to erupt in areas of greater crustal density, a three dimensional model of crustal density is developed for three study areas. Forward gravity modeling using a previously developed Fortran code (Black et al., 2002) was used with geologic information to create the crustal model, and a Geographic Information System (GIS) was used to spatially correlate the crustal density with the nature of erupted volcanics in the area.

2.2 Choice of Study Areas

The area under consideration in the regional studies includes the extensional environments of the Basin and Range province in Nevada and California, and the Mojave Desert in California. The specific areas studied at the volcanic field scale are shown on Figure 2.1. Study areas include Central Nevada, Mojave, and an area along the California and Nevada border that includes the Eastern Sierra Nevada and Western Basin and Range (SNBR). These areas have late Tertiary to Quaternary (<16 Ma) volcanism, are well mapped, and have excellent gravity data coverage. Also included in the report is a summary of a model of southeastern California which includes the Coso volcanic field, an area where a correlation between crustal density and magmatic style has already been noted (Black et al., 2002).

2.3 Data

2.3.1 Gravity Data and Corrections

Gravity data used for gravity modeling were the California and Nevada regional gravity data sets from the 1994 National Geophysical Data Center Gravity CD (Hittelman et al., 1994). Isostatic anomaly values, as given in this data set, were used to interpolate gridded data used in the modeling. The data set contains raw gravity data and gravity correction values for variations in elevation, terrain, and latitude as well as an isostatic correction based on the Airy-Heiskanen method. Although newer and larger gravity data sets exist, the completeness of this set, with all correction values for each point provided in a table format, made it the best choice for this study. Uncertainties about the isostatic correction method, and the effect of these uncertainties on the results should be taken into consideration when interpreting the results. Please refer to Chapter 3 for details of the isostatic correction method comparison, including data used to prepare the isostatic correction models.

2.3.2 Geologic Maps

The geologic map of Nevada used was compiled by J.H. Stewart and J.E. Carlson (1978). The map is available in digital format (ArcView shapefile) via the internet. The digital California Geologic map was compiled by Charles W. Jennings et al. (1977). A geologic map of the Reveille quadrangle (Ekren et al., 1973), a geologic map of the Lunar Crater quadrangle (Snyder et al., 1972) and gravity and

basin depth maps of the Basin and Range Province (Saltus and Jachens, 1995) were also used to constrain model geometry.

2.3.3 Late Cenozoic Volcanic Rocks

The location, type, and age of late Cenozoic volcanic rocks (less than 16 Ma) in each study area were digitized from maps prepared by Luedke and Smith (1981). The Western North American Volcanic and Intrusive Rock Database (NAVDAT) was queried for the location, composition, and silica content of volcanic rock samples less than 16 Ma in each study area. The NAVDAT database is available at http://navdat.kgs.ku.edu/.

Information about late Cenozoic volcanics from the two sources overlaps but is not identical. Some samples from NAVDAT are from volcanics that are not included on maps by Luedke and Smith (1981). The NAVDAT data repository does not have sample information from all mapped areas. Maps with locations of volcanics (mapped and sampled) associated with each study area are included in Chapter 4.

2.4 Gravity modeling technique

2.4.1 Fortran Code

The forward gravity modeling was performed utilizing locally written Fortran code based on the Fourier domain subroutine 'glayer' from Blakely (1995). Input is a set of two-dimensional grids of density contrast values, each representing one layer in the overall model of the crust. The grid size, layer thickness and the number of layers is set independently and is easily changed as the model is refined. The code is

a three-dimensional implementation, which uses 'glayer' to generate the vertical component gravity response for each layer and then sums the responses. Black et al. (2002) initially developed the code. A listing is included in Appendix A.

2.4.2 Geographic Information System (GIS)

ESRI ArcGIS was used extensively in this project. Initial data input into the GIS included geologic maps (either available in digital format or scanned), gravity point data, and information about surface volcanics. The GIS software allowed the stacking of information to view the problem in a visual, rather than numeric format. For example, the model layers were created, displayed and modified in the GIS. Model layers were converted to ASCII grids for input to the Fortan code and were converted back into GIS coverages within the GIS software. A Fortran program was written which would integrate modified layers of modeled plutons or basins into the background basement density file. This speeded the modification and iteration process that is cumbersome in forward modeling. The GIS also supported spatial correlation (visual and statistical) of crustal density estimates with location of erupted volcanics.

2.4.3 Modeling Procedure

Forward modeling was utilized exclusively in the final analysis. Forward gravity modeling is nonunique and for each study area an infinite number of possible crustal geometries can produce the same gravity anomaly values. Surficial geological mapping turned out to be the single most helpful constraint in the modeling procedure and there is no substitute for human interpretation of the map

product in producing constraints during modeling. Geological constraints were more easily incorporated into the forward modeling procedure.

The modeling procedure consisted of several different parts, based on the half wavelength of the anomalies involved. The anomalies of interest in this study have widths or 'half wavelengths' of kilometers to tens of kilometers. Anomalies with widths of more than ten or twenty kilometers constitute regional anomalies in the exploration sense.

In the regional study area, longer wavelength anomalies are mainly caused by the isostatic support system, typically an Airy-Heiskanen or Pratt-Hayford model. The regional average of the isostatically corrected gravity should be equal to the regional average of the free-air corrected gravity, if the isostatic correction has been applied correctly. In the western U.S. this is not the case and detailed gravity studies tend to show unrealistically low density estimates. The error in the regional isostatic anomaly average is on the order of 12 mgal or, translated into near surface rock density, approximately 100 kg m^{-3}. This is probably due to the fact that neither of the standard isostatic models fits the situation in this geologically complex area. Chapter 3 describes details of the various isostatic correction techniques and the implications for this study.

Oliver (1977) showed that the gravity anomalies observed in the Sierra Nevada crustal block could be accounted for by density variations in the upper 10 km of the crustal section. The same parameters seemed reasonable in later, well constrained work (Black et al., 2002). Causative bodies at depths of greater than

10 km generate broader and flatter gravity signatures that tend to be lost in the regional gravity anomaly (Figure 2.2). Thus all anomalies at the kilometer to tens of kilometers scale were modeled as being generated in the upper ten kilometers of the crust.

Since consistent subsurface constraints were not available in all areas, but surficial geological mapping was consistently available, the geological mapping was used as the primary constraint in the initiation of each modeling project. Each study area was handled separately.

A scanned geologic map was used with a GIS system to prepare a shape file of the study area. Again, using a GIS system, all gravity points within the study area were interpolated to a grid using a simple inverse distance-weighting scheme. Figure 2.3a shows the grid generated for the Central Nevada study area with all NGDC gravity points for the study area. Next, those NGDC data points taken on 'basement' outcrop (areas of bedrock not covered by Cenozoic alluvium) were isolated and gridded alone. Figure 2.3b shows the grid generated by interpolation from only the points on 'basement'. This process effectively decouples the basement and basin contributions and the two can be modeled independently. After the initial step of separating the basin fill and basement gravity signatures, the basement contribution was modeled utilizing the mapped surficial geology as the major constraint. The process of basin-basement separation in modeling was developed by Saltus and Jachens (1995).

Once a ‘basement’ crustal density contrast model produced an isostatic anomaly that closely matched the general observed isostatic anomaly of the area, the basin isostatic anomaly values were included and modeled. The basin fill effect was modeled utilizing a depth-density function developed by the USGS for gravity studies within the Basin and Range. There are at least two such functions in common use. Black et al. (2002) utilized a modified version of the discrete layer model developed by Jachens and Moring (1990). In this study a newer empirical model estimating density as a continuous function (Kaban and Mooney, 2001) was utilized. Both models yield similar results, but the newer, continuous model is simpler to implement with models of layers of arbitrary thickness. The sediment density-depth relationship was estimated from data supplied by Mikhail Kaban (personal communication, 2002), based on well log and porosity data from Kennet et al. (1994), Beyer et al. (1985), and McCulloh (1967). The relationship is shown in graph form on Figure 2.4.

As basins were added to the layers, other short wavelength anomalies apparent in the observed isostatic anomaly grid were also modeled. A GIS was used to map basins and other areas where density should be increased or decreased within the model. After creating a layer and assigning density contrasts, the GIS coverage was converted into an ASCII grid for use as input into the Fortan computer code. The output from the model was viewed in a GIS and compared to the actual isostatic gravity anomaly. The difference between the actual and modeled anomaly values,

with basin depth information and geology guided adjustments to the model input (i.e., the layer depth, thickness, and density contrast values).

In general, any anomaly of any wavelength that could be correlated with a feature in the surficial geology was modeled as such. Approximate crustal density contrasts of mapped surface volcanics of interest in this study were used on the uppermost layer. Older volcanics which may have been present were not given special treatment but were modeled as part of the 'basement' crustal density contrast. Any short wavelength anomaly that could not be correlated with surficial geology was modeled as a shallow subsurface feature. Any longer wavelength anomaly that could not be correlated with a feature in surficial geological mapping was mapped as a through-going basement feature. In general, the simplest or most plausible geology that could explain an anomaly was the one that was used. Unless otherwise indicated (e.g. shallow basalt flow), surficial geology that correlated with gravity anomalies was allowed to continue with depth. The number and depth of layers was not constrained and varied with each study area. Layer depths were defined by surface geology and gravity anomaly values. The model was modified until the calculated anomaly was within approximately 5 mgal of the observed anomaly value. Small geographic areas with greater than 5 mgal difference in modeled and actual anomaly values were present in all study areas.

The end product of the modeling was a set of crustal density contrast values assembled in gridded layers of various thicknesses. Finally, correlation of erupted

volcanics with modeled crustal density contrasts was accomplished through tools available within the GIS and by visual inspection.

Figure 2.1 Topographic map of the western United States with areas used in forward gravity modeling boxed. Sierra Nevada Basin and Range, Central Nevada and Mojave study areas are subjects of the current study. The study area used by Black et al. (2002) (Coso volcanic field) is also shown.

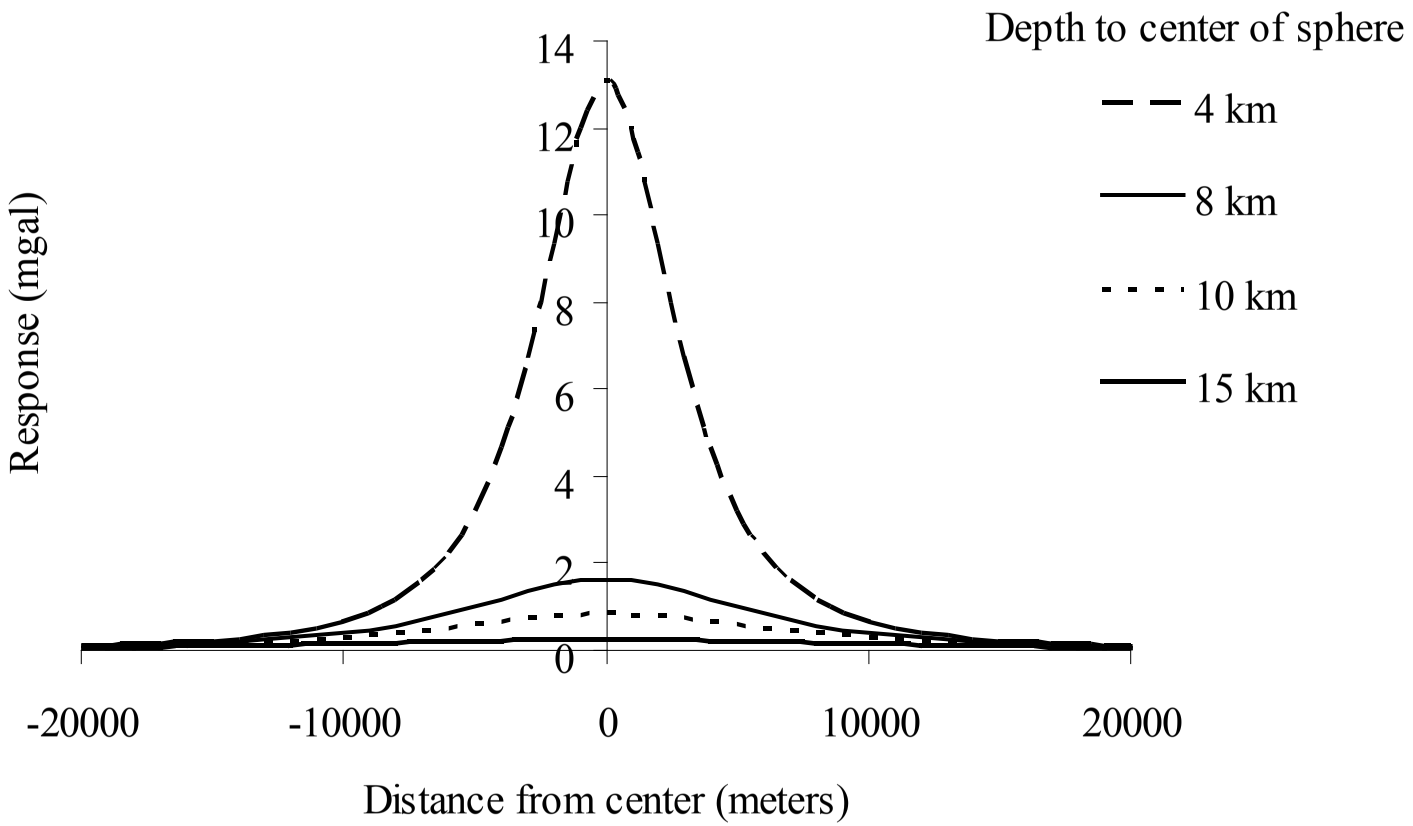

Figure 2.2 Gravitational response of a buried sphere 100 meters in diameter at 4, 8, 10, and 15 km depth. Density contrast between the sphere and its surroundings is 300 kg m^{-3}.

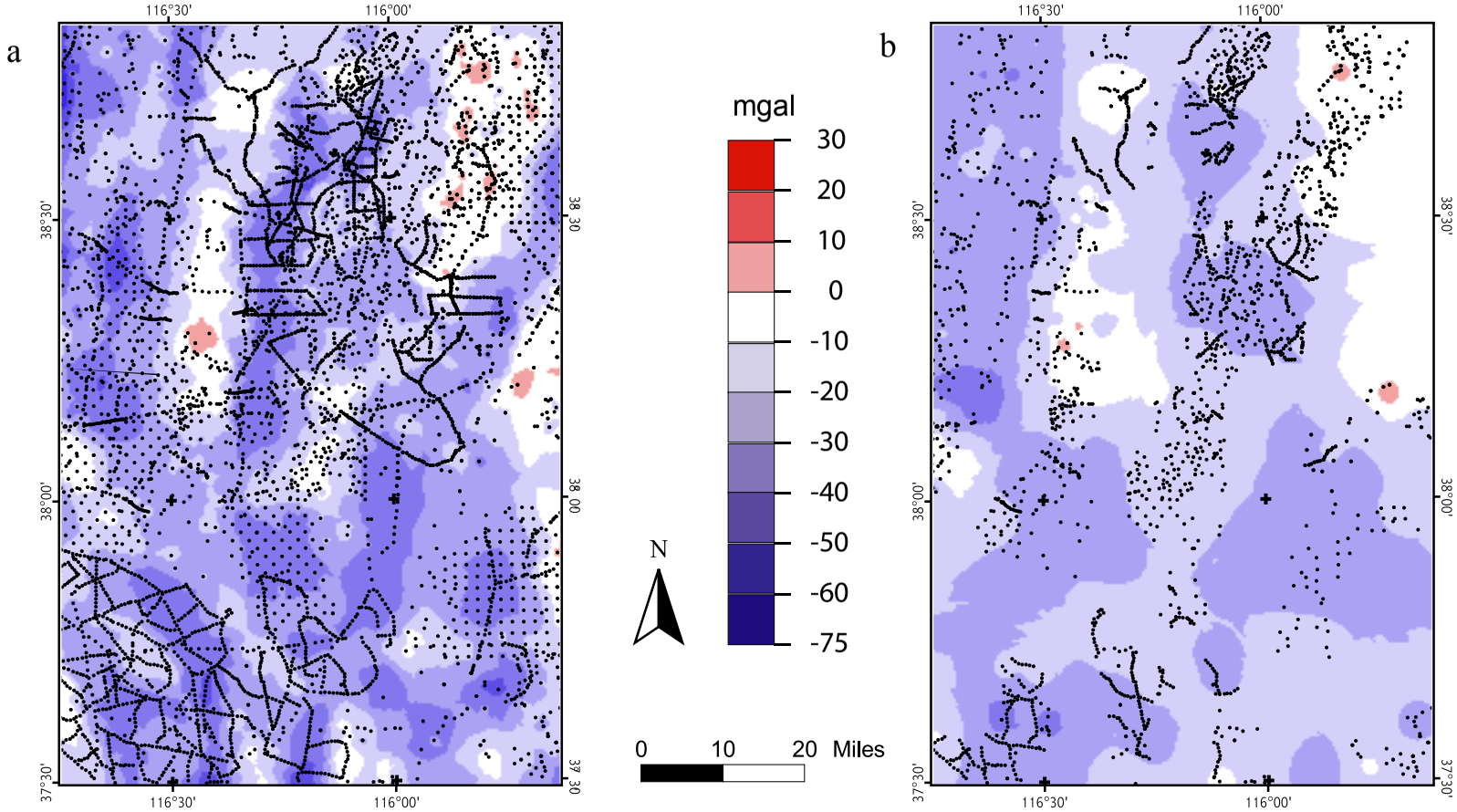

Figure 2.3 Examples of isostatic anomaly grids used to model crustal density contrasts. Grids shown are from the Central Nevada study area. a) Isostatic anomaly grid as interpolated from all available gravity data points. Location of data points shown in black. b) Isostatic anomaly grid as interpolated from points located on bedrock. Data points over sedimentary basins have been removed and are not included in the interpolation.

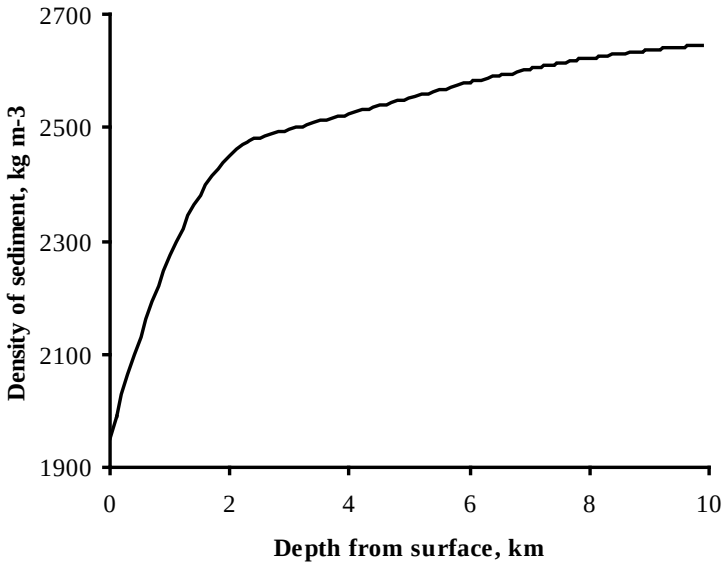

Figure 2.4 Estimated density of sediment with increasing depth. Based on data from Kennet et al., 1994; Beyer et al., 1985; and McCulloh, 1967. After Kaban and Mooney, 2001.

Chapter 3

Isostatic Compensation Model Comparisons

3.1 Introduction

The purpose of the many gravity corrections applied to a set of raw gravity measurements is to convert measurements made on the Earth's surface that reflect all rock mass beneath and nearby to a set of measurements that reflect density variations within the crust and upper mantle. A 'corrected' set of gravity values will have had the mass and shape of a normal earth accounted for (reference ellipsoid), as well as the gravitational effects of the sun and moon (tidal correction), the elevation above sea level of the measurement (free air correction), the rock between the measurement and sea level (Bouguer correction), the surrounding terrain (complete Bouguer correction) and possibly the long-wavelength gravitational effect of compensating mass (isostatic correction). After the application of these corrections to a data set, the remaining gravity values, the isostatic anomaly values, reflect changes in the gravity field caused by unaccounted for changes in density within the crust.

The goal of the isostatic correction model comparison was to analyze the effect the choice of isostatic compensation model has on the residual gravity anomaly data set. Previous comparisons between the two most common isostatic correction techniques, Airy-Heiskanen and Pratt-Hayford, were derived for points only. These values, presented by Watts (2001, pages 30-31) show differences in isostatic anomaly values between the two methods as well as within one method using different depths of compensation. In the current comparison, the Airy-

Heiskanen and Pratt-Hayford isostatic correction techniques have been used to estimate the isostatic correction to gravity data in California and Nevada. In this chapter, these techniques are compared on a regional basis with the goal of evaluating if the correction methods yield significantly different results (isostatic anomaly values) that could affect the interpretation of crustal density models. A new isostatic correction method, the Combined Effect Model (CEM), is also presented.

3.2 Data

The topographic database used to calculate the isostatic correction values was created from the combined GTOPO30 gridded elevation set for the western U.S. and the Digital Bathymetric Database Variable Resolution (DBDB-V) for the eastern Pacific Ocean. GTOPO30 was developed by a collaborative effort of several international agencies led by the U.S. Geological Survey (USGS) and is available from the USGS. DBDB-V is available from the U.S. Naval Oceanographic Office. Both datasets are available online. Any missing data were read from USGS topographic maps and entered manually into the grid. All data were regridded to 3 km resolution for greater processing speed.

Walter Mooney (personal communication, 2001) provided a sampled digital database of crustal thickness used in the CEM. This database was created from points where two dimensional velocity models had been determined from seismic information. The database includes the depth, thickness, and seismic velocity of crustal layers, as well as depth to Moho. Additions to Mooney's database were made from Fliedner et al. (2000), Fuis et al. (2001) and Catchings and Mooney (1991).

Data points were interpolated to a 3 km grid using ArcView software. Some areas, most notably Idaho, Utah, western Oregon, and ocean areas have poor data coverage, and the resulting grid of Moho depth is likely to be inaccurate there. The interpolation method used five of the nearest neighbors, inverse distance weighted, to calculate cell values. This method, while the best available, tends to produce circular patterns, which may not be realistic. Further work and additional data are needed to improve the quality of the depth to Moho grid.

As in the gravity modeling, gravity measurements used for the isostatic correction study are from the California and Nevada regional gravity data sets taken from the 1994 National Geophysical Data Center Gravity CD (Hittelman et al., 1994). The data were contributed by the USGS, and contain free air anomalies, simple and complete Bouguer anomalies, terrain corrections, and isostatic anomalies. Principal Investigators were Richard Saltus (Nevada) and David Snyder (California).

Isostatic corrections beyond 166.7 km from the calculation point were obtained from the far field isostatic correction grid generated by Karki et al. (1961). The far field data set was generated for an Airy isostatic correction model with a 30 km crustal depth and a density contrast across the Moho of 600 kg m^{-3}. This data set, although the best available of its type, was calculated with parameters different from those used in the following models.

3.3 Pratt-Hayford Isostatic Compensation Model

In the mid 1800s, G. Everest began mapping India. As the survey was being conducted, workers noticed that plumb lines were deflected from the vertical and

inconsistencies in calculations were common. Two individuals, John Henry Pratt and George Airy, responded with explanations for the discrepancy. Both Pratt and Airy concluded that the deflection of plumb lines and the resulting measurement errors resulted from the gravitational attraction created by the mass of the nearby Himalayan Mountains. Later, in related work, Pratt and Airy suggested separate mechanisms for the isostatic support of the topographically high Himalayas.

John Henry Pratt's hypothesis was that low elevations are underlain by high density rocks and high elevations are underlain by low density rocks. At some depth (the compensation depth) he assumed the overlying mass of all areas is equal. J.F. Hayford further developed Pratt's model in the early 1900s. This geometry and associated equations are shown on Figure 3.1.

A computer model of the Pratt-Hayford compensation method was developed. Model input parameters include crustal density above sea level, density of the sea level column (equal to the crustal density above sea level by definition) and the compensation depth. A column density ($\rho(x)$ on Figure 3.1), was calculated by assuming that the total mass of each column was equal at the compensation depth, and therefore equal to the sea level column.

As previously mentioned, the value of Earth density above sea level and for the column density for columns at sea level is assigned, as is the depth to equal pressure(i.e., compensation depth). The calculated column density increases with an increase in given sea level column density, and with a decrease in the compensation depth. Differences in the correction values arise from differences in column density

and the compensation depth. The isostatic correction value for each grid cell was then found from the column density values by calculating the difference in gravitational attraction between a column at sea level (assumed) and that at the grid location for all mass within a radius of 166.7 km. The subroutine 'gbox' written by Richard Blakely (Blakely, 1995) was used to calculate the vertical gravitational attraction of each cell to the appropriate depth. A listing of the computer program used to calculate Pratt-Hayford correction values, including GBOX, is included in Appendix A. Results from the Pratt-Hayford model are shown in Table 3.1, and discussed below.

3.4 Airy-Heiskanen Isostatic Compensation Model

George Biddell Airy also provided an explanation to the gravity data inconsistency in India. He suggested that the crust was less dense than a fluid layer underlying it and compared the behavior to that of blocks of wood floating on water. His idea was based on Archimedes' principal, which states that a block placed on a denser liquid will displace an amount of liquid with equivalent mass. W.A. Heiskanen put Airy's model in a more precise form. The model geometry and associated equations are shown on Figure 3.2.

Input parameters to the Airy-Heiskanen model include density of the crust, the difference in density between the crust and mantle, and the thickness of the crust at zero elevation. The depth of the compensating root (or anti-root if the topography is below sea level) was calculated for each grid cell from the topography and the set

of input parameters. Then, in similar fashion to the method used for the Pratt-Hayford model, the isostatic correction value was calculated.

A listing of the computer program used for the Airy-Heiskanen correction is included in Appendix A. As for the Pratt-Hayford program, the subroutine 'gbox' written by Richard Blakely (Blakely, 1995) was used to calculate the vertical gravitational attraction of each cell to the appropriate depth. Modified versions of two subroutines used in Airyroot (Simpson et al., 1983) were used to calculate the topographic load and depth to the supporting root. Example results of the Airy-Heiskanen isostatic correction model are shown in Table 3.1 and discussed below.

3.5 Combined Effect Model

A new isostatic compensation model has been developed. The Combined Effect Model (CEM) includes methodology from both the Pratt-Hayford and Airy-Heiskanen isostatic compensation techniques. It uses both a crustal root and variable mantle density for compensation of high topography. Using the depth to Moho values from the database of crustal thickness (described in section 3.2), a grid of Moho depth was interpolated. This grid was used as the crustal root instead of calculating one from topography as is done in the Airy-Heiskanen model. Figure 3.3 shows the interpolated depth to Moho grid. Figure 3.4 shows the depth to root as calculated by the Airy-Heiskanen model using a crustal density of 2670 kg m^{-3}, a mantle density of 3070 kg m^{-3}, and a compensation depth of 25 km. The greatest differences between the Airy-Heiskanen calculated root and the observation-based

crustal thickness are observed in the eastern central valley of California, coastal areas of Oregon, and basin and range areas in Nevada and Utah (Figure 3.5).

Pratt-Hayford methodology was then used to calculate density variations in the mantle that would be needed, along with the support from crustal root, to support the topography in isostatic equilibrium. Figure 3.6 shows the geometry and associated equations for the Combined Effect Model. Constant inputs into this model include elevation and interpolated grid of depth to crustal root. Variable input parameters include crustal density and mantle density at sea level. Mantle density for elevations other than sea level and isostatic correction are calculated based on the input values. The balance (see equations) uses a known depth to Moho at sea level elevation. The actual depth to Moho at sea level varies from 14.47 km to 30.45 km according to the interpolated grid. A value of 22.54 was used for the constant sea level Moho depth by averaging 1234 values with elevations at or near sea level (0 to 50 m underwater).

3.6 Discussion

All isostatic compensation models were run using the composite topographic database described above. Several modeling runs were made for each type of model and the value of the isostatic corrections were calculated. For each set of results, the isostatic anomaly values for California and Nevada were calculated, averaged and compared with the average free-air anomaly value and average isostatic anomaly value calculated from the 1994 National Geophysical Data Center gravity dataset. Example results are given in Table 3.1.

Over large isostatically stable areas, the average free air anomaly value is approximately zero (Turcotte and Schubert, 1982, p. 219). The average free air anomaly value over California and Nevada from the interpolated and gridded NGDC point data is -0.21 mgal, indicating that the area is essentially isostatically compensated. This suggests that an average isostatic anomaly value at sea level should also be near zero.

The most common isostatic compensation model applied to U.S. areas is the Airy-Heiskanen model with a 25 km crustal root depth at sea level elevation, crustal density value of 2670 kg m^{-3}, and a mantle density value of 3070 kg m^{-3}. This configuration was used to produce the isostatic correction in the NGDC gravity dataset. Figure 3.7 shows the difference between the NGDC isostatic correction values (interpolated to a grid), and the values calculated by the Airy-Heiskanen program written for this study. The vast majority of the values are within 3 mgal. Areas that show a more sizable difference in value, such as the coastal area of southern California, are apparently due to slight differences in elevation values used to calculate the isostatic correction. A similar published data set for the Pratt-Hayworth model is not available.

The average isostatic anomaly in California and Nevada from the interpolated anomaly values is –12.97 mgal. The results of the Airy-Heiskanen computer program developed for this study compare favorably with the NGDC data set with an average of -13.07 mgal. In this study an attempt was made to reproduce the average free air anomaly (-0.21 mgal), and the average anomaly produced by the commonly

used Airy configuration described above (-12.97 mgal) for each of the three compensation models. Comparisons made between the models are for similar average anomaly values (see Table 3.1). It should be noted that even though care is taken to compare results that are have similar average anomaly values, the different compensation depths and Moho densities produce widely different values, somewhat limiting the usefulness of the direct comparisons. The results of the comparisons, presented below, provide insight into the different character of the isostatic corrections produced by the different model geometries.

For consistency and ease of comparison, the calculated isostatic correction values were converted to isostatic anomaly values by adding the correction values with the far field isostatic correction values (Karki et al., 1961), and subtracting the result from the complete Bouguer anomaly data set. [Note: the far field isostatic correction (Karki et al., 1961) was calculated for an Airy-Heiskanen model configuration with a sea level compensation depth of 30 km and a density difference between crust and mantle of 600 kg m^{-3}. This difference in parameters has been estimated to cause an error of approximately 3 mgal at an elevation of 3000 feet for an Airy-Heiskanen model with a 25 km depth compensation depth and a density difference between crust and mantle of 400 kg m^{-3} (Simpson et al., 1983). This study does not recalculate the far-field correction.]

The Airy-Heiskanen isostatic model with a crustal density of 2670 kg m^{-3}, a mantle density of 3070 kg m^{-3}, and a 25 km depth to Moho at sea level yields an average isostatic anomaly of –13.03 mgal. A Pratt-Hayford isostatic model using a

crustal density of 2670 kg m^{-3} and a compensation depth of 62 km yields an average anomaly value of –13.21 mgal. Figure 3.8 shows the spatial differences between the results produced by the two model configurations described above. Differences in the anomaly values are correlated with topography. Anomaly values from the Pratt-Hayford model are more positive than those from the Airy-Heiskanen model for high elevations. For low elevations the Airy-Heiskanen model produces values that are more positive. Because rocks closest to the surface have the greatest impact on gravity values, the calculated isostatic correction value is strongly correlated with the rock density closest to the surface. The Pratt column changes spatially with topographic load producing higher amplitude changes in correction value. A difference in correction value of 30 mgal over a spatial distance of 36 km is seen in the boxed area of Figure 3.8. An error of this magnitude could result in mis-interpretation of 200 kg m^{-3} in the density value of a 4 km thick slab buried at approximately 6 km. This is approximately the density difference between granite and diorite.

Models with average anomaly values similar to the free air value also have a large variation in values. The Airy-Heiskanen isostatic model with a crustal density of 2800 kg m^{-3}, a mantle density of 3300 kg m^{-3}, and a 17.6 km depth to Moho at sea level yields an average isostatic anomaly of -0.22 mgal. A Pratt-Hayford isostatic model using a crustal density of 2800 kg m^{-3} and a compensation depth of 42.7 km yields an average isostatic anomaly value of -0.23 mgal. Figure 3.9 shows the difference in isostatic anomaly value between these two model configurations.

Preliminary results from the CEM are presented in Figures 3.10 and 3.11. An intermediate calculation in the CEM model produces mantle density values because both mantle density variations as well as the crustal root are used for isostatic support. When the 'given' value of sea level mantle density is subtracted from the calculated mantle density values for the entire area, a mantle density anomaly is produced. These mantle density anomaly values, shown in Figure 3.10, compare favorably with the upper mantle density anomaly presented by Kaban and Mooney (2001). The obvious differences are believed to be primarily a result of differences in basin treatment (especially the Great Valley in California) the grid interpolation, and in the assumed crustal density in the CEM.

Figure 3.11 shows the difference between values produced by the CEM with an average anomaly value of -0.22 mgal and the Airy-Heiskanen model with an average anomaly value of -0.22 mgal. The greatest differences are centered on areas where the depth to Moho map is greatly different from the depth to root generated by the Airy-Heiskanen calculations (Figure 3.5).

The three models compared in this study produce similar, but different isostatic correction values. In some areas, the isostatic correction values, and therefore isostatic anomaly values show differences of 30 to 50 mgal over distances of approximately 30 km. It is not possible at this time to determine which model is most accurate. It is well known that a supporting root underlies mountain ranges, suggesting that probably the best choices for models are the Airy-Heiskanen model, the CEM or some other similar configuration with a crustal root. The Airy-

Heiskanen correction included with the NCDC data is used for the crustal density study because the CEM is still considered under development. An improved map of the Moho is needed to improve the results, and further testing is needed.

The field areas chosen for crustal density modeling are shown graphically on Figure 3.11. In these areas the change in anomaly value that would be caused by the incorrect choice of isostatic correction model (between the CEM and Airy-Heiskanen models) is gradual but significant. Small scale anomalies would not be affected, but the larger scale modeling for basement density contrasts might be influenced.

Table 3.1 Comparison of isostatic correction technique average anomaly values with parameters used in calculations. See text for further description.

Method	**Crustal Density (kg m^{-3})**	**Mantle Density (kg m^{-3})**	**Crustal Thickness at Sea Level Elevation (Airy-Heiskanen) or Compensation Depth (Pratt-Hayford) (km)**	**Average Isostatic Anomaly California and Nevada (mgal)**	**Figure(s)**
Airy-Heiskanen	2670	3070	25.0	-13.03	3.2, 3.5
Airy-Heiskanen	2800	3400	17.6	-0.22	3.2, 3.7, 3.9
Pratt-Hayford	2670 (above sea level)	varies	62.0	-13.21	3.1, 3.6
Pratt-Hayford	2800 (above sea level)	varies	46.5	-0.23	3.1, 3.7
CEM	2800	3300 Sea level only Varies elsewhere	68.0	-0.22	3.4, 3.9

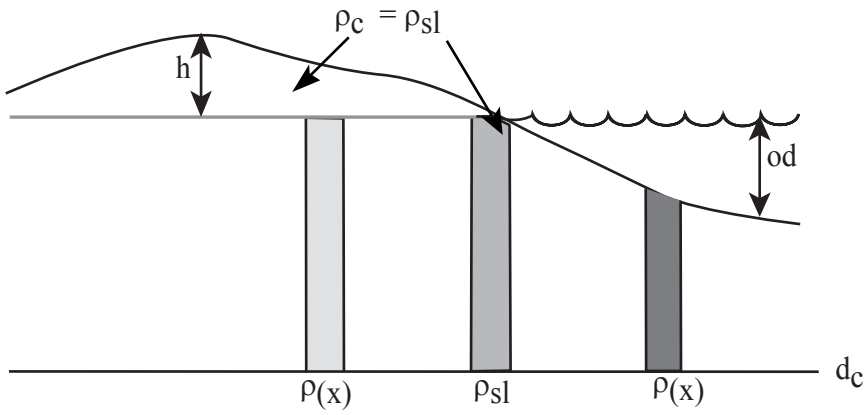

Pratt-Hayford Isostatic Compensation Model

Topographic support is provided by laterally varying substrate density.

h	=	topographic height above sea level
od	=	ocean depth
d_c	=	compensation depth
ρ_{sea}	=	seawater density
ρ_c	=	crustal density (equal to ρ_{sl})
ρ_{sl}	=	column density when topographic height is 0
$\rho_{(x)}$	=	calculated column density

On land the balance is described:
$\rho_{(x)}(d_c) + h(\rho_c) = \rho_{sl}\, d_c$

On the ocean the balance is described:
$\rho_{(x)}(d_c - od) + od(\rho_{sea}) = \rho_{sl}\, d_c$

Figure 3.1 Geometry and variables of the Pratt-Hayford isostatic compensation model. Isostatic correction is the change in gravitational attraction of a column due to the density difference between ρ_{sl} and $\rho_{(x)}$.

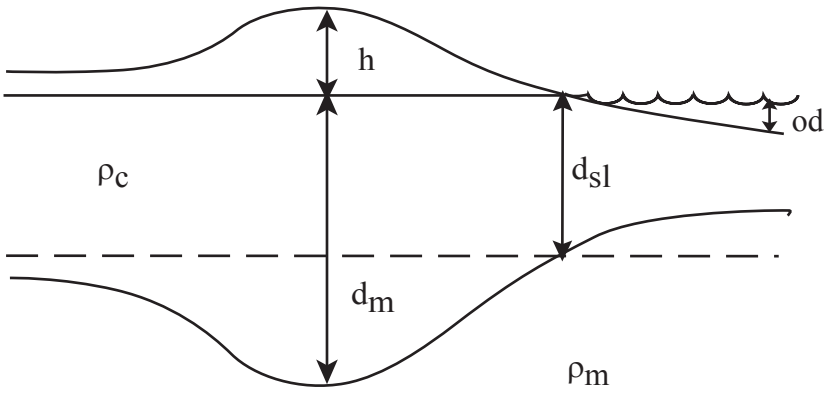

Airy-Heiskanen Isostatic Compensation Model

Topographic support is provided by a crustal root

h	=	topographic height above sea level
od	=	ocean depth
d_{sl}	=	depth of sea level root (specified in model)
d_m	=	depth of crustal root (calculated)
ρ_c	=	density of crust
ρ_m	=	mantle density
ρ_{sea}	=	density of seawater

On land the balance is described:
$(d_m - d_{sl})(\rho_m - \rho_c) = h(\rho_c)$

On the ocean the balance is described:
$(d_m - d_{sl})(\rho_m - \rho_c) = od(\rho_c - \rho_{sea})$

Figure 3.2 Geometry and variables of the Airy-Heiskanen isostatic compensation model. Isostatic correction is the difference in gravitational attraction of a column due to the difference in density between the crust and mantle and the difference in depth of the crustal root.

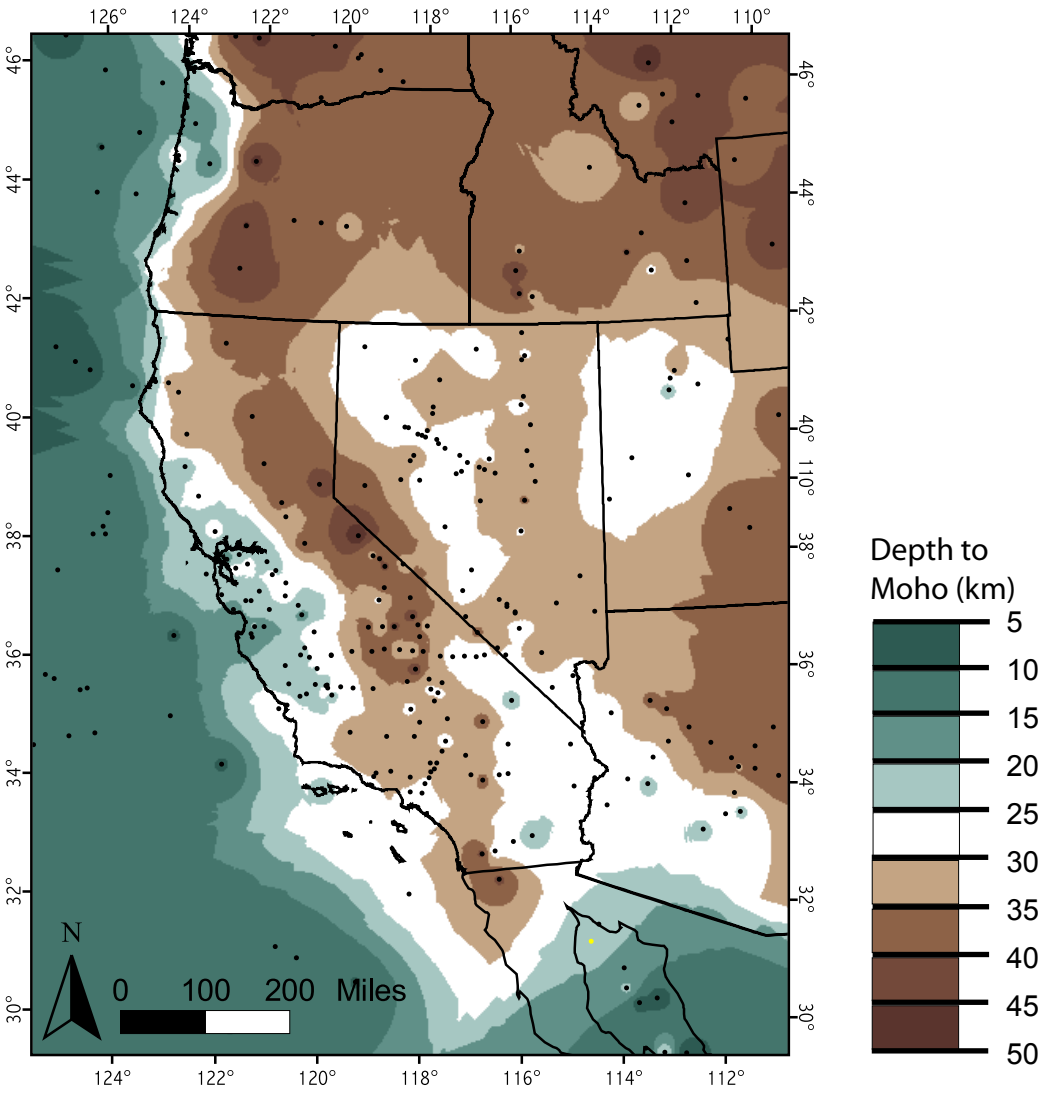

Figure 3.3 Depth to Moho interpolated from crustal thickness data from Walter Mooney (personal communication, 2001), Fliedner et al. (2000), Fuis et al. (2001) and Catchings and Mooney (1991). Locations of data points used in interpolation are shown as black dots.

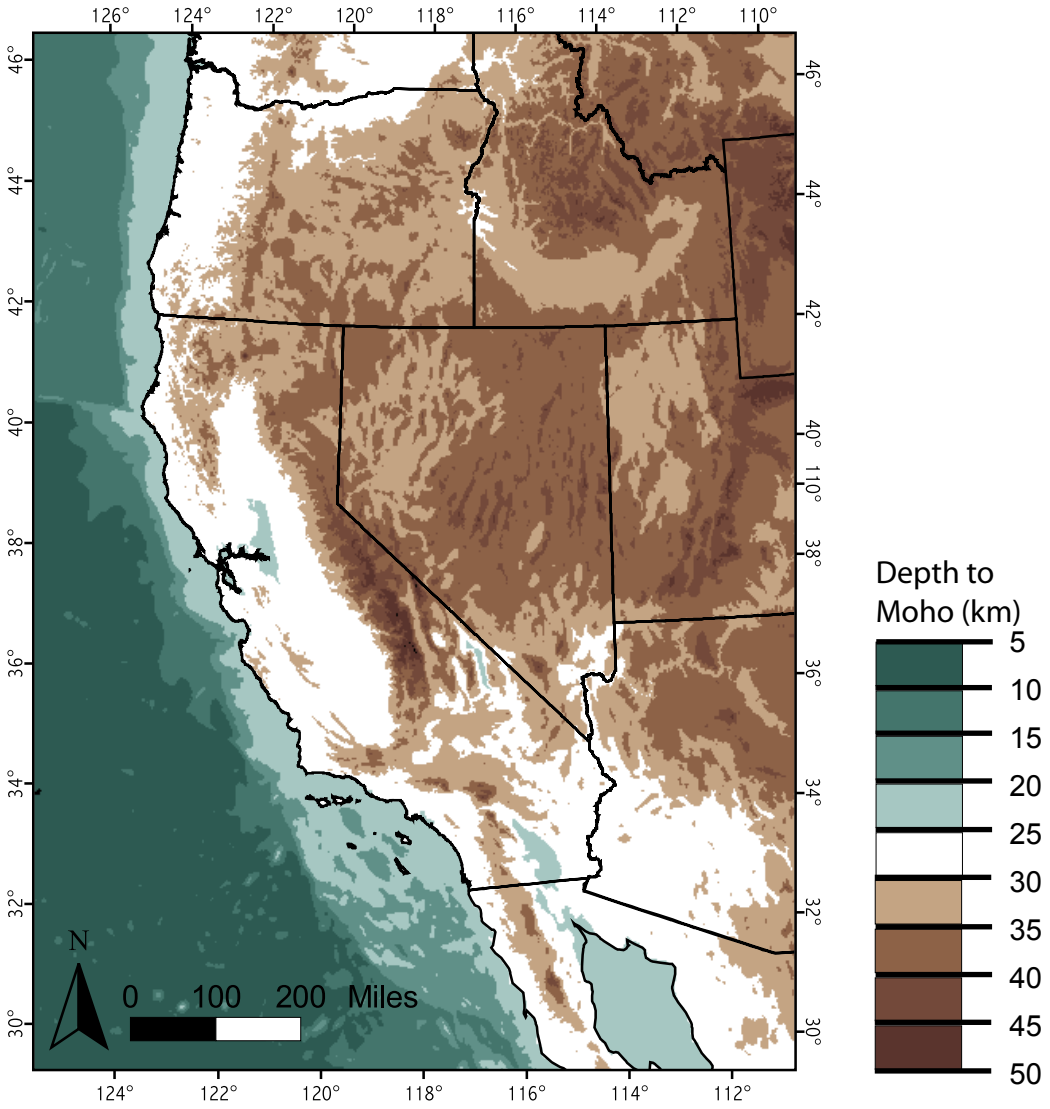

Figure 3.4 Moho depth generated by the Airy-Heiskanen isostatic correction computer model with crustal density 2670 kg m^{-3}, mantle density 3070 kg m^{-3}, and compensation depth 25 km.

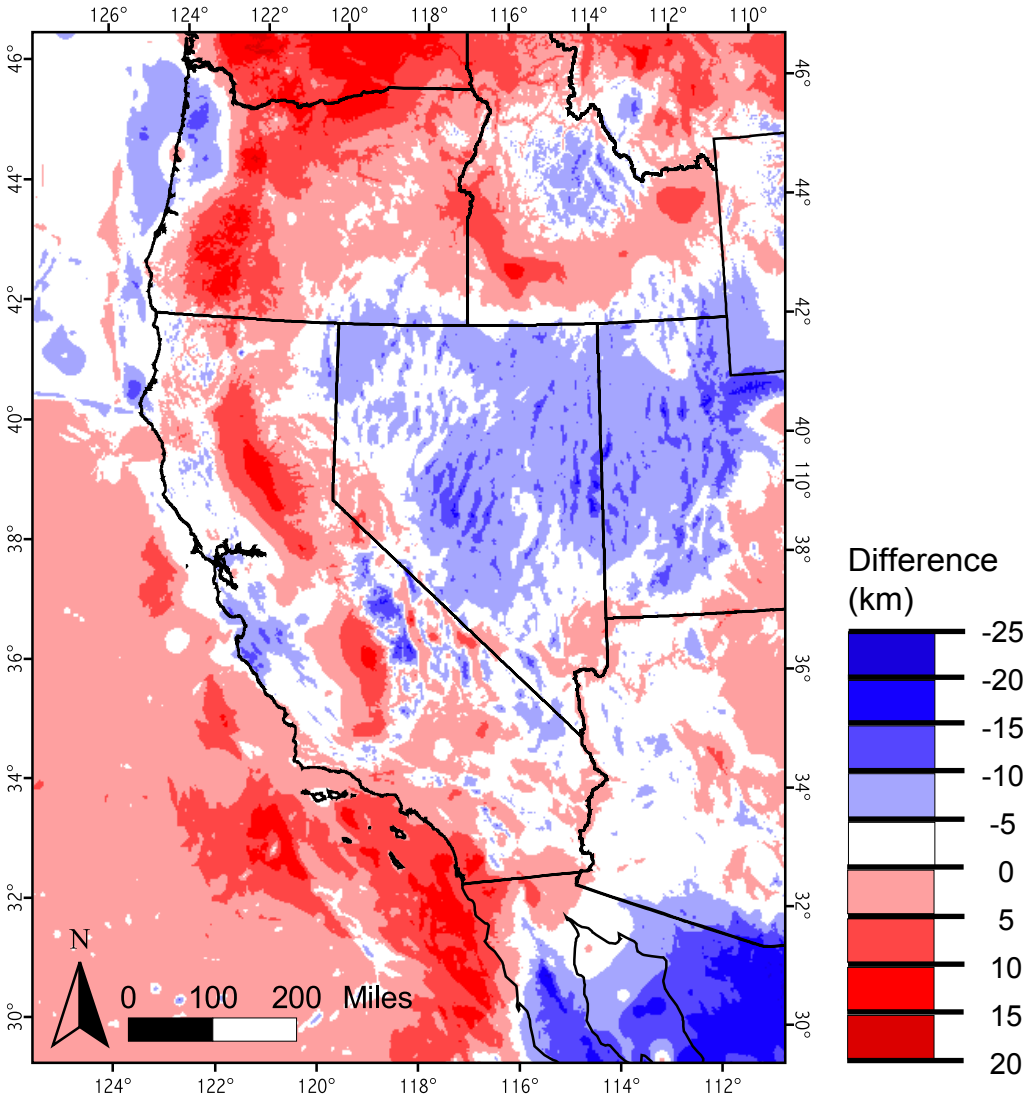

Figure 3.5 Difference between the depth to Moho interpolated from crustal thickness data (Figure 3.3), and the crustal root depth (Moho) generated by the Airy-Heiskanen isostatic correction computer model (Figure 3.4). Positive values indicate that the interpolated depth is greater than that calculated by the Airy-Heiskanen model, and negative values indicate that the Airy-Heiskanen calculated depth is greater.

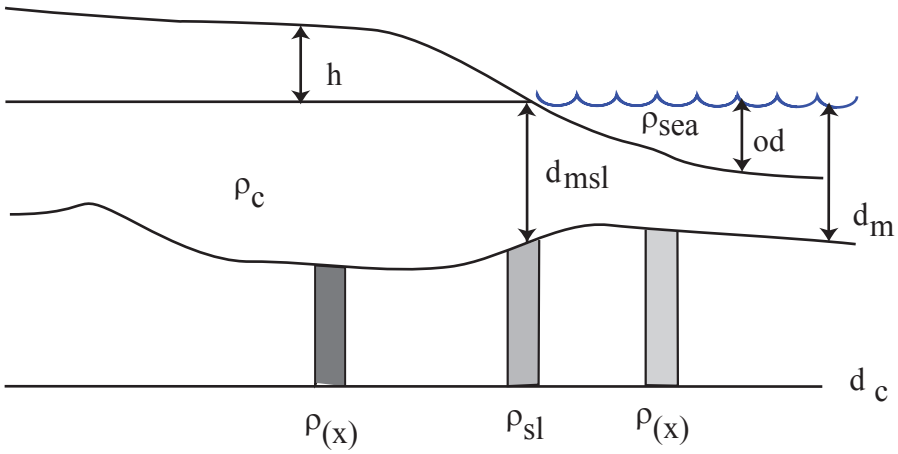

Combined Effect Isostatic Compensation Model

Topographic support is provided by crustal root and laterally varying mantle density. Crustal density is held constant.

h = topographic height above sea level
od = ocean depth
d_c = compensation depth
d_m = depth below sea level to moho (known)
d_{msl} = depth to moho at h = 0 (average value)
ρ_c = crustal density
ρ_{sea} = seawater density
ρ_{sl} = mantle density where topographic height is 0 (specified)
$\rho_{(x)}$ = calculated mantle density

On land the balance is described:
$\rho_{(x)}(d_c - d_m) + \rho_c(h + d_m) = \rho_{sl}(d_c - d_{msl}) + \rho_c(d_{msl})$

On the ocean the balance is described:
$\rho_{(x)}(d_c - d_m) + \rho_c(d_m - od) + od(\rho_{sea}) = \rho_{sl}(d_c - d_{msl}) + \rho_c(d_{msl})$

Figure 3.6 Geometry and variables of the combined effect model. Isostatic correction is the change in gravitational attraction (at sea level) of a column due to the difference in ρ_{sl} and $\rho_{(x)}$ and the changes in d_m.

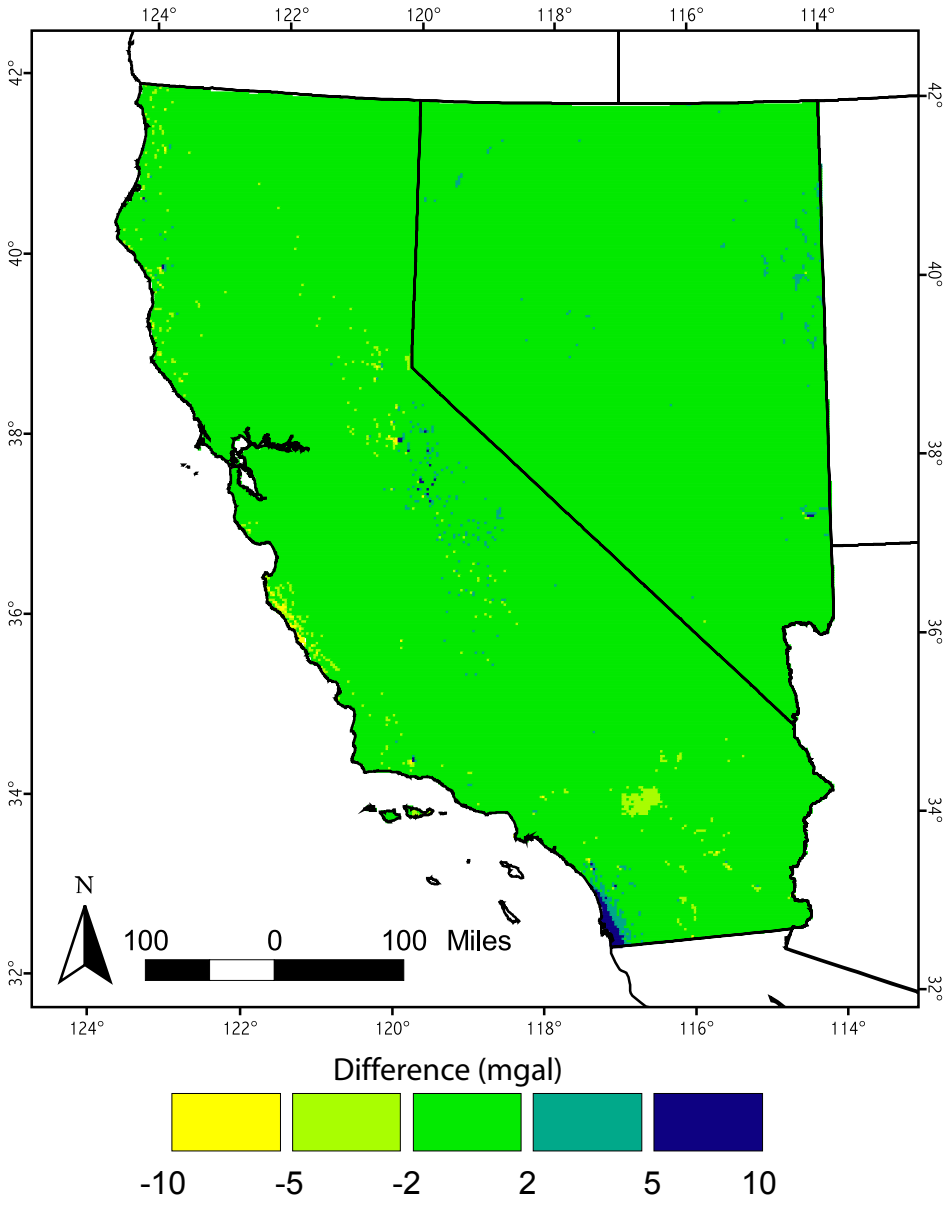

Figure 3.7 Difference between National Geophysical Data Center isostatic anomaly values and those generated by the Airy-Heiskanen computer model written for this study.

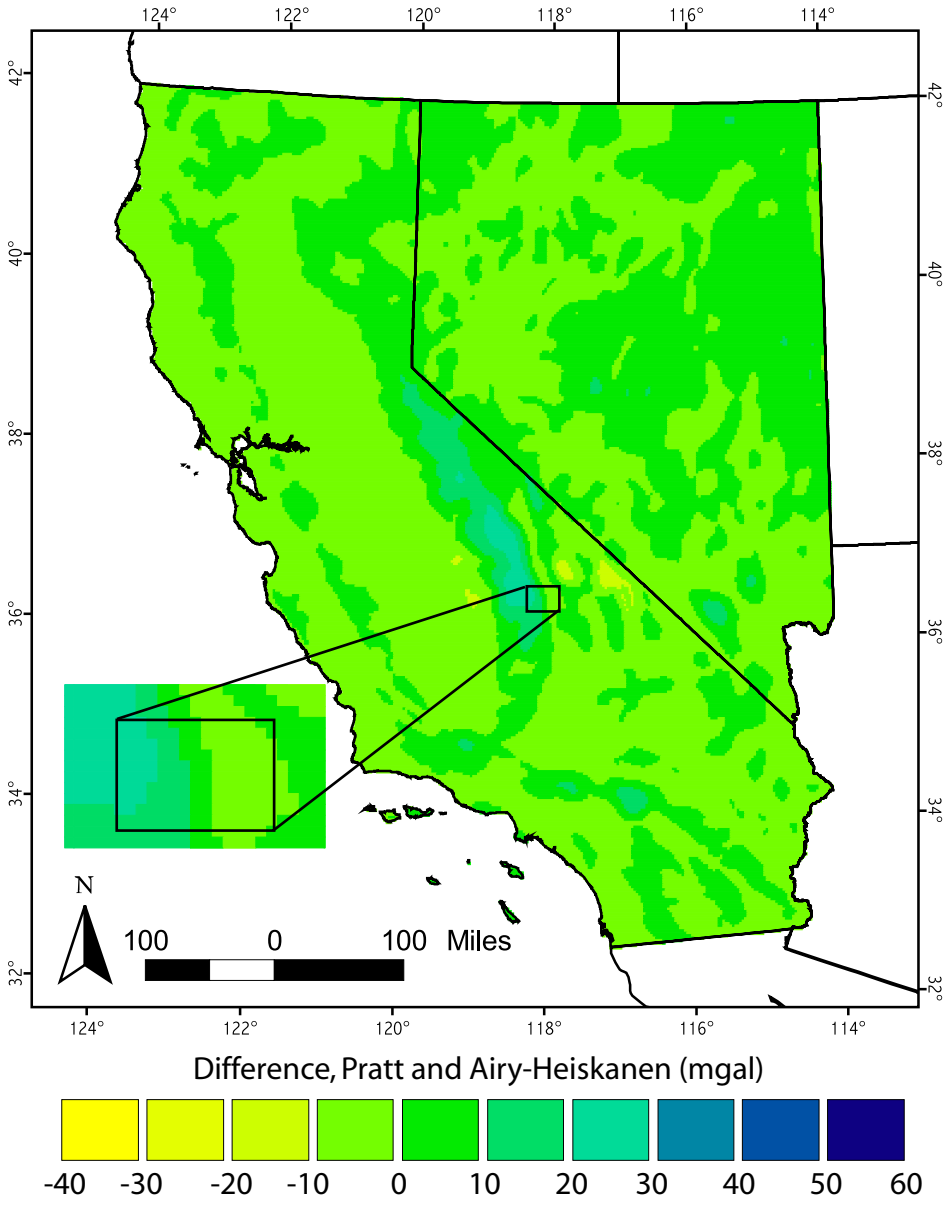

Figure 3.8 Difference between isostatic anomaly values generated by the Pratt-Hayford isostatic correction model and the Airy-Heiskanen isostatic correction model with average anomaly values of -13.21 mgal and -13.07 mgal respectively.

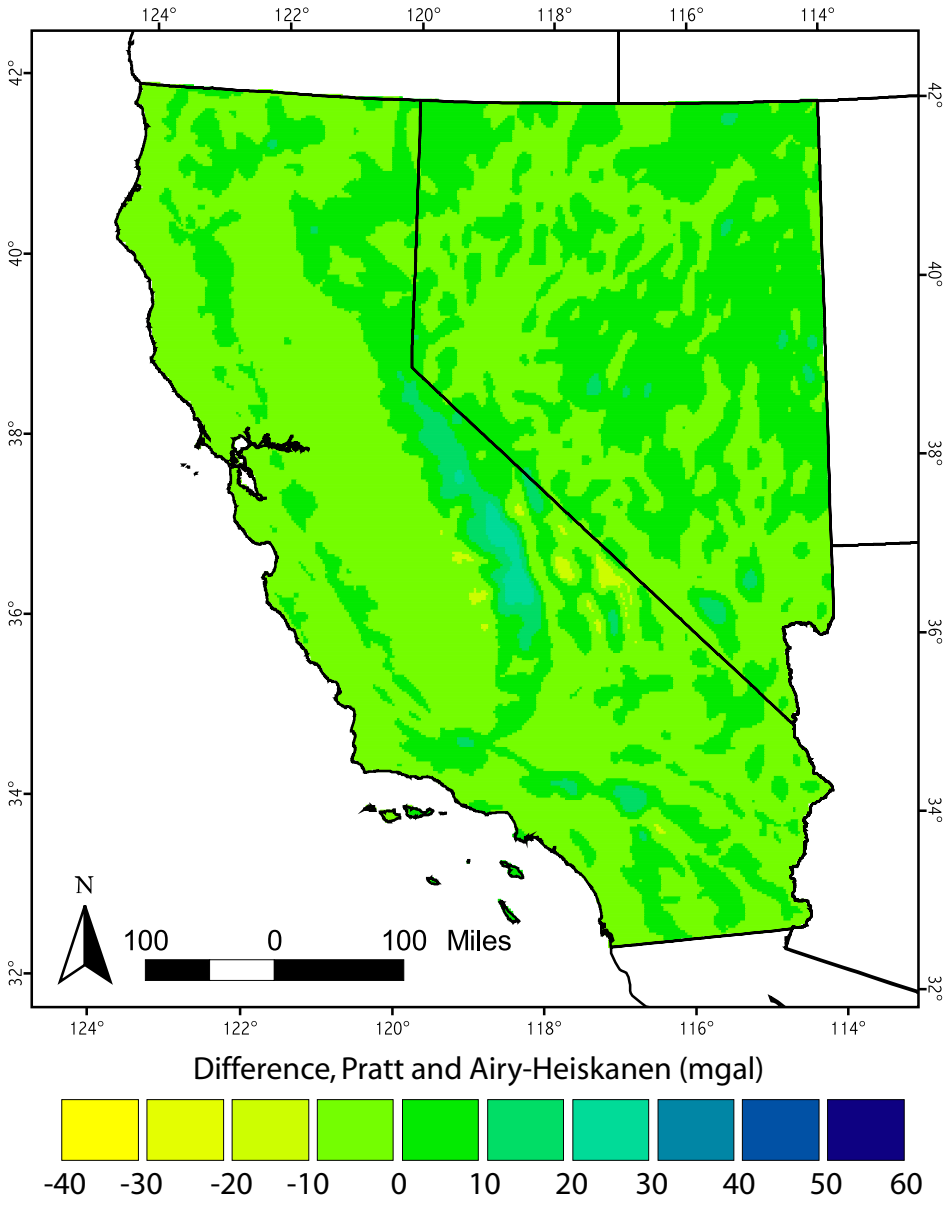

Figure 3.9 Difference between isostatic anomaly values generated by the Pratt-Hayford isostatic correction model and the Airy-Heiskanen isostatic correction model with average anomaly values of - 0.22 mgal and -0.22 mgal respectively.

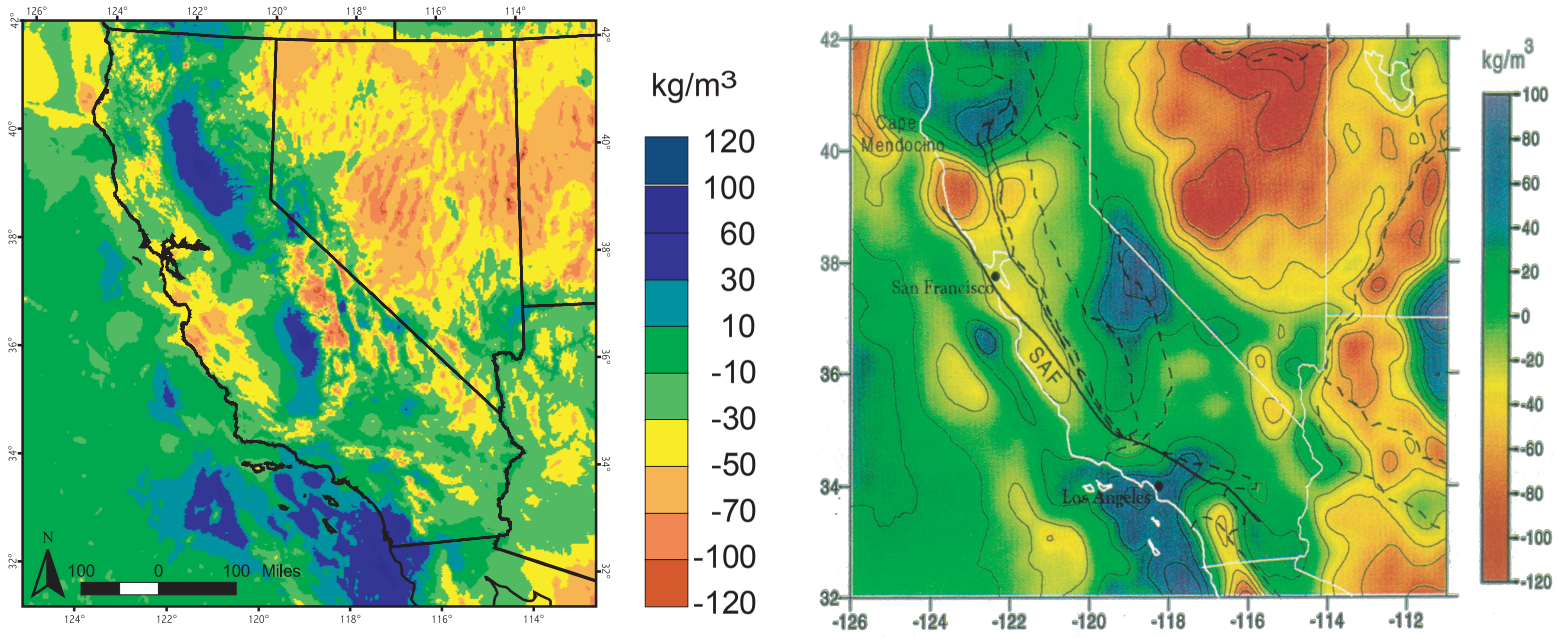

Figure 3.10 Mantle (Moho to 100 km) density anomaly computed by the Combined Effect Model (left) compared with the upper mantle density anomaly found by Kaban and Mooney (2001) from their isostatic lithosphere model and an inversion of isostatic anomalies (right).

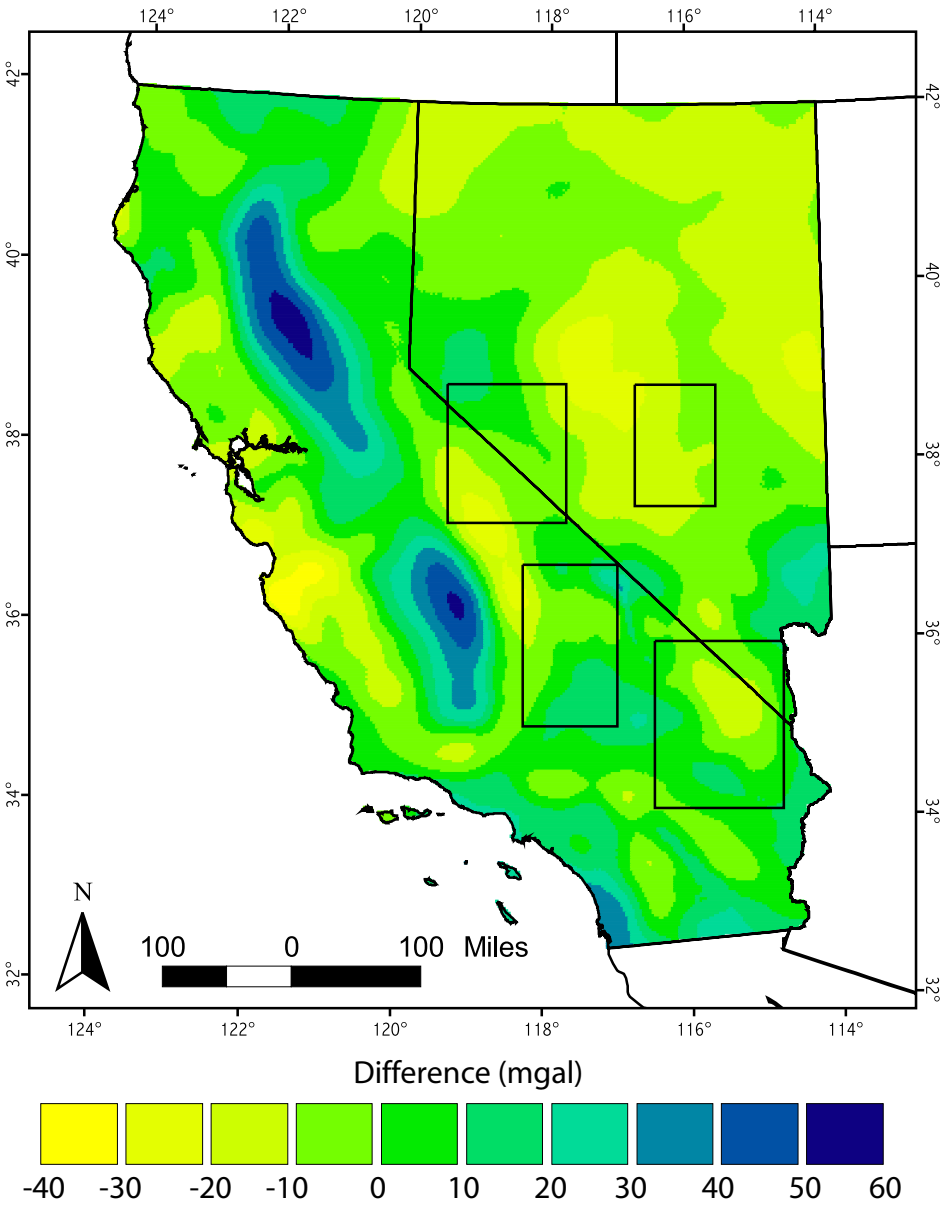

Figure 3.11 Difference between isostatic anomaly values generated by the CEM and the Airy-Heiskanen model with average anomaly values of -0.22 mgal and -0.22 mgal respectively.

Chapter 4

Modeling Results

4.1 Introduction

The areas selected for gravity modeling are shown on Figure 2.1, and include areas in the Mojave Desert in California and western Nevada, the eastern Sierra Nevada and western Basin and Range along the border of California and Nevada, and the Basin and Range in Central Nevada. In addition, gravity modeling performed by Black et al. (2002) in east central California near the Indian Wells Valley and Coso Volcanic Field is summarized in the following section.

All areas either are currently volcanically active, or have been active within the last 16 million years. Magmatism and tectonism within these areas is extensively studied and researchers strive to connect many different, yet related aspects of the behavior of the area. This chapter describes the results of gravity modeling for crustal density contrasts and the general spatial relationship of the crustal density with the nature of erupted volcanics. No attempt is made at this time to describe magma evolution or chemical relationships. The goal is to assess if there is a relationship between the crustal density and the density of erupted volcanics and likely intrusions that are used to describe gravity anomalies.

Numerical values describing crustal density are given as crustal density contrast values rather than actual densities. Isostatic anomaly values, by definition, reflect variations in the density of the upper crust. The goal of the gravity model was to reproduce those anomaly values by building a suitable model of the earth's upper

crust with density contrast values relative to the standard density. For example, a density contrast of -100 kg m^{-3} is used to describe crust that is 100 kg m^{-3} less dense than standard crust. Crustal density contrast values listed in tables 4.1, 4.2, and 4.3 refer to the density contrast values for the deepest model layer (basement) in each study area.

Many crustal density contrast values in the study areas are negative reflecting the negative character of the gravity anomaly values as included in the NGDC data set. As mentioned previously, the NGDC data set uses the Airy-Heiskanen isostatic correction method with a sea level root depth of 25 km, and a density contrast across the Moho of 400 kg m^{-3}. This configuration produces a generally negative average anomaly value. The crustal density contrast values must also be negative in character to reproduce this isostatic gravity anomaly signature. The crustal density contrast value for granitic basement can be estimated by the crustal density contrast value needed to reproduce the isostatic anomaly value over granite bedrock. This value is approximately -75 (±5) kg m^{-3} for all study areas.

With the exception of the area modeled by Black et al. (2002), a standard set of figures and tables is included for each study area. They show the geographic location of the study area, the type and location of recent (<16 ma) volcanics as mapped by Luedke and Smith, generalized geology, the NGDC isostatic anomaly grid, the isostatic anomaly produced by the crustal density contrast model, crustal density contrasts within each model layer, a table of the model layer thicknesses, figures relating the of volcanic rock type mapped by Luedke and Smith (1981) to the

crustal density contrast values of the deepest model layer (basement), and figures showing the relationship of silica content of volcanic rock samples in each area with crustal density contrast values for the deepest model layer.

4.2 Summary of Black et al. (2002)

Black et al. (2002) constructed a three-dimensional gravity model of the area of southeastern California surrounding the Indian Wells Valley. Their method was used as a model for the study described in this document.

The study area used by Black et al. (2002), shown on Figure 2.1, is bounded by Death Valley to the east and the Sierra Nevada mountains to the west. The Mojave Desert is in the southern part of the study area. Constraints for the model included surface geology, seismic reflection data, and deep well information.

The final model configuration consisted of nine layers of varying crustal density contrasts. The layers, with thicknesses ranging from 0.2 to 6.4 km, extended from the surface to 10 km. The final model results indicated low density crust in the northern portion of the study area and higher density crust in the south. Final crustal density contrast values for the basement rocks range from 0 to -120 kg m^{-3}. A wedge of lower density crust cuts across the northern study area from southeast to northwest. The wedge of low crustal density is at least partly bounded by the Wilson Canyon fault to the south, further supporting the possibility of significantly different crustal densities existing adjacent to each other. The Coso volcanic field is located on the surface above the low density crust. Black et al. (2002) conclude that the

crustal density may have been a determining factor in the location and nature of the surface volcanics in the area.

4.3 Mojave study area

This study area is located in the transitional zone between the Basin and Range extensional province and the Mojave block. Figure 4.1 shows the location of this study area and surface features within. Mapped faults in the area are confined to the west and trend generally northwest or west (USGS, 2006). The topography is generally "basin and range" type, with extensive sedimentary basins between mountains of basement rock. Basement outcrops include Precambrian crystalline rocks (primarily schist and gneiss), Precambrian, Mesozoic, and Cenozoic sedimentary and metamorphic rocks, Mesozoic granite, and Cenozoic granite. Tertiary and Quaternary volcanics overly both basement and basin fill in some areas. The location of volcanics less than 16 Ma, as mapped by Luedke and Smith (1981) is shown on Figure 4.2 and the geology of the area is shown on Figure 4.3. Volcanic rocks erupted in the last 16 million years include basalt, andesite and rhyolite. Later Pleistocene and Holocene eruptions have been basaltic in nature and include the Cima volcanic field, the Amboy volcanic field and the Pisgah lava field.

The modeled area for the Mojave Desert study area includes approximately 32,000 km^2. As described in Chapter 2, two isostatic gravity anomaly grids were used in the modeling. One interpolation used data points located only on bedrock, and the other was interpolated from all gravity points available. Figure 4.4 shows the isostatic anomaly grid interpolated from all gravity data points. A prominent

gravity anomaly low is found in the center of the study area. The highest gravity anomaly values are located to the north and west of the low, and an area of intermediate values is located to the south and east of the low.

For purposes of estimating the density of surface volcanics, and thus removing them from the underlying basement values which were of primary interest, the density contrast of granite was assumed to be -75 kg m^{-3}. The crustal density contrast value for basalt was estimated to be approximately 100 kg m^{-3}. The overall density contrast values of the basement (lowest layer) geology were assumed to reflect the gravity anomaly values interpolated from points on bedrock. The lateral extent of each basin was approximated from the surface geology. Maps produced by Saltus and Jachans (1995) were used as a guideline for basin depths. Gravity modeling in this study and that by Saltus and Jachens (1995) indicates that the basins in this area are generally shallow (less than 600 m).

The overall grid size for the Mojave study area was 414 rows by 308 columns. Each cell measured 500 m per side. The final model consists of five layers of various thickness (Table 4.1). Actual isostatic gravity anomaly values and those produced by the model are shown on Figures 4.4 and 4.5. The model produced a good match to the actual values with the greatest error associated with the prominent circular low in the central portion of the study area. Figures 4.6 to 4.10 show the 5 layers of crustal density contrasts as modeled in the Mojave study area.

The density trend displays low density crust (-55 to -85 kg m^{-3} contrast) in the center of the area, with denser (-20 kg m^{-3} contrast) crust to the south, and the

densest crust to the north (0 kg m^{-3} contrast). A wedge of high density crust (40 kg m^{-3} contrast) was indicated in the north central portion of the area. Short wavelength gravity highs were modeled as high density intrusions within a less dense crust. The "intrusions" in the Mojave study area are scattered across the entire region and are not isolated to one particular crustal density contrast value. The Independence dike swarm is an extensive system of mafic to silicic dikes which intruded eastern California about 148 Ma. The Garlock fault cuts across the swarm and the southern extent is mapped at the surface in the western part of the Mojave study area (Carl and Glazner, 2002). The small high density "intrusions" may be related to subsurface portions of the swarm.

Late Tertiary and Quaternary volcanics, ranging in composition from silicic to mafic (Luedke and Smith, 1981) are located over the central gravity anomaly low, and associated low values for crustal density. Figure 4.12 shows the crustal density contrast value of the basement (deepest layer) directly beneath these volcanics. The association shown on the figure, and on similar figures in the other study areas, is that between the type of volcanic rock (basalt, andesite, dacite or rhyolite) mapped in a particular grid cell and the modeled density contrast of the basement in the same grid cell. The associations and percentages show trends only, as melt can travel significant distances from the point of eruption. Basalt is found above all but the densest basement (deepest layer) crust and is primarily associated with the lowest basement crustal density contrast values (Figures 4.11, 4.12). The greatest lateral extent of late Tertiary and Quaternary (<16 Ma) volcanic deposits are located above

crust of comparatively low density (crustal density contrast value -55 kg m^{-3}) and include basalt, andesite, and rhyolite (Figure 4.12). Volcanics erupted in the area during the late Pleistocene and Holocene are almost exclusively basaltic in nature (Amboy, Pisgah, and some Cima deposits) and erupted through crust with density contrast values of 0 to -55 kg m^{-3}. However, because the isostatic gravity anomaly values are all negative in character and granitic basement is modeled with approximately a -75 kg m^{-3} value, most basalt erupts through crust denser than that of granite.

Volcanic rock sample data from the Mojave study area that include silica content information are plotted against modeled crustal density contrast values on Figure 4.13. Silica content of samples taken in the area varies from 46% to 76% by weight. The widest variation of silica content is associated with the least dense crust (-85 to -55 kg m^{-3} contrast value), perhaps indicating ponding of basaltic magma, and melting of crustal rocks creating silicic magma.

4.4 Eastern Sierra Nevada, Western Basin and Range study area (SNBR)

The SNBR study area is a region of approximately 24,276 km^2 in size on the eastern side of the Sierra Nevada in California. It is bounded on the west by the Sierra Nevada mountains and is open to the Basin and Range extensional province on the east. Figure 4.14 shows the location of the SNBR study area and features within. Late Tertiary to recent volcanics are abundant in this area and include rhyolite, andesite and basalt (Figure 4.15). The area, much of which is currently volcanically active, includes Long Valley Caldera, Mono Craters, Mono Lake, the

Aurora-Bodie volcanic field and the Adobe Hills. Basalt flows in the Adobe Hills occurred at several times in the late Tertiary and Quaternary. NAVDAT ages range from 13 to 3.5 Ma for the Adobe Hills. Felsic to intermediate composition volcanics erupted in the Aurora-Bodie volcanic field from about 15 to 8 Ma. Long Valley caldera was created about 760,000 years ago by a massive eruption. Ash flow deposits from the caldera-forming blast created the Rhyolitic Bishop Tuff located just north of Bishop, California. Rhyolite, dacite and basalt have since been deposited within the boundary of the caldera. The Mono-Inyo craters are even younger in age, with eruptions from several thousand to several hundred years ago, the most recent of which is the Paoha island andesite estimated at 250 years old. Figure 4.16 shows the geology of the SNBR area.

The overall grid size for this study area was 335 rows by 290 columns. Each cell measured 500 m per side. Model constraints or guidelines included surface mapping (Jennings et al., 1977; Stewart and Carlson, 1978; Luedke and Smith, 1981) and inferred structure from previous two and three-dimensional gravity modeling, seismic modeling and drilling on the Long Valley Caldera (Carle, 1988; Abers, 1985). Previous work by Carle (1988) and Abers (1985) is concentrated on the 30 km by 50 km Long Valley caldera, which is the most complex part of the area to model.

Figure 4.17 shows the isostatic gravity anomaly grid interpolated from NGDC data. Anomaly values range from -71 to 11 mgal and generally grade from low to high from the southwest to northeast. The Long Valley Caldera is a significant

low within the field. The gravity low associated with the caldera has been attributed to either low density sediment (alluvium, lake sediment, and fall back deposits of Bishop Tuff) or a shallow magma body (Carle, 1988; Abers, 1985). These previous models, constrained with drill hole and seismic data modeled the caldera sediment depth from 2 to 3 km. Carle's model included a low density area, possibly magma, beneath the caldera.

Separating the gravity values measured over basin fill from those on bedrock was not as successful in the Long Valley area due to the large amount of young volcanics on the surface. In many cases it was not possible to differentiate between points on bedrock and points on volcanics that overly older basin fill.

The final model created in this study is composed of 11 layers of varying thickness from the surface to a depth of 10 km (Table 4.2). Agreement between the NGDC interpolated isostatic anomaly gravity data (Figure 4.17) and that produced by the model (Figure 4.18) is good. As in previous models, the lowest model layer represents basement rock and was modeled from a gravity anomaly grid interpolated from data measured on bedrock. Basement density contrast values include values of 0, -25, -70, -80, and -100 kg m^{-3}. The surface geology in the southwest portion of the study area is mapped as an extensive area of granitic plutonic outcrop. The crustal density contrast value in the area of the pluton outcrop is -70 kg m^{-3}, supporting the assumption that a valid crustal density contrast value for granite is approximately -75 kg m^{-3} in this area. Basins were identified by surface geology and gravity anomaly values. The depth of the Long Valley Caldera was constrained by

previous work (Carle, 1988). Although the fill within the caldera is primarily volcanic, the density-depth relationship (Figure 2.4) used for general basin fill was similar to fill density used by Carle (1988) in his more detailed model and was used in this simulation. Density contrast values within each layer are shown in Figures 4.19 to 4.29.

In the SNBR study area, volcanics have erupted through basement (deepest layer) crust of all density contrast values within the model. This includes density contrast values of 0, -25, -70, -80 and –100 kg m^{-3}. Figure 4.30 shows late Tertiary and Quaternary volcanics in relationship to estimated basement (deepest layer) density contrast values. A breakdown of volcanic rock type and the associated basement crustal density values are shown on Figure 4.31.

Most eruptions in the SNBR study area occur through basement crust of intermediate-high density, shown by the –25 kg m^{-3} crustal density contrast value. Basaltic flows are found primarily above the basement crust with a –25 kg m^{-3} crustal density contrast value, with less significant deposits above denser crust (0 kg m^{-3} crustal density contrast) and less dense crust (-70 and –80 kg m^{-3} density contrast). Very little basalt exists above the least dense estimate (-100 kg m^{-3} crustal density contrast). Andesites are most frequently found associated with basement crust of intermediate to high density (-25 kg m^{-3} density contrast), but are also frequently associated with less dense (-80 kg m^{-3} contrast) crust. Rhyolite flows occur in association with basement crustal density contrast values of -80 to -25 kg m^{-3}. The large rhyolite ash flow tuff (Bishop Tuff) in the south central

portion of the study area occurs near positive gravity anomalies which were modeled as very dense (100 to 200 kg m^{-3} contrast) plutons within basement crust of density similar to granite or granidiorite (-70 to -25 kg m^{-3} density contrast). A likely explanation for this result is the ponding of basaltic to intermediate magma due to neutral buoyancy. Due to the inexact nature of gravity modeling, it is possible that the "plutons" have a density contrast value less than 200 kg m^{-3} and continue deeper into the crust or are shallower than modeled. The short wavelength nature of the gravity anomalies indicate that they are most likely localized intrusions. The exact shape, depth and density contrast value are not well constrained at this time.

Figure 4.32 shows the relationship between silica content (wt%) of volcanic samples in the SNBR study area available through NAVDAT and the basement crustal density contrast values. Samples with the lowest and highest recorded silica content (44% to 78%) are associated with basement crust with a density contrast value of -70 kg m^{-3}, although basement of other density contrast values (-25 and -100 kg m^{-3}) show a wide range of silica content values as well. A definite relationship between the two variables is not evident, but may be due to the availability and spacing of sample data available on NAVDAT at this time.

4.5 Central Nevada study area

The modeled area in Central Nevada encompasses approximately 15,000 km^2 of the Basin and Range Province. It includes the north-south trending Reveille Range, Pancake Range, Quinn Canyon Range, Kawich Range and the southern Hot Creek and Monitor Ranges. Basin-bounding normal faults are oriented parallel to

the ranges. Basins include Railroad Valley and Sand Spring Valley. Figure 4.33 shows the location and features of the Central Nevada Study area.

Tertiary volcanics in this study area are primarily basaltic with lesser amounts of rhyolite and andesite. Felsic volcanism predominated until approximately 14 Ma, when lithospheric derived basaltic andesites erupted (Rash, 1995). Between 14 and 6 Ma the source for mafic volcanics shifted from the lithosphere to the asthenosphere (Rash, 1995; Dickson, 1995). Mafic volcanics erupted primarily in the Reveille and southern Pancake ranges (Lunar Crater Volcanic field) while those of felsic composition are found in the southwest portion of the study area (Figure 4.34). The youngest volcanic rocks are found in this study area are found in the Lunar Crater Volcanic field in the Pancake Range. Geology of the Central Nevada study area is shown on Figure 4.35 and consists primarily of Tertiary age volcanic and shallow intrusive ranges bounded by basins.

The overall grid size for this study area was 300 rows by 200 columns. Each cell measured 500 m per side. The isostatic anomaly grid interpolated from NGCD data is shown on Figure 4.36, and the isostatic anomaly grid generated by the gravity model for the area is shown on Figure 4.37.

The solution is composed of nine layers of gridded crustal density contrast values relative to the density of granite. Basement density contrasts include values of 0, -5, -25, -40, -55, -60, -65, and -80 kg m^{-3}. The density contrast value for Mesozoic plutonic granites in this area is approximately -80 kg m^{-3} as indicated by

geologic mapping on area bedrock. Layer thickness and depth are given on Table 4.3

A two-dimensional representation of each layer of crustal density contrast values is shown on Figures 4.38 through 4.46. Figure 4.46 is the two-dimensional representation of the basement density contrasts with the location of surface volcanics shown as an overlay.

Figure 4.48 categorizes erupted volcanics in the Reveille Range study area by modeled crustal density contrast values. Basaltic volcanics are grouped in a northeast to southwest band and overlie basement rocks with modeled densities varying from 0 to –65 kg m^{-3} contrast. The majority (51%) of the basalt deposits occur over the dense basement values (0 and –5 kg m^{-3} contrast), with a slightly lesser amount (45%) over basement of -50 to -60 kg m^{-3} crustal density contrast that lies between the denser values. No basalt is found over the least dense crust.

A small amount of Tertiary age andesite is found in this study area. Locations of andesite eruptions are split somewhat equally between crustal density contrast values of 0 to -5 kg m^{-3} contrast, -50 to -65 kg m^{-3} contrast, and -80 kg m^{-3} contrast.

Rhyolitic eruptions occur predominately in the southwest corner of the study area. A small amount is also found associated with basalt eruptions. Rhyolite magma reached the surface through crust of contrast values from 0 to -65 kg m^{-3}.

A number of high density (100 - 200 kg m^{-3} contrast) intrusions were used to model short wavelength variations in the gravity anomaly map. The largest of these

is centered in the northwest corner of the study area where the basement was found to be the least dense (-80 kg m^{-3} contrast). This intrusion is modeled as being connected to a smaller and shallower body in denser (-5 kg m^{-3} contrast) crust found adjacent. Andesite eruptions occur in close proximity to this "intrusion", in both densities of crust. Smaller plutons were modeled in the southern portion of the study area near rhyolite volcanics. The basement in this area is modeled to vary from –25 to –60 kg m^{-3} density contrast. A small isolated intrusive body was modeled over dense (0 kg m^{-3} density contrast) basement near basalt eruptions.

Figure 4.49 shows the relationship between silica content (wt%) of volcanic samples in the Central Nevada study area available through NAVDAT and the basement crustal density contrast values. Rocks with the lowest silica content for this study area (42%) are associated with a basement crustal density contrast value of -5 kg m^{-3}. Rocks with the highest silica content (60%) are associated with the crust of the same basement density contrast, but in a different geographic location. Volcanic rocks with silica content ranging from 45% to 50% are associated with basement crustal density contrast values of -50. Since the contrast value for granite is -75 ± 5 kg m^{-3}, all basalts erupted through basement crust are denser than granite.

Table 4.1 Mojave study area gravity model layer depth and thickness

Layer identifier (associated figure)	Depth range (meters)	Thickness (meters)
A (Figure 4.6)	0 - 100	100
B (Figure 4.7)	100 - 200	100
C (Figure 4.8)	200 - 400	200
D (Figure 4.9)	400 - 600	200
E (Figure 4.10) 'basement'	600 - 10000	9400

Table 4.2 SNBR gravity model layer depth and thickness

Layer identifier (associated figure)	Depth range (meters)	Thickness (meters)
A (Figure 4.19)	0 - 100	100
B (Figure 4.20)	100 - 300	200
C (Figure 4.21)	300 - 500	200
D (Figure 4.22)	500 - 700	200
E (Figure 4.23)	700 - 900	200
F (Figure 4.24)	900 -1100	200
G (Figure 4.25)	1100 - 1500	400
H (Figure 4.26)	1500 - 2000	500
I (Figure 4.27)	2000 - 2400	400
J (Figure 4.28)	2400 - 3000	600
K (Figure 4.29) 'basement'	3000 - 10000	7000

Table 4.3 Central Nevada gravity model layer depth and thickness

Layer identifier (associated figure)	Depth range	Layer thickness in meters
A (Figure 4.38)	0-100	100
B (Figure 4.39)	100-300	200
C (Figure 4.40)	300-500	200
D (Figure 4.41)	500-700	200
E (Figure 4.42)	700-900	200
F (Figure 4.43)	900-1100	200
G (Figure 4.44)	1100-1300	200
H (Figure 4.45)	1300-1600	300
I (Figure 4.46) 'basement'	1600-10000	8400

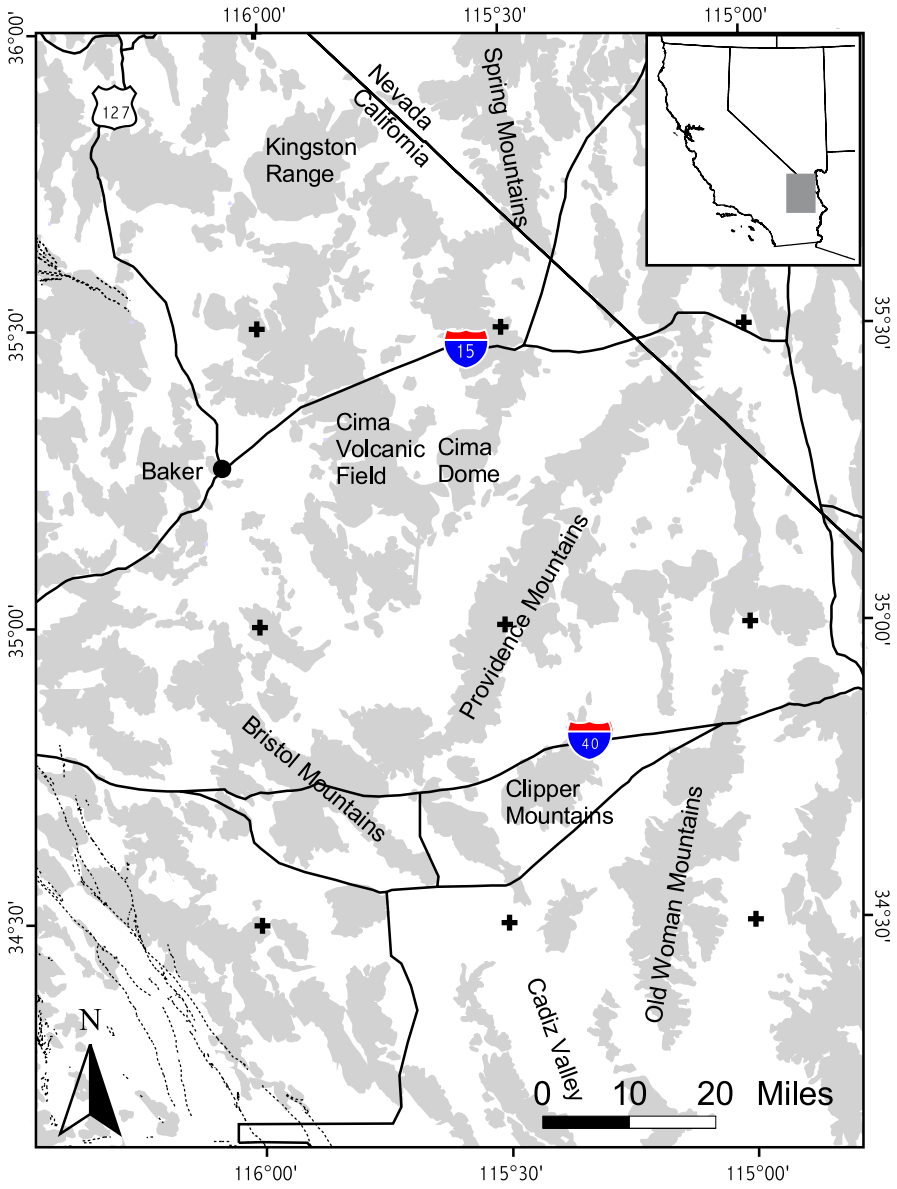

Figure 4.1 Location and features of Mohave study area.

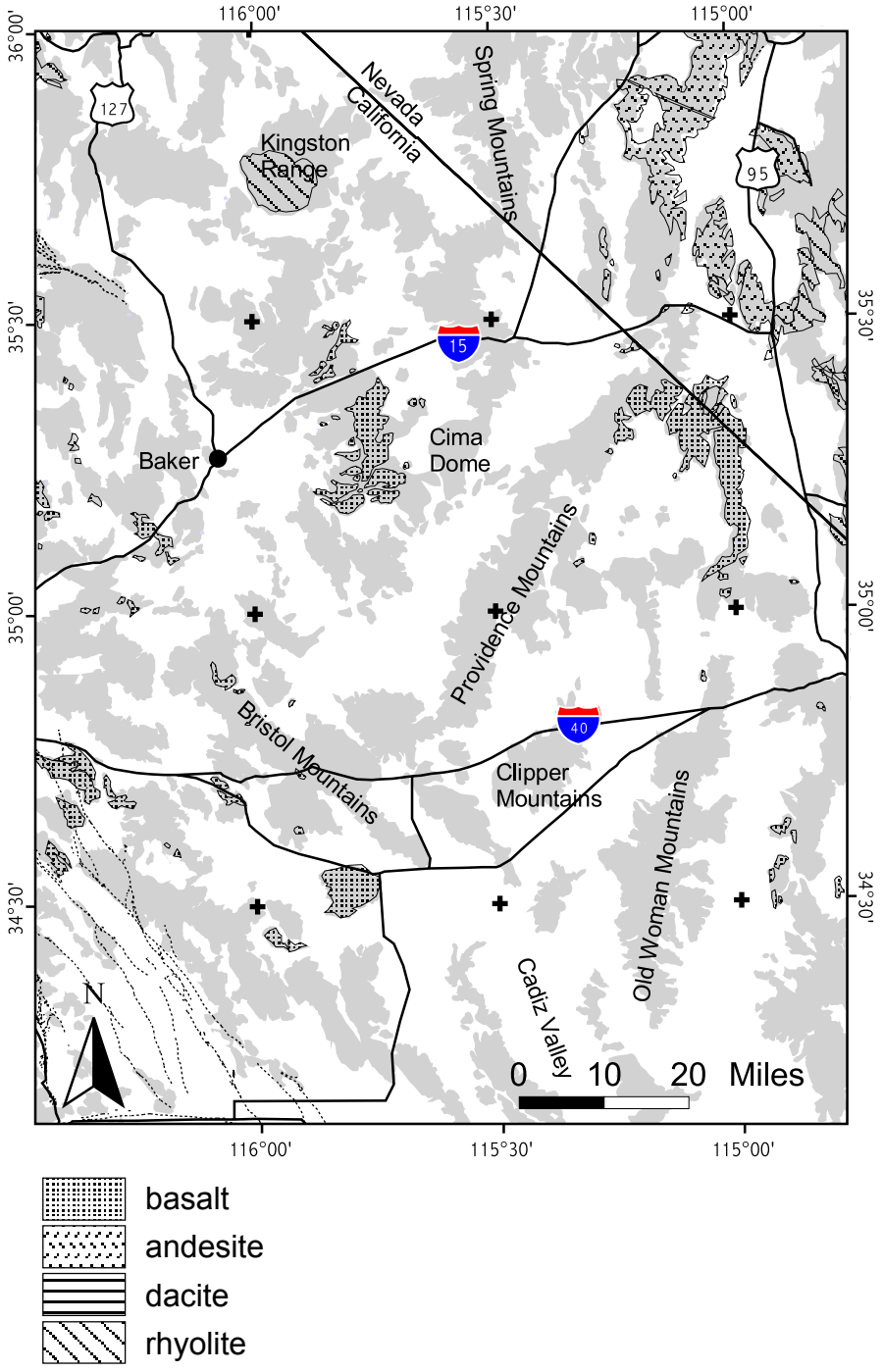

Figure 4.2 Late Tertiary and Quaternary volcanics in the Mojave study area as mapped by Luedke and Smith (1981).

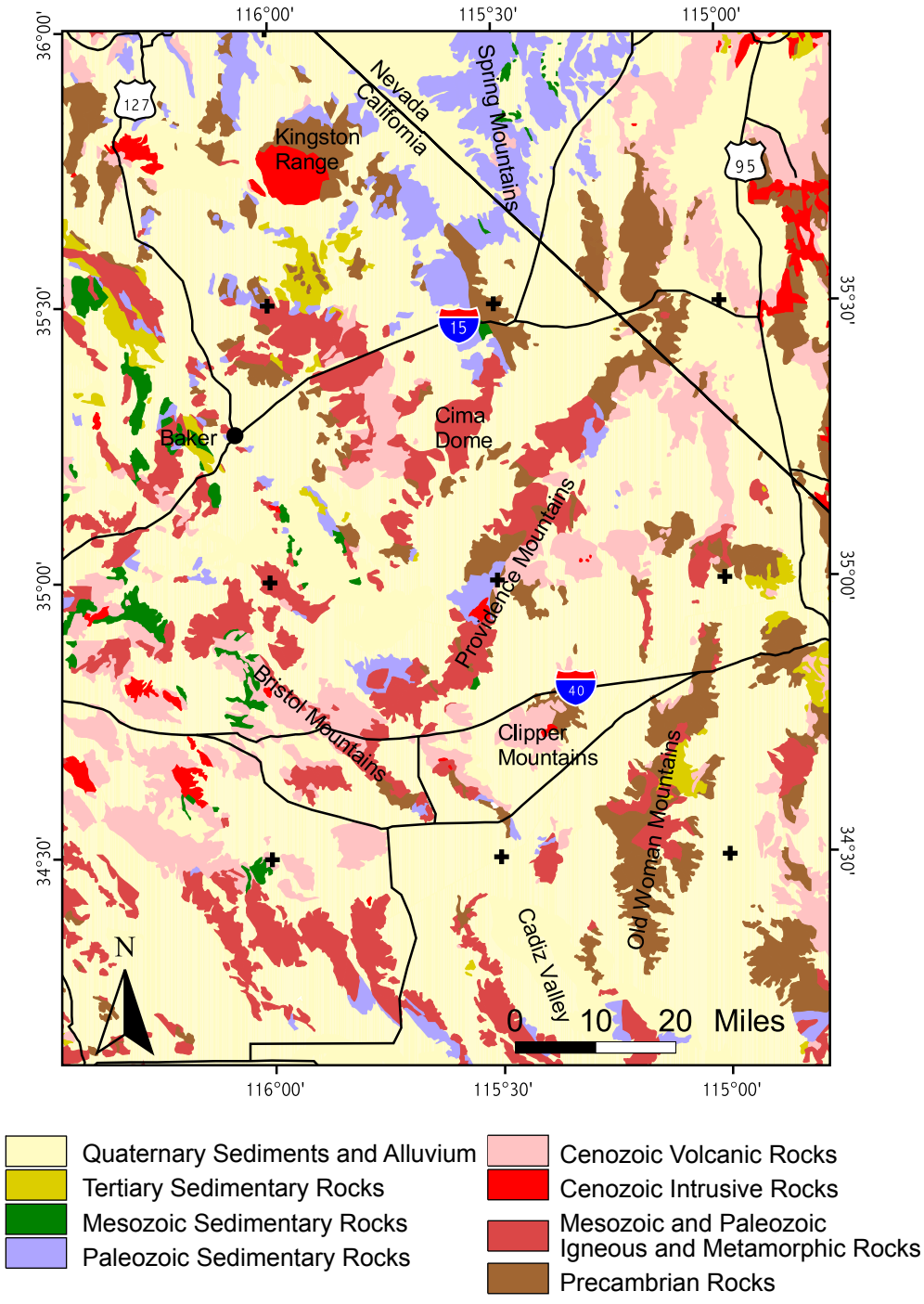

Figure 4.3 Geology of the Mojave study area. Modified from Jennings et al. (1977).

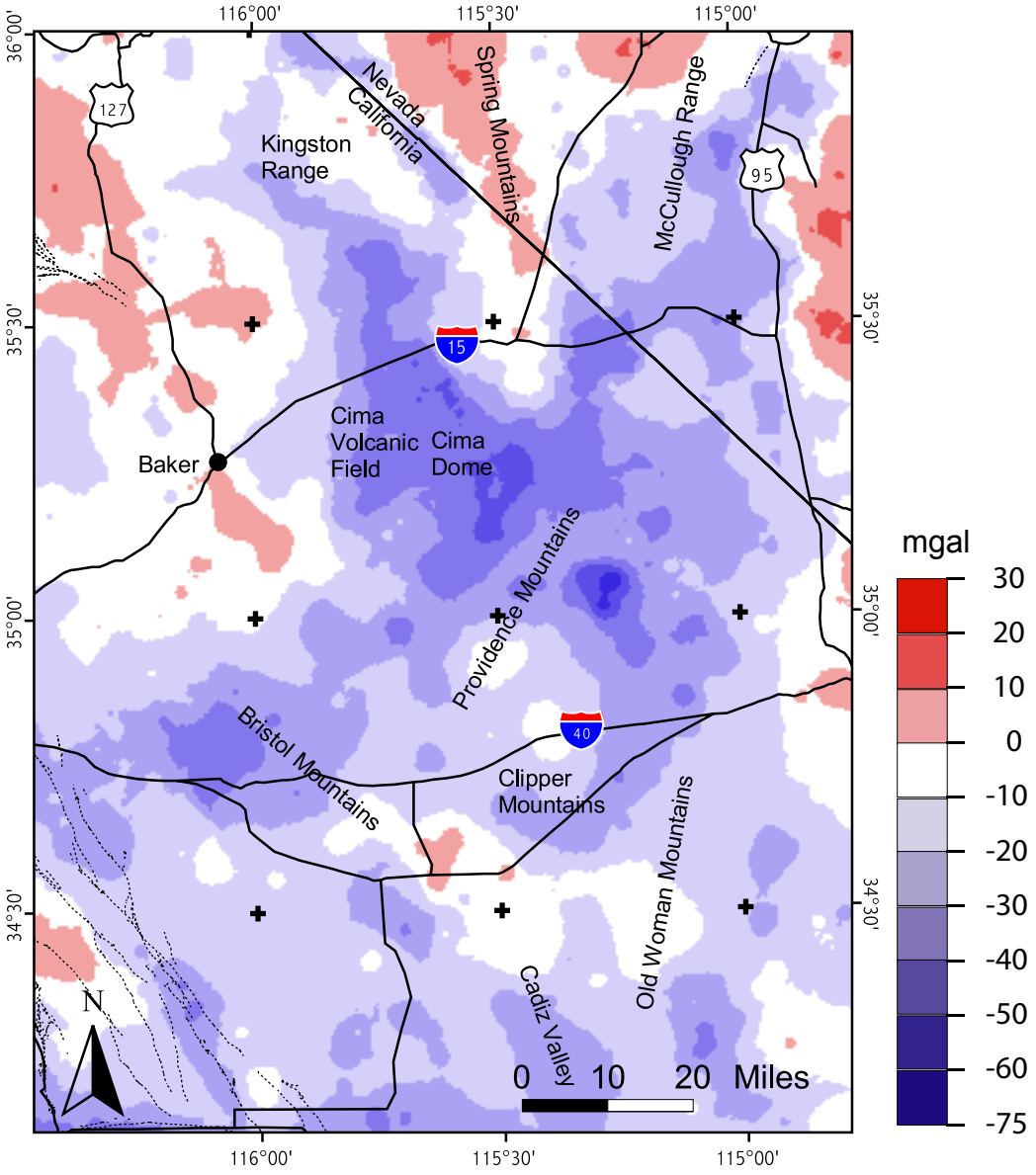

Figure 4.4 Isostatic gravity anomaly grid interpolated from NGDC isostatic anomaly data, Mojave study area.

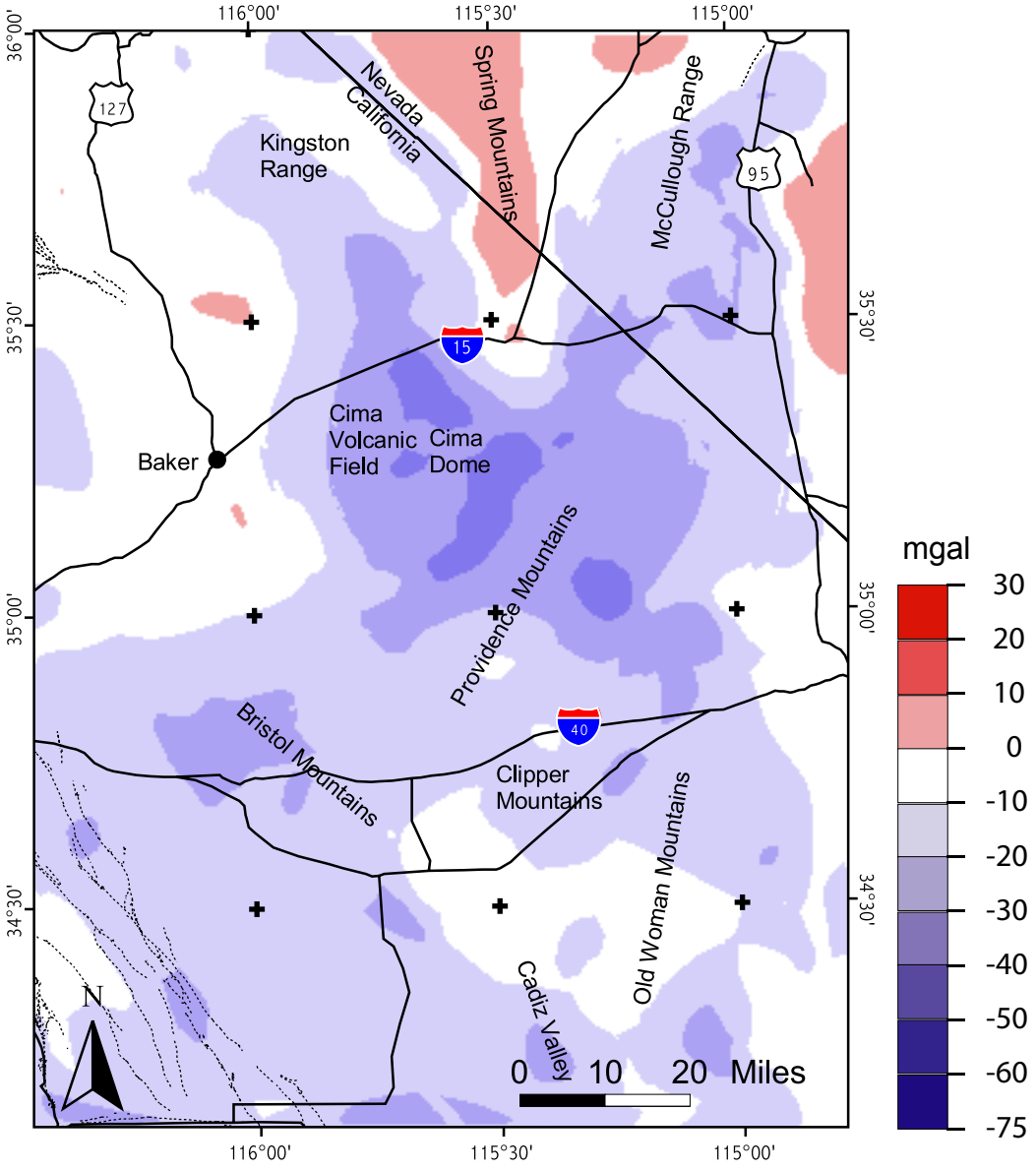

Figure 4.5 Isostatic gravity anomaly grid calculated from crustal density contrast model, Mojave study area.

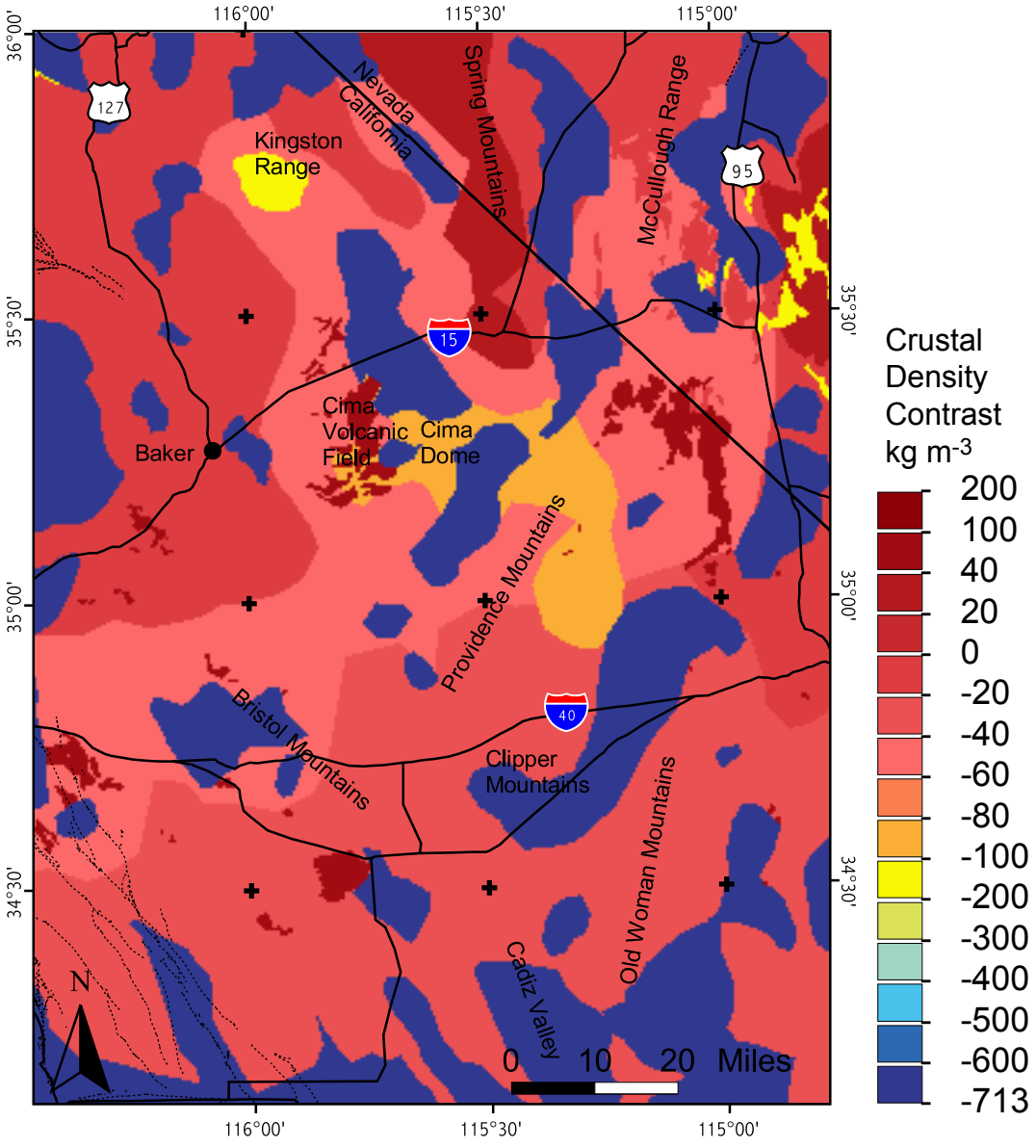

Figure 4.6 Modeled crustal density contrasts for layer A, 0 - 100 meters depth, Mojave study area.

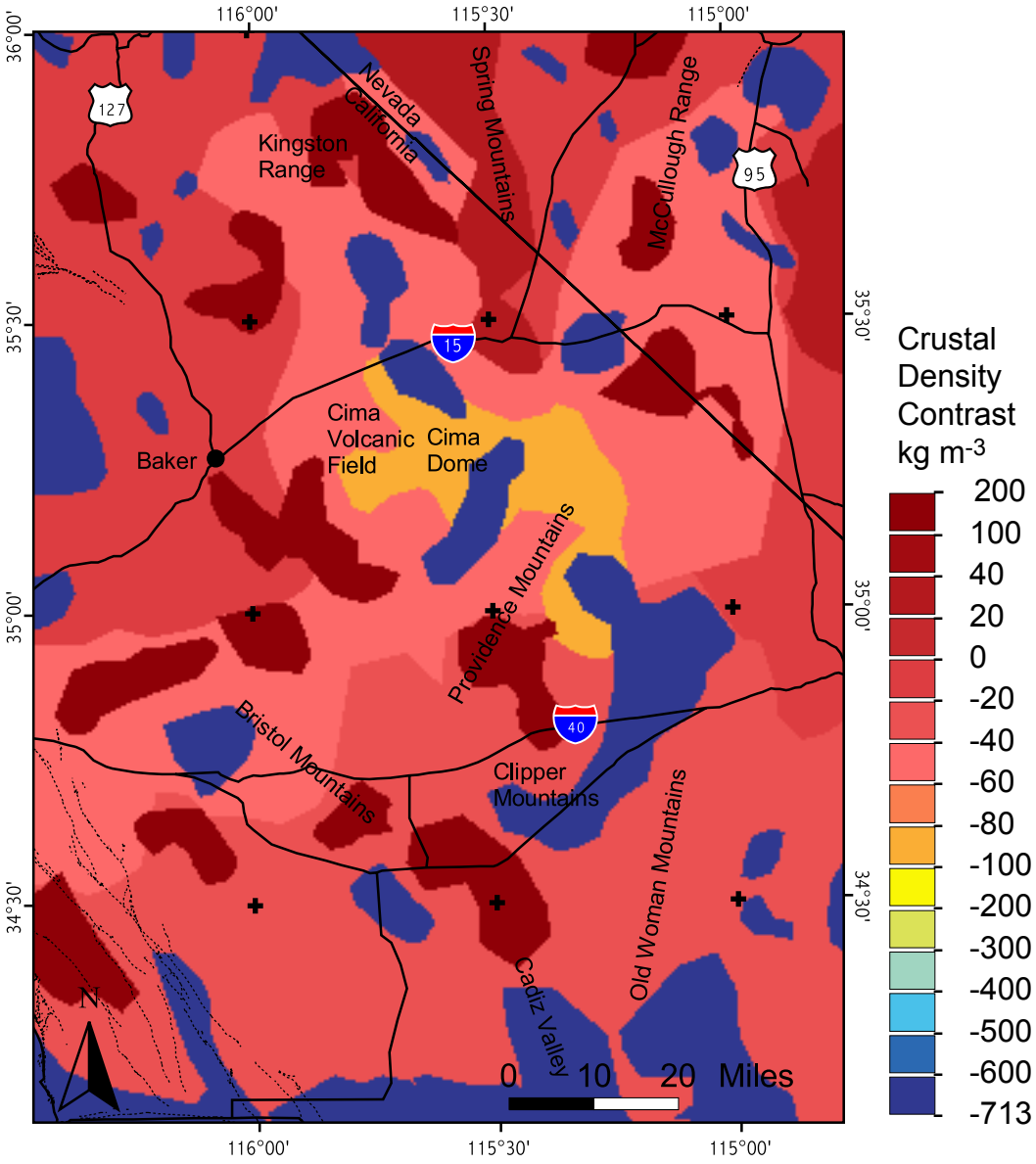

Figure 4.7 Modeled crustal density contrasts for layer B, 100 - 200 meters depth, Mojave study area.

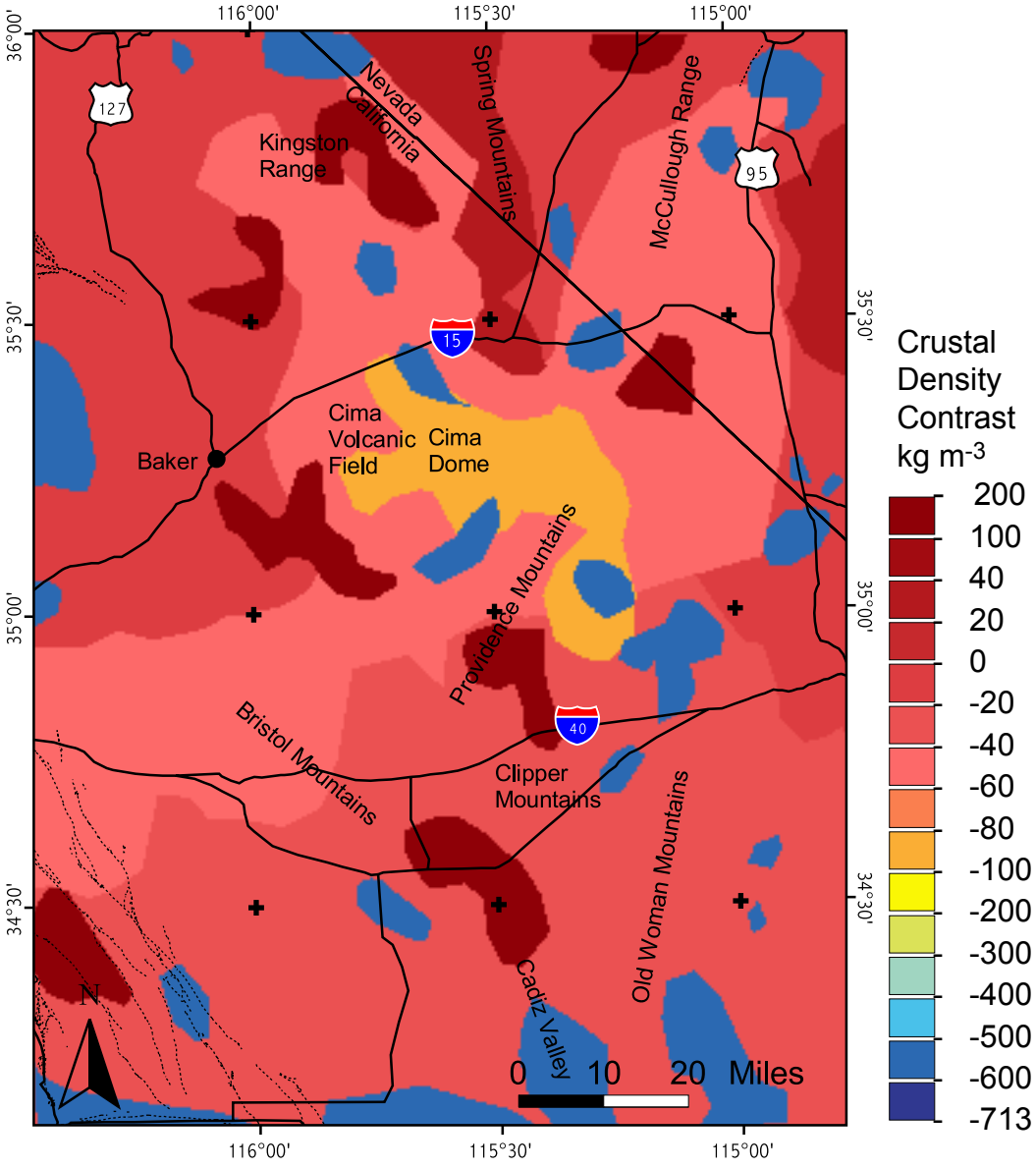

Figure 4.8 Modeled crustal density contrasts for layer C, 200 - 400 meters depth, Mojave study area.

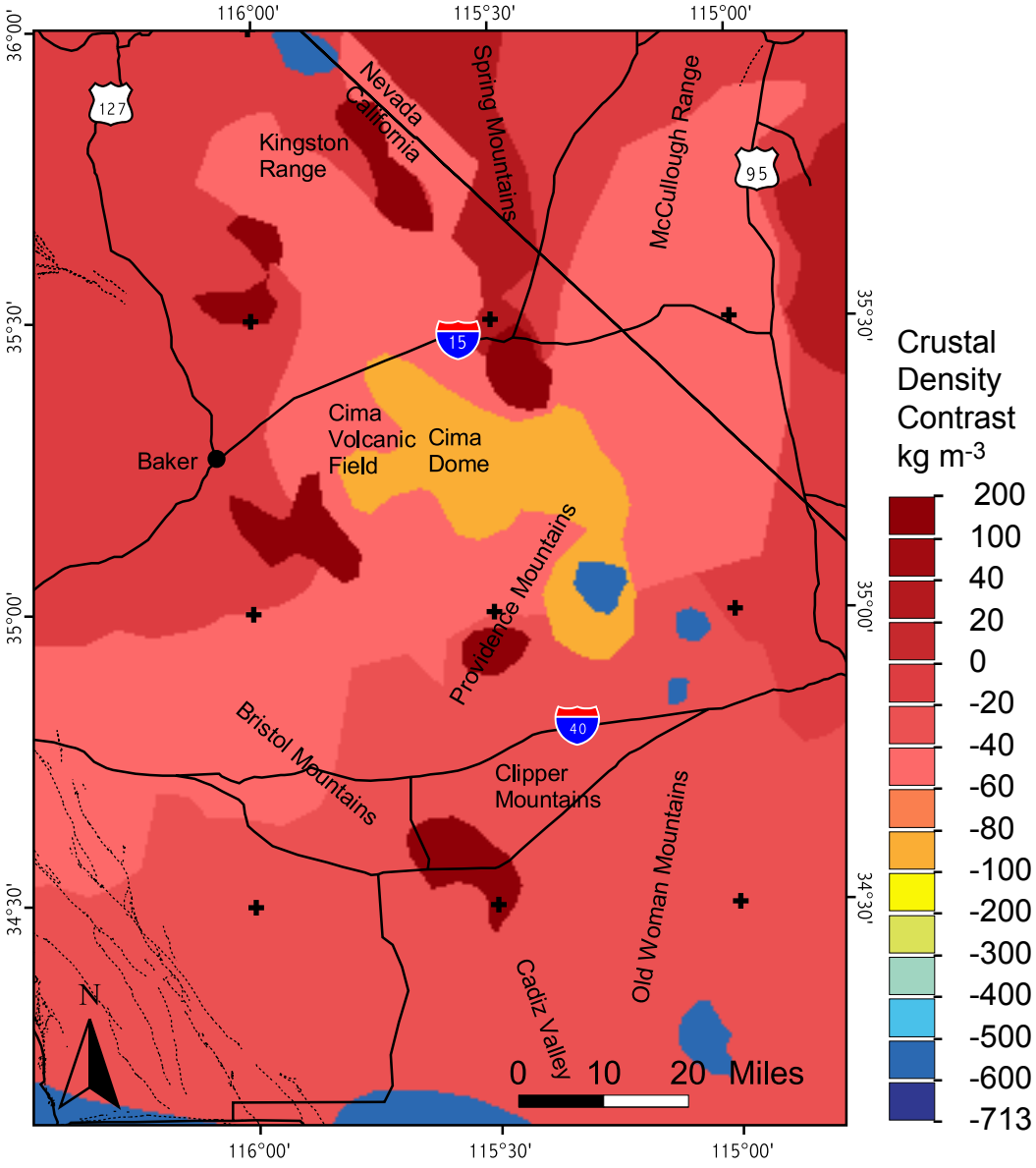

Figure 4.9 Modeled crustal density contrasts for layer D, 400 - 600 meters depth, Mojave study area.

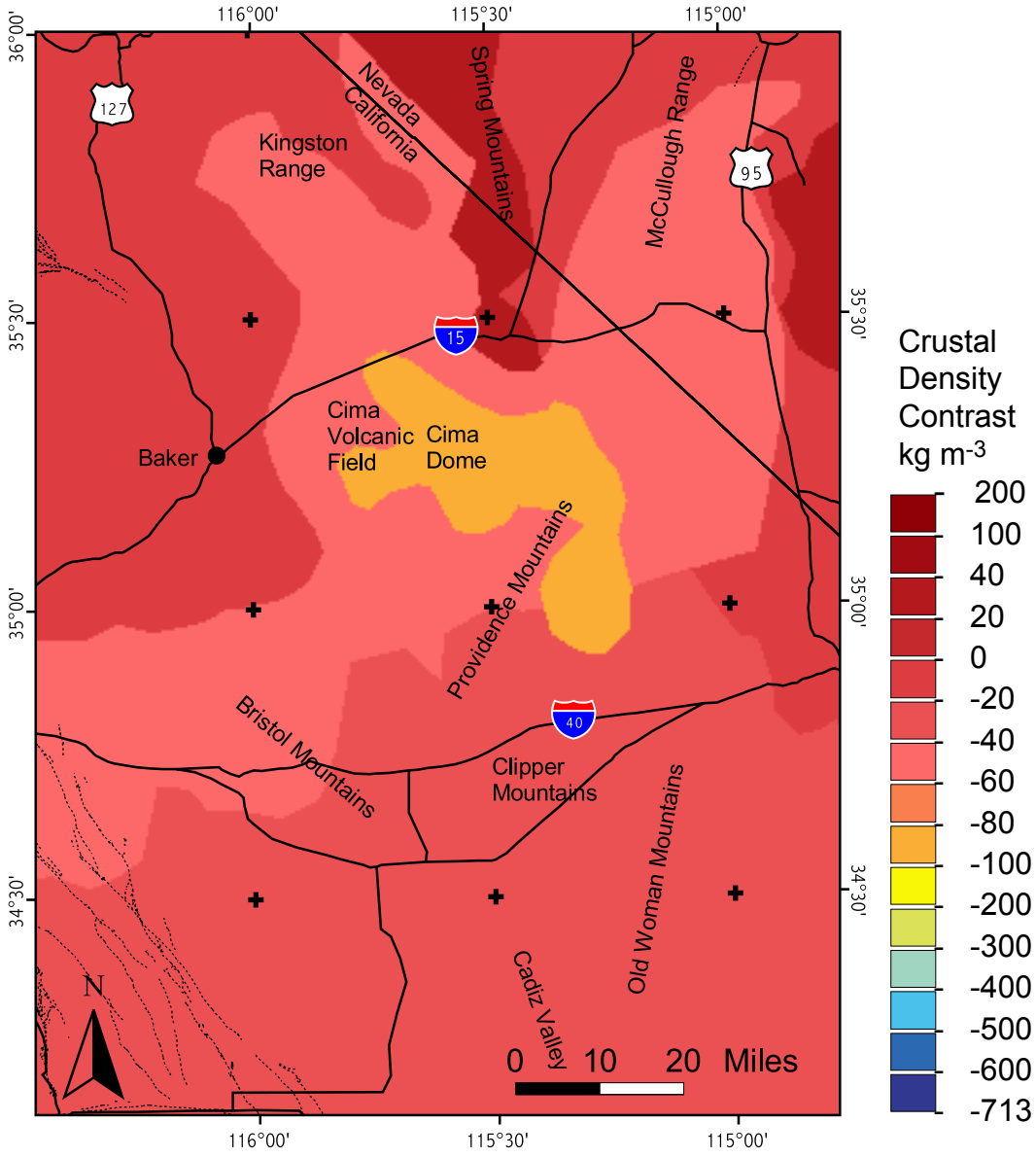

Figure 4.10 Modeled crustal density contrasts for layer E (basement), 600 - 10,000 meters depth, Mojave study area.

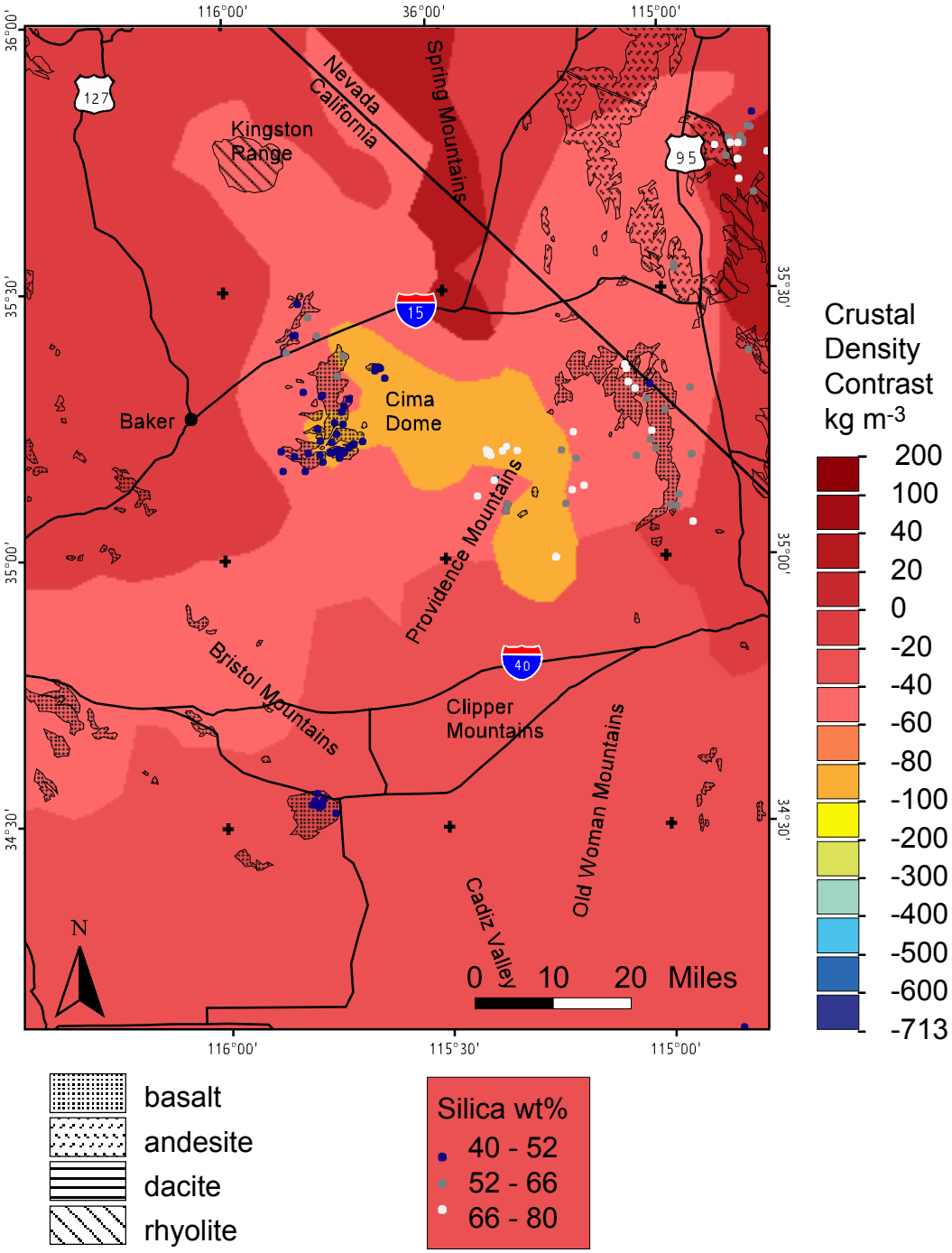

Figure 4.11 Modeled crustal density contrasts for layer E (basement), for the Mojave study area shown with late Tertiary and Quaternary volcanics as mapped by Luedke and Smith (1981), and silica content values of sampled volcanics from NAVDAT database.

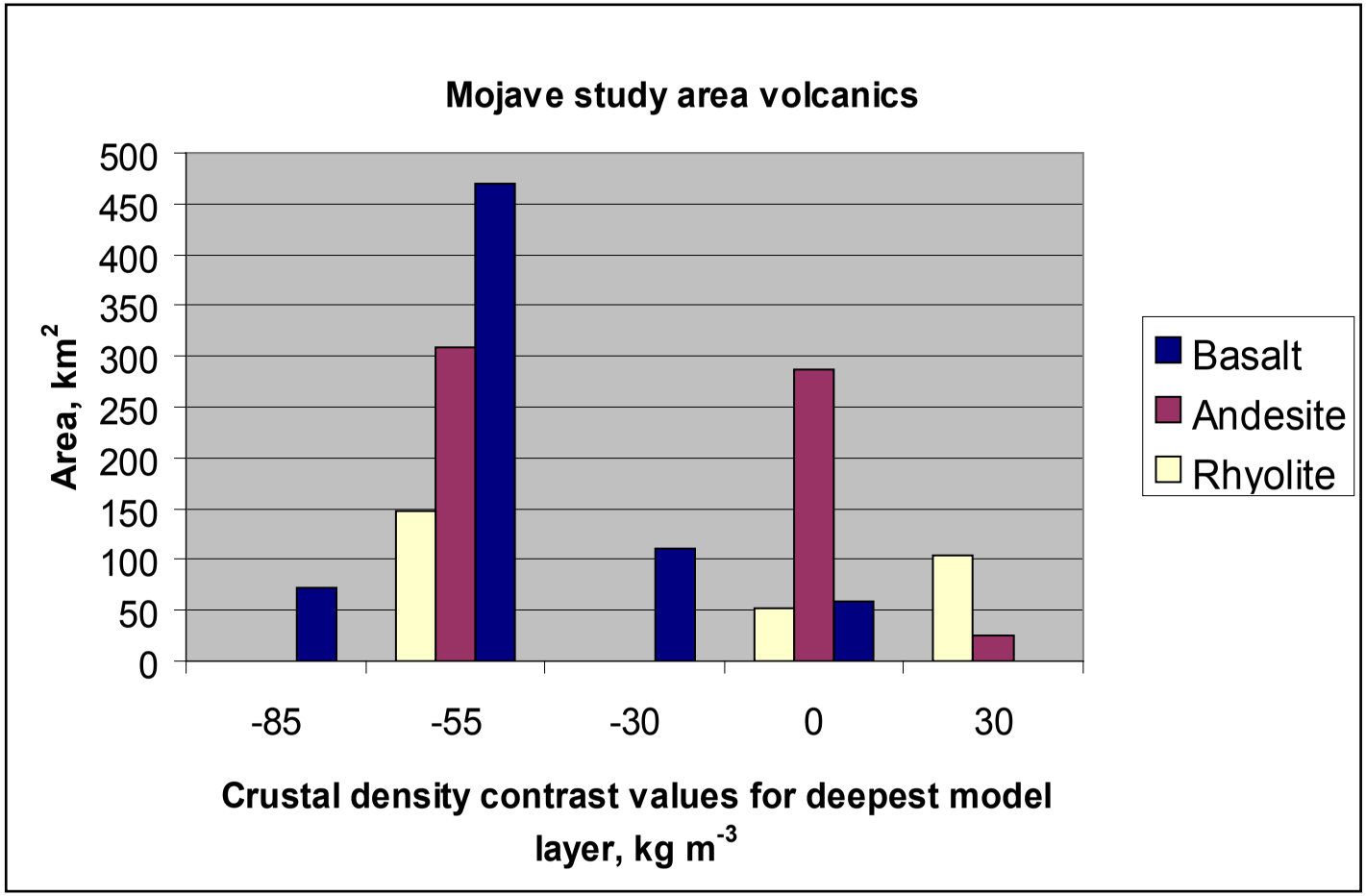

Figure 4.12 Surface area of late Tertiary and Quaternary (<16 Ma) volcanics, as mapped by Luedke and Smith (1981), erupted through each crustal density contrast value in basement model layer (E), Mojave study area.

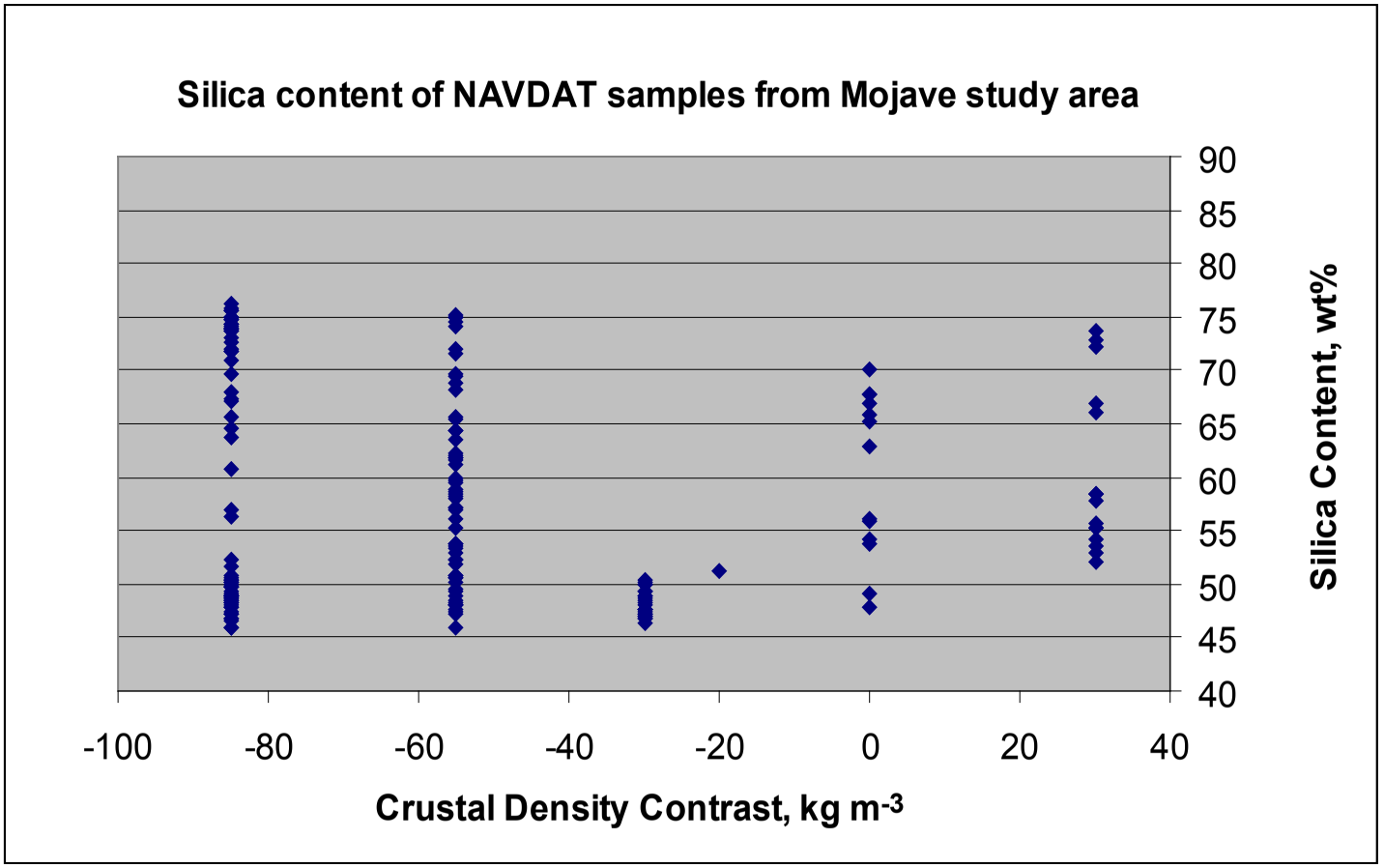

Figure 4.13 Relationship of silica content of NAVDAT samples of late Tertiary and Quaternary volcanics with modeled basement crustal density contrast values.
Figure 4.11 shows the location of samples used in this plot.

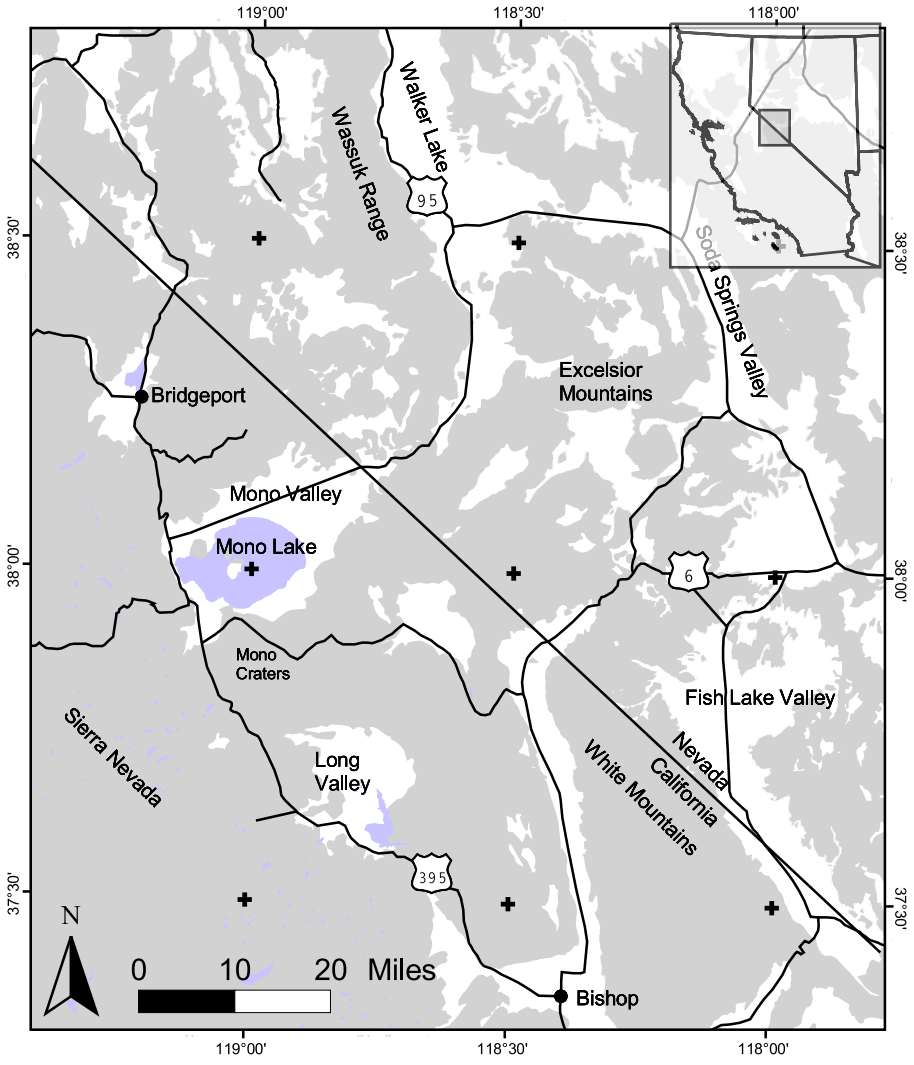

Figure 4.14 Location and features of Eastern Sierra Nevada and Western Basin and Range (SNBR) study area.

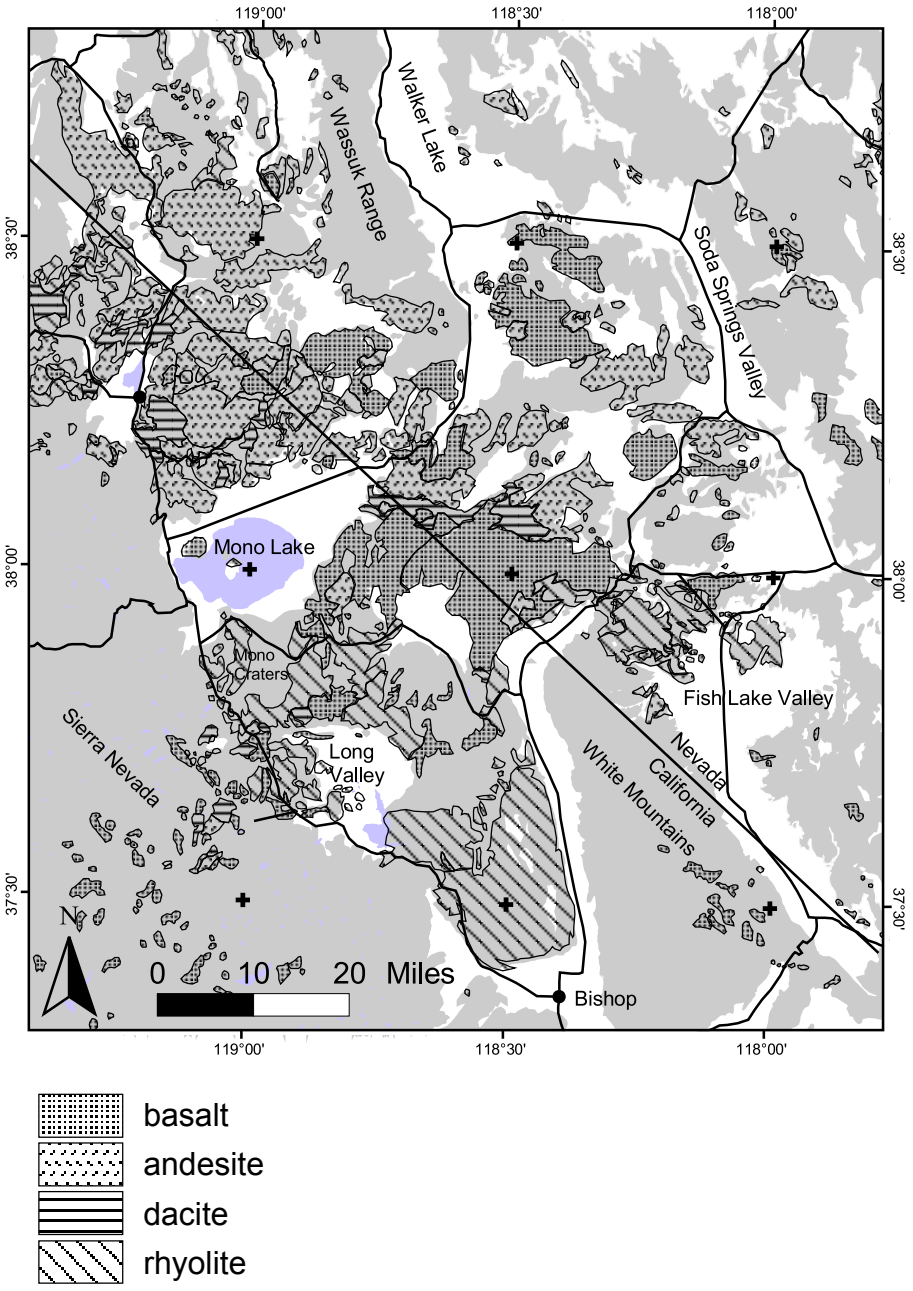

Figure 4.15 Late Tertiary and Quaternary volcanics in the SNBR study area as mapped by Luedke and Smith (1981).

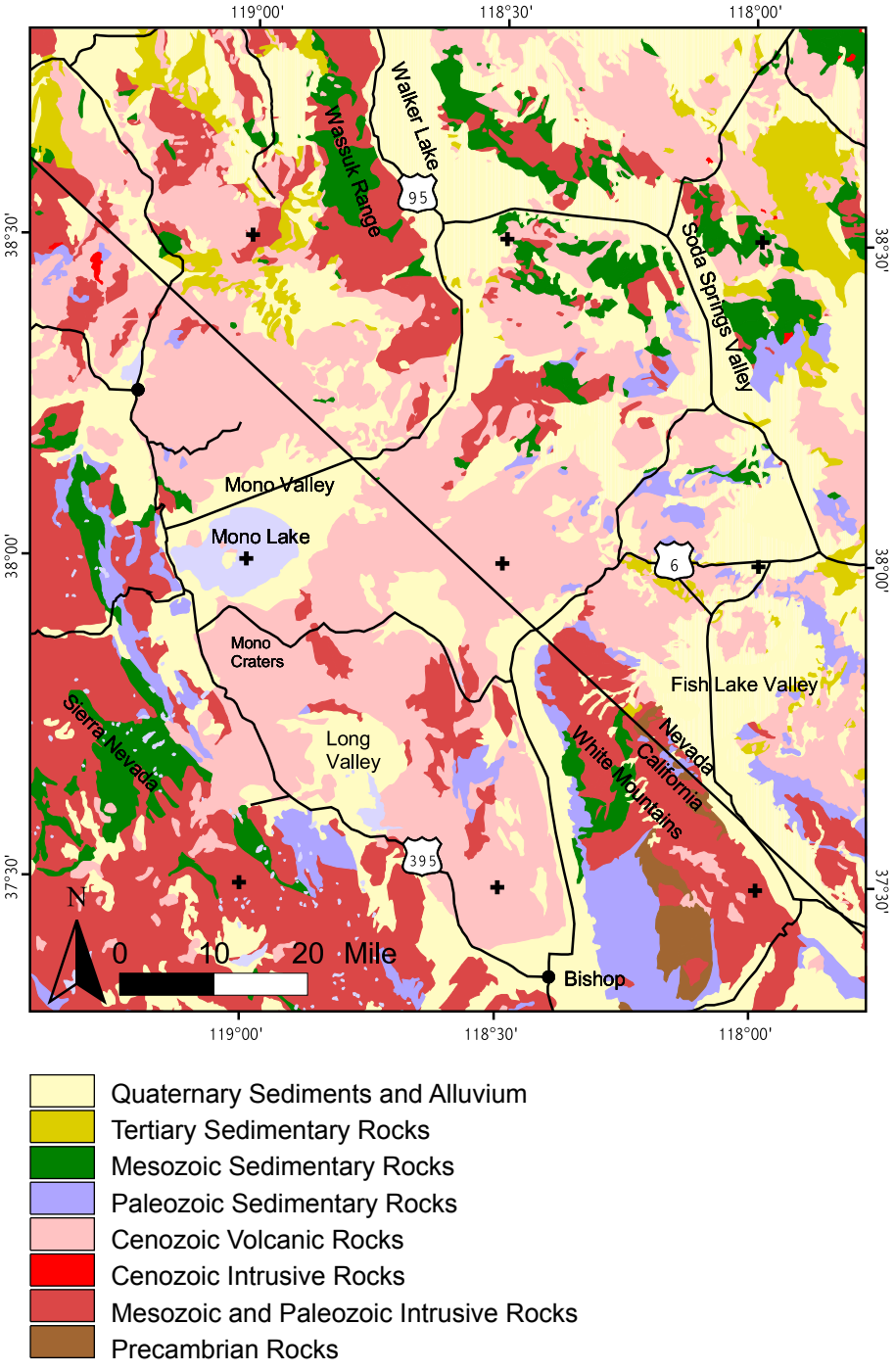

Figure 4.16 Geologic map of the SNBR study area. Modified from Stewart and Carlson (1978) and Jennings (1977).

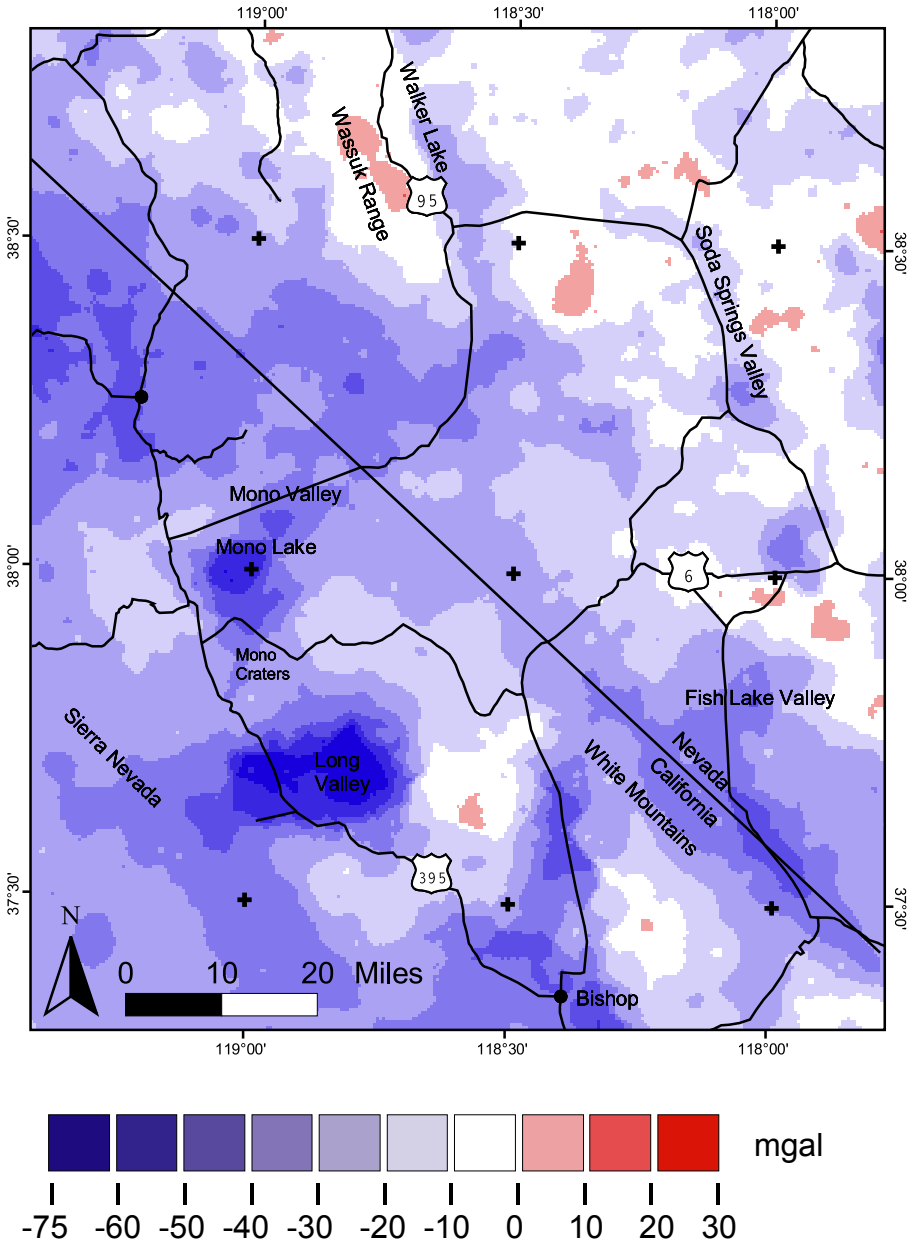

Figure 4.17 Isostatic gravity anomaly grid interpolated from NGDC isostatic gravity anomaly values, SNBR study area.

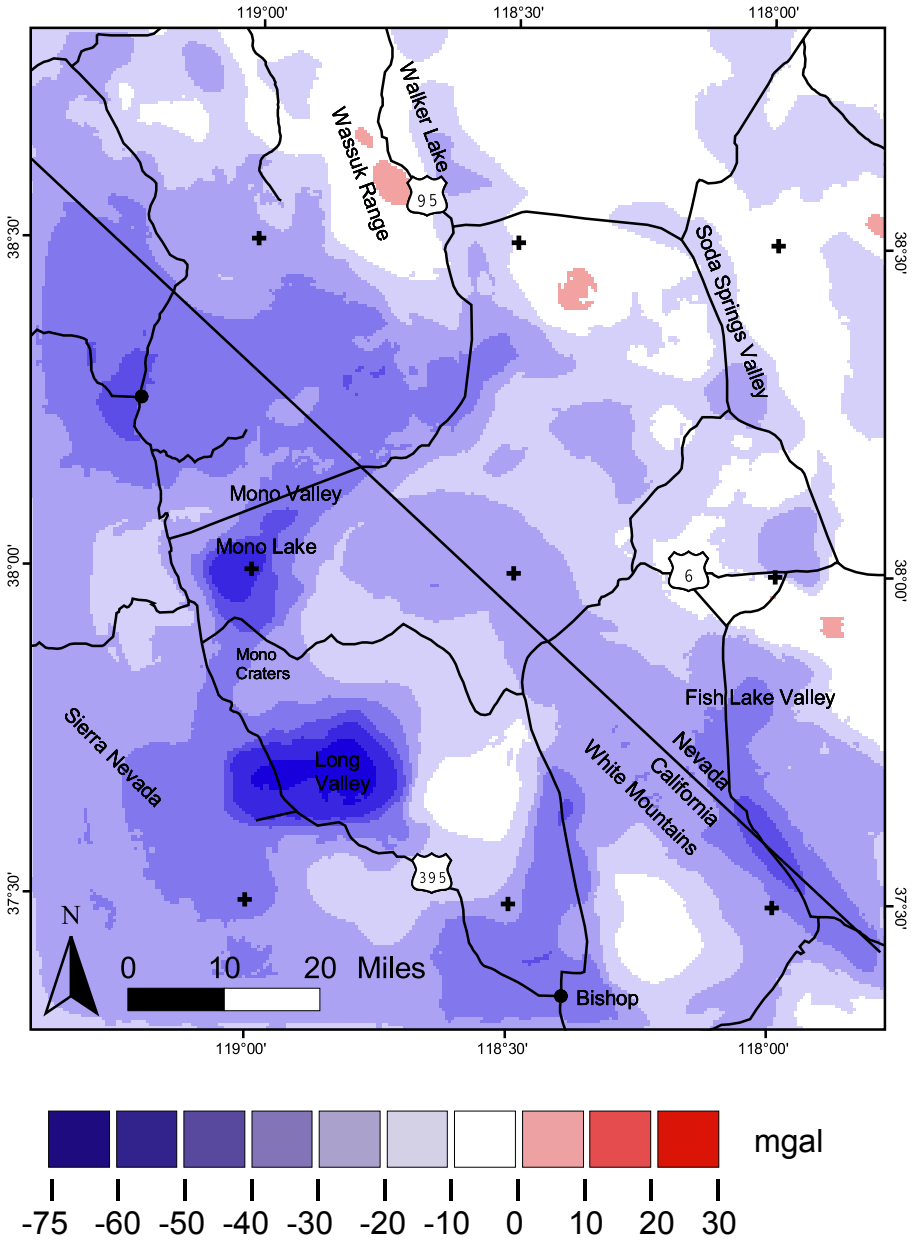

Figure 4.18 Isostatic gravity anomaly calculated from crustal density contrast model, SNBR study area.

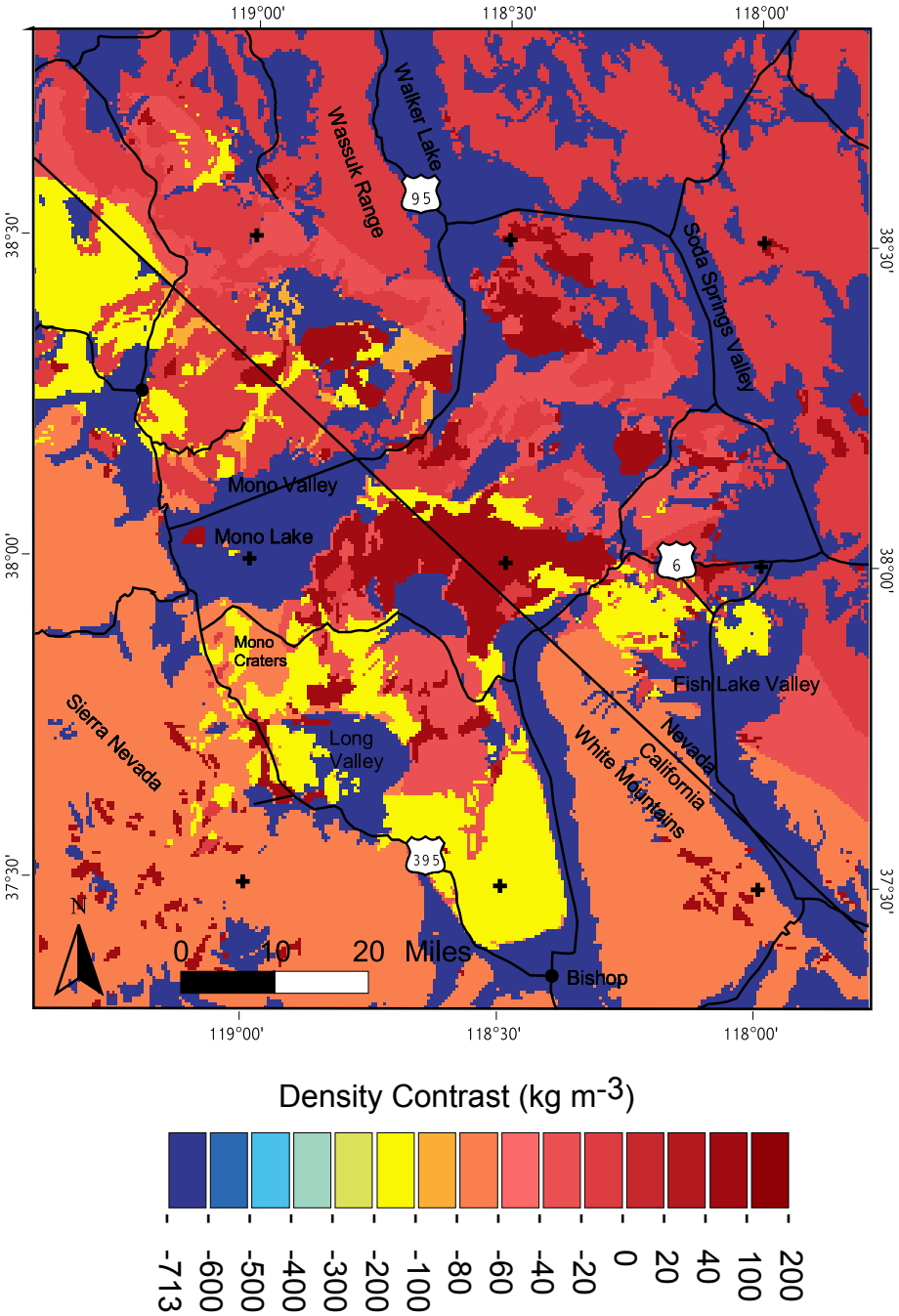

Figure 4.19 Modeled crustal density contrasts for layer A, 0 - 100 meters depth, SNBR study area.

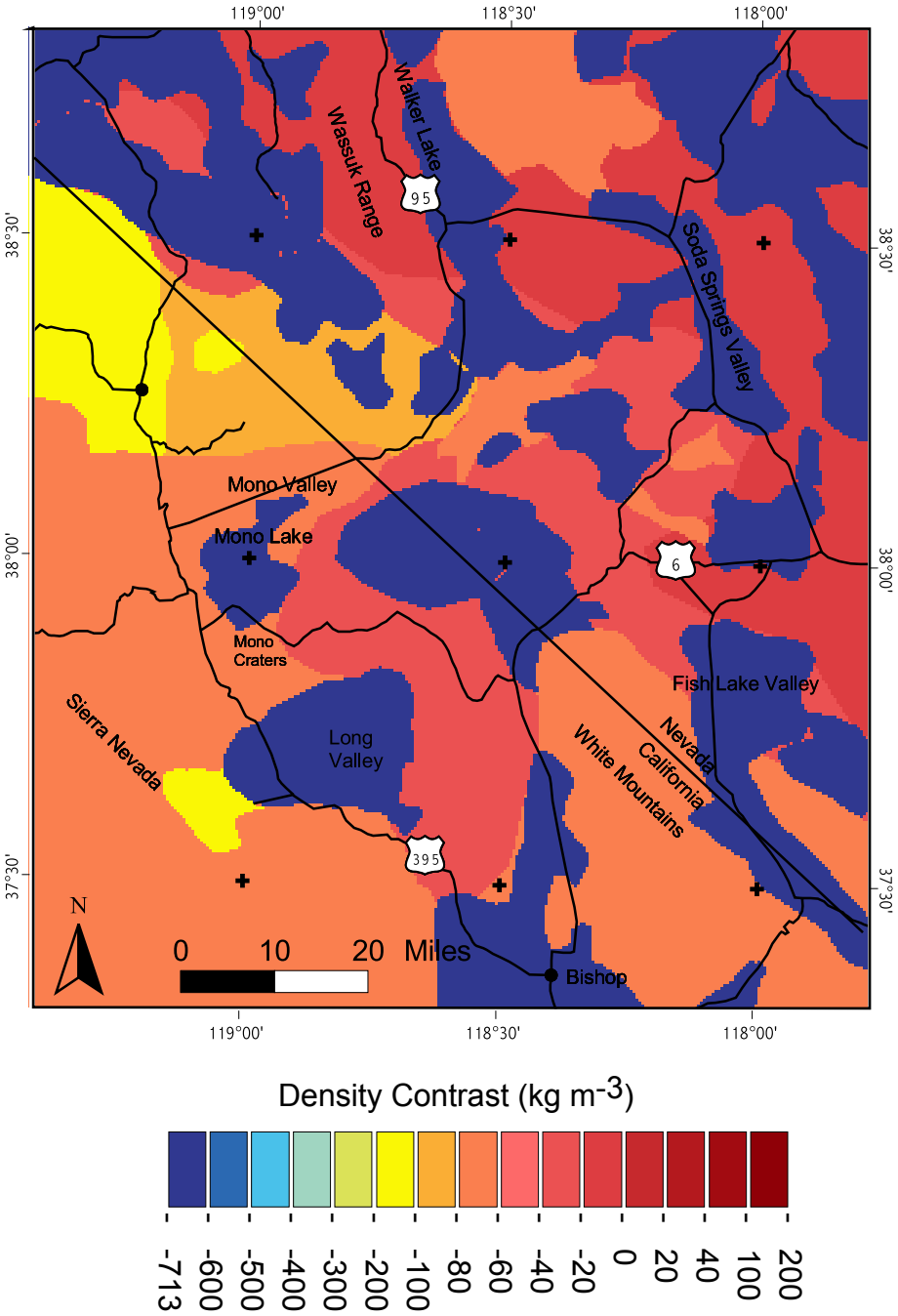

Figure 4.20 Modeled crustal density contrasts for layer B, 100 - 300 meters depth, SNBR study area.

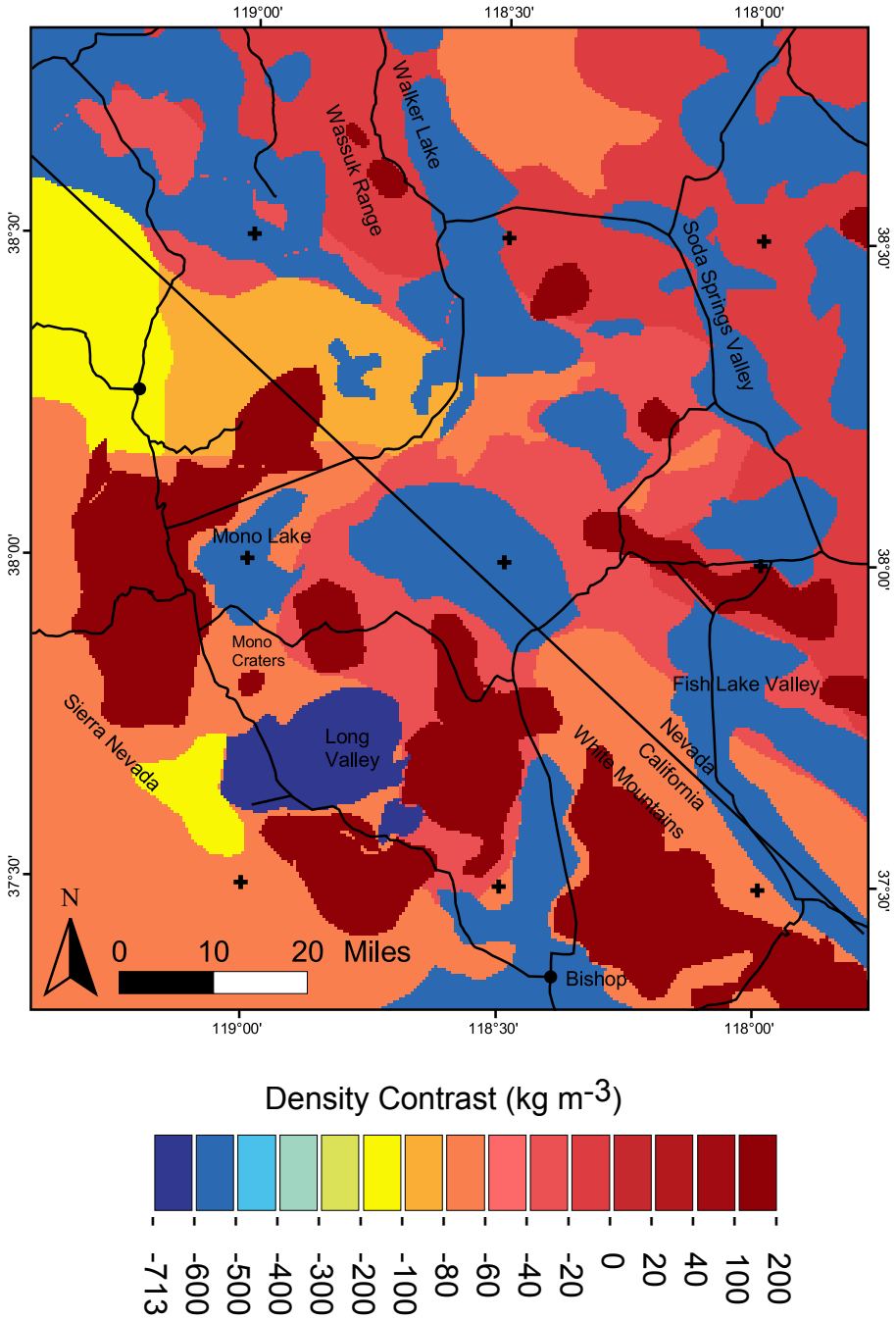

Figure 4.21 Modeled crustal density contrasts for layer C, 300 - 500 meters depth, SNBR study area.

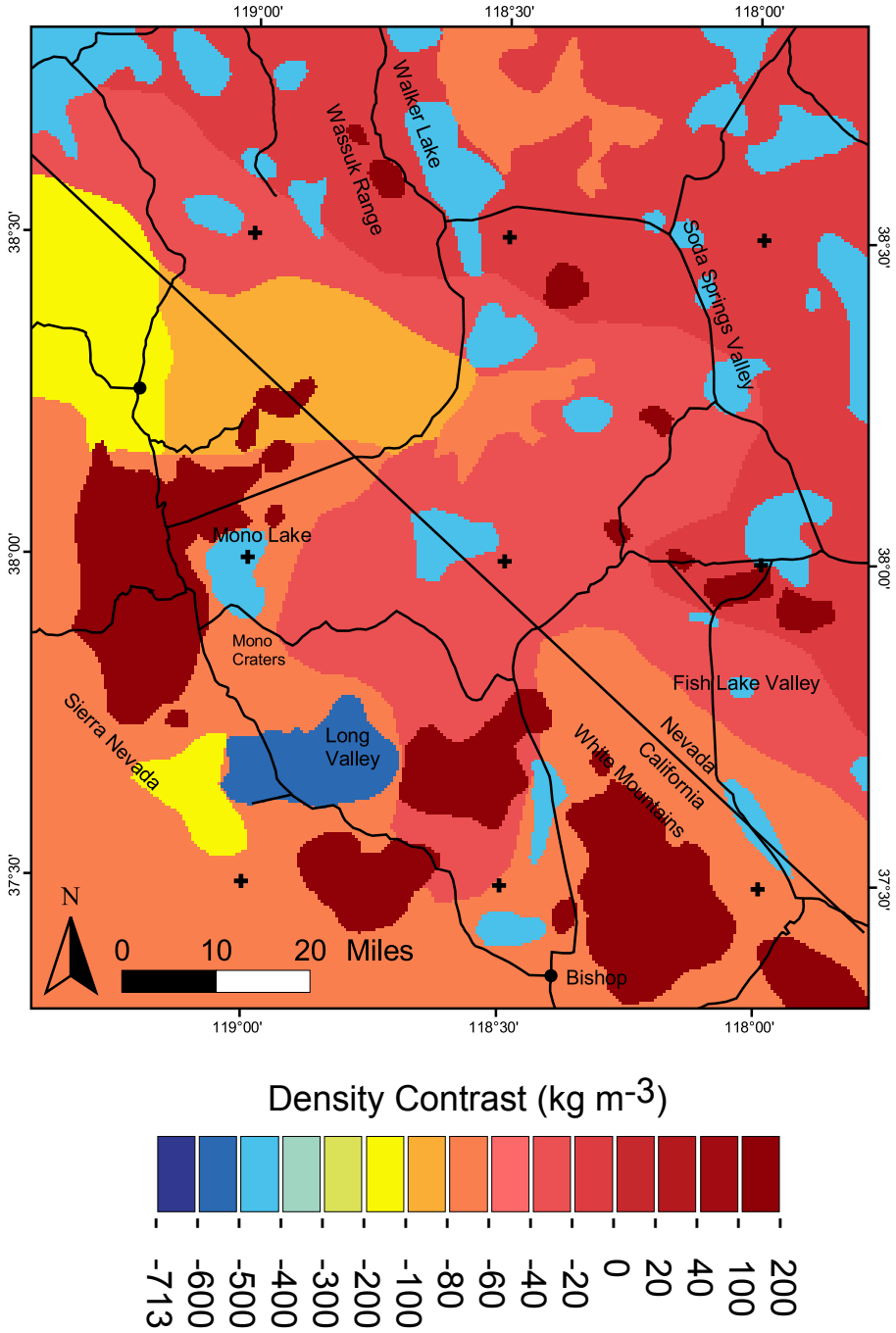

Figure 4.22 Modeled crustal density contrasts for layer D, 500 - 700 meters depth, SNBR study area.

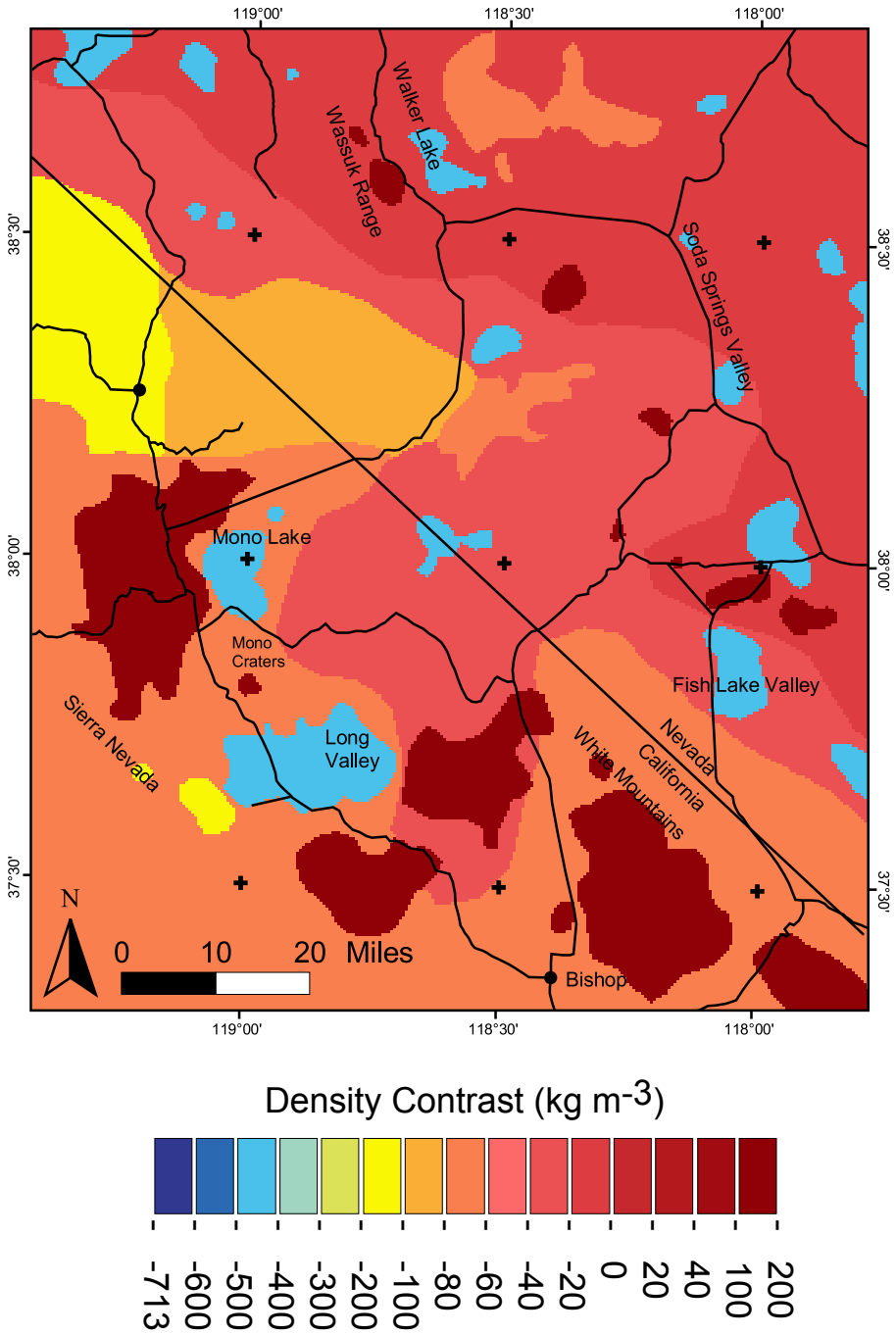

Figure 4.23 Modeled crustal density contrasts for layer E, 700 - 900 meters depth, SNBR study area.

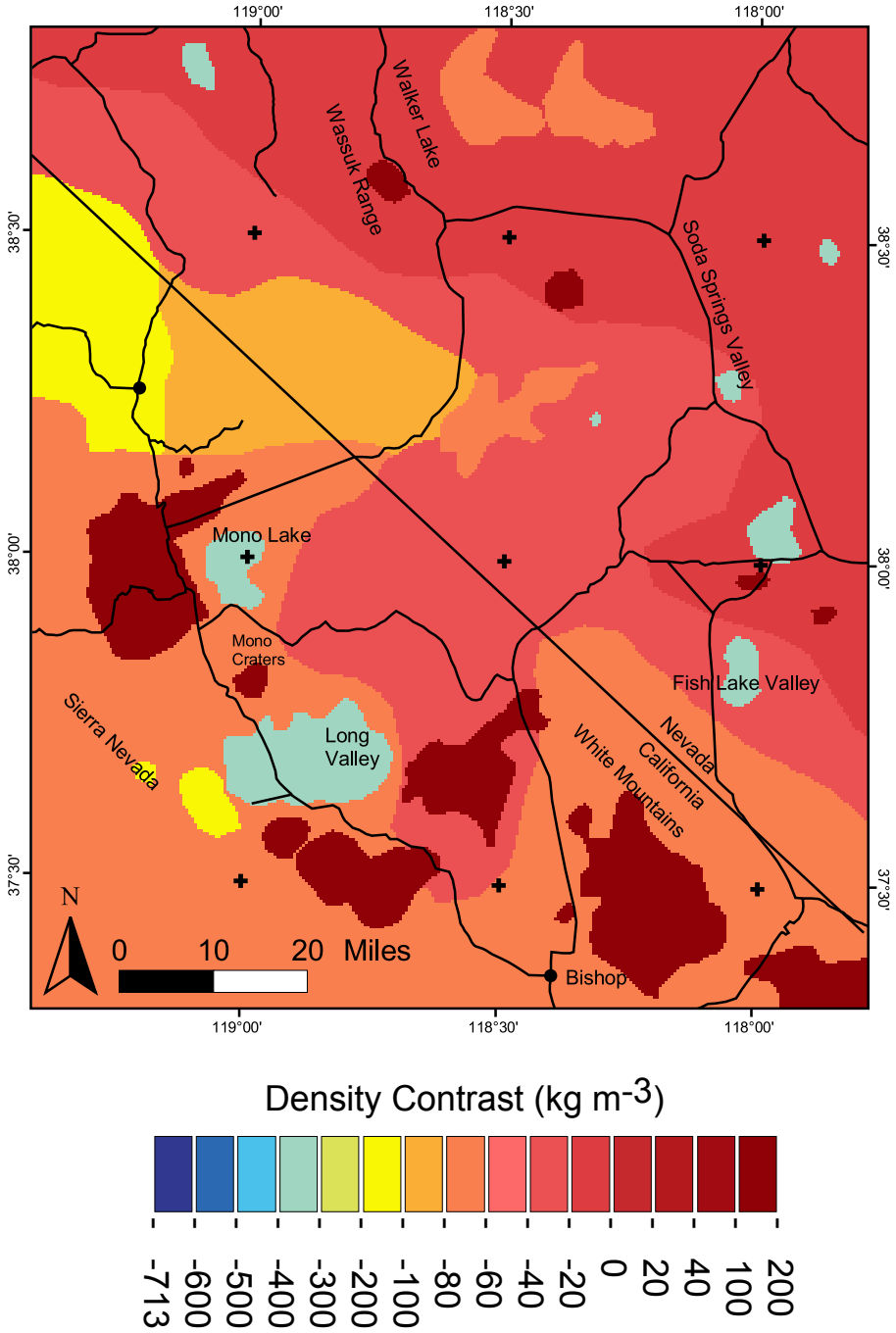

Figure 4.24 Modeled crustal density contrasts for layer F, 900 - 1100 meters depth, SNBR study area.

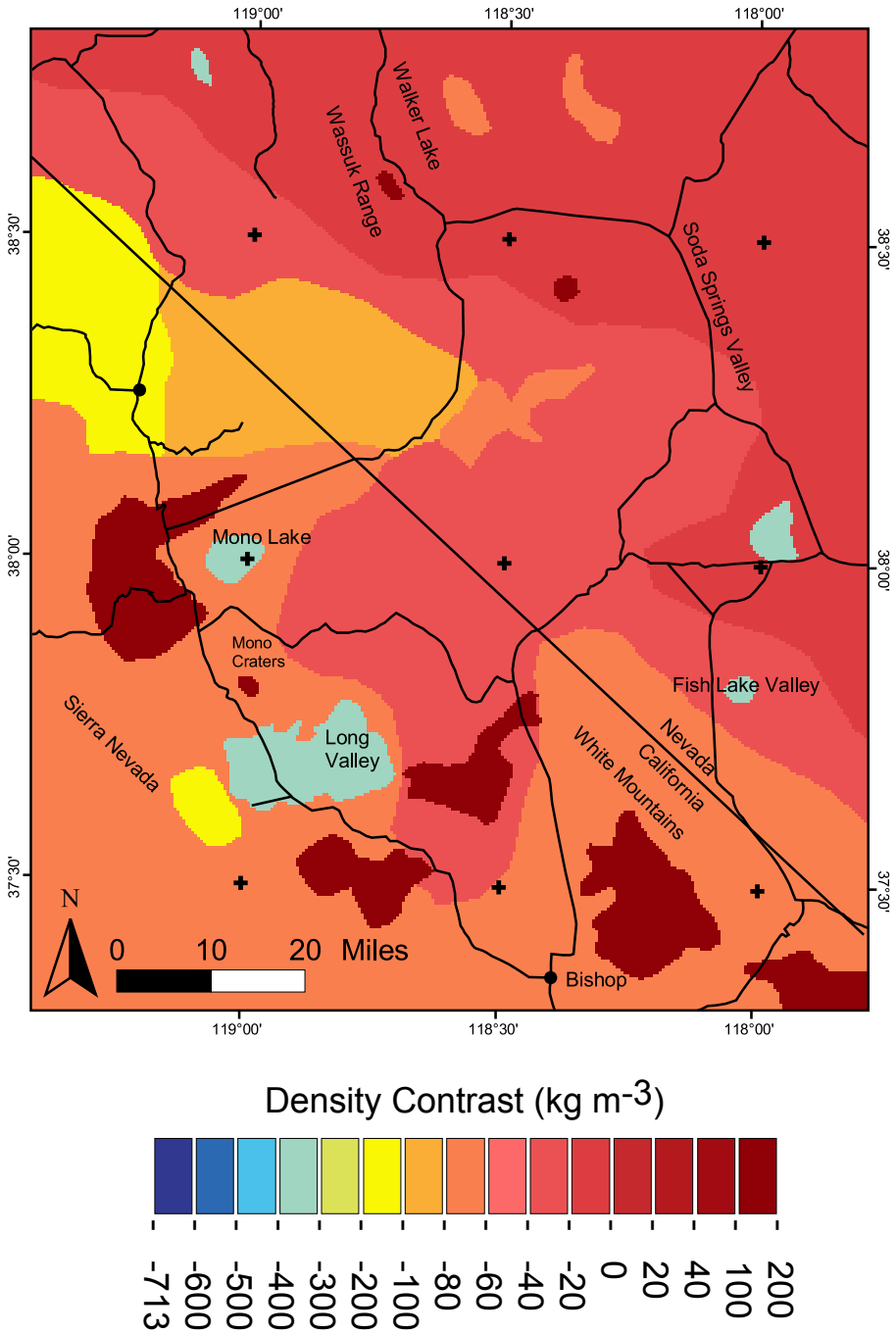

Figure 4.25 Modeled crustal density contrasts for layer G, 1100 - 1500 meters depth, SNBR study area.

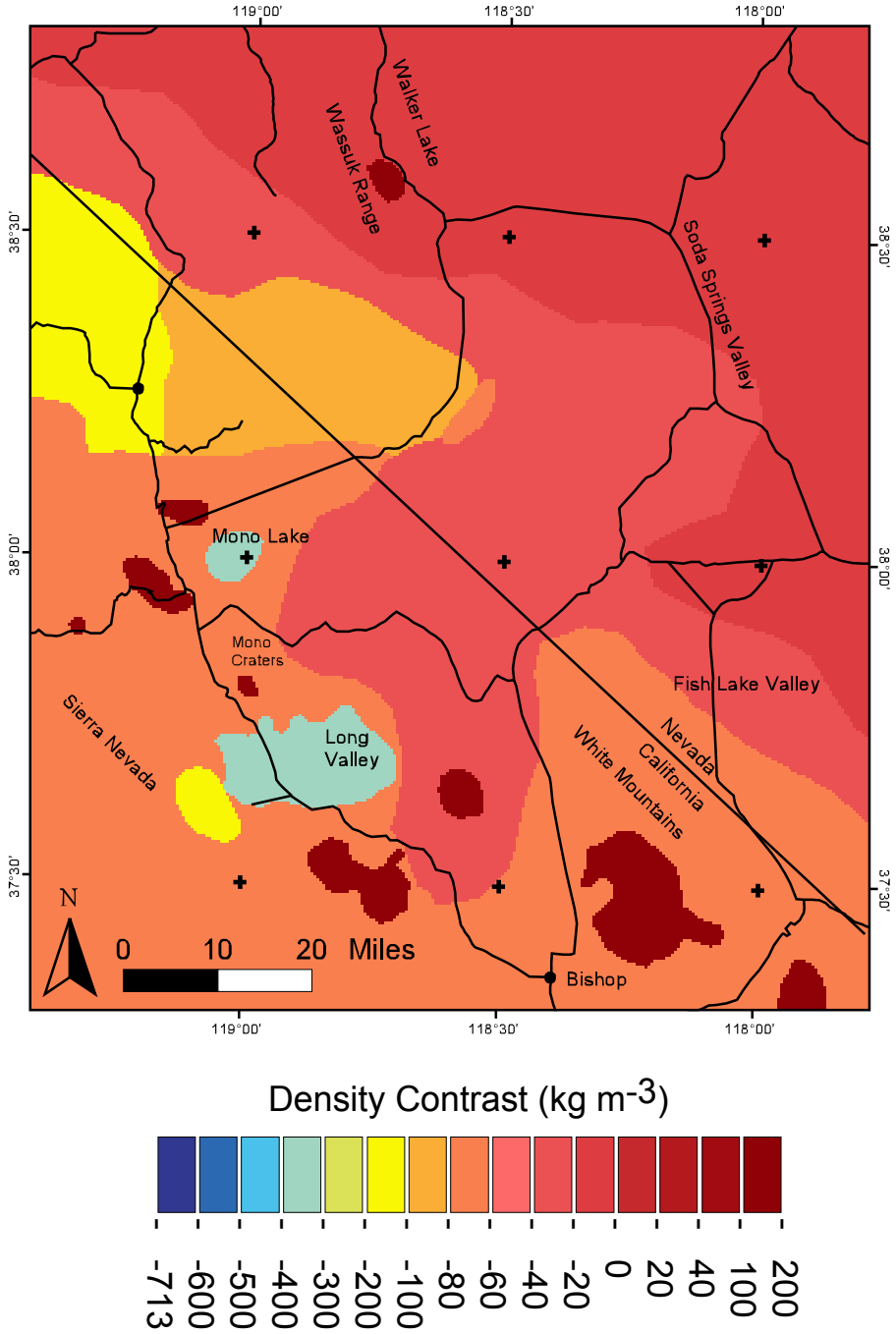

Figure 4.26 Modeled crustal density contrasts for layer H, 1500 - 2000 meters depth, SNBR study area.

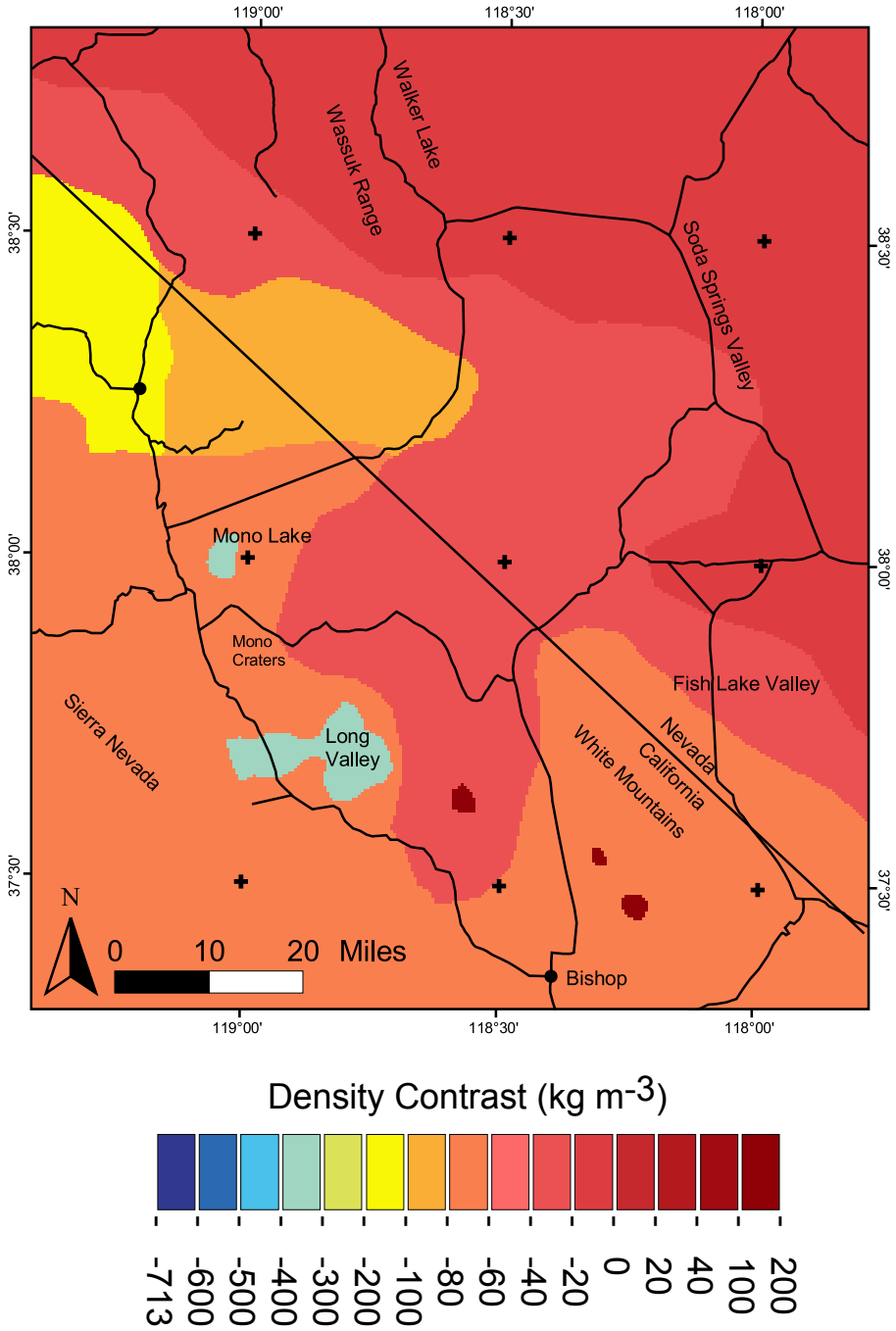

Figure 4.27 Modeled crustal density contrasts for layer I, 2000 - 2400 meters depth, SNBR study area.

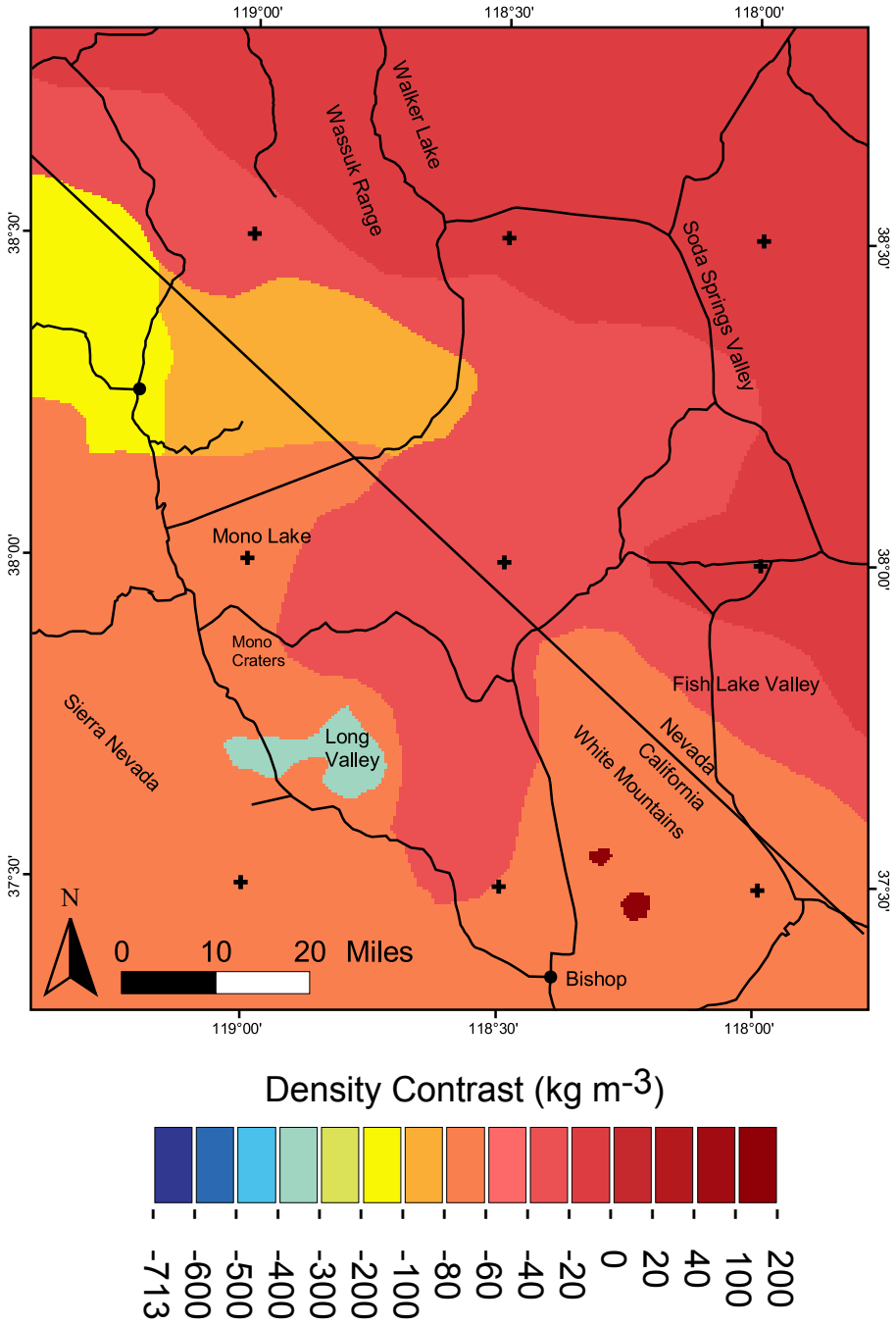

Figure 4.28 Modeled crustal density contrasts for layer J, 2400 - 3000 meters depth, SNBR study area.

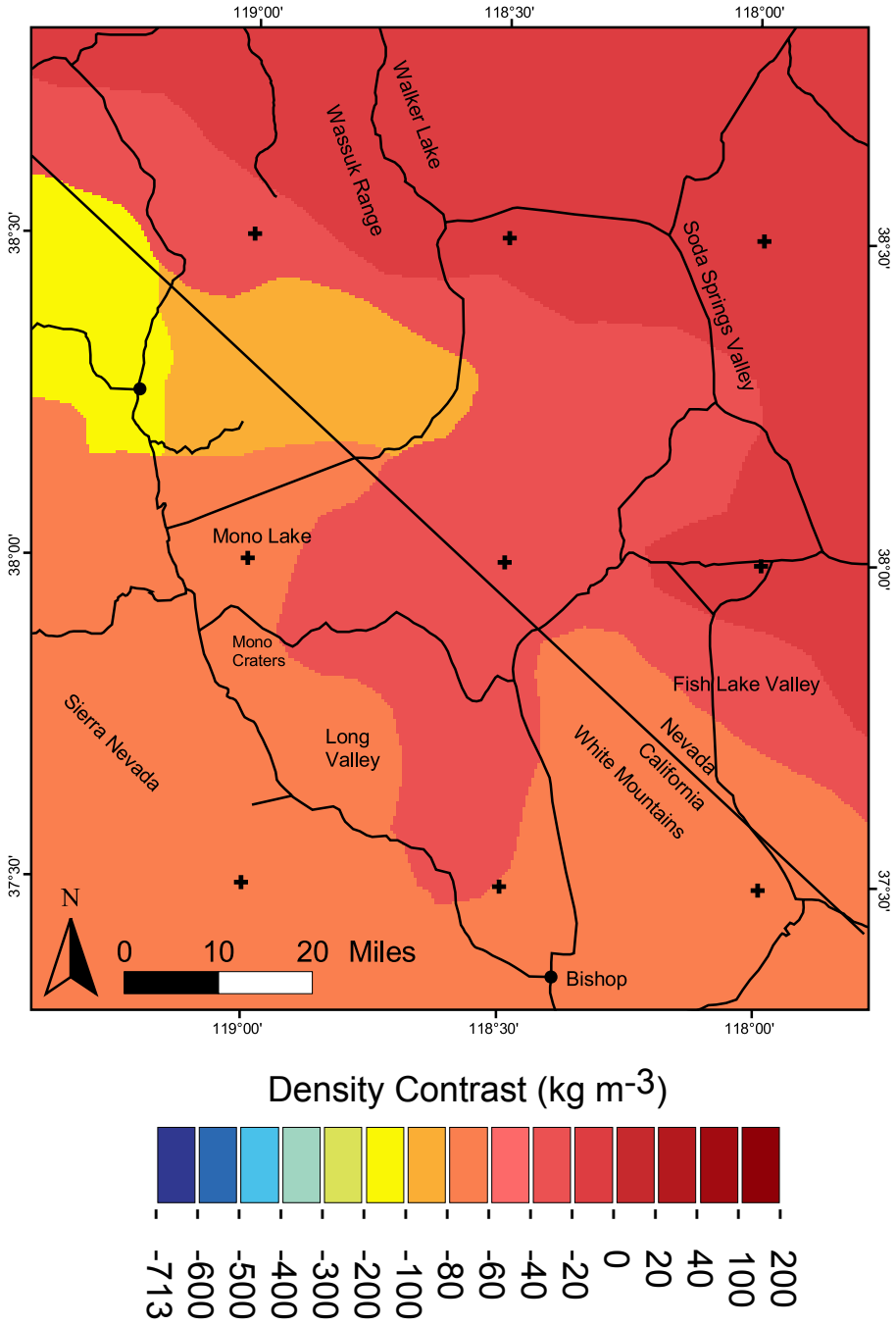

Figure 4.29 Modeled crustal density contrasts for layer K (basement), 3,000 - 10,000 meters depth, SNBR study area.

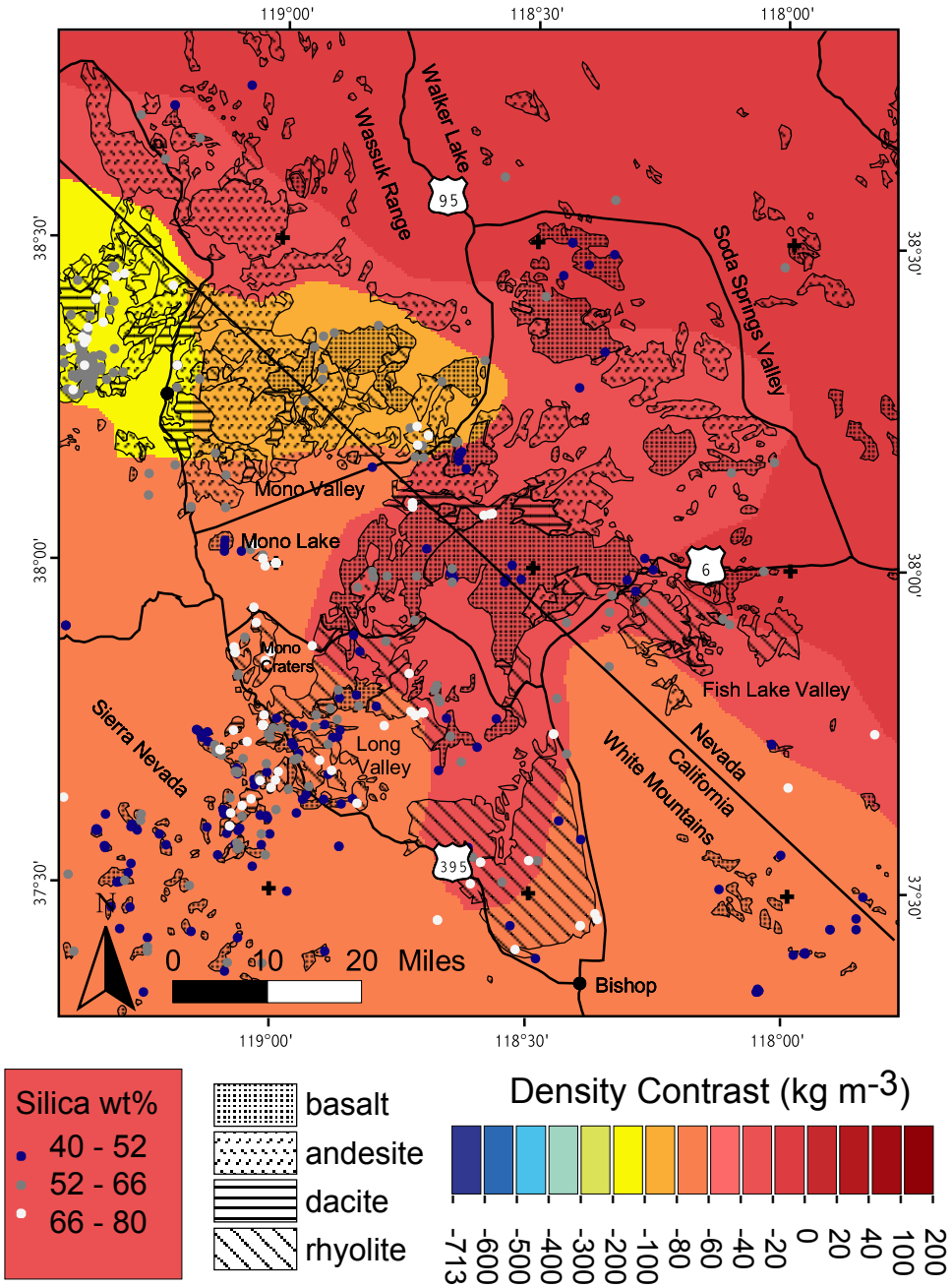

Figure 4.30 Basement (deepest layer) crustal density contrast values in the SNBR study area shown with late Tertiary and Quaternary volcanics as mapped by Luedke and Smith (1981) and silica content values of sampled volcanics from NAVDAT database.

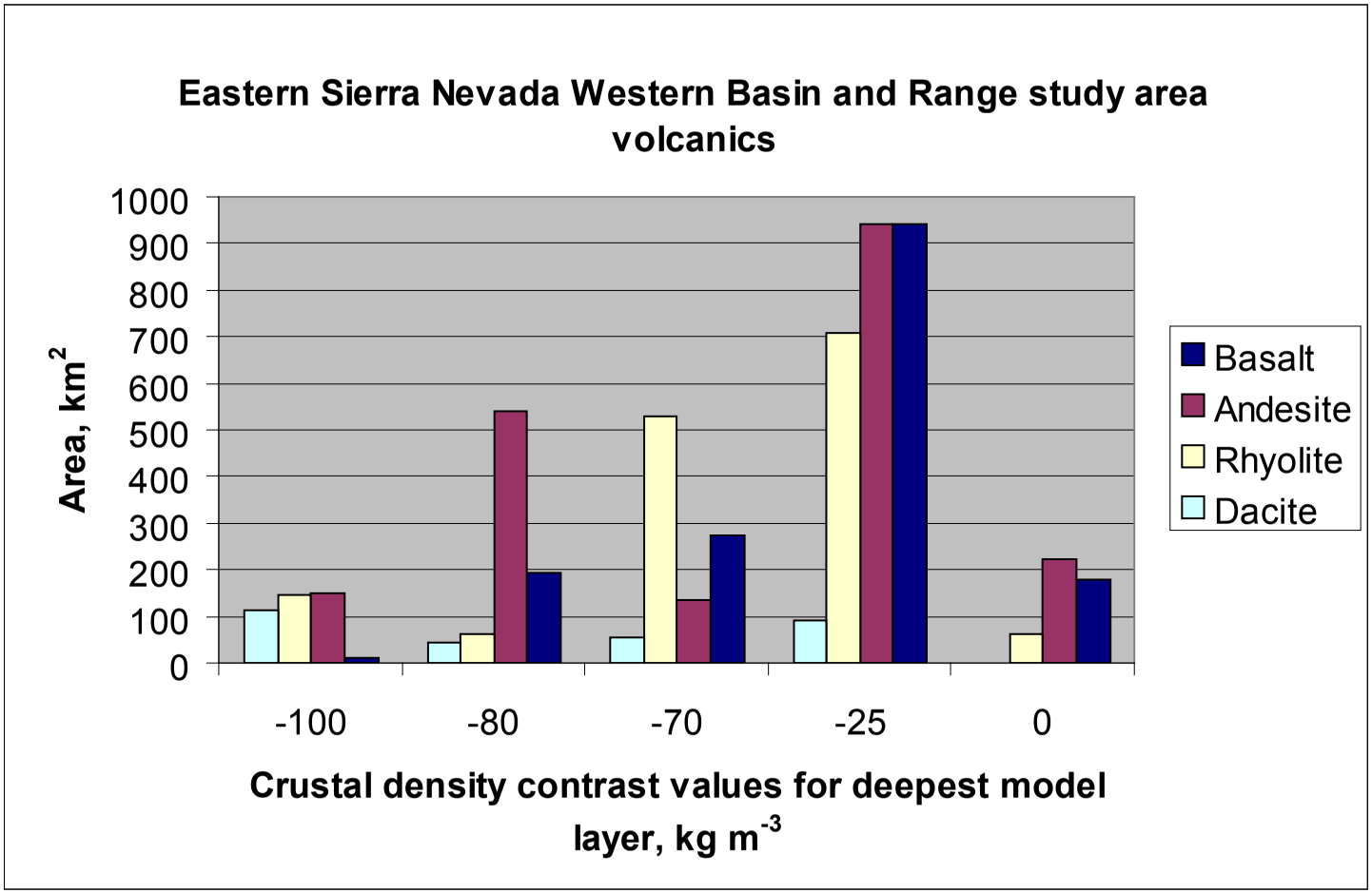

Figure 4.31 Surface area of late Tertiary and Quaternary (<16 Ma) volcanics, as mapped by Luedke and Smith (1981), erupted through each crustal density contrast value in basement model layer (K), Eastern Sierra Nevada, Western Basin and Range study area.

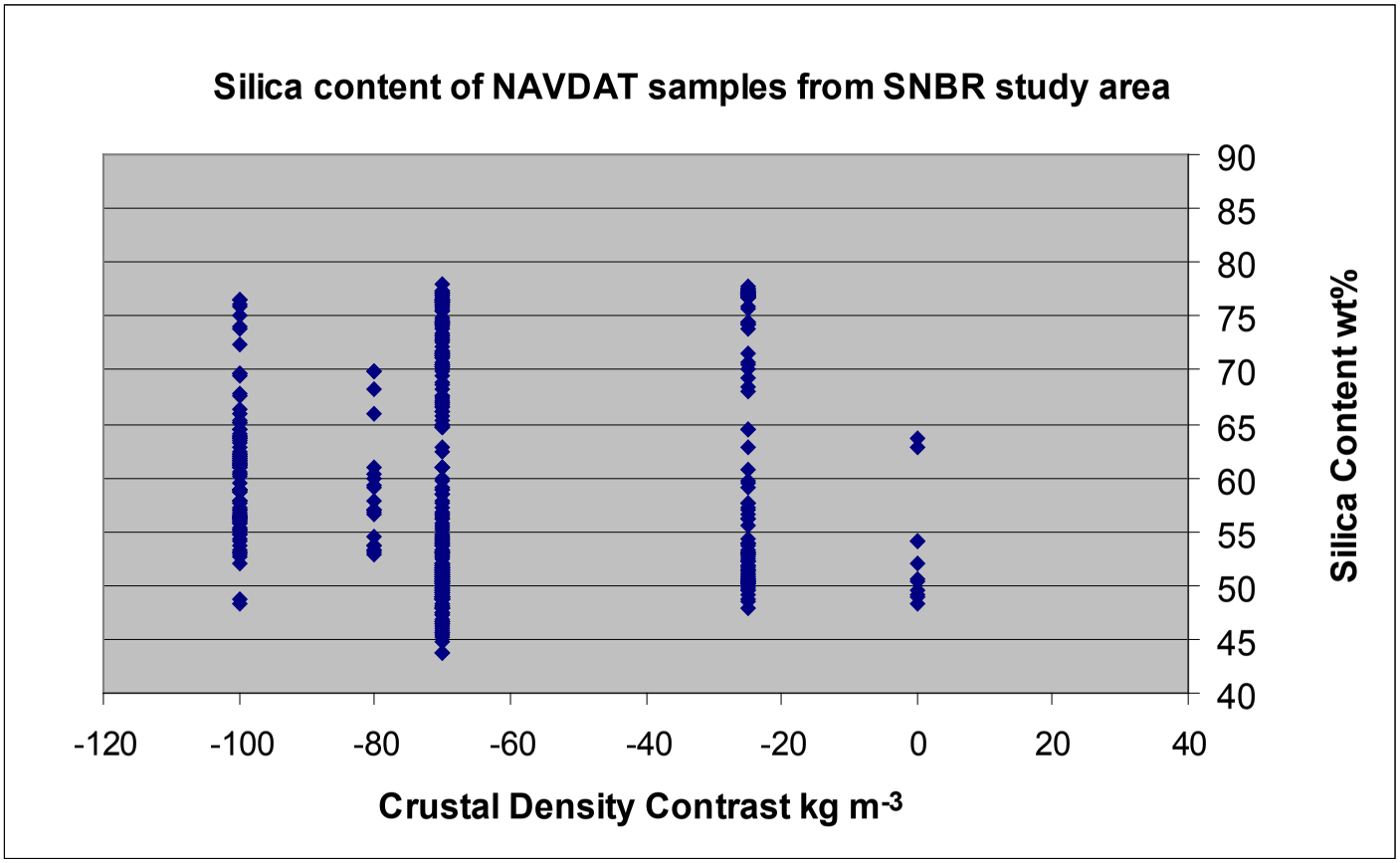

Figure 4.32 Relationship of silica content of NAVDAT samples of late Tertiary and Quaternary volcanics with modeled basement crustal density contrast values in the SNBR study area. Figure 4.30 shows the location of samples used in this plot.

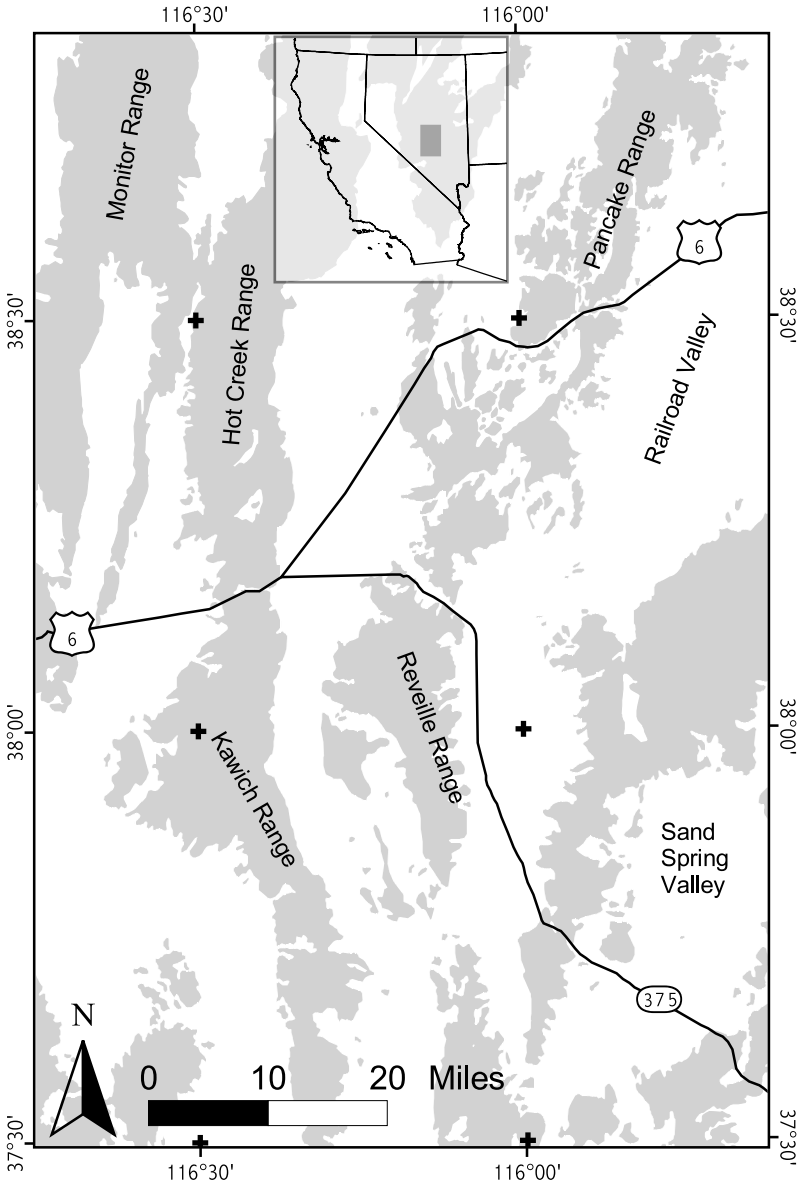

Figure 4.33 Location and features of the Central Nevada Study area.

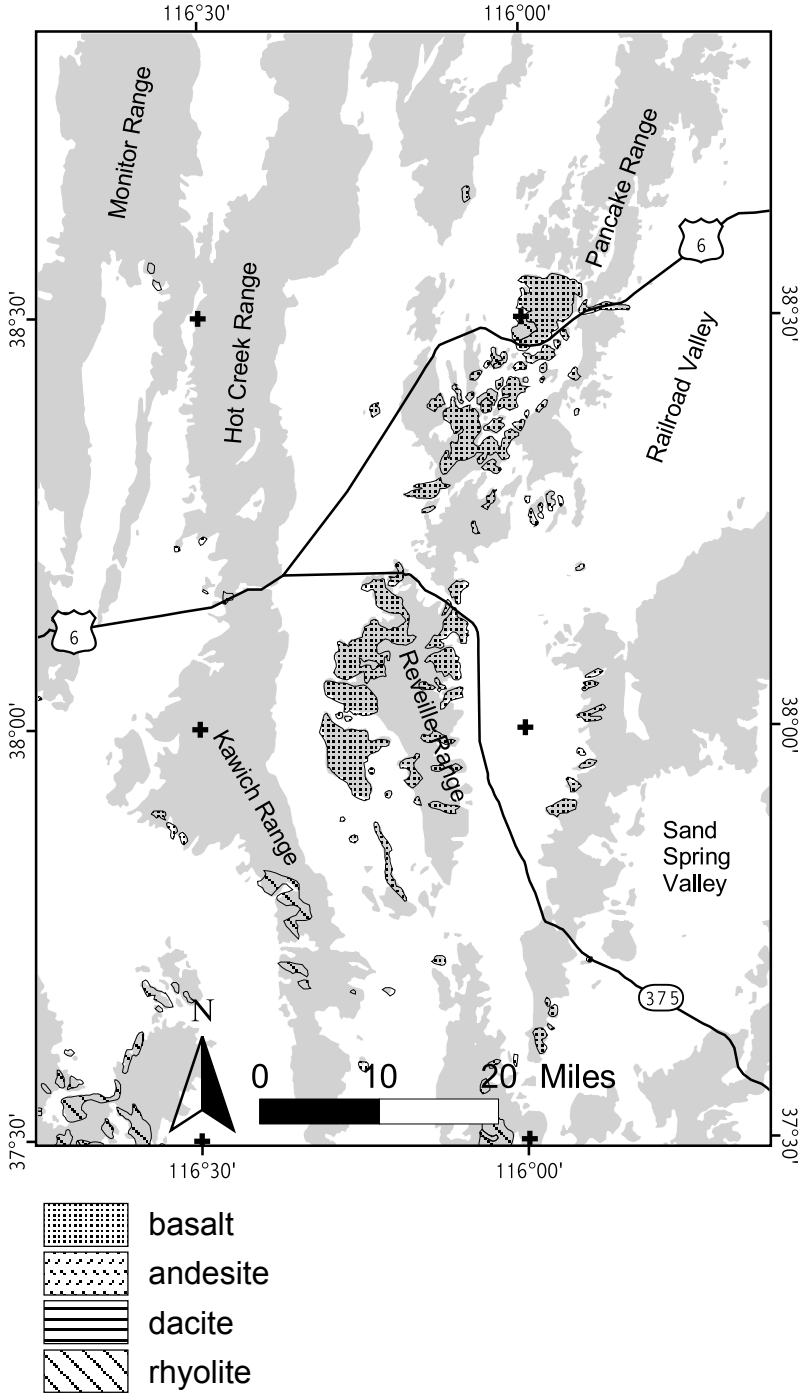

Figure 4.34 Late Tertiary and Quaternary volcanics in the Central Nevada study area as mapped by Luedke and Smith (1981).

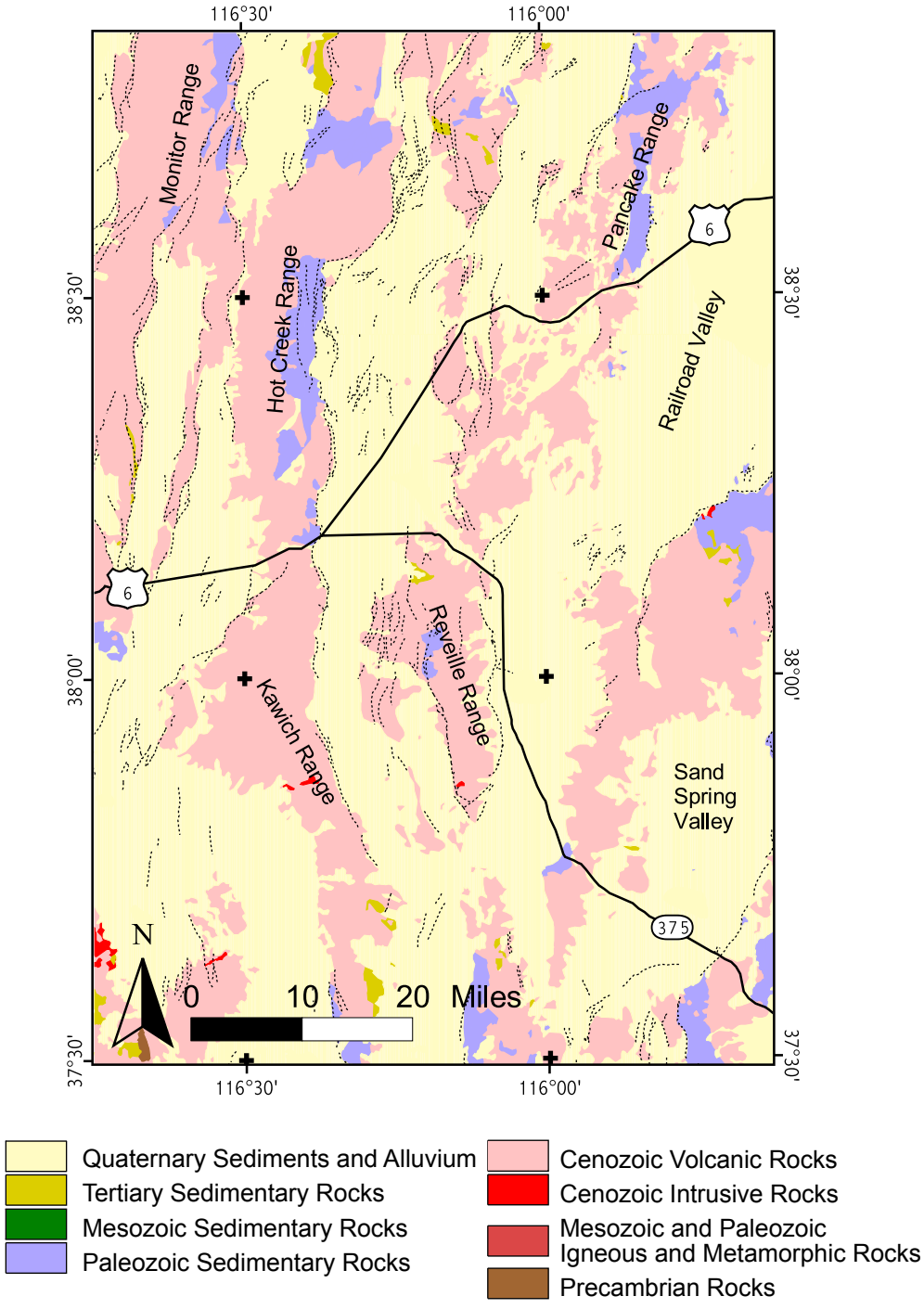

Figure 4.35 Geology of the Central Nevada study area.
Modified from Jennings et al. (1977).

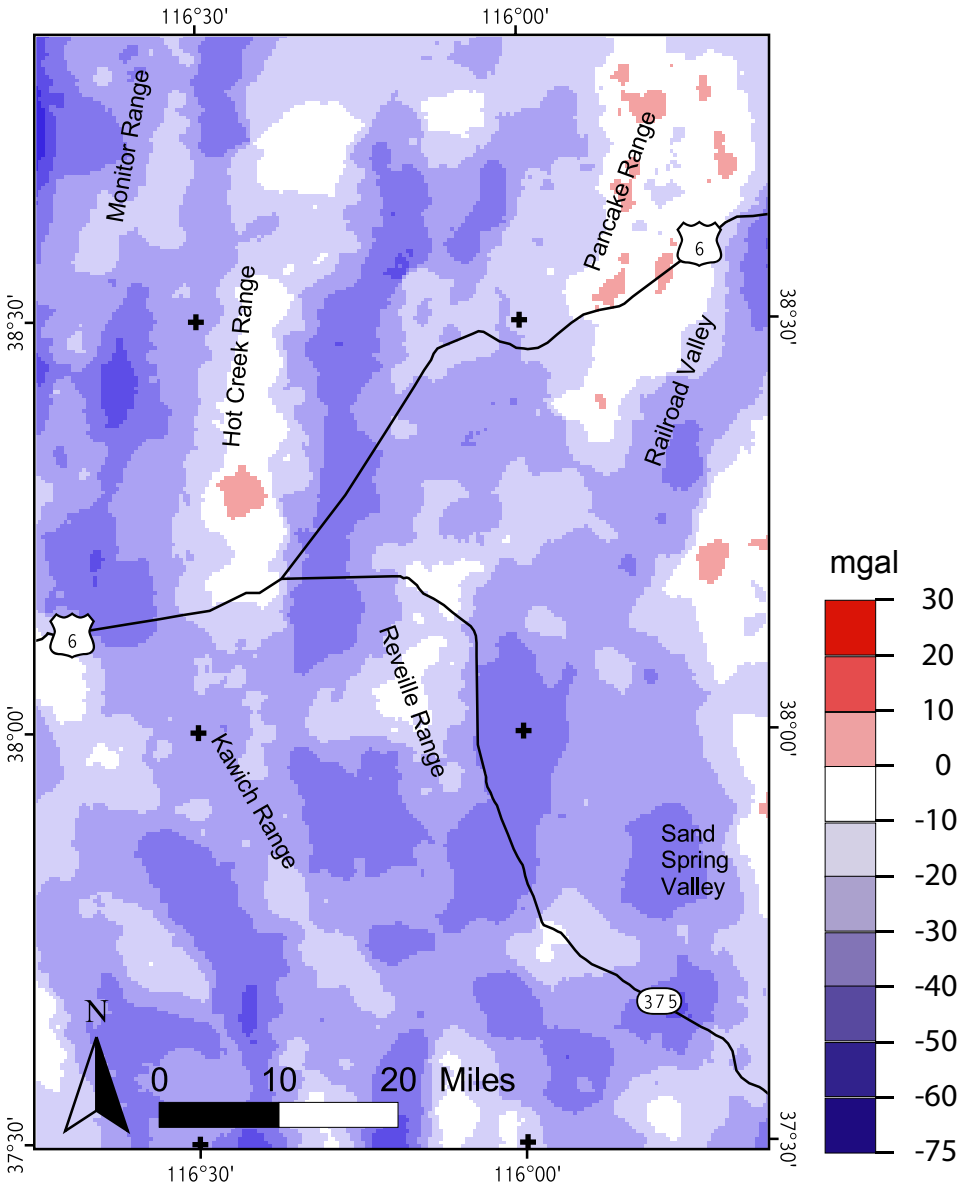

Figure 4.36 Isostatic anomaly grid interpolated from NGCD isostatic anomaly data, Central Nevada study area.

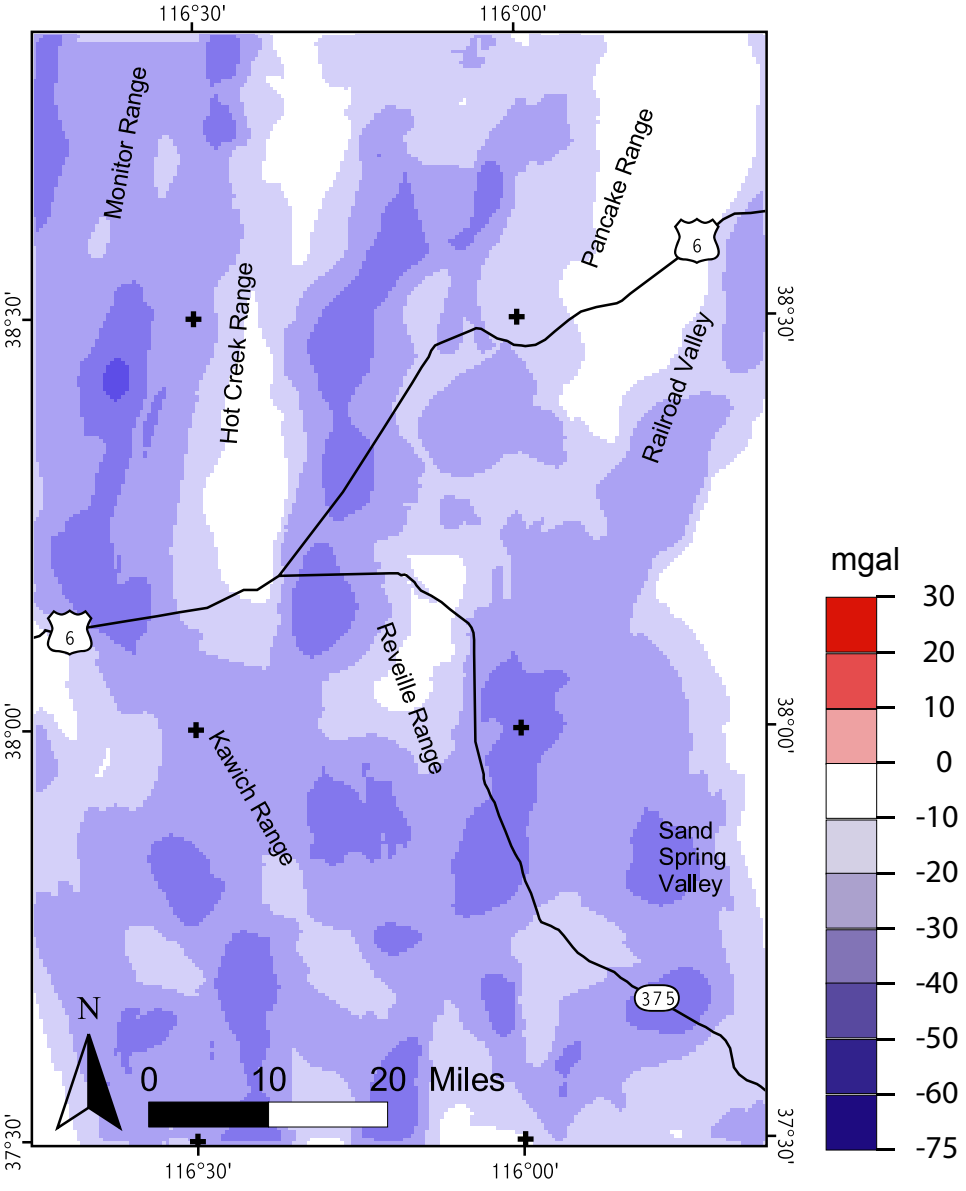

Figure 4.37 Isostatic gravity anomaly grid calculated from crustal density contrast model, Central Nevada Study area.

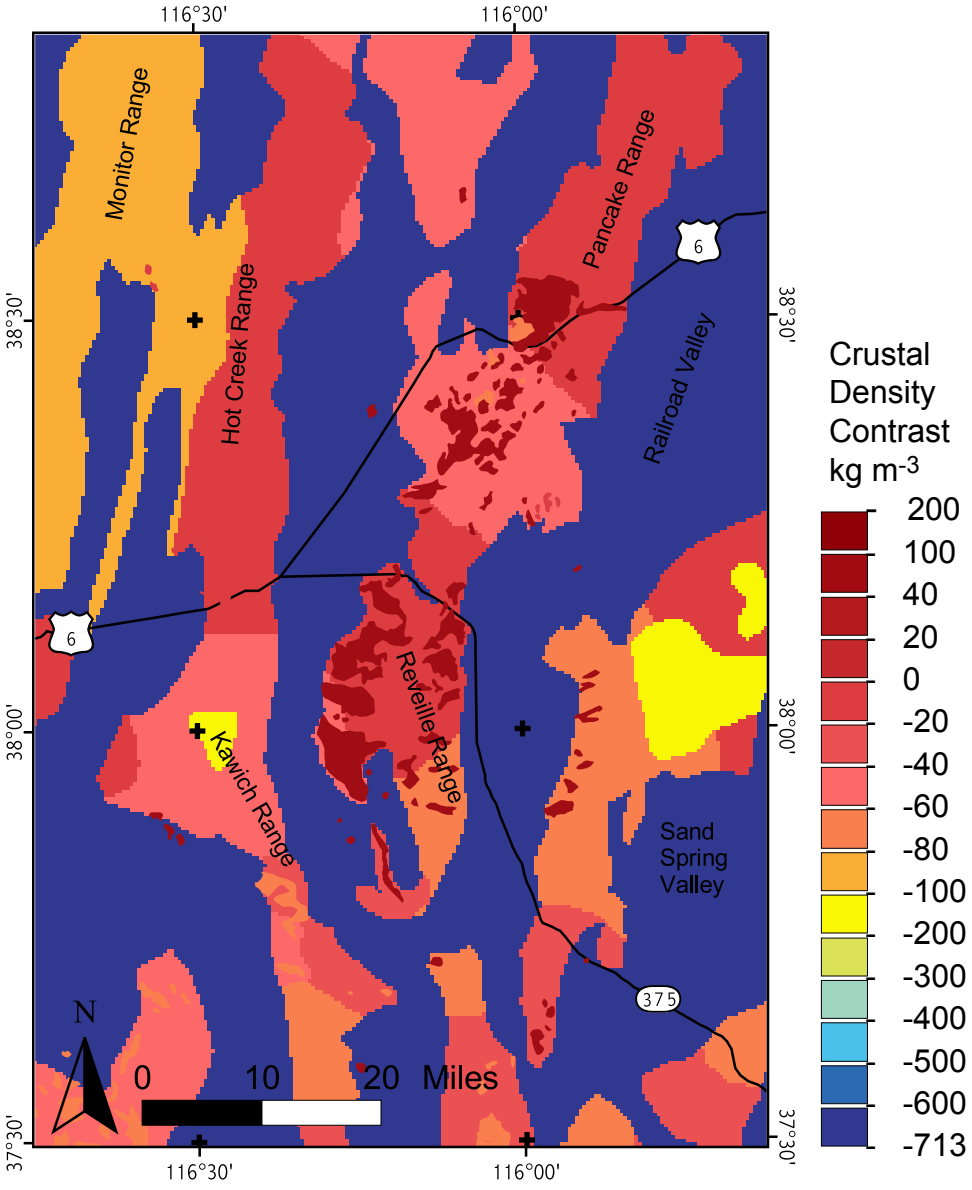

Figure 4.38 Modeled crustal density contrasts for layer A, 0 - 100 meters depth, Central Nevada study area.

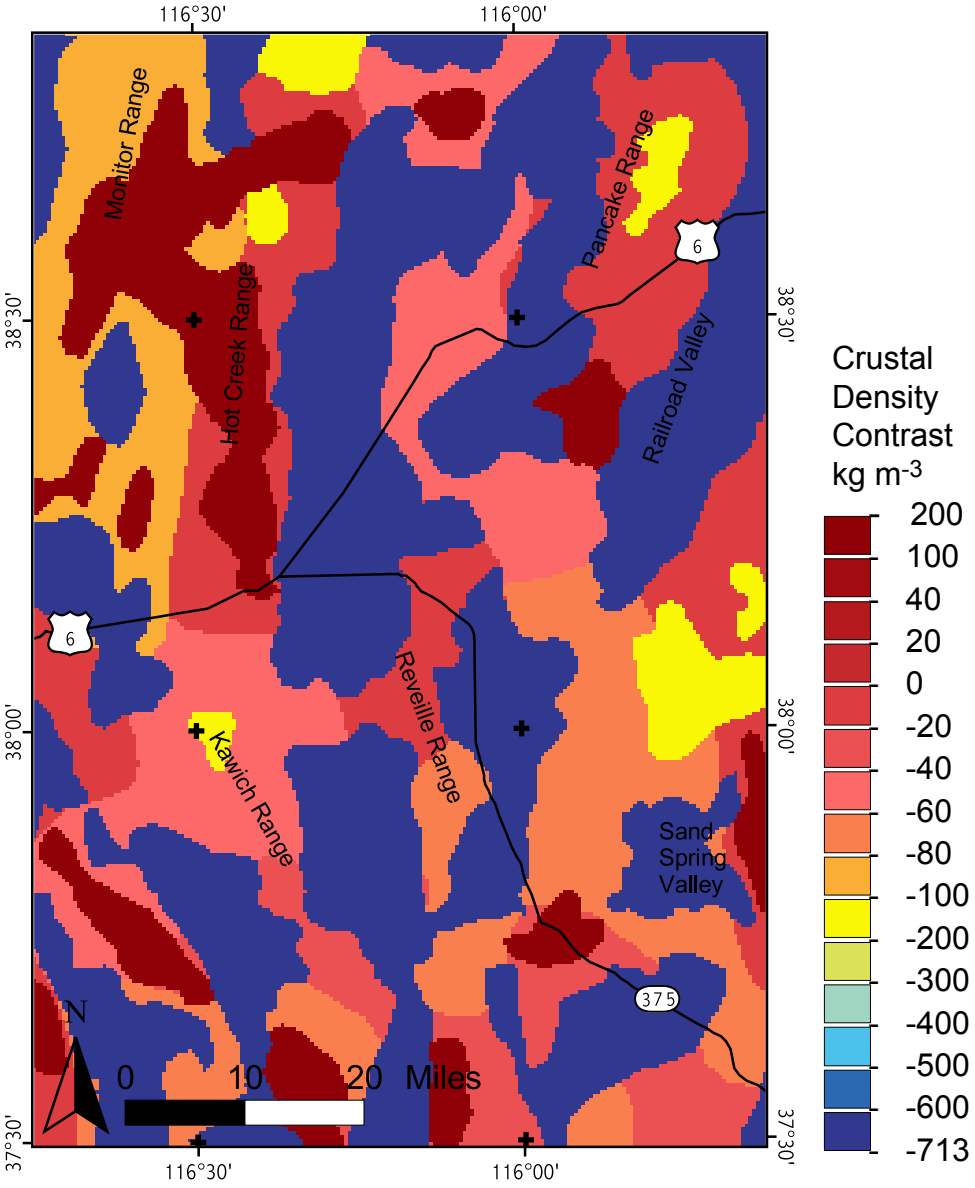

Figure 4.39 Modeled crustal density contrasts for layer B, 100 - 300 meters depth, Central Nevada study area.

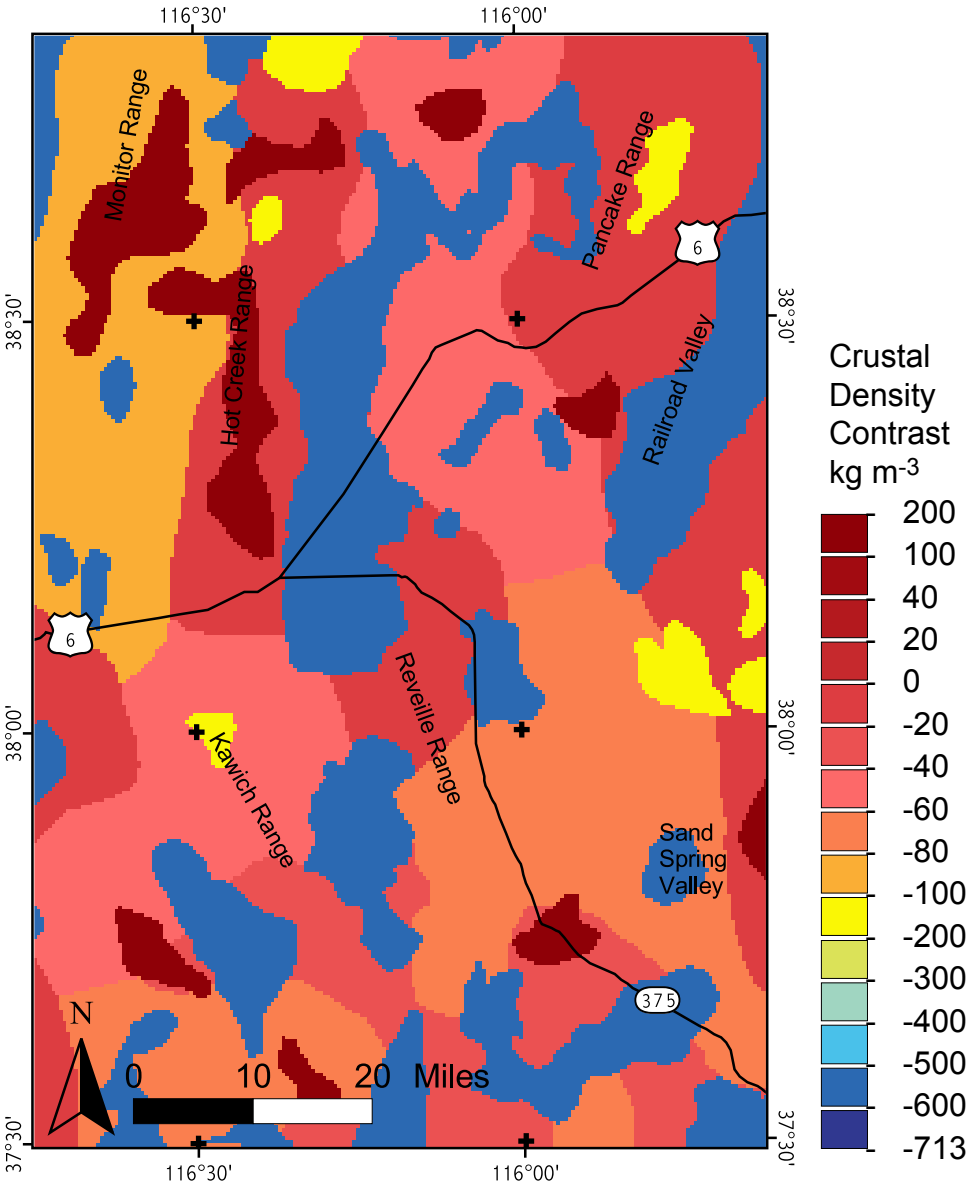

Figure 4.40 Modeled crustal density contrasts for layer C, 300 - 500 meters depth, Central Nevada study area.

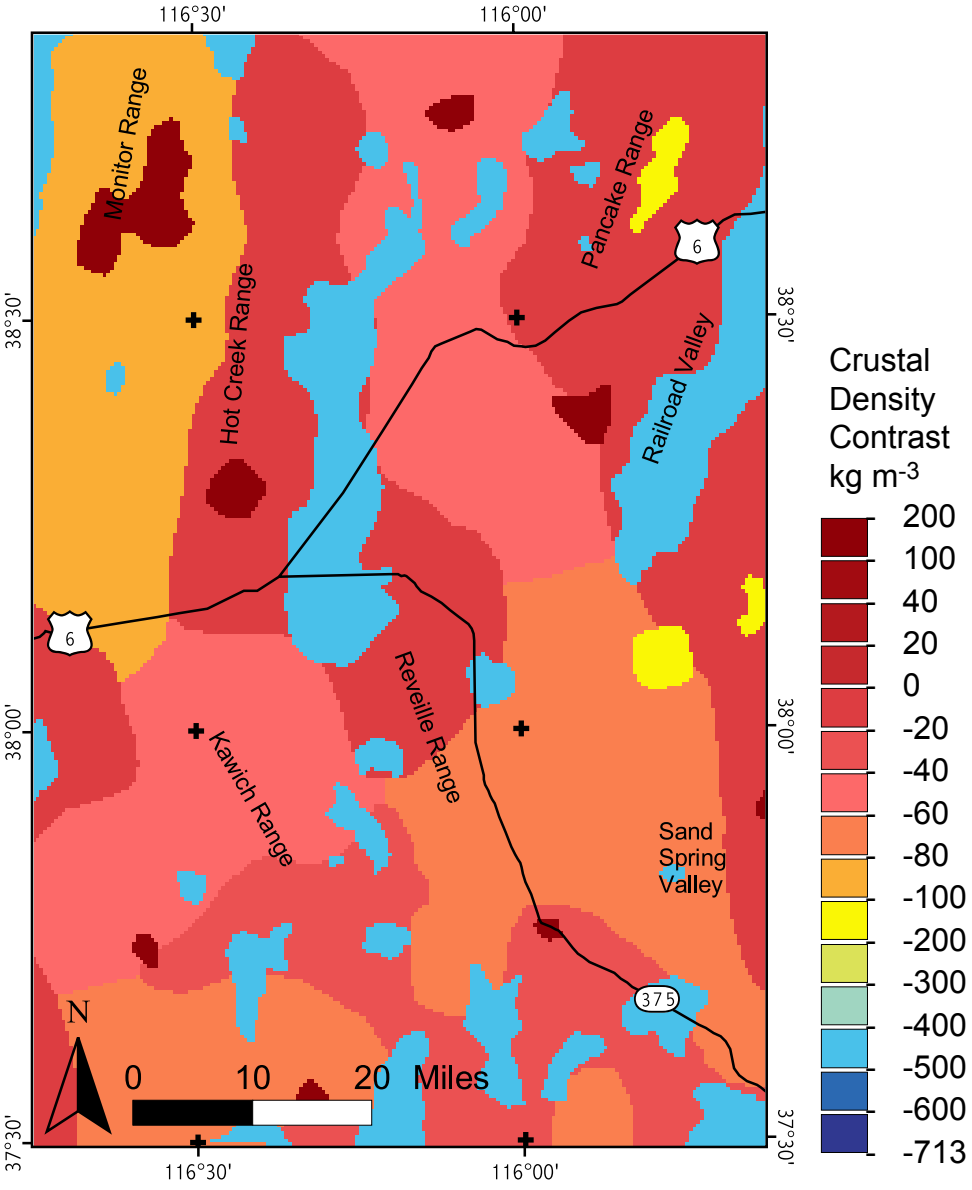

Figure 4.41 Modeled crustal density contrasts for layer D, 500 - 700 meters depth, Central Nevada study area.

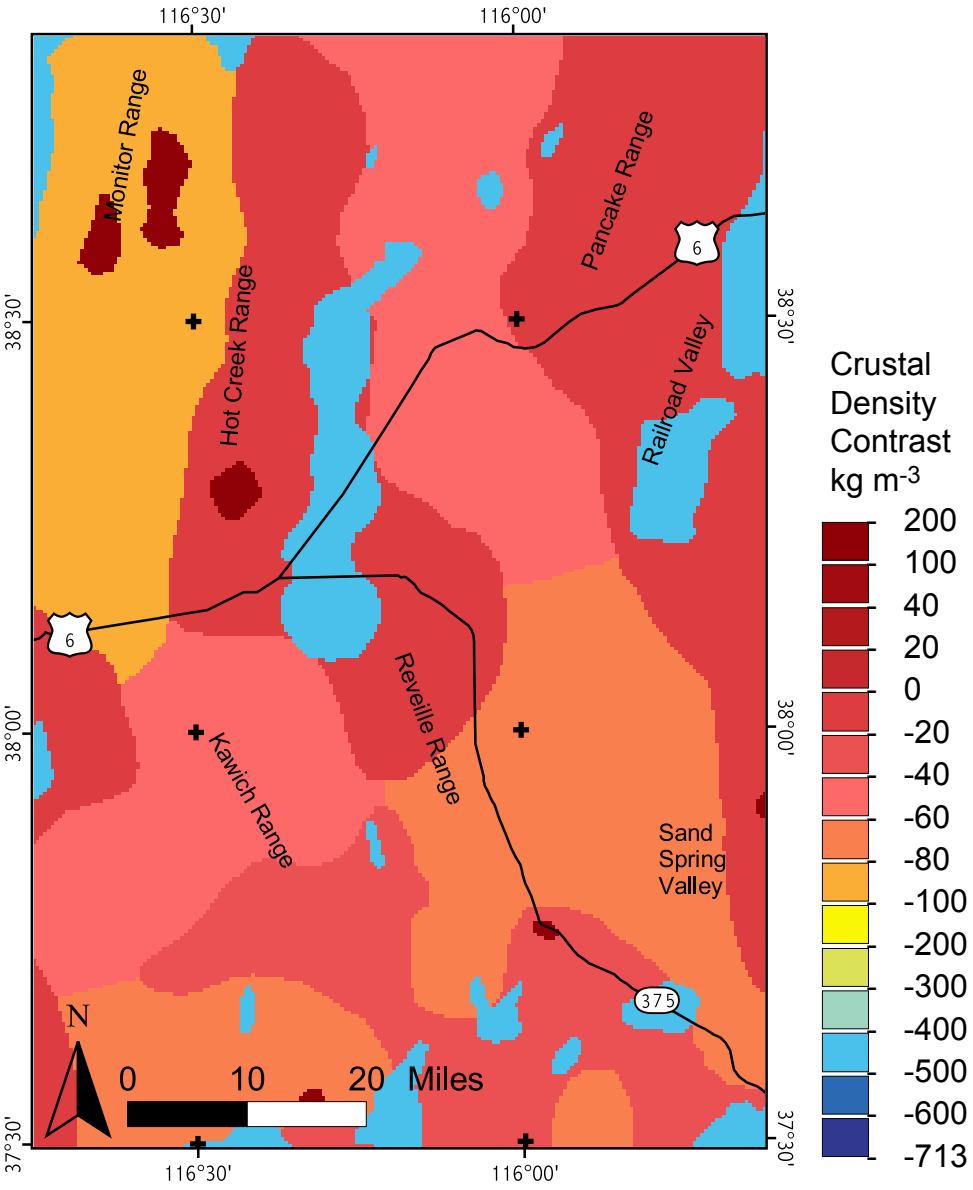

Figure 4.42 Modeled crustal density contrasts for layer E, 700 - 900 meters depth, Central Nevada study area.

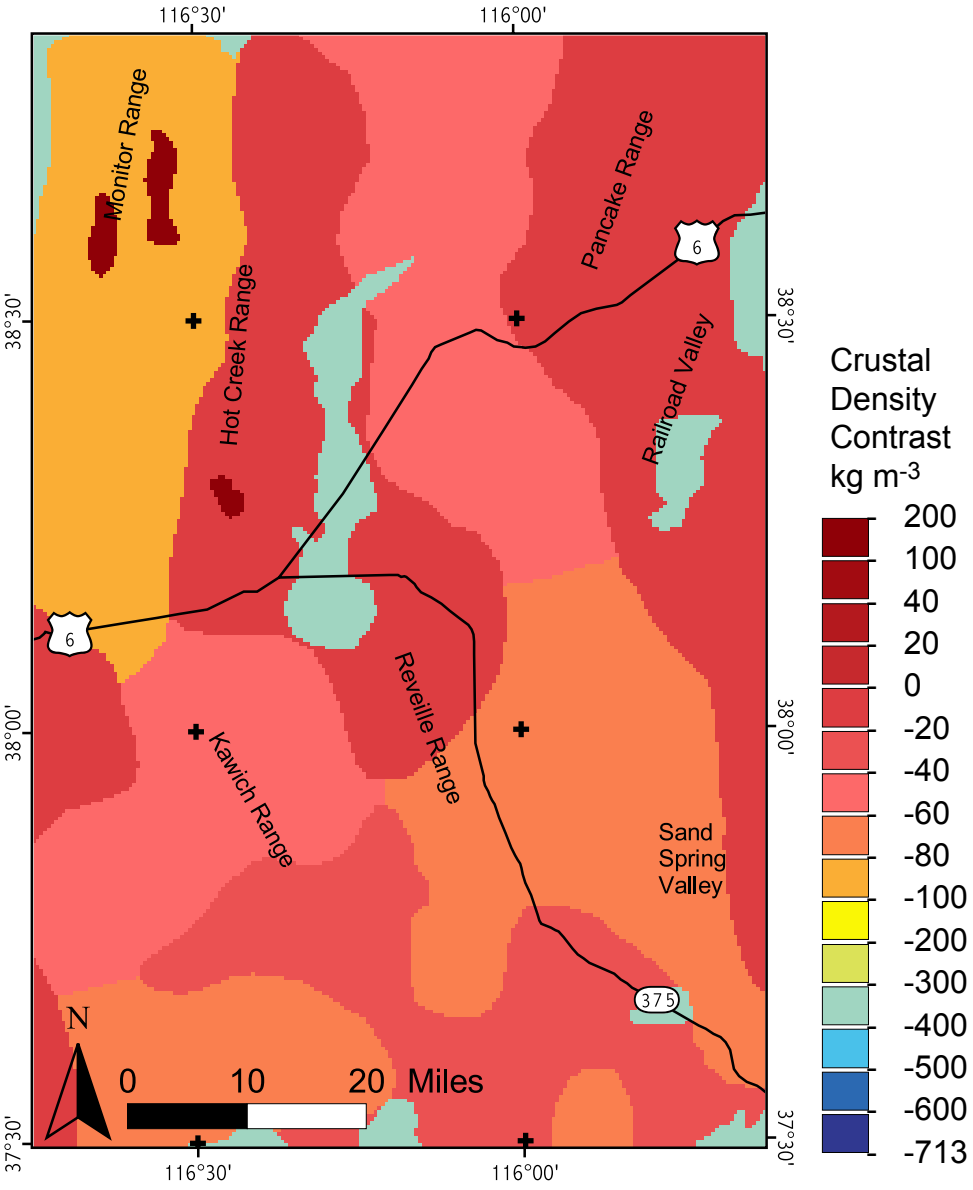

Figure 4.43 Modeled crustal density contrasts for layer F, 900 - 1100 meters depth, Central Nevada study area.

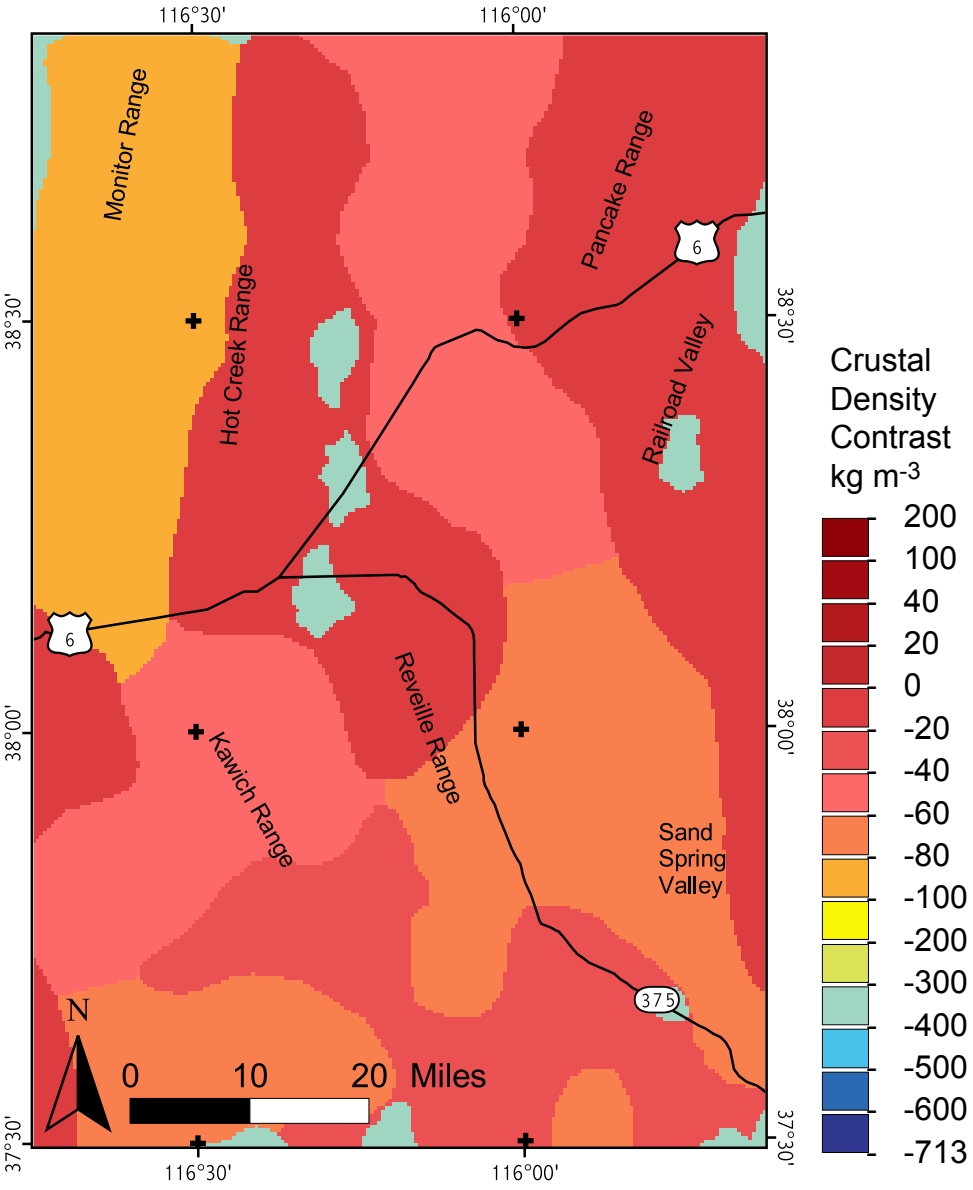

Figure 4.44 Modeled crustal density contrasts for layer G, 1100 - 1300 meters depth, Central Nevada study area.

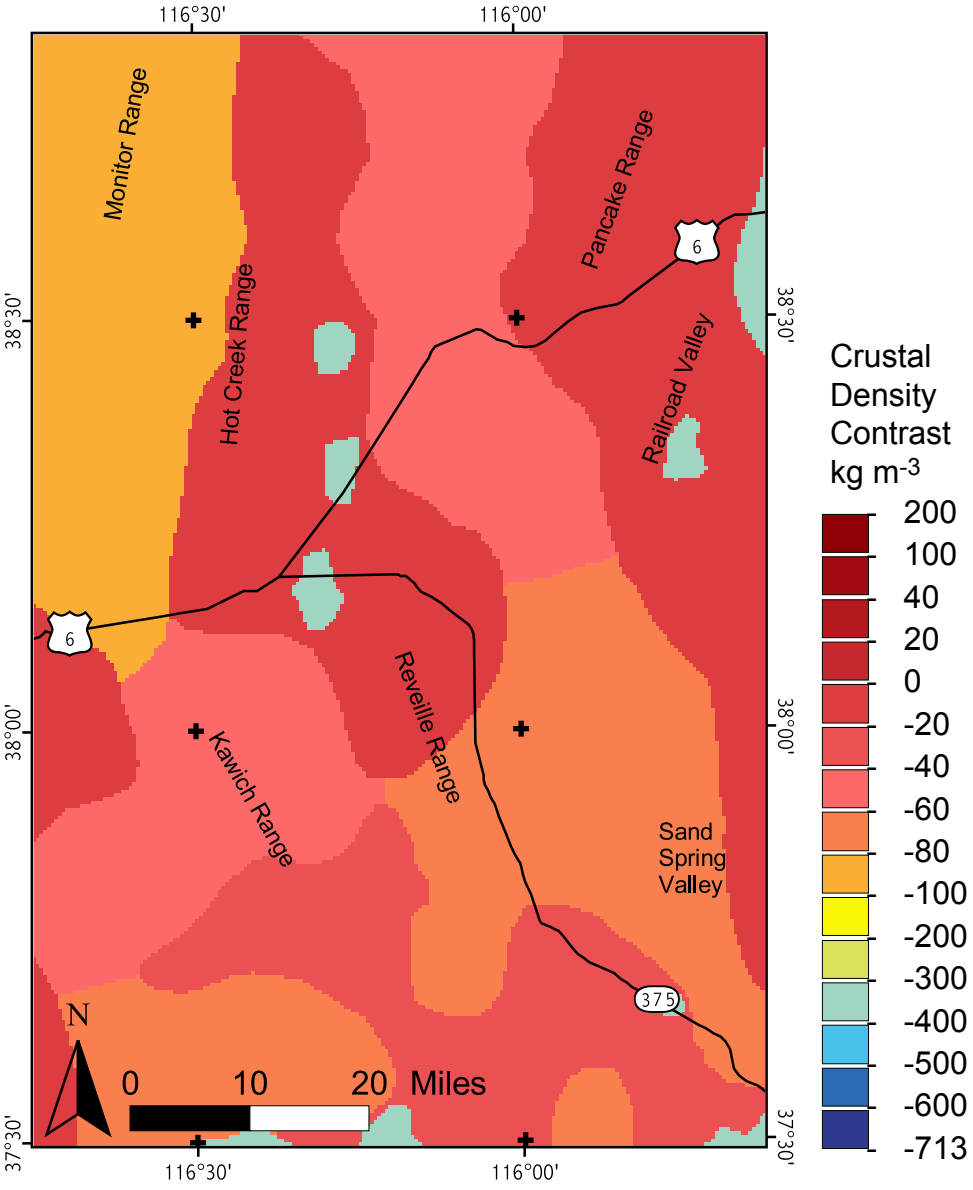

Figure 4.45 Modeled crustal density contrasts for layer H, 1300 - 1600 meters depth, Central Nevada study area.

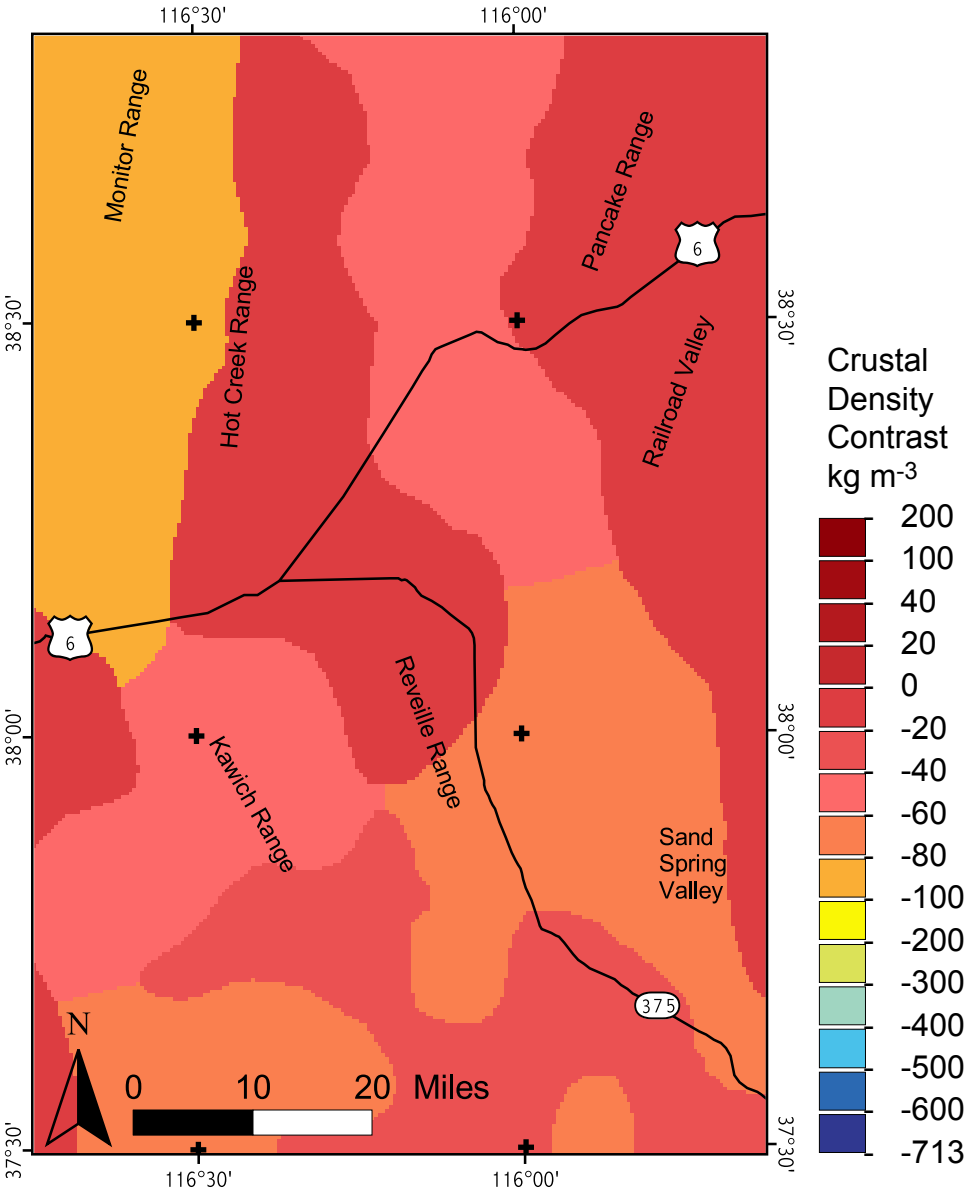

Figure 4.46 Modeled crustal density contrasts for layer I (basement), 1600 - 10,000 meters depth, Central Nevada study area.

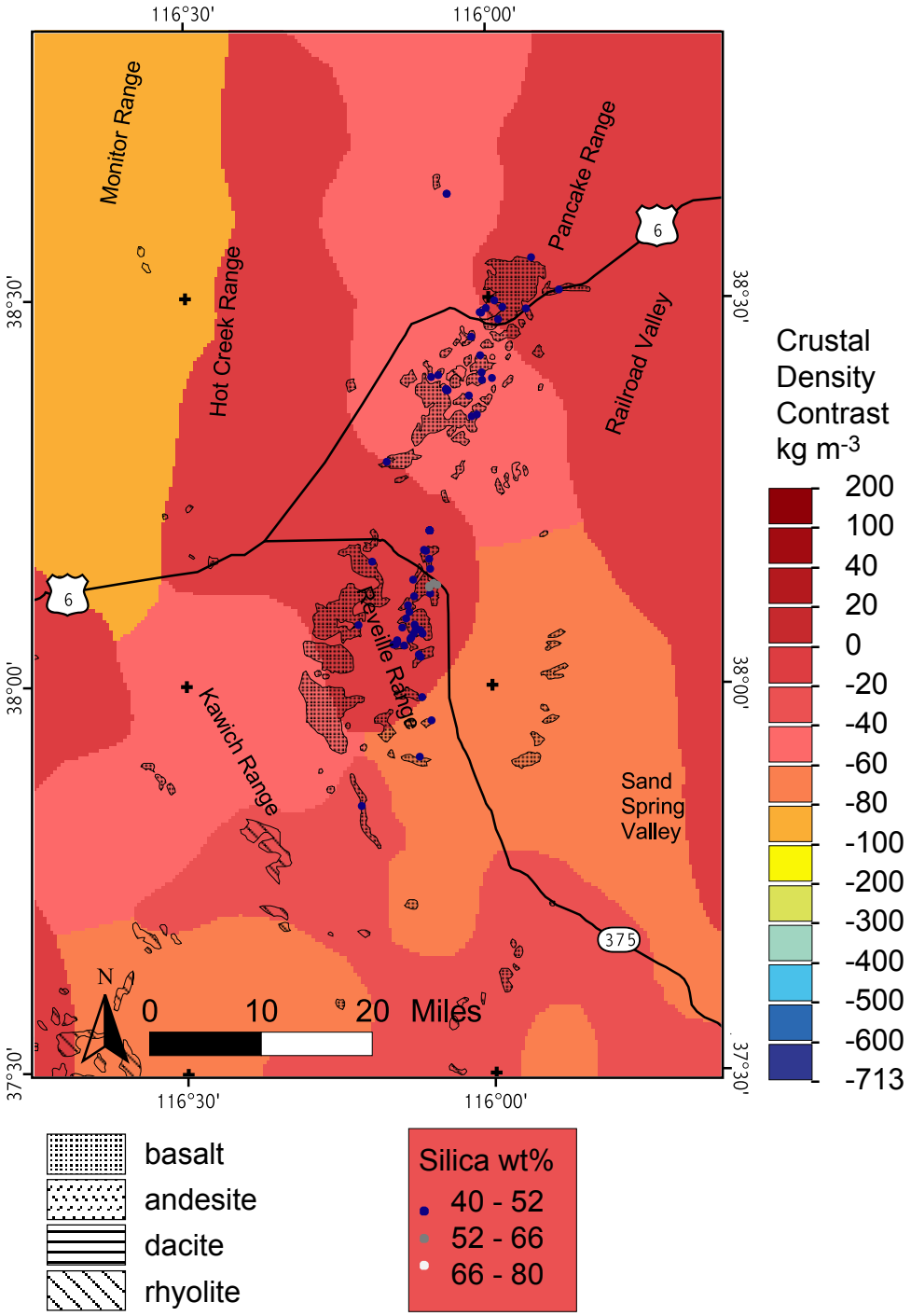

Figure 4.47 Modeled crustal density contrasts for layer I (basement), for the Central Nevada study area shown with late Tertiary and Quaternary volcanics as mapped by Luedke and Smith (1981), and silica content values of sampled volcanics from NAVDAT database.

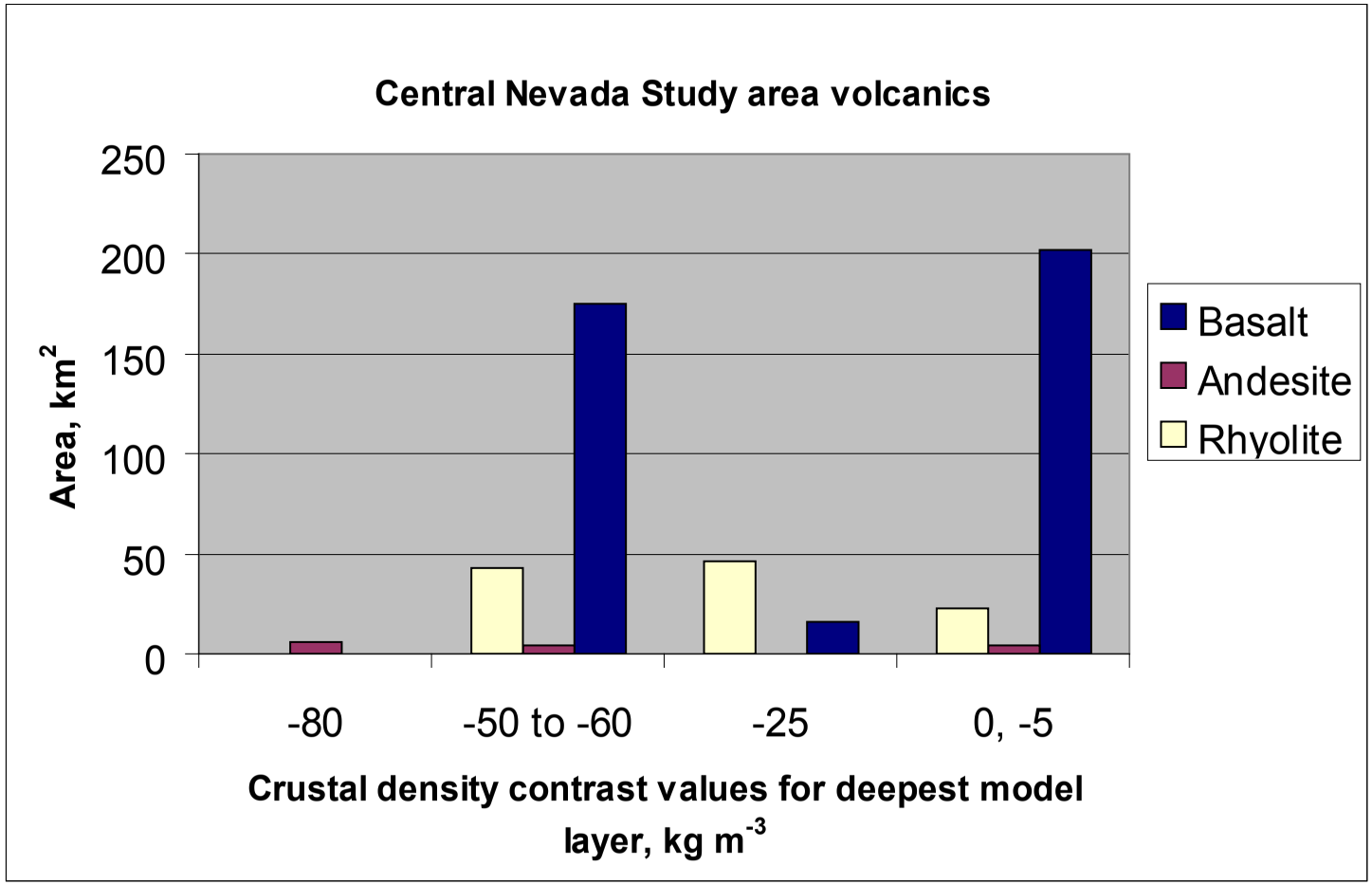

Figure 4.48 Surface area of late Tertiary and Quaternary (<16 Ma) volcanics, as mapped by Luedke and Smith (1981), erupted through each crustal density contrast value in basement model layer (I), Central Nevada study area.

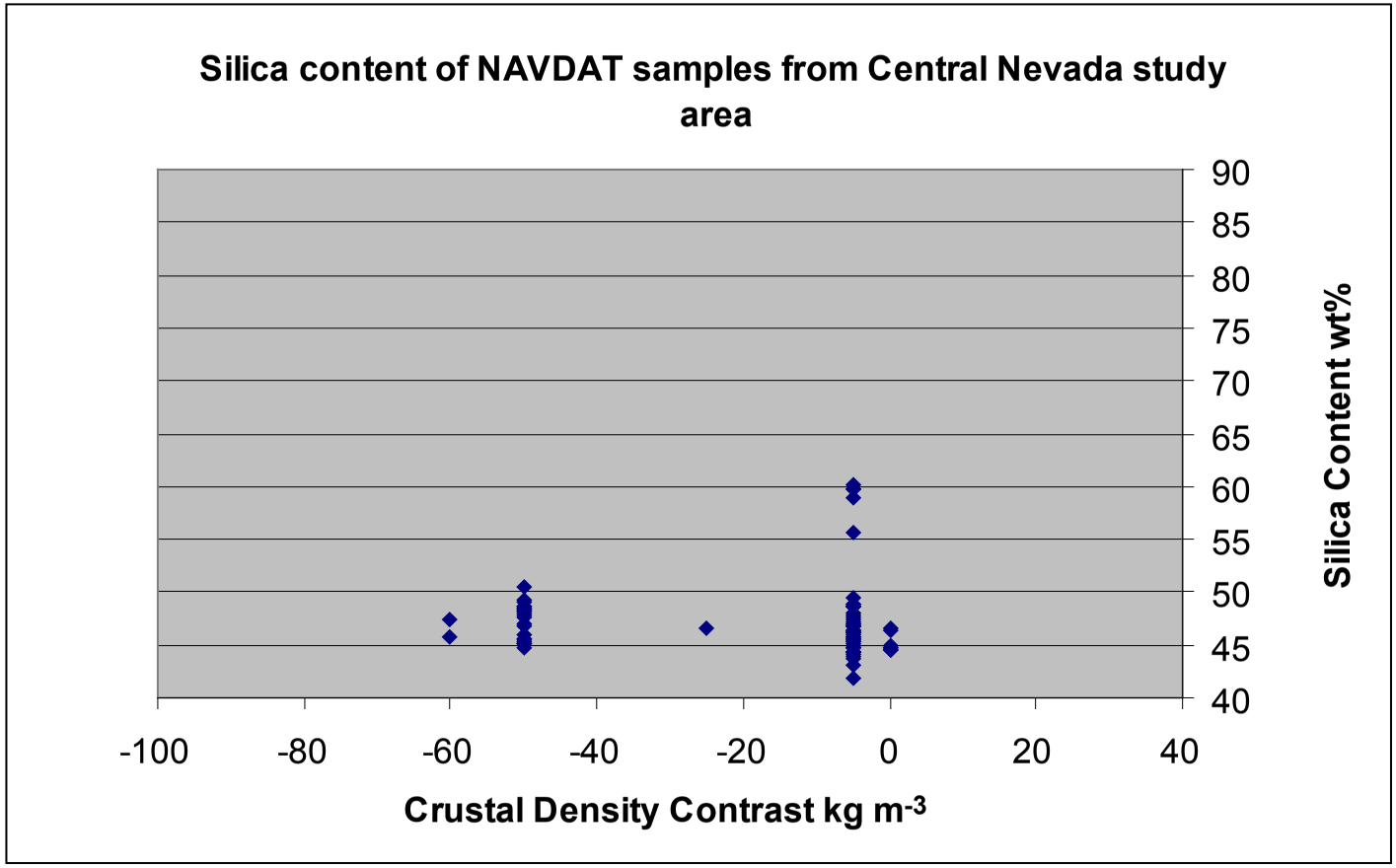

Figure 4.49 Relationship between silica content of NAVDAT samples of erupted late Tertiary and Quaternary volcanics and modeled basement crustal density contrast values.
Figure 4.47 shows the location of samples used in this plot.

Chapter 5

Conclusions

5.1 Introduction

The work described in Chapters 1-4 was designed to test the hypothesis that crustal density controls the nature of magmatic activity due to buoyancy effects. The hypothesis states that basaltic magmas will have a tendency to pond within the crust in areas with lower crustal density, and are more likely to erupt in areas of greater crustal density due to differences in buoyancy forces. Areas in which the basaltic magmas pond within the crust should also correlate with areas where rhyolitic melts are generated and rhyolitic magmatic centers can be formed.

Isostatic gravity anomalies are intended to show density anomalies within the upper crust. An isostatic gravity set has had numerous corrections applied to the raw data, including an isostatic correction that accounts for deep mass supporting high topography. The value of the correction directly affects the value of the gravity anomaly, and so the value of isostatic anomalies used in the gravity modeling. A second part of the research presented here was a comparison of two commonly used isostatic correction techniques, the Airy-Heiskanen, and Pratt-Hayford methods and the introduction of a new isostatic compensation technique that combines aspects of both methods.

5.2 Isostatic Correction Models

The choice of isostatic correction model will affect the gravity anomaly value and so the crustal density contrast values found in the gravity models. This study has

shown that differences between the Pratt-Hayford and Airy-Heiskanen isostatic correction techniques are significant on a scale of tens of kilometers. Comparisons between models show that the greatest disagreement in correction value occurs with large variations in elevation. Differences between values generated by the Pratt-Hayford and Airy-Heiskanen models reach 30 mgal over approximately 36 km in some areas. The SNBR and Mojave study areas are most strongly influenced by the differences in correction values.

The CEM model is presented as an alternative method of isostatic compensation. Aspects of both the Airy-Heiskanen and the Pratt-Hayford isostatic compensation models are used in the CEM. It uses a 'map' of the Moho obtained from seismic data for crustal root geometry rather than calculating a crustal root, and then uses a calculated mantle density contrast value to further compensate high topography where needed. This method uses a more accurate concept of the actual geometry of the crust and mantle interface and the nature of the mantle than the compensation methods introduced by Pratt and Airy in the early twentieth century.

The development of the CEM isostatic correction model is an important step toward increasing the accuracy of this important gravity data correction. The CEM incorporates recent advancements in the understanding of the nature of the lower crust and upper mantle to increase the accuracy of the isostatic gravity data correction.

Free air anomaly data are highly correlated with terrain, but over scales of hundreds of kilometers average to near zero if the area under consideration is

isostatically compensated. As done in this work, using the averaged free air anomaly value as a guide to isostatically correcting gravity data (i.e., averaged isostatic anomaly values should equal averaged free air values) produces the most valid isostatic anomaly data sets, and in turn the most accurate crustal density anomaly models.

5.3 Crustal Density and Volcanic Rocks

Crustal density contrasts reflect the general crustal density trends within an area. With or without an actual firm number for crustal density (i.e., 2670 kg m^{-3} for granite), the spatial relationship between density contrast and location of erupted volcanics is of value in establishing the likelihood of a connection between the two entities.

Magma density can be determined in several ways. An estimate can be made using the partial molar volumes of the oxide components of the rock (e.g. Bottinga et al., 1982; Ochs and Lange, 1999). If rock chemical analysis is available this method is most accurate. Magma density is also sensitive to water content and temperature, neither of which can accurately be determined from rock chemistry. Test calculations using a density calculator (Wenner, personal communication) based on Ochs and Lange (1999) and using rock chemistry from samples in the Reveille Range (Wang, 1999) show that the density of the basaltic magma in the Reveille Range is approximately 3100 kg m^{-3}. This value is high, possibly due to incomplete analysis and unknown water content.

Another very simple method of estimating magma density is suggested by Philpotts (1990, p. 14). He suggests using the fact that when a rock melts it will expand about 10%. Thus most magmas will have a density about 91% of the solid form of the rock. Densities of solid basalt, based on known mineral densities can vary from 3000 to 3300 kg m^{-3}. Using the simple rule of thumb provided by Philpotts, the corresponding magma density will be approximately 91% of that value, or 2700 kg m^{-3} to 3000 kg m^{-3}. The test calculations show the sensitivity of the buoyancy mechanism due to slight variations in magma chemistry. Using the above numbers, basaltic magma with a density of 2700 kg m^{-3} rising solely due to buoyancy should have the potential to reach the surface through crust of density about 30 kg m^{-3} greater than that of granite. The crustal density contrast value needed to reproduce the isostatic anomaly value over granite bedrock provides an accurate estimate of the crustal density contrast value for granite in general. This value is approximately -75 (±5) kg m^{-3} for all study areas. Thus, the density contrast value that would allow basaltic magma of density 2700 kg m^{-3} to pass through is -45 kg m^{-3}. Figure 5.1 summarizes this condition in the three study areas and for the study as a whole. About 50% of basaltic magma in the study areas erupts through crust denser than 2700 kg m^{-3} and about 50% erupts through crust less dense than 2700 kg m^{-3}. Approximately half of the late Tertiary and Quaternary basalt in the study areas has erupted through crust that is less dense than the magma was. It is likely that in these cases, the simple model of a magma diapir rising through the crust due to buoyancy force is not correct.

In the areas where the upper crustal density does not appear to have controlled the eruptive location of basalt, it is possible that the magma is not rising due to buoyancy alone, but is connected to a deeper source through a conduit. In this situation the force needed for magma to reach the surface is partly or entirely supplied by buoyancy at depth where the density of the surrounding rock is greater and the connection to the deeper source (Stolper and Walker, 1980). The map of the depth to the Moho created for the CEM isostatic model shows that in all three study areas the seismically observed Moho is generally shallower than would be expected by the Airy-Heiskanen model, and denser mantle is 5 to 10 km nearer the surface than would be expected from the topography, perhaps providing the extra few kilometers of dense material needed to support a column of basaltic magma all the way to the surface.

This study has shown that magma sometimes erupts through crust of a higher density than the magma. In these instances the magma must maintain a connection to a deep source. Substantiating this condition may be possible through the use of isotopic data from rock samples in each study area.

5.4 Correlation of Crustal Density with Apparent High Density Intrusive Rocks

Short wavelength positive anomalies within an otherwise generally negative larger scale anomaly were modeled as small, high density intrusives. With the exception of the Mojave study area the intrusives occurred within lower density crust. In the Mojave study area, intrusive structures were scattered among all

modeled crustal densities, and are in the correct location to be part of the Independence dike swarm. The occurrence of high density intrusives in the low density crust supports the idea that dense magma will pond and solidify beneath the surface. In the Central Nevada and SNBR study areas this idea is further supported by the occurrence of felsic volcanics near the intrusions, indicating that melting of felsic crust occurred nearby.

5.5 Future Directions

This study did not differentiate between magma that rose as a diapir and magma that rose due to the combined buoyancy force acting on a column of magma connected to a deep source. Geochemical information from sampled rocks can be used to infer the source of the magma and the likely speed of ascent. Magma which remained connected to a deep source and rose quickly through an open conduit will show little crustal contamination. Samples containing mantle xenoliths most certainly rose to the surface quickly through a conduit. Geochemical data from NAVDAT database will be combined with crustal density contrast data produced in this study to differentiate between the two mechanisms of magma ascent and further define the role crustal density plays in the location of volcanism.

The accuracy of gravity modeling using isostatic anomalies is very sensitive to differences in the anomaly value, especially short wavelength changes. Further development and testing of the CEM isostatic compensation method will contribute to advancements in the accuracy of gravity anomaly data and the overall understanding of the mechanism that supports high topography.

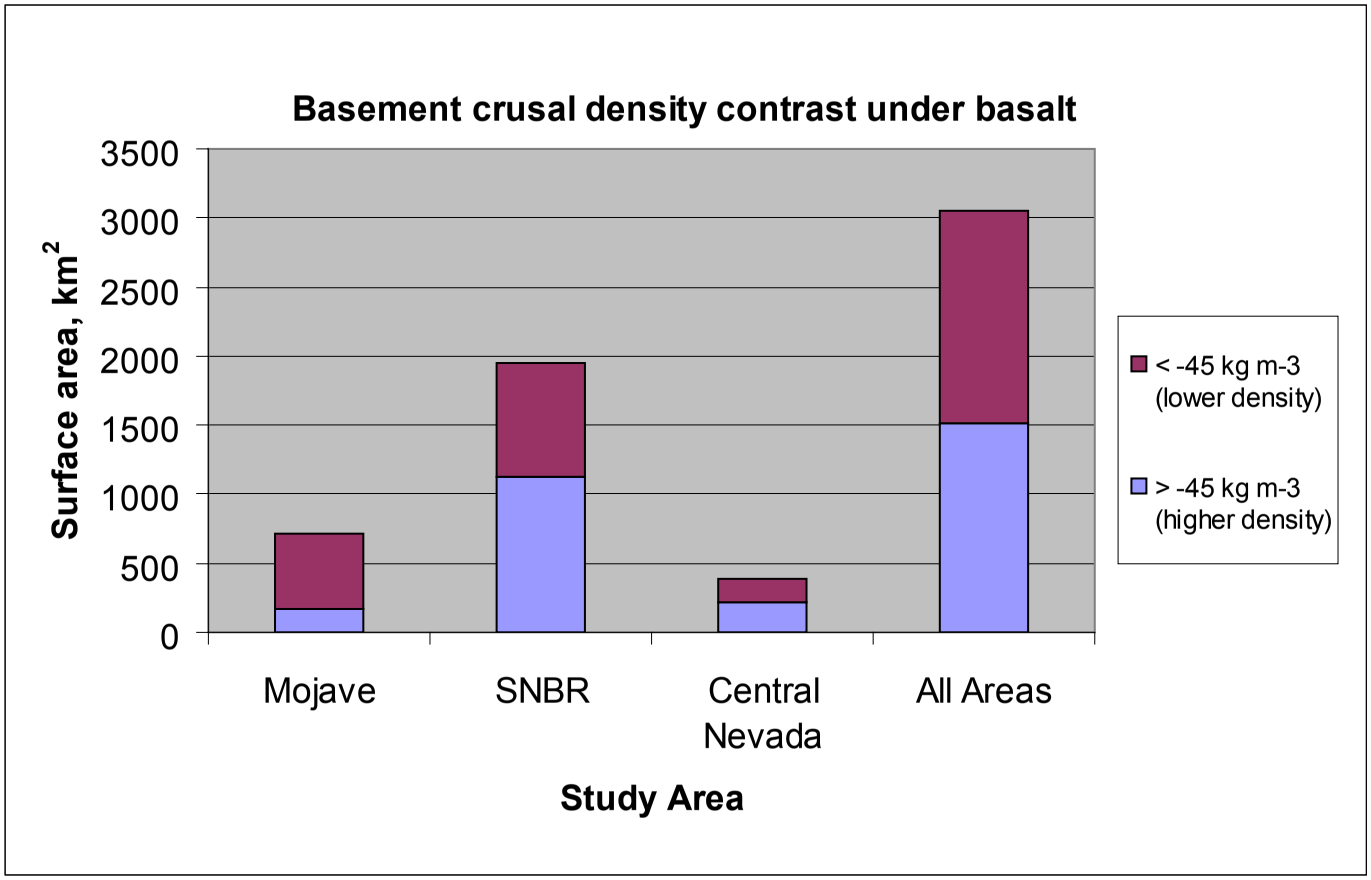

Figure 5.1 Summary of the crustal density contrast value under basaltic volcanics in all study areas. Quantities shown are the surface areas of late Tertiary and Quaternary basalt as mapped by Luedke and Smith (1981). The density contrast value of -45 kg m^{-3} translates into approximately 2700 kg m^{-3}, the minimum density of crust through which basaltic magma can reach the surface as a discrete parcel disconnected from a deep source.

References:

Abers, G. (1985), The subsurface structure of Long Valley Caldera, Mono County, California; a preliminary synthesis of gravity, seismic, and drilling information, *J. Geophys. Res.*, *90*(B5), 3627-3636.

Beyer, L. A., S.L. Robbins and F.G. Clutsom (1985), Basic data and preliminary density and porosity profiles for twelve borehole gravity surveys made in the Los Angeles, San Joaquin, Santa Maria and Ventura Basins, California, *Open File Rep. 85-42*, 67 pp., U. S. Geol. Surv., Reston, VA.

Birch, F. (1961), The velocity of compressional waves in rocks to 10 kilobars, Part 2, *J. Geophys. Res.*, *66*(7), 2199-2224.

Black, R.A, J.D. Walker and G.S. Baker (2002), Three-dimensional gravity modeling and crustal-density variations, Panamint Range to the eastern Sierra Nevada, southeastern California, in *Geologic Evolution of the Mojave Desert and Southwestern Basin and Range*, Geological Society of America Memoir 195, edited by A.F. Glazner, J.D. Walker and J.M. Bartley, pp. 229-241, Geological Society of America, Boulder, CO.

Blakely, R.J. (1995), *Potential Theory in Gravity and Magnetic Applications*, 441 pp., Cambridge University Press, Cambridge.

Bottinga, Y., D.F. Weill and P.Richet (1982), Density calculations for silicate liquids-I. Revised method for aluminosilicate compositions, *Geochim. Cosmochim. Acta, 46*, 909-919.

Carle, S.F. (1988), Three-dimensional gravity modeling of the geologic structure of Long Valley Caldera, *J. Geophys. Res.*, *93*(B11), 13237-13250.

Carl, B.S., and A. Glazner (2002), Extent and significance of the Independence dike swarm, eastern California, in *Geologic Evolution of the Mojave Desert and Southwestern Basin and Range*, Geological Society of America Memoir 195, edited by A.F. Glazner, J.D. Walker and J.M. Bartley, pp. 117-130, Geological Society of America, Boulder, CO.

Catchings, R.D. and W.D. Mooney (1991), Basin and Range crustal and upper mantle structure, northwest to central Nevada, *J. Geophys. Res.*, *96*(B4), 6247-6267.

Dickson, L.D. (1997), Volcanology and geochemistry of pliocene and quaternary basalts on Citadel Mountain, Lunar Crater Volcanic field, Pancake Range, Nevada, M.S. Thesis, 146 pp., University of Nevada, Las Vegas.

Ekren, E.B., C. L. Rogers, and G.L. Dixon (1973), Geologic and Bouguer gravity map of the Reveille Quadrangle, Nye County, Nevada, *Map I-806*, Miscellaneous Geologic Investigations, U.S. Geol. Surv., Reston, VA.

Fliedner, M.M., S. Ruppert, P.E. Malin, S.K. Park, G. Jiracek, R.A. Phinney, J.B. Saleeby, B. Wernicke, R. Clayton, R. Keller, K. Miller, C. Jones, J.H. Luetgert, W.D. Mooney, H. Oliver, S.L. Klemperer and G.A. Thompson (1996), Three-dimensional crustal structure of the southern Sierra Nevada from seismic fan profiles and gravity modeling, *Geology*, *24*(4), 367-370.

Fuis, G.S., T. Ryberg, N.J. Godfrey, D.A. Okaya, J.M. Murphy (2001), Crustal structure and tectonics from the Los Angeles Basin to the Mojave Desert, southern California, *Geology*, *29*(1), 15-18.

Glazner, A.F., J.M. Bartley, D.S. Coleman, W. Gray, R.Z. Taylor (2004), Are plutons assembled over millions of years by amalgamation from small magma chambers?, *GSA Today*, *14*(4/5), 4-11.

Glazner, A.F., and W.U. Ussler, III (1988), Trapping of magma at midcrustal density discontinuities, *Geophys. Res. Lett.*, *15*(7), 673-675.

Glazner, A.F., and W.U. Ussler, III (1989), Crustal extension, crustal density, and the evolution of Cenozoic magmatism in the basin and range of the Western United States, *J. Geophys. Res.*, *94*(B6), 7952-7960.

Hittelman, A.M., D.T. Dater, R.W. Buhmann, and S.D. Racey (1994), Gravity CD-ROM and User's Manual (1994 Edition), National Oceanic and Atmospheric Administration, Natl. Geophys. Data Cent., Boulder, CO.

Jachens, R.C. and B.C. Moring (1990), Maps of the thickness of Cenozoic deposits and the isostatic residual gravity over basement for Nevada, *Open File Report 90-404*, 15 pp., U.S. Geol. Surv., Reston, VA.

Jennings, C.W., R.G. Strand and T.H. Rogers (1977), Geologic Map of California (scale 1:750000), digital version, Calif. Div. Mines and Geology, Sacramento, CA.

Kaban, M.K., and W.D. Mooney (2001), Density structure of the lithosphere in the southwestern United States and its tectonic significance, *J. Geophys. Res.*, *106*(B1), 721-739.

Karki, P., L. Kivioja, and W.A. Heiskanen (1961), Topographic-isostatic reduction maps for the world for the Hayford zones 18-1, Airy-Heiskanen system, T=30 km, *Publications of the Isostatic Institute of the International Association of Geodesy*, 23pp., Intl. Assoc. Geodesy, Helsinki.

Kennett, J.P., J.G. Baldauf, R. Behl, W.R. Bryant, M. Fuller, K., Grimm, L. Heusser, A. Kemp, C. Lange, S.P. Lund, R. Merrill, F. Olivier, E. Polgreen, L. Pratt, F. Rack, A. Schimmelmann, M. Schwartz, R. Stein, J. Thurow and R.J. Musgrave (1994), Site 893, *Proceedings of the Ocean Drilling Program, Initial Reports, 146*, Part 2, pp. 15-50, College Station, TX.

Luedke, R.G. and R.L. Smith (1981), Map showing distribution, composition, and age of late Cenozoic volcanic centers in California and Nevada, *Map I-1091-C*, Miscellaneous Investigations Series, U.S. Geol. Surv., Reston, VA.

McCulloh, T.H. (1967), Mass properties of sedimentary rocks and gravimetric effects of petroleum and natural-gas reservoirs, *Prof. Pap., 528-A*, 50 pp., U.S. Geol. Surv., Reston, VA.

Ochs F. A, III and R. A. Lange (1999), The density of hydrous magmatic liquids, *Science, 283*(5406), 1314-1317.

Oliver, H. W. (1977), Gravity and magnetic investigations of the Sierra Nevada batholith, California, *Geol. Soc. Amer. Bull., 88*(3), 445-461.

Pakiser, L.C. (1976), Seismic exploration of Mono Basin, California, *J. Geophys. Res., 81*(20), 3607-3618.

Philpotts, Anthony R. (1990), *Principles of Igneous and Metamorphic Petrology*, 498 pp., Prentice Hall, Upper Saddle River, NJ.

Raines, G.L., K.A. Connors, L.A. Moyer and R.J. Miller (2003), Spatial Digital Database for the Geologic Map of Nevada, *Open File Report 03-66*, 32 pp., U.S. Geol. Surv., Reston, VA. (http://pubs.usgs.gov/of/2003/of03-66/)

Rash, K.B. (1995), Geology and geochemistry of Tertiary volcanic rocks in the northern Reveille and southern Pancake ranges, Nye County, Nevada, M.S. Thesis, 171 pp., University of Nevada, Las Vegas.

Ruppert, S., M.M. Fliedner, and G. Zandt (1998), Thin crust and active upper mantle beneath the Southern Sierra Nevada in the western United States, *Tectonophysics, 286*(1-4), 237-252.

Saltus, R.W. and R.C. Jachens (1995), Gravity and basin-depth maps of the Basin and Range Province, western United States, *Map GP-1012*, Geophysical Investigations Map, U.S. Geol. Surv., Reston, VA.

Simpson, R.W., R.C. Jachens and R.J. Blakely (1983), AIRYROOT: a Fortan program for calculating the gravitational attraction of an Airy isostatic root out to 166.7 km, *Open File Rep. 83-883*, 66 pp. U.S. Geol. Survey, Reston, VA.

Snyder, R.P., E.B. Ekren and G.L. Dixon (1972), Geologic map of the Lunar Crater Quadrangle, Nye County, Nevada, *Map I-700*, Miscellaneous Geologic Investigations, U.S. Geol. Surv., Reston, VA.

Stewart, J.H. and J.E. Carlson (1978), Geologic map of Nevada, 1:500,000 scale, 2 sheets, prepared in cooperation with the Nev. Bur. Mines and Geology, U.S. Geol. Surv., Reston, VA.

Stolper, E, and D. Walker (1980), Melt density and the average composition of basalt, *Contrib. Mineral. Petrol., 74*, 7-12.

Turcotte, D.L. and G. Schubert (1982), *Geodynamics: Applications of Continuum Physics to Geological Problems*, 450 pp., Wiley, New York.

U.S. Geological Survey, Calif. Geological Survey and Nev. Bureau of Mines and Geology (2006), Quaternary fault and fold database for the United States, accessed Jan 9, 2006, from USGS web site, http://earthquake.usgs.gov/regional/qfaults/.

Wang, K. (1999), Crust-mantle interaction and mantle chemical systematics during Basin and Range extension, SW USA: evidences from late Cenozoic volcanic rocks, *Ph.D. Dissertation*, 310 pp., University of Kansas, Lawrence, KS.

Watts, A. B., (2001), *Isostasy and Flexure of the Lithosphere*, 458 pp, Cambridge University Press, Cambridge.

Appendix A

Listing A.1 program layergrav

```
      program layergrav
c
c  Modified from gross.f written by Ross Black
c
c  calculate the gravitational attraction
c  from a series of Arc gridascii grids
c  the output grid is the same size as
c  the input grid in xy and
c  is  also an ascii grid
c
c  the Arc ascii grid starts with the northwest corner
c  of the data and is stored row by row.
c
c  Subroutines by Richard Blakely
c
      real data(500,500),grav(500,500)
      real data2(262144)
      real store(524288)
      real ztop(25),zbot(25)
      integer nx,ny
      character*14 junk(6),junk2
      character*40 rhofile,layerfile,outfile
      print*,'input density file name'
      read(5,10) rhofile
 10   format(a40)
      open(1,file=rhofile,status='old')
      print*,'input layer information file name'
      read(5,10) layerfile
      open(2,file=layerfile,status='old')
      print*,'enter output gravity file name'
      read(5,10) outfile
      open(3,file=outfile,status='new')
      read(1,15) junk(1),nx
 15   format(a14,i3)
      write(6,20) nx
 20   format('ncols ',i4)
      read(1,30) junk(2),ny
 30   format(a14,i3)
      write(6,35) ny
 35   format('nrows ',i4)
      read(1,40) junk(3),ixllc
 40   format(a14,i6)
      xllc = float(ixllc)
      write(6,45) xllc
 45   format('xllc ',f8.1)
      read(1,50) junk(4),iyllc
 50   format(a14,i7)
      yllc = float(iyllc)
      write(6,55) yllc
 55   format('yllc ',f9.1)
      read(1,60) junk(5),icellsize
 60   format(a14,i3)
      write(6,65) icellsize
 65   format('icellsize ',i4)
      read(1,70) junk(6),inodata
 70   format(a14,i5)
      read(2,*) nlayers
```

```
      print*,' nlayers=',nlayers
      dx = float(icellsize)/1000.
      dy = float(icellsize)/1000.
c
c  layer top, bottom depths in m
c
      do k=1,nlayers
        read(2,*) ztop(k),zbot(k)
      end do
      cellhalf = float(icellsize)/2.
      iwindhalf = int(radius/float(icellsize))
      print*,'xllc,yllc=',xllc,yllc
      print*,'icellsize,cellhalf=',icellsize,cellhalf
      xulcent = xllc+cellhalf
      yulcent = (yllc+(ny*icellsize))-cellhalf
c
c  start the calculations
c  use UTM coords converted to KM until the call to glayer
c     UL map corner is 1st data element on input
c  use NEV coords in KM on the call to gbox
c     LL map corner is 1st data element in 1D array going
c     to glayer
c
c  in this version all layers must have exactly the same number of
c  rows and columns and must be in exactly the same spatial location
c
      do k=1,nlayers
        print*,' starting layer ',k
        if (k.gt.1) then
          do j=1,6
            read(1,11) junk2
            print*,junk2
 11         format(a14)
          end do
        end if
        do i=1,ny
          print*,i
          read(1,*) (data(j,i),j=1,nx)
          do j=1,nx
            if (data(j,i).lt.-998.0) data(j,i) = 0.
          end do
        end do
        do i=1,524288
          store(i) = 0.
        end do
c start fourier stuff

        z1 = (ztop(k)+0.1)/1000.
        z2 = zbot(k)/1000.
c
c gbox uses NEV coords for xyz, not UTM where EN=xy
c  so flip the x and y coords around in subroutine call
c
        nnx = 512
        nny = 512
        do ii=1,ny
          do jj=1,nx
            irow = 1+ny-ii
            in = jj+(ii-1)*nnx
            data2(in) = data(jj,irow)
```

```
          end do
        end do
        call glayer(data2,nny,nnx,dy,dx,z1,z2,store)
        do ii=1,ny
          do jj=1,nx
            irow = 1+ny-ii
            in = jj+(ii-1)*nnx
            grav(jj,irow) = data2(in)+grav(jj,irow)
          end do
        end do
      end do
      write(6,76)
 76   format(' finished ')
      write(3,15) junk(1),nx
      write(3,30) junk(2),ny
      write(3,40) junk(3),ixllc
      write(3,50) junk(4),iyllc
      write(3,60) junk(5),icellsize
      write(3,70) junk(6),inodata
      do i=1,ny
        write(3,80) (grav(j,i),j=1,nx)
 80     format(1200f10.4)
      end do
      stop
      end
c=============================================================
      subroutine glayer(rho,nx,ny,dx,dy,z1,z2,store)
c
c  Subroutine GLAYER calculates the vertical gravitational
c  attraction on a two-dimensional grid caused by a two-
c  dimensional density confined to a horizontal layer.  The
c  following steps are involved:  (1) Fourier transform the
c  density, (2) multiply by the earth filter, and (3) inverse
c  Fourier transform the product.  Density is specified on a
c  rectangular grid with x and y axes directed north and east,
c  respectively.  Z axis is down.  Requires subroutines FOURN,
c  KVALUE, and GFILT.
c
c  Input parameters:
c    nx - number of elements in the south-to-north direction.
c    ny - number of elements in the west-to-east direction.
c         (NOTE: Both nx and ny must be powers of two.
c    rho - a singly dimensioned real array containing the
c         two-dimensional density, in kg/(m**3).  Elements
c         should be in order of west to east, then south to
c         north (i.e., element 1 is the southwest corner,
c         element ny is the southeast corner, element
c         (nx-1)*ny+1 is the northwest corner, and element ny*nx
c         is the northeast corner.
c    store - a singly dimensioned real array used internally.
c         It should be dimensioned at least 2*nx*ny.
c    dx - sample interval in the x direction, in km.
c    dy - sample interval in the y direction, in km.
c    z1 - depth to top of layer, in km.  Must be > 0.
c    z2 - depth to bottom of layer, in km.  Must be > z1.
c
c  Output parameters:
c    rho - upon output, rho will contain the gravity anomaly,
c         in mGal, with same orientation as above.
c
```

```
      complex crho,cmplx
      real kx,ky,km2m
      dimension rho(262144),store(524288),nn(2)
      data pi/3.14159265/,si2mg/1.e5/,km2m/1.e3/

      nn(1) = ny
      nn(2) = nx
      ndim = 2
      dkx = 2.*pi/(nx*dx)
      dky = 2.*pi/(ny*dy)
      do 10 j=1,nx
        do 10 i=1,ny
          ij = (j-1)*ny+i
          store(2*ij-1) = rho(ij)
   10 store(2*ij) = 0.
      isssign = 1
      call fourn(store,nn,ndim,isssign)
      do 20 j=1,nx
        do 20 i=1,ny
          ij = (j-1)*ny+i
          call kvalue(i,j,nx,ny,dkx,dky,kx,ky)
          crho = cmplx(store(2*ij-1),store(2*ij))
          crho = crho*gfilt(kx,ky,z1,z2)
          store(2*ij-1) = real(crho)
   20 store(2*ij) = aimag(crho)
      isssign = -1
      call fourn(store,nn,ndim,isssign)
      do 30 j=1,nx
        do 30 i=1,ny
          ij = (j-1)*ny+i
   30 rho(ij) = store(2*ij-1)*si2mg*km2m/(nx*ny)
      return
      end

c=============================================================

      subroutine kvalue(i,j,nx,ny,dkx,dky,kx,ky)
c  Subroutine KVALUE finds the wavenumber coordinates of one
c  element of a rectangular grid from subroutine FOURN.
c
c  Input parameters:
c    i  - index in the ky direction.
c    j  - index in the kx direction.
c    nx - dimension of grid in ky direction (a power of two).
c    ny - dimension of grid in kx direction (a power of two).
c    dkx - sample interval in the kx direction.
c    dky - sample interval in the ky direction.
c
c  Output parameters:
c    kx - the wavenumber coordinate in the kx direction.
c    ky - the wavenumber coordinate in the ky direction.
c
      real kx,ky
      nyqx = nx/2+1
      nyqy = ny/2+1
      if (j.le.nyqx) then
        kx = (j-1)*dkx
      else
        kx = (j-nx-1)*dkx
      end if
```

```
      if (i.le.nyqy) then
        ky = (i-1)*dky
      else
        ky = (i-ny-1)*dky
      end if
      return
      end

c=============================================================

      subroutine fourn(data,nn,ndim,isign)
c
c  Replaces DATA by its NDIM-dimensional discrete Fourier transform,
c  if ISIGN is input as 1.  NN is an integer array of length NDIM,
c  containing the lengths of each dimension (number of complex values),
c  which must all be powers of 2.  DATA is a real array of length twice
c  the product of these lengths, in which the data are stored as in a
c  multidimensional complex Fortran array.  If ISIGN is input as -1,
c  DATA is replaced by its inverse transform times the product of the
c  lengths of all dimensions.  From Press, W.H., Flannery, B.P.,
c  Teukolsky, S.A., and Vetterling, W.T., 1986, Numerical Recipes,
c  Cambridge Univ. Press, p. 451-453.
c
      real*8 wr,wi,wpr,wpi,wtemp,theta
      dimension nn(2),data(524288)
      ntot = 1
      do 11 iidim=1,ndim
        ntot = ntot*nn(iidim)
11    continue
      nprev = 1
      do 18 iidim=1,ndim
        n = nn(iidim)
        nrem = ntot/(n*nprev)
        ip1 = 2*nprev
        ip2 = ip1*n
        ip3 = ip2*nrem
        i2rev = 1
        do 14 i2=1,ip2,ip1
          if (i2.lt.i2rev) then
            do 13 i1=i2,i2+ip1-2,2
              do 12 i3=i1,ip3,ip2
                i3rev = i2rev+i3-i2
                tempr = data(i3)
                tempi = data(i3+1)
                data(i3) = data(i3rev)
                data(i3+1) = data(i3rev+1)
                data(i3rev) = tempr
                data(i3rev+1) = tempi
12            continue
13          continue
          end if
          ibit = ip2/2
1         if ((ibit.ge.ip1).and.(i2rev.gt.ibit)) then
            i2rev = i2rev-ibit
            ibit = ibit/2
          go to 1
          end if
          i2rev = i2rev+ibit
14      continue
        ifp1 = ip1
```

```
2       if (ifp1.lt.ip2) then
          ifp2 = 2*ifp1
          theta = isign*6.28318530717959d0/(ifp2/ip1)
          wpr = -2.d0*dsin(0.5d0*theta)**2
          wpi = dsin(theta)
          wr = 1.d0
          wi = 0.d0
          do 17 i3=1,ifp1,ip1
            do 16 i1=i3,i3+ip1-2,2
              do 15 i2=i1,ip3,ifp2
                k1 = i2
                k2 = k1+ifp1
                tempr = sngl(wr)*data(k2)-sngl(wi)*data(k2+1)
                tempi = sngl(wr)*data(k2+1)+sngl(wi)*data(k2)
                data(k2) = data(k1)-tempr
                data(k2+1) = data(k1+1)-tempi
                data(k1) = data(k1)+tempr
                data(k1+1) = data(k1+1)+tempi
15            continue
16          continue
            wtemp = wr
            wr = wr*wpr-wi*wpi+wr
            wi = wi*wpr+wtemp*wpi+wi
17        continue
          ifp1=ifp2
          go to 2
        end if
        nprev = n*nprev
18    continue
      return
      end

c=============================================================

      function gfilt(kx,ky,z1,z2)
c
c  Function GFILT calculates the value of the gravitational
c  earth filter at a single (kx,ky) location.
c
c  Input parameters:
c    kx - the wavenumber coordinate in the kx direction, in
c         units of 1/km.
c    ky - the wavenumber coordinate in the ky direction, in
c         units of 1/km.
c    z1 - the depth to the top of the layer, in km.
c    z2 - the depth to the bottom of the layer, in km.
c
c  Output parameters:
c    gfilt - the value of the earth filter.
c
      real kx,ky,k
      data pi/3.14159265/,gamma/6.67e-11/
      k = sqrt(kx**2+ky**2)
      if (k.eq.0.) then
        gfilt = 2.*pi*gamma*(z2-z1)
      else
        gfilt = 2.*pi*gamma*(exp(-k*z1)-exp(-k*z2))/k
      end if
      return
      end
```

Listing A.2 program pratthayford

```
      program pratthayford

ccccccccccccccccccccccccccccccccccccccccccccccccccccccccccccccccccccccccccc
c  October, 07
c  Correction values are upward continued.
c  by Linda Pickett Garinger with subroutines by Richard J. Blakely (from
c  Potential theory in Gravity and Magnetic Applications).  This program
c  calculates an isostatic correction using the Pratt method.
c  This program is a two layer model.  Density above sea level is
c  constant and equal to seacoast density.  Other densities below sea level
c  are calculated for each grid column according to topographic load.
c  The program uses these densities to calculate the vertical gravitational
c  isostatic correction.  An area of 166.7 km radius is considered for each
c  grid point.
c  This program reads gridded values of elevation.
c  June 11, 2007.  Changing correction calculation to consider the anomalous
c  water density over ocean areas per Watts. The gravitational attraction of
c  each column is considered - including water, and calculated column
density.
c  Then the gravitational attraction of the sea level column is subtracted.


      real rhosl,rad,compdpth,xllcorner,yllcorner
      real cellsize,xnodat,rhockgm,gravsum
      real topogrid(2000,2000),rhogrd(2000,2000)
      real prattgrid(2000,2000)
      integer ncol,nrow,inodat
      character*50 topofile,label(8),notefile,rhofile,prattfile

c**********constants ******************
      print*, 'input crustal density (above sea level) in kg/m**3'
      read*, rhockgm
      rhosl = rhockgm
      rhosea = 1027.
      rad = 166.7
      gravsum = 0.0
      do i=1,2000
        do j=1,2000
          prattgrid(i,j) = 0.0
        end do
      end do
C***Rho is held constant only to sea level.

c***compdpth is the compensation depth(km). Lithosperic density between
c***compdpth and sea level will adjust according to topographic load.
      print*,'input compensation depth (km)'
      read*,compdpth
c********input topo acsii grid**************
c***this is an ascii grid.  Elevations are in m*****
      print*,'input gridascii topo file name'
      read(5,10) topofile
  10  format(a50)
      open(9,file=topofile, status='old')
      read(9,15) label(1), ncol
      read(9,16) label(2), nrow
      read(9,25) label(3), xllcorner
      read(9,25) label(4), yllcorner
```

```
      read(9,25) label(5), cellsize
      read(9,35) label(6), inodat
      xnodat = float(inodat)
   15 format(a14,i3)
   16 format(a14,i4)
   25 format(a14,f15.5)
   35 format(a14,i5)
      do i=1,nrow
        read(9,*,end=45)(topogrid(i,j),j=1,ncol)
      end do
   45 continue
      close(9)
c*****Calculate the density of column .....

      do 50 j=1,ncol
        do 50 i=1,nrow
          if (topogrid(i,j).eq.xnodat) then
            rhogrd(i,j) = xnodat
            go to 50
          else if (topogrid(i,j).le.-50000.) then
            od = -1.*(topogrid(i,j)+50000.)/1000.
c for ocean areas balance is:
            rhogrd(i,j) = (compdpth*rhosl -
     +                    (od*rhosea))/(compdpth - od)

            go to 50
          else if(topogrid(i,j).ge.0.) then
c for continental areas above sea level balance is:
            rhogrd(i,j) = ((rhosl*compdpth - ((topogrid(i,j)/1000.)
     +                      *rhockgm)))/compdpth
          else
c for continental areas below sea level the balance is:
            rhogrd(i,j) = (rhosl*compdpth)/
     +                    (compdpth+(topogrid(i,j)/1000.))
          end if
   50 continue

c****write the density grid***************
      print*, 'input density (rho) file name'
      read(5,10) rhofile
      open (3, file = rhofile,status = 'new')
      do 55 k=1,nrow
        write(3,56) (rhogrd(k,l),l=1,ncol)
   55 continue
   56 format(2000f12.3)
      close(3)

c****calculate the gravitational correction
      print*,'input note file name'
      read(5,10) notefile
      print*,'input pratt correction file name'
      read(5,10) prattfile
      open (12, file = notefile, status = 'new')
      open (13,file = prattfile, status = 'new')
      write(12,*) 'run name:', prattfile
      write(12,*) 'Two layer model, variable mantle density'
      write(12,*) 'crustal density = ', rhockgm
      write(12,*) 'column density at sea level = ',rhosl
      write(12,*) 'compensation depth = ',compdpth
      close(12)
```

```
c  write header for ascii grid output file
      write(13,15) label(1), ncol
      write(13,15) label(2), nrow
      write(13,25) label(3), xllcorner
      write(13,25) label(4), yllcorner
      write(13,25) label(5), cellsize
      write(13,35) label(6), inodat

      del = int(180/(cellsize/1000.))

*************************************************************************
      do 300 j=1,ncol
      if ((j.lt.50).or.(j.gt.(ncol-50))) then
        go to 300
      end if
      print*, j
        do 300 k = 1,nrow

          if ((k.lt.50).or.(k.gt.(nrow-50))) then
            go to 300
          end if

          X0 = (xllcorner + (cellsize*(float(j)-.5)))/1000.
          Y0 = (yllcorner + (cellsize *(float(nrow-k)+.5)))/1000.

          if (topogrid(k,j).le.-50000.) then
            Z0 = 0.0
          else if((topogrid(k,j).le.0.).and.
     &            (topogrid(k,j).gt.-50000.)) then
            Z0 = -1.* (topogrid(k,j)/1000.)
          else
            Z0 = -1. * (topogrid(k,j)/1000.)
          end if

c*****define the box to use for near calculations***********
          jjstart = j-del
          jjend = j+del
          kkstart = k-del
          kkend = k+del
          if (jjstart.le.0) jjstart = 1
          if (jjend.gt.ncol) jjend = ncol
          if (kkstart.le.0) kkstart = 1
          if (kkend.gt.nrow) kkend = nrow

c*************************************************************************
*
          do 400 jj = jjstart, jjend
            do 400 kk = kkstart, kkend

              if (rhogrd(kk,jj).eq.xnodat) go to 400

                X1 = (xllcorner + (cellsize * float(jj-1)))/1000.
                Y1 = (yllcorner + (cellsize * float(nrow - kk)))/1000.
                X2 = (xllcorner + (cellsize * float(jj)))/1000.
                Y2 = (yllcorner + (cellsize * float(nrow-kk+1)))/1000.

                mdptx =(X1+X2)/2
                mdpty =(Y1+Y2)/2

              if ((mdptx.lt.0).and.(X0.ge.0)) then
```

```
                xdist = abs((X1+X2)/2) + abs(X0)
              else if ((mdptx.ge.0).and.(X0.lt.0)) then
                xdist = abs((X1+X2)/2) + abs(X0)
              else
                xdist = abs((X1+X2)/2) - abs(X0)
              end if

              if ((mdpty.lt.0).and.(Y0.ge.0)) then
                ydist = abs((Y1+Y2)/2) + abs(Y0)
              else if ((mdpty.ge.0).and.(Y0.lt.0))then
                ydist = abs((Y1+Y2)/2) + abs(Y0)
              else
                ydist = abs((Y1+Y2)/2) - abs(Y0)
              end if

c  Begin modification to include water in calcs

              if (sqrt(xdist**2+ydist**2).le.rad) then

                if (topogrid(kk,jj).le.-50000)then
                  Z1 = 0.0
                  Z2 = -1.*(topogrid(kk,jj)+50000.)/(1000.)
                  Z3 = compdpth

                  rhocol= rhogrd(kk,jj)
                  call gbox(X0,Y0,Z0,X1,Y1,Z1,X2,Y2,Z2,rhosea,g1)
                  call gbox(X0,Y0,Z0,X1,Y1,Z2,X2,Y2,Z3,rhocol,g2)
                  call gbox(X0,Y0,Z0,X1,Y1,Z1,X2,Y2,Z3,rhosl,gsl)

                  g = g1+g2-gsl

                  g1 = 0.0
                  g2 = 0.0
                  gsl= 0.0

                else if (topogrid(kk,jj).ge.0.)then
                  Z1 = 0.0
                  Z2 = compdpth
                  call gbox(X0,Y0,Z0,X1,Y1,Z1,X2,Y2,Z2,rhogrd(kk,jj),g1)
                  call gbox(X0,Y0,Z0,X1,Y1,Z1,X2,Y2,Z2,rhosl,g2)
                  g = g1-g2

                else if ((topogrid(kk,jj).lt.0.).and.
     +                   (topogrid(kk,jj).gt.-50000.))then

                  Z1 = -1.*(topogrid(kk,jj)/1000.)
                  Z2 = compdpth
                  Z3 = 0.0
                  call gbox(X0,Y0,Z0,X1,Y1,Z1,X2,Y2,Z2,rhogrd(kk,jj),g1)
                  call gbox(X0,Y0,Z0,X1,Y1,Z3,X2,Y2,Z2,rhosl,g2)
                  g = g1-g2

                else
                  print*, "error"
                end if

                gravsum = gravsum + g

                g1 = 0.0
                g2 = 0.0
```

```
                gsl = 0.0
                g = 0.0
              else
                continue
              end if

  400     continue
          prattgrid(k,j) = gravsum

          gravsum = 0.0

  91      format(2000f13.6)

c**********************
  300 continue
      do 303 k=1,nrow
        write(13,91) (prattgrid(k,l),l=1,ncol)
  303 continue

      close(13)

      end

*************************************************************
      subroutine gbox(x0,y0,z0,x1,y1,z1,x2,y2,z2,rho,g)
c
c  Subroutine GBOX computes the vertical attraction of a
c  rectangular prism.  Sides of prism are parallel to x,y,z axes,
c  and z axis is vertical down.
c
c  Input parameters:
c    Observation point is (x0,y0,z0).  The prism extends from x1
c    to x2, from y1 to y2, and from z1 to z2 in the x, y, and z
c    directions, respectively.  Density of prism is rho.  All
c    distance parameters in units of km; rho in units of
c    kg/(m**3).
c
c  Output parameters:
c    Vertical attraction of gravity, g, in mGal.
c
      real km2m
      dimension x(2),y(2),z(2),isign(2)
      data isign/-1,1/,gamma/6.670e-11/,twopi/6.2831853/,
     &     si2mg/1.e5/,km2m/1.e3/
      x(1) = x0-x1
      y(1) = y0-y1
      z(1) = z0-z1
      x(2) = x0-x2
      y(2) = y0-y2
      z(2) = z0-z2
      sum = 0.0
      do 1 i=1,2
        do 1 j=1,2
          do 1 k=1,2
            rijk = sqrt(x(i)**2+y(j)**2+z(k)**2)
            ijk = isign(i)*isign(j)*isign(k)
            arg1 = atan2((x(i)*y(j)),(z(k)*rijk))
            if (arg1.lt.0.) arg1=arg1+twopi
            arg2 = rijk+y(j)
```

```
        arg3 = rijk+x(i)
        if (arg2.le.0.) pause 'GBOX:  Bad field point'
        if (arg3.le.0.) pause 'GBOX:  Bad field point'
        arg2 = alog(arg2)
        arg3 = alog(arg3)
        sum = sum+ijk*(z(k)*arg1-x(i)*arg2-y(j)*arg3)
1 continue
  g = rho*gamma*sum*si2mg*km2m
  return
  end
```

Listing A.3 program airyheisk

```
      program airyheisk

c  Aug 14,07
ccccccccccccccccccccccccccccccccccccccccccccccccccccccccccccccccccccccccccccc
c  by Linda Pickett Garinger with subroutines by Richard J. Blakely (from
c  Potential theory in Gravity and Magnetic Applications) and modified from
c  Simpson, Jachens and Blakely (AIRYROOT: a fortran program for
c  calculating the gravitational attraction of an airy isostatic root out to
c  166.7 km)
c  This program reads gridded values of elevation. Root geometry
c  is found from the topo map. It then calculates
c  the gravitational attraction of a rectangular prism due to the
c  root for a circular area to 166.7 km.
c
c  As per the "airyroot" program, upward continued calculations.

      real rhocrust,rhoman,delrho,rad,compdpth,xllcorner,yllcorner
      real cellsize,xnodat,rhockgm,drhokgm,gravsum
      real topogrid(2000,2000), ldgrd(2000,2000), rootgrd (2000,2000)
      real airygrid(2000,2000),rhosea
      integer ncol,nrow,inodat,del
      character*50 topofile,label(8),loadfile,rootfile,airyfile
c**********constants ******************
      print*, 'input crustal density in kg/m**3'
      read*, rhockgm
      print*, 'input mantle density in kg/m**3'
      read*, rhomankgm
      rhocrust = rhockgm/1000.
      rhoman = rhomankgm/1000.
      delrho = rhocrust-rhoman
      drhokgm = rhockgm - rhomankgm

      rad = 166.7
      rhosea = 1027.
      delrhosw = rhosea - rhockgm
      gravsum = 0.0
c***compdpth is the depth of root at sea level elevation (km)****
      print*,'compensation depth is the depth of the root at '
      print*,'sea level elevation.'
      print*,'input compensation depth (km)'
      read*,compdpth

c********input topo acsii grid**************
c***this is an ascii grid.  Elevations are in m*****
      print*,'input gridascii topo file name'
      read(5,10) topofile
  10  format(a50)
      open(10,file=topofile, status='old')
      read(10,15) label(1), ncol
      read(10,16) label(2), nrow
      read(10,25) label(3), xllcorner
      read(10,25) label(4), yllcorner
      read(10,25) label(5), cellsize
      read(10,35) label(6), inodat
      xnodat = float(inodat)
      write(*,15) label(1), ncol
      write(*,16) label(2), nrow
```

```
      write(*,25) label(3), xllcorner
      write(*,25) label(4), yllcorner
      write(*,25) label(5), cellsize
      write(*,35) label(6), inodat
      xnodat = float(inodat)

   15 format(a14,i3)
   16 format(a14,i4)
   25 format(a14,f15.5)
   35 format(a14,i7)

      do i=1,nrow
        read(10,*,end=45)(topogrid(i,j),j=1,ncol)
      end do
   45 continue

c****convert to load grid**************
      call topo2load(topogrid,ncol,nrow,rhocrust,xnodat,ldgrd)

c...write ldgrd
      print*,'input load file name'
      read(5,10) loadfile
      open(12,file = loadfile, status = 'new')
      do i=1,nrow
        write(12,80) (ldgrd(i,j),j=1,ncol)
 80     format(2000f15.4)
      end do
      continue

c****  Convert load to depth of root in km.
c****  grid will contain root after this step.

      call load2root(ldgrd,ncol,nrow,compdpth,delrho,xnodat,rootgrd)
c***write rootgrd
      print*,'input root output file name'
      read(5,10) rootfile

      open (3,file = rootfile, status = 'new')
      do i=1,nrow
        write(3,90) (rootgrd(i,j),j=1,ncol)
 90     format(2000f12.4)
      end do
      close(3)
c initialize airygrid vals
      do k=1,nrow
        do l=1,ncol
          airygrid(k,l) = xnodat
        end do
      end do

      print*,'input airy root gravity file name'
      read(5,10) airyfile

c****calculate the gravitational effect of the root

*****************************************************************
c set up so that the edge cells aren't calculated (saves time)
      ntop = 50
      nbot = 50
      nleft = 50
```

```
 nright = 50
 nrow2 = nrow-ntop-nbot
 ncol2 = ncol-nleft-nright
 xllcorner2 = xllcorner + cellsize*nleft
 yllcorner2 = yllcorner + cellsize*nbot
 del = int(175/(cellsize/1000.))
 do 300 j = 1,ncol
   if ((j.lt.50).or.(j.gt.(ncol-50))) then
     go to 300
   end if

   print*, j

   do 300 k = 1,nrow
     if ((k.lt.50).or.(k.gt.(nrow-50))) then
       go to 300
     end if

     X0 = (xllcorner + (cellsize*(float(j)-.5)))/1000.
     Y0 = (yllcorner + (cellsize *(float(nrow-k)+.5)))/1000.
     if (topogrid(k,j).le.-50000.)then
       Z0 = 0.0
     else if((topogrid(k,j).le.0.).and.
&            (topogrid(k,j).gt.-50000.))then
       Z0 = -1. * (topogrid(k,j)/1000.)
     else
       Z0 = -1. * (topogrid(k,j)/1000.)
     end if

     jjstart = j-del
     jjend = j+del
     kkstart = k-del
     kkend = k+ del
     if (jjstart.le.0) jjstart = 1
     if (jjend.gt.ncol) jjend = ncol
     if (kkstart.le.0) kkstart = 1
     if (kkend.gt.nrow) kkend = nrow
     do 400 jj = jjstart, jjend
       do 400 kk = kkstart, kkend
         X1 = (xllcorner + (cellsize * float(jj-1)))/1000.
         Y1 = (yllcorner + (cellsize * float(nrow - kk)))/1000.
         X2 = (xllcorner + (cellsize * float(jj)))/1000.
         Y2 = (yllcorner + (cellsize * float(nrow-kk+1)))/1000.

         mdptx =(X1+X2)/2
         mdpty =(Y1+Y2)/2

         if ((mdptx.lt.0).and.(X0.ge.0)) then
           xdist = abs((X1+X2)/2) + abs(X0)
         else if ((mdptx.ge.0).and.(X0.lt.0)) then
           xdist = abs((X1+X2)/2) + abs(X0)
         else
           xdist = abs((X1+X2)/2) - abs(X0)
         end if

         if ((mdpty.lt.0).and.(Y0.ge.0)) then
           ydist = abs((Y1+Y2)/2) + abs(Y0)
         else if ((mdpty.ge.0).and.(Y0.lt.0))then
           ydist = abs((Y1+Y2)/2) + abs(Y0)
         else
```

```
              ydist = abs((Y1+Y2)/2) - abs(Y0)
            end if

            if (sqrt(xdist**2+ydist**2).le.rad) then
              if (topogrid(kk,jj).le.-50000.) then
                Z1 = 0.0
                Z2= -1.*(topogrid(kk,jj)+ 50000.)/1000.
                Z3 = rootgrd(kk,jj)
                Z4 = compdpth

                call gbox(X0,Y0,Z0,X1,Y1,Z1,X2,Y2,Z2,rhosea,g1)
                call gbox(X0,Y0,Z0,X1,Y1,Z2,X2,Y2,Z3,rhockgm,g2)
                call gbox(X0,Y0,Z0,X1,Y1,Z3,X2,Y2,Z4,rhomankgm,g3)
                call gbox(X0,Y0,Z0,X1,Y1,Z1,X2,Y2,Z4,rhockgm,g4)
                g=g1+g2+g3-g4

                g1 = 0.0
                g2 = 0.0
                g3 = 0.0
                g4 = 0.0
              else if (((topogrid(kk,jj)).lt.0.).and.
     &                  ((topogrid(kk,jj)).gt.-50000.)) then
                Z1 = -1*(topogrid(kk,jj))/1000.
                Z2 = -1*(topogrid(kk,jj))/1000.
                Z3 = rootgrd(kk,jj)
                Z4 = compdpth

                call gbox(X0,Y0,Z0,X1,Y1,Z2,X2,Y2,Z3,rhockgm,g2)
                call gbox(X0,Y0,Z0,X1,Y1,Z3,X2,Y2,Z4,rhomankgm,g3)
                call gbox(X0,Y0,Z0,X1,Y1,Z1,X2,Y2,Z4,rhockgm,g4)
                g = g2+g3-g4
                g2 = 0.0
                g3 = 0.0
                g4 = 0.0

              else
                Z1 = compdpth
                Z2 = rootgrd(kk,jj)
                call gbox(X0,Y0,Z0,X1,Y1,Z1,X2,Y2,Z2,drhokgm,g)
              end if

              gravsum = gravsum + g

              g = 0

            else
              continue
            end if

400     continue

        airygrid(k,j) = gravsum
        gravsum = 0.0


91      format(2000f15.6)


300 continue
```

```
      open (13,file = airyfile, status = 'new')
c  write header for ascii grid output file
      write(13,15) label(1), ncol
      write(13,16) label(2), nrow
      write(13,25) label(3), xllcorner
      write(13,25) label(4), yllcorner
      write(13,25) label(5), cellsize
      write(13,35) label(6), inodat
      print*, ncol, nrow, xllcorner, yllcorner, inodat


      do k=1,nrow
        write(13,91) (airygrid(k,l),l=1,ncol)
      end do

      close(13)

      end

c*******************************************************
      subroutine topo2load(grid, ncol,nrow,rho,xnodat,ldgrd)
c      Grid starts out as topography (in meters)
c      It ends up as surface load (in g/cm**2)
c      Positive and negative elevations >50000. are
c       assumed to be on land.
c      Ocean depths must be flagged by adding -50000 to them
c      Assume density of seawater is in parameter statement

      real grid(2000,2000),ldgrd(2000,2000),load, m2cm
      parameter (m2cm=100., seawater=1.027)

      delrhosea = rho - seawater

      do 101 i=1,nrow
        do 101 j=1,ncol
          elev = grid(i,j)
          if(elev.eq.xnodat) then
            load = xnodat
          else if (elev.gt.-50000.) then
            load = elev*m2cm*rho
          else
            load = (elev+50000.)*m2cm*delrhosea
          end if
          ldgrd(i,j) = load
 101  continue
      return
      end

c*******************************************************
      subroutine load2root(ldgrd, ncol, nrow, compdpth,delrho,
     + xnodat,rootgrd)
c***   Grid starts out as the surface topographic load (g/cm**2),
c***   ends up as depth to airy isostatic root (km).
c***   compdpth = Positive depth to root for sealevel topo (km)
c***   delrho = density contrast at depth (g/cc) = rhomantle-rhocrust.

      real ldgrd(2000,2000),rootgrd(2000,2000)
      parameter (cm2km = 1.0e-5)
      do 201 ii=1,nrow
        do 201 jj=1,ncol
```

```
          if (ldgrd(ii,jj).eq.xnodat) then
            rtdepth = xnodat
            go to 200
          else
            rtdepth = compdpth + ldgrd(ii,jj) * cm2km/abs(delrho)
          end if
          if (rtdepth.lt.1.0) rtdepth = 1.0
  200     rootgrd(ii,jj) = rtdepth
  201 continue
      return
      end

*************************************************************
      subroutine gbox(x0,y0,z0,x1,y1,z1,x2,y2,z2,rho,g)
c
c  Subroutine GBOX computes the vertical attraction of a
c  rectangular prism.  Sides of prism are parallel to x,y,z axes,
c  and z axis is vertical down.
c
c  Input parameters:
c    Observation point is (x0,y0,z0).  The prism extends from x1
c    to x2, from y1 to y2, and from z1 to z2 in the x, y, and z
c    directions, respectively.  Density of prism is rho.  All
c    distance parameters in units of km; rho in units of
c    kg/(m**3).
c
c  Output parameters:
c    Vertical attraction of gravity, g, in mGal.
c
      real km2m
      dimension x(2),y(2),z(2),isign(2)
      data isign/-1,1/,gamma/6.670e-11/,twopi/6.2831853/,
     &     si2mg/1.0e5/,km2m/1.0e3/
      x(1) = x0-x1
      y(1) = y0-y1
      z(1) = z0-z1
      x(2) = x0-x2
      y(2) = y0-y2
      z(2) = z0-z2
      sum = 0.0
      do 1 i=1,2
        do 1 j=1,2
          do 1 k=1,2
            rijk = sqrt(x(i)**2+y(j)**2+z(k)**2)
            ijk = isign(i)*isign(j)*isign(k)
            arg1 = atan2((x(i)*y(j)),(z(k)*rijk))
            if (arg1.lt.0.) arg1=arg1+twopi
            arg2 = rijk+y(j)
            arg3 = rijk+x(i)
            if (arg2.le.0.) pause 'GBOX:  Bad field point'
            if (arg3.le.0.) pause 'GBOX:  Bad field point'
            arg2 = alog(arg2)
            arg3 = alog(arg3)
            sum = sum+ijk*(z(k)*arg1-x(i)*arg2-y(j)*arg3)
    1 continue
      g = rho*gamma*sum*si2mg*km2m
      return
      end
```

Listing A.4 program CEM

```
      program CEM
c  latest modification....Oct 8, 2007 (upward continued)
ccccccccccccccccccccccccccccccccccccccccccccccccccccccccccccccccccccccccc
c Correction values are for sea level elevation
c Topo map must have flagged (-50000 added) ocean values.
c  Values on land below sea level are not flagged.
c  by Linda Pickett Garinger with subroutines by Richard J. Blakely (from
c  Potential theory in Gravity and Magnetic Applications).  This program
c  reads gridded values of elevation and
c  calculates an isostatic correction using a modified Pratt-Hayford method.
c  It is a two layer model.  The uppermost layer is maintains a constant
c  density.  The depth of this layer is read from gridded values of moho
depth
c  provided by Walter Mooney. In this program the density of the second
layer
c  (mantle) will be calculated according to the topographic load. Then
c  the program uses these densities to calculate the vertical gravitational
c  attraction to 166.7 km.
c  This version uses the mohomap instead of calculating a root.

      real rad,compdpth,xllcorner,yllcorner
      real cellsize,xnodat,rhockgm,od,gravsum,g1sl,g2sl
         real deldpthsl, mohosl,mdptx,mdpty,mohosum
      real topogrid(2000,2000), moho(2000,2000),rhogrd(2000,2000)
      real lpggrid(2000,2000),deldpth(2000,2000)

      integer ncol,nrow,inodat,del
      character*50 topofile,label(8),notefile,rhofile,lpgfile
      character*50 statfile
c**********constants ******************
      print*, 'input crustal density in kg/m**3'
      read*, rhockgm
      print*,'input sea level mantle density kg/m**3'
      read*,rhomansl
c***compdpth is the compensation depth(km). Lithospheric density between
c***compdpth and moho will adjust according to topographic load.
      print*,'input compensation depth (km)'
      read*,compdpth

      rhosea = 1027.0
      rad = 166.7
      gravsum = 0.0
      counter = 0.0
      do i=1,2000
        do j=1,2000
          lpggrid(i,j)=0.0
        end do
      end do
c***crstdpth is the depth (km) of the first "layer" in the model.  Rho is
held
c***constant to this depth.
c***read moho depth grid
      open(14, file="moho821b.asc", status='old')
      read(14,15) label(1), ncol
      read(14,16) label(2), nrow
      read(14,25) label(3), xllcorner
      read(14,25) label(4), yllcorner
```

```
      read(14,25) label(5), cellsize
      read(14,35) label(6), inodat
      xnodat = float(inodat)
      do i=1,nrow
        read(14,*,end=44)(moho(i,j),j=1,ncol)
      end do
   44 continue



c********input topo acsii grid**************
c***this is an ascii grid.  Elevations are in m*****
      print*,'input gridascii topo file name'
      read(5,10) topofile
  10  format(a50)
      open(7,file=topofile, status='old')
      read(7,15) label(1), ncol
      read(7,16) label(2), nrow
      read(7,25) label(3), xllcorner
      read(7,25) label(4), yllcorner
      read(7,25) label(5), cellsize
      read(7,35) label(6), inodat
      xnodat = float(inodat)
   15 format(a14,i3)
   16 format(a14,i4)
   25 format(a14,f12.4)
   35 format(a14,i5)
      do i=1,nrow
        read(7,*,end=45)(topogrid(i,j),j=1,ncol)
      end do
   45 continue
      close(7)

c***calculate the deldpth grid
      do 60 j=1,ncol
        do 60 i=1,nrow
          deldpth(i,j) = compdpth - moho(i,j)
   60 continue
c calculate avg moho at sea level
      mohosum = 0.
      do 61 j=1,ncol
        do 61 i=1,ncol
          if (topogrid(i,j).le.-50000.) then
            odpt = -1. * (topogrid(i,j)+50000.)
          else
            go to 61
          end if

          if((odpt.le.100.).and.(odpt.ge.0.)) then
            mohosum = mohosum + moho(i,j)*1000.-odpt
            counter = counter + 1.
            print*, moho(i,j),odpt
          else
            go to 61
          end if
   61 continue
      mohosl = (mohosum/counter)/1000.
      print*, mohosl
      deldpthsl = compdpth - mohosl
c*****Calculate the density of column.....
```

```
      do 50 j = 1,ncol
        do 50 i = 1,nrow

          if (topogrid(i,j).le.-50000.) then
            od = -1.*(topogrid(i,j)+50000.)/1000.
            rhogrd(i,j) = (deldpthsl*rhomansl + rhockgm*(mohosl-
     +                    moho(i,j)+od) - (od*rhosea))/deldpth(i,j)
            go to 50

          else if (topogrid(i,j).gt.-50000.) then
            rhogrd(i,j) = (deldpthsl*rhomansl + (mohosl
     +                    -topogrid(i,j)/1000.-moho(i,j))*rhockgm)/
     +                    deldpth(i,j)

            go to 50

          else
            rhogrd(i,j) = xnodat

          end if

   50 continue

c****write the density grid****************
      print*, 'input density (rho) file name'
      read(5,10) rhofile
      open (9, file = rhofile,status = 'new')
c  write header for ascii grid output file
      write(9,15) label(1), ncol
      write(9,16) label(2), nrow
      write(9,25) label(3), xllcorner
      write(9,25) label(4), yllcorner
      write(9,25) label(5), cellsize
      write(9,35) label(6), inodat

      do 55 k=1,nrow
        write(9,56) (rhogrd(k,l),l=1,ncol)
   55 continue
   56 format(2000f12.3)
      close(9)

c****calculate the gravitational correction
      print*,'input note file name'
      read(5,10) notefile
      print*,'input status file name'
      read(5,10) statfile
      print*,'input isostatic correction file name'
      read(5,10) lpgfile
      open (12, file = notefile, status = 'new')
      open (13,file = lpgfile, status = 'new')
      write(12,*) 'run name:', lpgfile
      write(12,*) 'Two layer model, mohomap, variable mantle density'
      write(12,*) 'crustal density = ', rhockgm
      write(12,*) 'mantle density at sea level = ',rhomansl
      write(12,*) 'crustal depth = mohomap'
      write(12,*) 'compensation depth = ',compdpth
      close(12)
c  write header for ascii grid output file
      write(13,15) label(1), ncol
```

```
      write(13,16) label(2), nrow
      write(13,25) label(3), xllcorner
      write(13,25) label(4), yllcorner
      write(13,25) label(5), cellsize
      write(13,35) label(6), inodat

      del = int(175/(cellsize/1000.))
cXXXXXXXXXXXXXXXXXXXXXXXXXXXXXXXXXXXX

c loop through grid

      do 300 j=1,ncol
        open(8,file = statfile, status = 'unknown')
        write(8,*) j
        close(8)
        do 300 k=1,nrow

c leave out part of full grid

          if ((j.lt.50).or.(j.gt.(ncol-50))) then
            go to 299
          else if ((k.lt.50).or.(k.gt.(nrow-50))) then
            go to 299
          end if
c some constants!!!!************************************8888
          X0 = (xllcorner + (cellsize*(float(j)-.5)))/1000.
          Y0 = (yllcorner + (cellsize *(float(nrow-k)+.5)))/1000.
c "upward continued"
          if (topogrid(k,j).le.-50000.) then
            Z0 = 0.0
          else if((topogrid(k,j).le.0.).and.
     +            (topogrid(k,j).gt.-50000.)) then
            Z0 = -1.* (topogrid(k,j)/1000.)
          else
            Z0 = -1. * (topogrid(k,j)/1000.)
          end if

          Zsl = 0.0
          Zmsl = mohosl
          Zc = compdpth

c*****define the box to use for near calculations***********
          jjstart = j-del
          jjend = j+del
          kkstart = k-del
          kkend = k+ del
          if (jjstart.le.0) jjstart = 1
          if (jjend.gt.ncol) jjend = ncol
          if (kkstart.le.0) kkstart = 1
          if (kkend.gt.nrow) kkend = nrow
c*********************************************************************
*
          do 400 jj=jjstart, jjend
            do 400 kk=kkstart, kkend

              X1 = (xllcorner + (cellsize * float(jj-1)))/1000.
              Y1 = (yllcorner + (cellsize * float(nrow - kk)))/1000.
              X2 = (xllcorner + (cellsize * float(jj)))/1000.
              Y2 = (yllcorner + (cellsize * float(nrow-kk+1)))/1000.
```

```
              if (rhogrd(kk,jj).eq.xnodat) go to 400
              mdptx =(X1+X2)/2
              mdpty =(Y1+Y2)/2

              if ((mdptx.lt.0).and.(X0.ge.0)) then
                xdist = abs((X1+X2)/2) + abs(X0)
              else if ((mdptx.ge.0).and.(X0.lt.0)) then
                xdist = abs((X1+X2)/2) + abs(X0)
              else
                xdist = abs((X1+X2)/2) - abs(X0)
              end if

              if ((mdpty.lt.0).and.(Y0.ge.0)) then
                ydist = abs((Y1+Y2)/2) + abs(Y0)
              else if ((mdpty.ge.0).and.(Y0.lt.0))then
                ydist = abs((Y1+Y2)/2) + abs(Y0)
              else
                ydist = abs((Y1+Y2)/2) - abs(Y0)
              end if

c calculate the gravitational attraction

              if (sqrt(xdist**2+ydist**2).le.rad) then
c values for given sea level column:
                call gbox(X0,Y0,Z0,X1,Y1,Zsl,X2,Y2,Zmsl,rhockgm,g1sl)
                call gbox(X0,Y0,Z0,X1,Y1,Zmsl,X2,Y2,Zc,rhomansl,g2sl)

c oceanic conditions
                if (topogrid(kk,jj).le.-50000.) then

                  Z2 = (topogrid(kk,jj)+50000.)/(-1.*1000.)
                  Z3 = moho(kk,jj)
                  rhocalc = rhogrd(kk,jj)

c values for ocean column:
                  call gbox(X0,Y0,Z0,X1,Y1,Zsl,X2,Y2,Z2,rhosea,g1)
                  call gbox(X0,Y0,Z0,X1,Y1,Z2,X2,Y2,Z3,rhockgm,g2)
                  call gbox(X0,Y0,Z0,X1,Y1,Z3,X2,Y2,Zc,rhocalc,g3)
                  g = g1+g2+g3-g1sl-g2sl
c land values
                else if (topogrid(kk,jj).ge.0.) then
                  Z3 = moho(kk,jj)
                  rhocalc = rhogrd(kk,jj)
                  call gbox(X0,Y0,Z0,X1,Y1,Zsl,X2,Y2,Z3,rhockgm,gl1)
                  call gbox(X0,Y0,Z0,X1,Y1,Z3,X2,Y2,Zc,rhocalc,gl2)
                  g = gl1+gl2-g1sl-g2sl
c land below sea level
                else if ((topogrid(kk,jj).gt.-50000.).and.
     +                   (topogrid(kk,jj).lt.0.)) then
                  Z = topogrid(kk,jj)*(-1./1000.)
                  Z3 = moho(kk,jj)
                  rhocalc = rhogrd(kk,jj)
                  call gbox(X0,Y0,Z0,X1,Y1,Z,X2,Y2,Z3,rhockgm,gl1)
                  call gbox(X0,Y0,Z0,X1,Y1,Z3,X2,Y2,Zc,rhocalc,gl2)
                  g = gl1+gl2-g1sl-g2sl
                else
                  print*, "error"
                end if

                gravsum = gravsum + g
```

```
                g = 0.0
                g1 = 0.0
                g2 = 0.0
                g3 = 0.0
                g1sl = 0.0
                g2sl = 0.0
                gl1 = 0.0
                gl2 = 0.0

              else
                continue
              end if
  400     continue

          lpggrid(k,j) = gravsum

          gravsum = 0.0

  299     continue
  300 continue

c**********************************************************************
      do 303 k=1,nrow
        write(13,91) (lpggrid(k,l),l=1,ncol)
 91     format(2000f13.6)

  303 continue
      close(13)

      end

*************************************************************
      subroutine gbox(x0,y0,z0,x1,y1,z1,x2,y2,z2,rho,g)
c
c  Subroutine GBOX computes the vertical attraction of a
c  rectangular prism.  Sides of prism are parallel to x,y,z axes,
c  and z axis is vertical down.
c
c  Input parameters:
c    Observation point is (x0,y0,z0).  The prism extends from x1
c    to x2, from y1 to y2, and from z1 to z2 in the x, y, and z
c    directions, respectively.  Density of prism is rho.  All
c    distance parameters in units of km; rho in units of
c    kg/(m**3).
c
c  Output parameters:
c    Vertical attraction of gravity, g, in mGal.
c
      real km2m
      dimension x(2),y(2),z(2),isign(2)
      data isign/-1,1/,gamma/6.670e-11/,twopi/6.2831853/,
     &     si2mg/1.e5/,km2m/1.e3/
      x(1) = x0-x1
      y(1) = y0-y1
      z(1) = z0-z1
      x(2) = x0-x2
      y(2) = y0-y2
      z(2) = z0-z2
      sum=0.0
```

```
  do 1 i=1,2
    do 1 j=1,2
      do 1 k=1,2
        rijk = sqrt(x(i)**2+y(j)**2+z(k)**2)
        ijk = isign(i)*isign(j)*isign(k)
        arg1 = atan2((x(i)*y(j)),(z(k)*rijk))
        if (arg1.lt.0.) arg1=arg1+twopi
        arg2 = rijk+y(j)
        arg3 = rijk+x(i)
        if (arg2.le.0.) pause 'GBOX:  Bad field point'
        if (arg3.le.0.) pause 'GBOX:  Bad field point'
        arg2 = alog(arg2)
        arg3 = alog(arg3)
        sum = sum+ijk*(z(k)*arg1-x(i)*arg2-y(j)*arg3)
1 continue
  g = rho*gamma*sum*si2mg*km2m
  return
  end
```

Appendix B

Table B.1 NAVDAT entries (volcanics only) for Sierra Nevada, Basin and Range study area

Sample ID	Sample Num	Calc Age	Latitude	Longitude	GeoRef	Composition	Rock Name
KA 996	368842	9.9	37.304	-118.4869	1963-009923	mafic	basalt
KA 998	368843	9.8	37.124	-119.3957	1963-009923	mafic	basalt
KA 997	368844	3.6	37.3369	-119.0295	1963-009923	mafic	basalt
KA 988	368845	3.7	37.3976	-118.8882	1963-009923	mafic	basalt
KA 973	368846	2.7	37.5849	-118.8191	1963-009923	mafic	basalt
KA 1013	368847	3.3	37.5532	-118.6046	1963-009923	mafic	basalt
KA 968	368848	11.1	37.4134	-117.9632	1963-009923	mafic	basalt
KA 982	368849	11.2	37.4134	-117.9632	1963-009923	felsic	tuff
KA 305	368855	1.01	37.3	-118.4	1964-007048	felsic	tuff
KA 320	368856	1.01	37.3	-118.4	1964-007048	felsic	tuff
KA 321	368857	0.93	37.3	-118.4	1964-007048	felsic	tuff
KA 328	368858	0.94	37.3	-118.4	1964-007048	felsic	tuff
KA 414	368859	11.5	38.49	-118.9	1964-007048	felsic	tuff
KA 482	368866	10.78	38.49	-118.89	1964-007048	felsic	tuff
KA 482II	368867	11.5	38.49	-118.89	1964-007048	felsic	tuff
KA 500	368870	10.88	38.5	-118.9	1964-007048	felsic	tuff
KA 551	368871	11.09	38.49	-118.89	1964-007048	felsic	tuff
KA 552	368872	11.29	38.5	-118.9	1964-007048	felsic	tuff
KA 1134	368894	0.97	37.654	-119.055	1964-010952	mafic	basalt
KA 1013	368907	3.2	37.558	-118.596	1964-012355	mafic	basalt
KA 1268	368923	12.7	37.989	-117.865	1964-012355	felsic	tuff
KA 1070	368940	3.3	37.7558	-118.5824	1964-013614	mafic	basalt
KA 1071	368941	3.3	37.7552	-118.5824	1964-013614	mafic	basalt
KA 1092	368948	3.2	37.6094	-118.999	1964-013614	mafic	basalt

Table B.1 NAVDAT entries (volcanics only) for Sierra Nevada, Basin and Range study area (continued)

Sample ID	Sample Num	Calc Age	Latitude	Longitude	GeoRef	Composition	Rock Name
KA 1093	368949	3.9	37.375	-119.0833	1964-013614	mafic	basalt
KA 1103	368956	3.2	37.6803	-119.0554	1964-013614	mafic	basalt
KA 1135	368973	3.1	37.7134	-119.1	1964-013614	intermediate	latite
KA 1167	368975	0.38	37.6394	-119.0471	1964-013614	intermediate	latite
KA 1186	368976	3.6	37.5118	-119.1777	1964-013614	mafic	basalt
KA 1187	368977	3.4	37.5572	-119.1928	1964-013614	mafic	basalt
S21	369057	3.12	37.6161	-119.001	1966-000404	mafic	basalt
S22	369058	3.41	37.76	-118.5779	1966-000404	mafic	basalt
KA-1661	369176	11.8	37.9838	-118.7286	1968-058802	intermediate	latite
KA-1694	369177	10.6	37.9831	-118.7333	1968-058802	felsic	rhyolite
KA-1851	369178	3.4	38.0701	-118.7152	1968-058802	intermediate	latite
KA-1852	369179	11.9	38.0592	-118.5783	1968-058802	intermediate	latite
KA-1907	369180	10.1	38.1831	-119.0629	1968-058802	intermediate	latite
KA-1908	369181	9.9	38.2434	-118.9926	1968-058802	intermediate	latite
KA-1909	369182	9.8	38.2434	-118.9926	1968-058802	intermediate	latite
KA-1911	369183	11.6	38.0615	-118.4306	1968-058802	felsic	rhyolite
KA-1912	369184	2.8	38.1754	-118.8187	1968-058802	intermediate	latite
KA-1915	369185	11.7	38.121	-118.7745	1968-058802	intermediate	andesite
KA-1984	369186	3.5	38.2048	-118.8488	1968-058802	intermediate	andesite
KA-2004	369187	2.6	38.1865	-118.8202	1968-058802		vitrophyre
KA-2049	369189	9.5	38.154	-119.0884	1968-058802	intermediate	andesite
KA-1857	369190	6.4	38.1805	-118.8248	1968-058802	intermediate	andesite
KA-1859	369191	2.9	38.1762	-118.8191	1968-058802	intermediate	latite
KA-1906	369192	12	38.121	-118.7745	1968-058802	intermediate	andesite

Table B.1 NAVDAT entries (volcanics only) for Sierra Nevada, Basin and Range study area (continued)

Sample ID	Sample Num	Calc Age	Latitude	Longitude	GeoRef	Composition	Rock Name
KA-1972	369193	9.1	38.1922	-118.9783	1968-058802	intermediate	andesite
KA-1973	369194	8	38.1753	-119.194	1968-058802	intermediate	andesite
KA-1980	369195	3.3	38.1531	-119.0079	1968-058802	felsic	ignimbrite
KA-1990	369199	8.6	38.2348	-119.0881	1968-058802	intermediate	andesite
KA-1993	369200	2.4	38.2048	-118.8488	1968-058802		not-given
KA-1998	369201	9.8	38.154	-119.0884	1968-058802	intermediate	andesite
KA-1999	369202	1	38.174	-118.8337	1968-058802	felsic	ignimbrite
KA2002	369204	2.6	38.1865	-118.8202	1968-058802	intermediate	andesite
KA-2003	369205	2.8	38.1801	-118.8279	1968-058802	intermediate	andesite
KA-2048	369206	12.8	38.2533	-118.9143	1968-058802	intermediate	andesite
KA-2076	369207	3.7	38.1816	-118.8928	1968-058802	felsic	tuff
KA-1813	369208	3.6	38.1888	-118.7123	1968-058802	intermediate	latite
KA-1850	369209	3.5	38.1782	-118.7396	1968-058802	intermediate	latite
KA-1855	369210	11.5	38.1131	-118.7733	1968-058802	intermediate	latite
KA-1856	369211	11.4	38.1131	-118.7733	1968-058802	intermediate	latite
KA-1860	369212	11.5	38.0676	-118.5637	1968-058802	intermediate	latite
KA-1916	369213	11.6	38.0591	-118.6688	1968-058802	felsic	vitrophere
KA-2045	369218	12.2	37.9396	-118.9397	1968-058802	felsic	ignimbrite
KA-2066	369220	3.7	38.2447	-118.9449	1968-058802	felsic	rhyolite
KA-2081	369222	0.9	37.7816	-118.6871	1968-058802	mafic	basalt
KA-1811	369223	4.3	38.0654	-118.8064	1968-058802	mafic	basalt
KA-1866	369224	4.6	38.1711	-118.6946	1968-058802	mafic	basalt
KA-1867	369225	3.8	38.1777	-118.7375	1968-058802	mafic	basalt
KA-1876	369226	4	38.1844	-118.6995	1968-058802	mafic	basalt

Table B.1 NAVDAT entries (volcanics only) for Sierra Nevada, Basin and Range study area (continued)

Sample ID	Sample Num	Calc Age	Latitude	Longitude	GeoRef	Composition	Rock Name
KA-2015	369227	3.2	38.0361	-118.5385	1968-058802	mafic	basalt
KA-2016	369228	2.8	38.0361	-118.5385	1968-058802	mafic	basalt
KA-2086	369229	2.9	38.2596	-118.9508	1968-058802	mafic	basalt
KA-2089	369230	1.6	38.2348	-118.8216	1968-058802	mafic	basalt
KA-1693	369231	11.5	37.9838	-118.7286	1968-058802	intermediate	latite
5G201	369271	0.0071	37.8131	-119.0325	1968-062978	felsic	rhyolite
6G005	369272	0.0089	37.8139	-119.0297	1968-062978	felsic	rhyolite
5G202	369273	0.0063	37.8192	-119.0247	1968-062978	felsic	rhyolite
5G204	369275	0.0065	37.8253	-119.015	1968-062978	felsic	rhyolite
6G007	369277	0.0127	37.8244	-119.0186	1968-062978	felsic	rhyolite
6G008	369278	0.0127	37.8331	-119.0097	1968-062978	felsic	rhyolite
6G016	369280	0.0107	37.8778	-119.0019	1968-062978	felsic	rhyolite
USGSM-711-67	370420	13.9	38.2894	-118.9092	1973-004168	intermediate	andesite
USGSM-668-G10	370421	14.8	38.2403	-118.8917	1973-004168	intermediate	andesite
USGSM-711-8	370422	15.8	38.2681	-118.8917	1973-004168	intermediate	diorite
KA2048	370423	12.8	38.2522	-118.9175	1973-004168	intermediate	andesite
USGSM-712-1	370424	11.9	38.2522	-118.9175	1973-004168	intermediate	diorite
USGSM-710-7	370425	11.5	38.2822	-118.9281	1973-004168	felsic	rhyolite
USGSM-NTS10B	370426	11.3	38.3011	-118.8967	1973-004168	felsic	rhyolite
USGSM-670G4	370428	2.6	38.2811	-118.8842	1973-004168	felsic	rhyolite
USGSM-610-1B	370429	2.8	38.2778	-118.8586	1973-004168	intermediate	andesite
USGSM-672-2	370430	0.26	38.3128	-118.8825	1973-004168	intermediate	basaltic-andesite
USGSM-611-5	370431	2.3	38.2578	-118.8558	1973-004168	intermediate	andesite
KA2089	370432	1.6	38.2392	-118.8264	1973-004168	mafic	basalt

Table B.1 NAVDAT entries (volcanics only) for Sierra Nevada, Basin and Range study area (continued)

Sample ID	Sample Num	Calc Age	Latitude	Longitude	GeoRef	Composition	Rock Name
KA2066	370433	3.7	38.2561	-118.8086	1973-004168	felsic	rhyolite
KA2003	370434	2.8	38.1783	-118.82	1973-004168	intermediate	andesite
KA1859	370435	2.9	38.1783	-118.82	1973-004168	intermediate	andesite
KA1912	370436	2.8	38.1783	-118.82	1973-004168	felsic	pyroclastic-fall
W19 , no. 1	370437	3.41	38.1897	-118.7122	1973-004168	intermediate	latite
W19 , no. 2	370438	3.28	38.1897	-118.7122	1973-004168	intermediate	latite
KA1813	370439	3.6	38.1897	-118.7122	1973-004168	intermediate	latite
W20	370440	3.87	38.1919	-118.715	1973-004168	intermediate	andesite
KA1850	370441	3.5	38.1778	-118.7467	1973-004168	felsic	pyroclastic fall
W21	370442	3.59	38.19	-118.7133	1973-004168	mafic	basalt
KA1867	370443	3.8	38.1775	-118.7361	1973-004168	mafic	basalt
KA1876	370444	4	38.1825	-118.6992	1973-004168	mafic	basalt
KA1866	370445	4.6	38.1672	-118.7031	1973-004168	mafic	basalt
KA2016	370446	2.8	38.0714	-118.5633	1973-004168	mafic	basalt
KA2015	370447	3.2	38.0461	-118.5294	1973-004168	mafic	basalt
W23	370448	9.77	38.1761	-118.7428	1973-004168	felsic	pyroclastic-fall
KA1852	370449	11.9	38.0725	-118.6036	1973-004168	felsic	pyroclastic flow
KA1916 , 1918	370450	11.6	38.0756	-118.6031	1973-004168	felsic	pyroclastic flow
KA1860	370451	11.5	38.0806	-118.5897	1973-004168	felsic	pyroclastic flow
KA1911	370452	11.6	38.1122	-118.7289	1973-004168	felsic	pyroclastic flow
KA552	370455	11.3	38.4833	-118.9	1973-004168	felsic	rhyolite
KA414	370456	11.5	38.4925	-118.9042	1973-004168	felsic	rhyolite
KA482 , 482II	370457	11.1	38.4933	-118.91	1973-004168	felsic	rhyolite
KA500	370458	10.9	38.4917	-118.9042	1973-004168	felsic	rhyolite

Table B.1 NAVDAT entries (volcanics only) for Sierra Nevada, Basin and Range study area (continued)

Sample ID	Sample Num	Calc Age	Latitude	Longitude	GeoRef	Composition	Rock Name
KA551	370459	11.1	38.4933	-118.91	1973-004168	felsic	pyroclastic-flow
KA485	370460	9.5	38.8167	-119.2333	1973-004168	felsic	pyroclastic-fall
KA480	370464	11.4	37.9333	-118.0833	1973-004168	felsic	pyroclastic-flow
KA499	370465	11.7	37.9333	-118.0833	1973-004168	felsic	pyroclastic-fall
Gilbert	370466	15.5	38.0833	-117.7	1973-004168	intermediate	andesite
KA577	370467	11.8	38.5333	-117.75	1973-004168	felsic	rhyolite
KA452	370468	11	38.5333	-117.75	1973-004168	felsic	pyroclastic-fall
KA1268	370470	13	38	-117.85	1973-004168	felsic	pyroclastic-fall
6	370472	6.2	37.8	-117.8333	1973-004168	felsic	rhyolite
7	370473	4.9	37.7167	-118.0333	1973-004168	mafic	basalt
8	370474	6.1	37.7	-117.75	1973-004168	felsic	pyroclastic flow
5	370475	6.3	37.65	-117.8167	1973-004168	felsic	pyroclastic flow
13	370476	7.1	37.85	-117.6333	1973-004168	felsic	pyroclastic fall
Pigeon Spring	370477	4.6	37.4167	-117.6667	1973-004168	felsic	pyroclastic flow
G-B0642/NBM-AD13	370188	11.6	38.8633	-117.905	1972-010381	intermediate	granodiorite
USGSM-BH15	370319	8.9	38.2025	-119.009	1972-022655	felsic	dacite
USGSM-S1	370320	8.8	38.188	-119.0084	1972-022655	felsic	dacite
USGSM-B271	370321	8.7	38.2152	-119.0017	1972-022655	felsic	dacite
USGSM-856-8	370322	8.4	38.2152	-119.0017	1972-022655	felsic	dacite
USGSM-BH17	370323	9.4	38.1914	-119.0079	1972-022655	felsic	dacite
USGSM-7346-1	370324	2.8	38.2167	-118.9799	1972-022655	intermediate	andesite
USGSM-BH32	370325	9	38.1928	-119.0022	1972-022655	felsic	dacite
USGSM-856-32	370326	9.1	38.2055	-118.9967	1972-022655	felsic	dacite
USGSM-856-10	370327	9.1	38.2022	-119.029	1972-022655	felsic	rhyodacite

Table B.1 NAVDAT entries (volcanics only) for Sierra Nevada, Basin and Range study area (continued)

Sample ID	Sample Num	Calc Age	Latitude	Longitude	GeoRef	Composition	Rock Name
USGSM-BH26	370328	9.3	38.1948	-119.0065	1972-022655	felsic	dacite
USGSM-BH16	370329	9.7	38.2019	-118.9972	1972-022655	felsic	dacite
USGSM-854-1	370330	8.9	38.181	-119.003	1972-022655	felsic	dacite
USGSM-BH29	370331	8.9	38.1953	-118.9617	1972-022655	felsic	dacite
USGSM-BM2	370332	9.3	38.2204	-119.0577	1972-022655	felsic	dacite
USGSM-BH9	370333	9.5	38.1517	-119.1179	1972-022655	mafic	basalt
USGSM-MTB1	370334	9.8	38.1443	-119.0718	1972-022655	intermediate	andesite
USGSM-BH27	370335	9.3	38.137	-119.0526	1972-022655	felsic	rhyolite
USGSM-BH19A	370336	8.2	38.2202	-119.1726	1972-022655	felsic	dacite
USGSM-BH6	370337	5.9	38.1651	-119.1505	1972-022655	felsic	rhyolite
USGSM-BH20	370338	5.3	38.2198	-119.1476	1972-022655	felsic	rhyodacite
TBQob-1	454075	0.9	37.62	-119.0917	1997-021098	mafic	alkali basalt
TBQob-2	454076	0.9	37.6192	-119.0917	1997-021098	mafic	alkali basalt
HLQpb	454077	0.9	37.6125	-119.02	1997-021098	mafic	alkali basalt
TFQpb	454078	0.9	37.6117	-119.0083	1997-021098	mafic	alkali basalt
PBQa	454079	0.22	37.57	-119.05	1997-021098	mafic	alkali basalt
PBQa-2	454080	0.22	37.5633	-119.0583	1997-021098	mafic	alkali basalt
PBQa-3	454081	0.22	37.56	-119.0617	1997-021098	mafic	alkali basalt
RMQa	454082	0.22	37.6083	-119.0717	1997-021098	mafic	alkali basalt
MMQpb	454083	0.22	37.6583	-119.0317	1997-021098	mafic	alkali basalt
DCQgb-1	454084	0.22	37.6983	-118.9567	1997-021098	mafic	alkali basalt
DPQpb	454085	0.22	37.6383	-119.0783	1997-021098	mafic	alkali basalt
JLQa	454086	0.22	37.8267	-119.0683	1997-021098	mafic	alkali basalt
BSQpb	454087	0.22	37.75	-118.9417	1997-021098	mafic	alkali basalt

Table B.1 NAVDAT entries (volcanics only) for Sierra Nevada, Basin and Range study area (continued)

Sample ID	Sample Num	Calc Age	Latitude	Longitude	GeoRef	Composition	Rock Name
LMQa-1	454088	0.22	37.72	-118.9583	1997-021098	mafic	alkali basalt
LMQa-3	454089	0.22	37.753	-118.9567	1997-021098	mafic	alkali basalt
HCQpb	454090	0.22	37.735	-118.8733	1997-021098	mafic	alkali basalt
MLQab	454091	0.22	37.6383	-118.9383	1997-021098	mafic	alkali basalt
LVQpb	454092	0.22	37.745	-118.8683	1997-021098	mafic	alkali basalt
DCQab	454093	0.22	37.7467	-118.9817	1997-021098	mafic	alkali basalt
DPQaq	454094	1.8	37.615	-119.0767	1997-021098	felsic	rhyodacite
RCQyb-1	454095	0.013	37.5917	-119.0583	1997-021098	mafic	basalt
RCQyb-2	454096	0.013	37.5883	-119.0617	1997-021098	mafic	basalt
BPQyb	454097	0.013	38.0333	-119.1	1997-021098	mafic	basalt
MSTba	454098	2.9	37.8	-118.8383	1997-021098	mafic	basalt
WCTba	454099	2.9	37.7233	-118.6033	1997-021098	mafic	basalt
GSTba	454100	2.9	37.8917	-118.8467	1997-021098	mafic	basalt
Black Balls	371458	7.2	38.2314	-117.6058	1976-029758		not-given
GL-2	371459	14	37.1328	-117.7081	1976-029758	intermediate	andesite
73.8	454105	0.22	37.75	-119	1997-021098	mafic	basalt
127.8	454106	0.22	37.75	-119	1997-021098	mafic	basalt
405.8	454107	0.22	37.75	-119	1997-021098	mafic	basalt
503.4	454108	0.22	37.75	-119	1997-021098	mafic	basalt
527	454109	0.22	37.75	-119	1997-021098	mafic	basalt
540.4	454110	0.22	37.75	-119	1997-021098	mafic	basalt
686.8	454111	0.22	37.75	-119	1997-021098	mafic	basalt
883.3	454112	0.22	37.75	-119	1997-021098	mafic	basalt
2123.5	454113	0.22	37.75	-119	1997-021098	mafic	basalt

Table B.1 NAVDAT entries (volcanics only) for Sierra Nevada, Basin and Range study area (continued)

Sample ID	Sample Num	Calc Age	Latitude	Longitude	GeoRef	Composition	Rock Name
2130.4	454114	0.22	37.75	-119	1997-021098	mafic	basalt
2159.1	454115	0.22	37.75	-119	1997-021098	mafic	basalt
2209	454116	0.22	37.75	-119	1997-021098	mafic	basalt
BP83-1	454117	0.02	37.5917	-119.0583	1997-021098	mafic	basalt
JLB-1	454118	0.0138	37.75	-118.9417	1997-021098	mafic	basalt
D85-56	454119	0.013	37.5917	-119.0583	1997-021098	mafic	basalt
SSQab	454120	0.22	37.75	-118.9417	1997-021098	mafic	basalt
F-36	437020	10.75	38.4142	-119.3451	1978-010575	felsic	rhyolite
F-38	437021	9.65	38.3999	-119.3629	1978-010575	felsic	rhyolite
F-40	437022	9.65	38.3966	-119.3265	1978-010575	intermediate	andesite
F-49	437023	9.65	38.3759	-119.447	1978-010575	intermediate	latite
F-55	437026	9.65	38.3204	-119.4382	1978-010575	intermediate	andesite
F-58	437028	9.65	38.237	-119.4845	1978-010575	intermediate	latite
F-61	437030	9.65	38.2585	-119.4024	1978-010575	intermediate	latite
F-65	437032	9.65	38.2948	-119.3489	1978-010575	intermediate	andesite
F-67	437033	9.65	38.311	-119.347	1978-010575	intermediate	latite
F-68	437034	9.65	38.3127	-119.3523	1978-010575	intermediate	andesite
F-69-1	437035	9.65	38.4199	-119.4471	1978-010575	felsic	pyroclastic fall
F-69-b	437036	9.65	38.4301	-119.4487	1978-010575	felsic	tuff
F-69-t	437037	9.65	38.4301	-119.4487	1978-010575	felsic	tuff
F-72	437038	9.65	38.4181	-119.4326	1978-010575	felsic	pyroclastic fall
F-73	437039	9.65	38.2964	-119.3718	1978-010575	intermediate	andesite
F-74	437040	9.65	38.2918	-119.3692	1978-010575	intermediate	andesite
F-76	437041	10.75	38.4499	-119.3275	1978-010575	intermediate	andesite

Table B.1 NAVDAT entries (volcanics only) for Sierra Nevada, Basin and Range study area (continued)

Sample ID	Sample Num	Calc Age	Latitude	Longitude	GeoRef	Composition	Rock Name
F-78	437042	10.75	38.4394	-119.3069	1978-010575	felsic	rhyolite
F-79	437043	10.75	38.4348	-119.3233	1978-010575	felsic	rhyolite
F-80	437044	10.75	38.4497	-119.3307	1978-010575	intermediate	andesite
F-81	437045	8.75	38.2839	-119.4847	1978-010575	intermediate	andesite
GM-9	437046	9.75	37.9845	-118.726	1978-010575	intermediate	latite
GM-10	437047	3.55	37.976	-118.657	1978-010575	intermediate	andesite
GM-12	437048	3.55	37.9814	-118.6533	1978-010575	mafic	basalt
GM-14	437049	3.55	37.99	-118.6609	1978-010575	mafic	basalt
GM-15	437050	3.55	37.9903	-118.6577	1978-010575	mafic	basalt
GM-16	437051	3.55	37.9818	-118.5229	1978-010575	mafic	basalt
GM-20	437052	3.55	37.9822	-118.5524	1978-010575	mafic	basalt
GM-22	437053	3.55	37.9773	-118.5545	1978-010575	mafic	basalt
HV-1	437054	11.5	38.0033	-118.541	1978-010575	mafic	basalt
HV-2	437055	11.9	38.185	-118.7192	1978-010575	intermediate	andesite
HV-4	437056	11.9	38.1857	-118.7285	1978-010575	intermediate	latite
HV-7	437057	11.9	38.2002	-118.708	1978-010575	intermediate	latite
HV-9	437058	11.9	38.2139	-118.731	1978-010575	intermediate	latite
HV-10	437059	11.9	38.2115	-118.744	1978-010575	intermediate	latite
HV-11	437060	11.5	38.0907	-118.7369	1978-010575	felsic	pyroclastic fall
HV-12	437061	11.5	38.0907	-118.7369	1978-010575	felsic	pyroclastic fall
HV-13	437062	11.5	38.0967	-118.7366	1978-010575	intermediate	latite
B-88	371164	0.76	37.4699	-118.3705	1989-073447	felsic	tuff
B-107	371165	0.76	37.4512	-118.3981	1989-073447	felsic	rhyolite
B-72	371166	0.76	37.8744	-118.9255	1989-073447	felsic	tuff

Table B.1 NAVDAT entries (volcanics only) for Sierra Nevada, Basin and Range study area (continued)

Sample ID	Sample Num	Calc Age	Latitude	Longitude	GeoRef	Composition	Rock Name
B-78	371167	0.76	37.8616	-119.0752	1989-073447	felsic	tuff
B-77	371168	0.76	37.8609	-119.0751	1989-073447	felsic	tuff
B-48	371169	0.76	37.4135	-118.5232	1989-073447	felsic	rhyolite
B-52	371170	0.76	37.515	-118.6323	1989-073447	felsic	rhyolite
B-69	371171	0.76	37.8043	-118.7965	1989-073447	felsic	tuff
B-75	371172	0.76	37.7819	-118.9203	1989-073447	felsic	rhyolite
B-79	371173	0.76	37.8695	-119.077	1989-073447	felsic	vitrophere
B-83	371174	0.76	37.4017	-118.4803	1989-073447		
B-81	371175	0.76	37.513	-118.6118	1989-073447	felsic	vitrophere
B-104	371176	0.76	37.7446	-118.4552	1989-073447		
B-105	371177	0.76	37.7446	-118.4552	1989-073447	felsic	tuff
B-111	371178	0.76	37.5946	-119.078	1989-073447	felsic	vitrophere
B-136	371179	0.76	37.8369	-118.7941	1989-073447		
B-143	371180	0.76	37.6023	-119.0961	1989-073447	felsic	vitrophere
B-93	371181	0.76	37.5463	-118.593	1989-073447		
B-94	371182	0.76	37.5463	-118.593	1989-073447		
B-109	371183	0.76	37.4509	-118.3987	1989-073447	felsic	tuff
B-108	371184	0.76	37.451	-118.3984	1989-073447	felsic	tuff
B-138	371185	0.76	37.8343	-118.7368	1989-073447	felsic	rhyolite
B-14	371186	0.76	37.4327	-118.4022	1989-073447	felsic	rhyolite
B-20	371187	0.76	37.4116	-118.4813	1989-073447	felsic	rhyolite
B-70	371188	0.76	37.8588	-118.7492	1989-073447	felsic	rhyolite
B-73	371189	0.76	37.7838	-118.9245	1989-073447	felsic	rhyolite
B-87	371190	0.76	37.4699	-118.3705	1989-073447	felsic	rhyolite

Table B.1 NAVDAT entries (volcanics only) for Sierra Nevada, Basin and Range study area (continued)

Sample ID	Sample Num	Calc Age	Latitude	Longitude	GeoRef	Composition	Rock Name
B-95	371191	0.76	37.5463	-118.593	1989-073447	felsic	rhyolite
B-98	371192	0.76	37.7899	-118.5329	1989-073447	felsic	rhyolite
B-103	371193	0.76	37.7985	-118.5283	1989-073447	felsic	rhyolite
B-110	371194	0.76	37.5434	-118.3309	1989-073447	felsic	rhyolite
B-112	371195	0.76	37.6284	-119.0717	1989-073447	felsic	rhyolite
B-120	371196	0.76	37.4599	-118.3953	1989-073447	felsic	rhyolite
B-128	371197	0.76	37.6188	-119.0699	1989-073447	felsic	rhyolite
B-129	371198	0.76	37.6194	-119.0717	1989-073447	felsic	rhyolite
B-135	371199	0.76	37.8308	-118.7826	1989-073447	felsic	rhyolite
B-140	371200	0.76	37.6306	-118.5257	1989-073447	felsic	rhyolite
B-141	371201	0.76	37.6023	-119.0961	1989-073447	felsic	vitrophere
B-131	371202	0.76	37.6459	-118.671	1989-073447		
B-132	371203	0.76	37.6459	-118.671	1989-073447		
B-85	371204	0.76	37.6459	-118.671	1989-073447		
B-96	371205	0.76	37.6459	-118.671	1989-073447		
B-91	371206	0.76	37.6459	-118.671	1989-073447		
B-116	371207	0.76	37.6459	-118.671	1989-073447		
USGS-D2391R	372201	2.8	38.1575	-118.0817	1977-900002	mafic	basalt
USGS-D2392R	372202	2.9	38.1631	-118.05	1977-900002	mafic	basalt
USGS-D2390R	372204	15.7	38.1444	-118.0922	1977-900002	intermediate	andesite
SW-1	372227	14.8	38.7333	-119.3583	1977-900034	intermediate	andesite
OP-1	372229	11	38.8638	-119.4987	1977-900034	felsic	dacite
2605-5	372236	15.4	38.6433	-118.175	1977-900034	intermediate	andesite
11920-2	372237	15.4	38.5367	-117.9633	1977-900034	intermediate	andesite

Table B.1 NAVDAT entries (volcanics only) for Sierra Nevada, Basin and Range study area (continued)

Sample ID	Sample Num	Calc Age	Latitude	Longitude	GeoRef	Composition	Rock Name
HV-14	437063	11.5	38.0967	-118.7366	1978-010575	intermediate	latite
HV-17	437064	11.5	38.0814	-118.5852	1978-010575	intermediate	latite
HV-19	437065	11.5	38.0821	-118.5814	1978-010575	intermediate	latite
HV-21	437066	11.5	38.0797	-118.5973	1978-010575	intermediate	latite
HV-22	437067	11.5	38.1621	-118.6474	1978-010575	mafic	basalt
HV-23	437068	11.5	38.1664	-118.6493	1978-010575	mafic	basalt
HV-24	437069	11.5	38.1692	-118.6475	1978-010575	mafic	basalt
HV-26	437070	11.5	38.1733	-118.6466	1978-010575	mafic	basalt
HV-27	437071	11.5	38.1766	-118.6427	1978-010575	mafic	basalt
HV-28	437072	11.9	38.1916	-118.651	1978-010575	intermediate	andesite
HV-30	437073	11.9	38.1908	-118.6533	1978-010575	intermediate	andesite
HV-31	437074	11.5	38.1906	-118.6543	1978-010575	intermediate	andesite
HV-33	437075	11.5	38.1906	-118.6548	1978-010575	intermediate	andesite
PP-6A	437076	3.55	37.7299	-119.1363	1978-010575	mafic	basalt
PP-6C	437077	3.55	37.7299	-119.1363	1978-010575	mafic	basalt
7TABLE 1	437106	0.9	37.4111	-118.4692	1980-045824		not-given
8TABLE 1	437107	5.28	37.9425	-118.5689	1980-045824		not-given
8TABLE 1	437108	3.2	37.9425	-118.5689	1980-045824		not-given
4TABLE 6	437109	5.1	37.9425	-118.5689	1980-045824		not-given
C-1	437146	9.4	37.8967	-119.405	1982-017260	mafic	basalt
C-2	437147	9.4	37.8967	-119.405	1982-017260	mafic	basalt
C-3	437148	9.4	37.8967	-119.405	1982-017260	mafic	basalt
D-1	437149	3.1	37.85	-119.0167	1982-017260	felsic	rhyolite
CAN-2	371461	4	38.1542	-118.0833	1976-029758	mafic	basalt

Table B.1 NAVDAT entries (volcanics only) for Sierra Nevada, Basin and Range study area (continued)

Sample ID	Sample Num	Calc Age	Latitude	Longitude	GeoRef	Composition	Rock Name
2701-2	371462	8.7	38.515	-118.4667	1976-029758	mafic	basalt
CD-8	371467	15.4	38.3408	-118.2005	1976-029758		alteration
BPQ-1	436985	10.75	38.4229	-119.2118	1978-010575	felsic	rhyolite
CD-1	436987	3.55	37.5724	-118.6109	1978-010575	intermediate	latite
CT-6	436988	6	37.7778	-118.8879	1978-010575	intermediate	andesite
CT-8a	436989	3.55	37.7816	-118.8551	1978-010575	mafic	basalt
CT-8d	436990	3.55	37.7816	-118.8551	1978-010575	intermediate	andesite
CT-8g	436991	3.55	37.7821	-118.9445	1978-010575	intermediate	andesite
CT-13	436992	11.9	37.99	-118.8121	1978-010575	intermediate	andesite
F-1	437000	9.65	38.3068	-119.3821	1978-010575	intermediate	andesite
F-2	437001	9.65	38.3071	-119.3759	1978-010575	intermediate	latite
F-4	437003	9.65	38.2835	-119.3922	1978-010575	intermediate	andesite
F-6	437004	9.65	38.2776	-119.3957	1978-010575	intermediate	andesite
F-10	437005	9.65	38.4266	-119.3993	1978-010575	intermediate	andesite
F-12	437006	9.65	38.3258	-119.3937	1978-010575	intermediate	andesite
F-13	437007	10.7	38.3483	-119.3769	1978-010575	intermediate	andesite
F-14	437008	9.65	38.3368	-119.3777	1978-010575	felsic	tuff
F-22	437011	9.65	38.3555	-119.3769	1978-010575	intermediate	latite
F-23	437012	9.65	38.2687	-119.377	1978-010575	intermediate	andesite
F-24	437013	9.65	38.2613	-119.367	1978-010575	intermediate	latite
F-26	437014	9.75	38.2879	-119.3059	1978-010575	felsic	pyroclastic fall
F-27	437015	9.75	38.2872	-119.3152	1978-010575	felsic	pyroclastic fall
F-28	437016	9.65	38.2532	-119.3909	1978-010575	intermediate	latite
F-30	437017	9.65	38.2534	-119.3968	1978-010575	intermediate	latite

Table B.1 NAVDAT entries (volcanics only) for Sierra Nevada, Basin and Range study area (continued)

Sample ID	Sample Num	Calc Age	Latitude	Longitude	GeoRef	Composition	Rock Name
F-34	437018	9.65	38.3821	-119.3348	1978-010575	intermediate	andesite
F-35	437019	9.65	38.3635	-119.3472	1978-010575	felsic	rhyolite
D-106	371803	8.9	38.308	-119.375	1977-007325	mafic	basalt
F-167	371805	8.9	38.2863	-119.325	1977-007325	mafic	basalt
F-172	371806	8.9	38.2758	-119.3374	1977-007325	intermediate	andesite
TML-1	371819	8.9	38.2513	-119.3999	1977-007325	intermediate	latite
177-2	371821	8.9	38.2527	-119.3965	1977-007325	intermediate	latite
177-4	371823	8.9	38.2539	-119.3974	1977-007325	intermediate	latite
177-5	371824	8.9	38.2539	-119.3974	1977-007325	intermediate	latite
TML-6	371826	8.9	38.2906	-119.3494	1977-007325	intermediate	latite
F-330	371828	8.9	38.2747	-119.3654	1977-007325	intermediate	latite
F329	371830	8.9	38.2699	-119.3646	1977-007325	intermediate	latite
D-180	371831	8.9	38.27	-119.366	1977-007325	intermediate	latite
F-316	371832	8.9	38.27	-119.366	1977-007325	intermediate	latite
177-7	371833	8.9	38.2545	-119.3997	1977-007325	intermediate	latite
177-8	371834	8.9	38.2545	-119.3997	1977-007325	intermediate	latite
F-293	371835	8.9	38.2567	-119.4058	1977-007325	intermediate	latite
F-10	371836	8.9	38.3731	-119.3732	1977-007325	intermediate	latite
F-69-1	371837	8.9	38.374	-119.41	1977-007325	intermediate	latite
C-82-1	371838	8.9	38.3761	-119.447	1977-007325	intermediate	latite
C-82-2	371839	8.9	38.3761	-119.447	1977-007325	intermediate	latite
F-212	371840	8.9	38.374	-119.41	1977-007325	intermediate	latite
F-41	371841	8.9	38.2647	-119.3815	1977-007325	intermediate	latite
F-319	371842	8.9	38.2763	-119.3711	1977-007325	intermediate	latite

Table B.1 NAVDAT entries (volcanics only) for Sierra Nevada, Basin and Range study area (continued)

Sample ID	Sample Num	Calc Age	Latitude	Longitude	GeoRef	Composition	Rock Name
F-320	371843	8.9	38.277	-119.3733	1977-007325	intermediate	latite
F-70	371844	8.9	38.3976	-119.3633	1977-007325	intermediate	latite
THF	371845	8.9	38.332	-119.382	1977-007325	intermediate	latite
F-317	371846	8.9	38.2707	-119.3687	1977-007325	intermediate	latite
BD	371847	8.9	38.2707	-119.3687	1977-007325	intermediate	latite
RHV	371848	8.9	38.3399	-119.3874	1977-007325	intermediate	latite
D-77	371849	8.9	38.3234	-119.4093	1977-007325	intermediate	latite
F-351	371850	8.9	38.332	-119.382	1977-007325	intermediate	latite
D-1	371856	9.5	38.3255	-119.3876	1977-007325	intermediate	latite
D-12	371857	9.5	38.3461	-119.3819	1977-007325	intermediate	latite
N-41	371858	9.5	38.3235	-119.385	1977-007325	intermediate	latite
D-74	371859	9.5	38.3168	-119.3855	1977-007325	intermediate	latite
D-289	371860	9.5	38.3108	-119.3644	1977-007325	intermediate	latite
LW-37	371861	8.1	38.2942	-119.3844	1977-007325	intermediate	latite
D-44	371862	8.1	38.3235	-119.3235	1977-007325	intermediate	latite
D-71	371863	8.1	38.3168	-119.3895	1977-007325	intermediate	latite
D-91	371864	8.1	38.3173	-119.4228	1977-007325	intermediate	latite
D-112	371865	8.1	38.3092	-119.3827	1977-007325	intermediate	latite
D-112-2	371866	8.1	38.3128	-119.3829	1977-007325	intermediate	latite
D-240	371867	8.1	38.3181	-119.4251	1977-007325	intermediate	latite
F-99	371868	8.1	38.3048	-119.3898	1977-007325	intermediate	latite
F-265-2	371869	8.1	38.2596	-119.4138	1977-007325	intermediate	latite
F-297	371870	8.1	38.2795	-119.4043	1977-007325	intermediate	latite
F-300	371871	8.1	38.2801	-119.4035	1977-007325	intermediate	latite

Table B.1 NAVDAT entries (volcanics only) for Sierra Nevada, Basin and Range study area (continued)

Sample ID	Sample Num	Calc Age	Latitude	Longitude	GeoRef	Composition	Rock Name
F-322	371872	8.1	38.2812	-119.38	1977-007325	intermediate	latite
F-324	371873	8.1	38.2845	-119.3797	1977-007325	intermediate	latite
F-331	371874	8.1	38.2846	-119.4689	1977-007325	intermediate	latite
F-165	371875	8.1	38.25	-119.5	1977-007325	intermediate	latite
F-127	371876	8.1	38.2846	-119.4689	1977-007325	intermediate	latite
LW-4	371877	8.1	38.317	-119.4395	1977-007325	intermediate	latite
F-109	371878	8.1	38.299	-119.421	1977-007325	intermediate	latite
F-206	371879	8.1	38.2813	-119.4037	1977-007325	intermediate	latite
F-266	371880	8.1	38.2593	-119.4114	1977-007325	intermediate	latite
D-4	371881	8.1	38.2967	-119.3807	1977-007325	intermediate	latite
D-129	371882	8.1	38.3018	-119.3651	1977-007325	intermediate	latite
D-175	371883	8.1	38.2945	-119.3598	1977-007325	intermediate	latite
D-210	371884	8.1	38.2739	-119.3732	1977-007325	intermediate	latite
D-218	371885	8.1	38.2823	-119.3621	1977-007325	intermediate	latite
BP73-1	374041	2.66	37.0558	-118.3242	1978-010582	felsic	rhyolite
USGSD-HLV-100	374208	9.9	37.2181	-119.1397	1978-034495	mafic	basalt
USGSD-73-RCB-7	374221	5.7	38.3483	-118.3472	1978-034495	mafic	trachybasalt
SQ16	375096	7.5	38.9317	-118.9733	1981-009079	intermediate	basaltic-andesite
SQ24	375097	10	38.8483	-118.8	1981-009079	intermediate	basaltic-andesite
SQ34	375098	14.1	38.8033	-118.905	1981-009079	mafic	basalt
SQ10	375099	14.3	38.985	-118.9083	1981-009079	intermediate	latite
SQ14	375100	14	38.9883	-118.9467	1981-009079	intermediate	latite
2C530	375138	0.675	37.6306	-119.0694	1981-011633	felsic	rhyolite
427f	375139	1.1	37.6183	-119.0728	1981-011633	felsic	pyroclastic flow

Table B.1 NAVDAT entries (volcanics only) for Sierra Nevada, Basin and Range study area (continued)

Sample ID	Sample Num	Calc Age	Latitude	Longitude	GeoRef	Composition	Rock Name
64G001	375140	0.764	37.4592	-118.3672	1981-011633	felsic	rhyolite
64G002	375141	0.726	37.5578	-118.6561	1981-011633	felsic	rhyolite
64G003	375142	0.691	37.8247	-118.7761	1981-011633	felsic	rhyolite
2-Mar	374465	9.5	37.4139	-117.9644	1980-010483	mafic	basalt
5-Mar	374466	3.7	37.9167	-118.7283	1980-010483	mafic	basalt
Mar-6A	374467	3.8	37.9966	-118.6571	1980-010483	mafic	basalt
12-Mar	374469	11.1	37.2361	-119.2558	1980-010483	mafic	basalt
14-Mar	374470	3.4	37.5069	-119.2778	1980-010483	mafic	basalt
17-Mar	374473	2.1	37.0858	-117.765	1980-010483	mafic	basalt
18-Mar	374474	2.2	37.0858	-117.7769	1980-010483	mafic	basalt
19-Mar	374475	2.2	37.0858	-117.7603	1980-010483	mafic	basalt
21-Mar	374476	11.1	37.5097	-118.1314	1980-010483	mafic	basalt
23-Mar	374477	11.6	37.5631	-118.0131	1980-010483	mafic	basalt
USGSD-742-45	374632	11.7	38.0833	-119.15	1980-028332	intermediate	andesite
MP410	375496	3.55	37.5233	-119.47	1981-050018	mafic	basanite
M72B	375500	3.5	37.6083	-119.3183	1981-050018	mafic	basalt
M32B	375503	3.5	37.5833	-119.335	1981-050018	mafic	basalt
M9	375505	3.5	37.505	-119.2883	1981-050018	mafic	basalt
M33	375506	3.5	37.5833	-119.335	1981-050018	mafic	basalt
MP265C	375508	3.5	37.605	-119.25	1981-050018	mafic	basalt
H98A	375509	3.5	37.2167	-119.1533	1981-050018	intermediate	andesite
SL112A	375511	11.1	37.265	-119.2967	1981-050018		
DS107A	375512	3.5	37.3667	-118.05	1981-050018		
8	438512	0.73	37.4611	-118.3653	1984-019557	felsic	pyroclastic-fall

Table B.1 NAVDAT entries (volcanics only) for Sierra Nevada, Basin and Range study area (continued)

Sample ID	Sample Num	Calc Age	Latitude	Longitude	GeoRef	Composition	Rock Name
13	438517	0.68	37.5464	-118.5906	1984-019557	felsic	pyroclastic-fall
14	438518	0.68	37.6264	-119.0556	1984-019557	felsic	tuff
17	438520	0.9	37.4567	-118.6736	1984-019557	felsic	pyroclastic-fall
19	438522	1	37.4567	-118.6736	1984-019557	felsic	pyroclastic-fall
N6036	423233	2.66	37.999	-118.052	1980-024531	mafic	basalt
N3016	423222	2.66	38.278	-118.415	1980-024531	mafic	basalt
B-13/AH-108	377269	7.73	38.2325	-119.2117	1983-046157	intermediate	andesite
B-22/AH-109	377270	10.8	38.2675	-119.1983	1983-046157	intermediate	andesite
C3014	423162	3.3	37.554	-118.608	1980-024531	mafic	basalt
4-23-10J	379103	7.8	38.7325	-119.3667	1985-023627	felsic	rhyodacite
4-7-35J	379104	10.1	38.6125	-119.3144	1985-023627	intermediate	andesite
1-115-30J	379105	12	38.0167	-118.2381	1985-023627	felsic	tuff
210-2	379113	15	38.3783	-118.6856	1985-023627	intermediate	andesite
149-6	379114	15.7	38.4061	-118.6653	1985-023627	intermediate	andesite
145-14	379115	15.8	38.4431	-118.65	1985-023627	intermediate	andesite
34	438537	2.3	37.1667	-118.2	1984-019557	felsic	pyroclastic-fall
72G001	380282	0.694	37.662	-118.941	1986-028002	felsic	rhyolite
72G002	380283	0.678	37.679	-118.922	1986-028002	felsic	rhyolite
72G003	380284	0.68	37.678	-118.891	1986-028002	felsic	rhyolite
72G004	380285	0.688	37.645	-118.899	1986-028002	felsic	rhyolite
72G005	380286	0.333	37.641	-118.808	1986-028002	felsic	rhyolite
72G006	380287	0.751	37.6615	-118.879	1986-028002	felsic	rhyolite
72G007	380288	0.11	37.678	-118.986	1986-028002	felsic	rhyolite
72G008	380289	0.097	37.659	-118.982	1986-028002	felsic	rhyolite

Table B.1 NAVDAT entries (volcanics only) for Sierra Nevada, Basin and Range study area (continued)

Sample ID	Sample Num	Calc Age	Latitude	Longitude	GeoRef	Composition	Rock Name
72G009	380290	0.106	37.655	-118.975	1986-028002	felsic	rhyolite
72G010	380291	0.692	37.726	-118.912	1986-028002	felsic	rhyolite
72G011	380292	0.481	37.731	-118.9	1986-028002	felsic	rhyolite
72G012	380293	0.523	37.72	-118.883	1986-028002	felsic	rhyolite
72G013	380294	0.677	37.7215	-118.912	1986-028002	felsic	rhyolite
72G014	380295	0.652	37.701	-118.938	1986-028002	felsic	rhyolite
72G015	380296	0.154	37.676	-118.959	1986-028002	mafic	basalt
72G016	380297	0.155	37.675	-118.959	1986-028002	mafic	basalt
72G017	380298	0.115	37.697	-119.011	1986-028002	felsic	rhyolite
73G001	380299	0.228	37.653	-118.965	1986-028002	intermediate	andesite
73G008	380300	0.149	37.717	-118.955	1986-028002	mafic	basalt
73G009	380301	0.108	37.749	-118.937	1986-028002	mafic	basalt
73G010	380302	2.95	37.746	-118.997	1986-028002	intermediate	andesite
73G012	380303	0.1755	37.645	-118.9315	1986-028002	mafic	basalt
73G014	380304	0.244	37.646	-118.938	1986-028002	mafic	basalt
73G016	380305	1.96	37.765	-118.773	1986-028002	felsic	rhyolite
73G017	380306	0.362	37.669	-118.807	1986-028002	felsic	rhyolite
73G018	380307	0.148	37.649	-119	1986-028002	felsic	dacite
73G019	380308	0.142	37.664	-119.001	1986-028002	felsic	dacite
73G021	380309	0.095	37.665	-119.025	1986-028002	mafic	basalt
73G023	380310	0.052	37.632	-119.037	1986-028002	felsic	dacite
73G024	380311	0.123	37.646	-119.031	1986-028002	felsic	dacite
73G025	380312	0.086	37.631	-119.001	1986-028002	intermediate	andesite
73G013	380313	0.141	37.6667	-118.9167	1986-028002	mafic	basalt

Table B.1 NAVDAT entries (volcanics only) for Sierra Nevada, Basin and Range study area (continued)

Sample ID	Sample Num	Calc Age	Latitude	Longitude	GeoRef	Composition	Rock Name
73G022	380314	0.07	37.635	-119.036	1986-028002	felsic	dacite
74G001	380315	0.527	37.712	-118.881	1986-028002	felsic	rhyolite
74G002	380316	0.505	37.704	-118.867	1986-028002	felsic	rhyolite
74G003	380317	0.329	37.659	-118.78	1986-028002	felsic	rhyolite
74G004	380318	0.256	37.624	-119.044	1986-028002	felsic	dacite
74G005	380319	0.215	37.639	-119.046	1986-028002	felsic	dacite
74G006	380320	0.103	37.673	-119.023	1986-028002	felsic	dacite
74G009	380321	0.212	37.643	-119.022	1986-028002	felsic	dacite
74G010	380322	0.729	37.6667	-118.9167	1986-028002	mafic	basalt
74G011	380323	0.239	37.635	-118.912	1986-028002	mafic	basalt
509-27-6	380324	0.288	37.627	-118.827	1986-028002	felsic	rhyolite
D85-16	383608	10.5	37.45	-117.9167	1988-052744	mafic	basalt
D85-227	383615	4.8	37.7333	-118.0333	1988-052744	mafic	basalt
D85-235	383617	2.6	37.5667	-118.8667	1988-052744	mafic	basalt
I-2-11	382934	0	37.751	-119.018	1988-001163	felsic	rhyolite
I-3-1	382936	0	37.751	-119.018	1988-001163	felsic	rhyolite
I-3-20	382938	0	37.751	-119.018	1988-001163	felsic	rhyolite
I-3-26	382939	0	37.751	-119.018	1988-001163	felsic	rhyolite
I-5-3	382941	0	37.751	-119.018	1988-001163	felsic	rhyolite
I-5-23	382943	0	37.751	-119.018	1988-001163	felsic	rhyolite
SS5-2	382945	0	37.751	-119.018	1988-001163	felsic	rhyolite
SS5-3	382946	0	37.751	-119.018	1988-001163	felsic	rhyolite
I-3-17	382948	0	37.751	-119.018	1988-001163	felsic	rhyolite
I-3-28	382950	0	37.751	-119.018	1988-001163	felsic	rhyolite

Table B.1 NAVDAT entries (volcanics only) for Sierra Nevada, Basin and Range study area (continued)

Sample ID	Sample Num	Calc Age	Latitude	Longitude	GeoRef	Composition	Rock Name
I-5-17	382952	0	37.751	-119.018	1988-001163	felsic	rhyolite
I-3-2g	382953	0	37.751	-119.018	1988-001163	felsic	rhyolite
U-1	437218	9.8	37.25	-119.3283	1982-017260	intermediate	andesite
U-2	437219	9.8	37.2367	-119.2583	1982-017260	mafic	basalt
U-3	437220	9.8	37.21	-119.265	1982-017260	intermediate	andesite
U-4	437221	9.8	37.21	-119.265	1982-017260	intermediate	andesite
U-5	437222	9.8	37.21	-119.265	1982-017260	intermediate	andesite
U-6	437223	9.8	37.1983	-119.255	1982-017260	mafic	basalt
U-7	437224	9.8	37.1717	-119.35	1982-017260	mafic	basalt
U-8	437225	9.8	37.1417	-119.45	1982-017260	intermediate	andesite
U-9	437226	9.8	37.14	-119.4183	1982-017260	mafic	basalt
U-10	437227	9.8	37.14	-119.4183	1982-017260	mafic	basalt
U-12	437228	9.8	37.1217	-119.3933	1982-017260	mafic	basalt
U-13	437229	9.8	37.1183	-119.4133	1982-017260	mafic	basalt
U-14	437230	9.8	37.105	-119.4367	1982-017260	mafic	basalt
V-1	437231	11.4	37.22	-119.1517	1982-017260	mafic	basalt
V-2	437232	11.4	37.1967	-119.1117	1982-017260	intermediate	andesite
V-3	437233	11.4	37.1967	-119.1117	1982-017260	intermediate	andesite
W-1	437234	3.85	37.1867	-118.7767	1982-017260	mafic	basalt
W-2	437235	3.85	37.025	-118.9067	1982-017260	mafic	basalt
W-3	437236	3.85	37.0067	-118.91	1982-017260	mafic	basalt
W-4	437237	3.85	37.0133	-118.8367	1982-017260	mafic	basalt
Y-1	437238	0.51	37.13	-118.2733	1982-017260	mafic	basalt
Y-2	437239	0.51	37.0567	-118.305	1982-017260	felsic	rhyolite

Table B.1 NAVDAT entries (volcanics only) for Sierra Nevada, Basin and Range study area (continued)

Sample ID	Sample Num	Calc Age	Latitude	Longitude	GeoRef	Composition	Rock Name
Y-3	437240	0.51	37.03	-118.2733	1982-017260	mafic	basalt
Z-1	437241	0.51	37.0133	-118.2317	1982-017260	mafic	basalt
Z-2	437242	0.51	37.0233	-118.17	1982-017260	mafic	basalt
Z-3	437243	0.51	37.0167	-118.1717	1982-017260	mafic	basalt
Z-4	437244	0.51	37.0133	-118.1883	1982-017260	mafic	basalt
Z-5	437245	0.51	37.0133	-118.1633	1982-017260	mafic	basalt
Z-6	437246	0.51	37.01	-118.1633	1982-017260	mafic	basalt
79G88S	383981	0.71	37.8354	-118.736	1988-079677	felsic	pyroclastic fall
79G88S-1	383982	0.76	37.8354	-118.736	1988-079677	felsic	pyroclastic fall
79G88S-2	383983	0.74	37.8354	-118.736	1988-079677	felsic	pyroclastic fall
79G94S	383984	0.75	37.8337	-118.7616	1988-079677	felsic	pyroclastic fall
64G003	383985	0.691	37.8248	-118.777	1988-079677	felsic	pyroclastic fall
B-96	383986	0.7	37.8946	-118.8444	1988-079677	felsic	pyroclastic fall
79G88P	383987	0.74	37.8353	-118.736	1988-079677	felsic	pyroclastic fall
77G88G	383988	0.93	37.8353	-118.736	1988-079677	felsic	pyroclastic fall
77G88B	383989	1.1	37.8353	-118.736	1988-079677	felsic	pyroclastic fall
77G88B	383990	0.34	37.8353	-118.736	1988-079677	felsic	pyroclastic fall
79G94P	383991	0.83	37.8337	-118.7616	1988-079677	felsic	pyroclastic fall
79G14S	383992	0.74	37.4611	-118.3651	1988-079677	felsic	pyroclastic-fall
79G14S-2	383993	0.75	37.4611	-118.3651	1988-079677	felsic	pyroclastic-fall
80G24	383994	0.74	37.4611	-118.3651	1988-079677	felsic	pyroclastic fall
80G24S	383995	0.71	37.4611	-118.3651	1988-079677	felsic	pyroclastic fall
80G21	383996	0.73	37.4611	-118.3651	1988-079677	felsic	pyroclastic fall
64G001	383997	0.764	37.4611	-118.3651	1988-079677	felsic	pyroclastic fall

Table B.1 NAVDAT entries (volcanics only) for Sierra Nevada, Basin and Range study area (continued)

Sample ID	Sample Num	Calc Age	Latitude	Longitude	GeoRef	Composition	Rock Name
64G002	383998	0.726	37.5581	-118.6571	1988-079677	felsic	pyroclastic fall
B-105	383999	0.75	37.7443	-118.4541	1988-079677	felsic	pyroclastic fall
B-109	384000	0.74	37.4521	-118.399	1988-079677	felsic	pyroclastic fall
79G14B	384001	1.14	37.4611	-118.3651	1988-079677	felsic	pyroclastic-fall
79G14PQ	384002	1.36	37.4611	-118.3651	1988-079677	felsic	pyroclastic-fall
80G21P	384003	0.66	37.4611	-118.3651	1988-079677	felsic	pyroclastic fall
USGSD75FB144	384787	15.6	38.9333	-118.0667	1989-042953		not-given
USGSDQb-1	384803	2.8	38.1583	-118.0767	1989-042953	mafic	basalt
USGSDQb-2	384804	2.9	38.1567	-118.0583	1989-042953	mafic	basalt
B	385763	9.75	38.3	-119.2	1989-065947	mafic	basalt
C	385764	9.75	38.3	-119.2	1989-065947	mafic	basalt
D	385765	9.75	38.3	-119.2	1989-065947	mafic	basalt
E	385766	9.75	38.3	-119.2	1989-065947	mafic	basalt
F	385767	9.75	38.3	-119.2	1989-065947	mafic	basalt
G	385768	9.75	38.3	-119.2	1989-065947	intermediate	latite
H	385769	9.75	38.3	-119.2	1989-065947	intermediate	latite
I	385770	9.75	38.3	-119.2	1989-065947	intermediate	latite
O	385776	9.75	38.3	-119.2	1989-065947	intermediate	latite
Q	385778	9.75	38.3	-119.2	1989-065947	felsic	rhyolite
D85-2	386031	3.55	37.4333	-117.6167	1989-079451	mafic	basalt
D85-3	386032	3.55	37.4333	-117.5833	1989-079451	mafic	basalt
D85-7	386034	0.9	37.8333	-117.6333	1989-079451	intermediate	mugearite
D85-8	386035	3.55	37.8833	-117.65	1989-079451	mafic	basalt
D85-13	386037	3.55	38.2667	-117.7833	1989-079451	intermediate	hawaiite

Table B.1 NAVDAT entries (volcanics only) for Sierra Nevada, Basin and Range study area (continued)

Sample ID	Sample Num	Calc Age	Latitude	Longitude	GeoRef	Composition	Rock Name
D85-16	386039	10.5	37.45	-117.9167	1989-079451	mafic	basalt
D85-20	386040	0.9	37.1183	-118.3137	1989-079451	mafic	basalt
D85-38	386048	0.9	37.0255	-118.2281	1989-079451	mafic	basalt
D85-40	386049	0.8	37.0096	-118.1773	1989-079451	mafic	basalt
D85-53	386057	12.5	37.4	-118.4833	1989-079451	mafic	basalt
D85-54	386058	12.5	37.45	-118.5333	1989-079451	mafic	basalt
D85-56	386060	0.2	37.5333	-119.0333	1989-079451	mafic	basalt
D85-58	386062	0.8	37.5833	-119.0833	1989-079451	mafic	basalt
D85-59	386063	0.2	37.6167	-118.95	1989-079451	mafic	basalt
L82-88	386079	7.3	38.9	-119.2333	1989-079451	intermediate	basaltic-andesite
L82-89	386080	6.59	38.6167	-119.2333	1989-079451	intermediate	basaltic-andesite
L82-90	386081	0.25	38.3333	-118.9333	1989-079451	intermediate	trachyandesite
L82-91	386082	0.25	38.2833	-118.9167	1989-079451	intermediate	trachyandesite
L82-93A	386083	0.013	38.0167	-119.1	1989-079451	mafic	basalt
L82-93C	386084	0.013	38.0167	-119.0667	1989-079451	mafic	basalt
L82-94	386085	5.7	38.3167	-118.5	1989-079451	intermediate	hawaiite
L82-95	386086	5.7	38.3333	-118.3667	1989-079451	intermediate	hawaiite
L82-96	386087	5.7	38.45	-118.45	1989-079451	mafic	basalt
L82-99	386090	3.1	38	-118.2667	1989-079451	intermediate	hawaiite
L82-100	386091	3.1	37.9833	-118.3167	1989-079451	intermediate	mugearite
L82-101	386092	3.1	37.9667	-118.3	1989-079451	intermediate	hawaiite
L82-102	386093	3.1	37.95	-118.2833	1989-079451	intermediate	mugearite
L82-103	386094	3.1	37.85	-118.35	1989-079451	intermediate	trachyandesite
L82-104	386095	3.1	37.8	-118.45	1989-079451	intermediate	hawaiite

Table B.1 NAVDAT entries (volcanics only) for Sierra Nevada, Basin and Range study area (continued)

Sample ID	Sample Num	Calc Age	Latitude	Longitude	GeoRef	Composition	Rock Name
L82-105	386096	3.1	37.7667	-118.5667	1989-079451	intermediate	hawaiite
L82-106	386097	3.1	37.9833	-118.7833	1989-079451	intermediate	trachyandesite
L82-107	386098	0.63	37.5667	-119.0667	1989-079451	mafic	basalt
L82-109	386099	0.104	37.7	-118.95	1989-079451	intermediate	trachyandesite
L82-110	386100	0.104	37.7333	-118.8833	1989-079451	mafic	basalt
L82-111	386101	0.9	37.1133	-118.2704	1989-079451	mafic	basalt
L82-112	386102	0.9	37.0714	-118.2516	1989-079451	intermediate	hawaiite
L82-113	386103	0.9	37.064	-118.2594	1989-079451	mafic	basalt
L82-116	386106	0.9	37.0352	-118.2308	1989-079451	mafic	basalt
L82-118	386107	3.55	37.1333	-117.6833	1989-079451	mafic	basalt
L82-119	386108	3.55	37.15	-117.6667	1989-079451	intermediate	basaltic-andesite
L82-120	386109	3.55	37.1667	-117.6333	1989-079451	intermediate	trachyandesite
L82-140	386125	15.1	38.4667	-118.0167	1989-079451	intermediate	trachyandesite
D85-150	386126	6.6	38.65	-119.1667	1989-079451	intermediate	trachyandesite
D85-151	386127	6.8	38.6833	-119.2833	1989-079451	intermediate	trachyandesite
D85-152	386128	6.8	38.7	-119.2167	1989-079451	mafic	basalt
D85-156	386129	7.4	38.7333	-119.0667	1989-079451	mafic	basalt
D85-158	386130	3.55	37.5833	-118.4	1989-079451	intermediate	hawaiite
D85-159	386131	2.01	37.55	-118.4833	1989-079451	intermediate	trachyandesite
D85-162	386132	14.55	38.9667	-118.6333	1989-079451	intermediate	trachyandesite
D85-163	386133	14.55	38.6	-118.5667	1989-079451	intermediate	trachyandesite
D85-164	386134	3.55	38.5667	-118.35	1989-079451	intermediate	trachyandesite
D85-165A	386135	14.55	38.5	-118.4333	1989-079451	mafic	basalt
D85-165B	386136	14.55	38.5	-118.4333	1989-079451	mafic	basalt

Table B.1 NAVDAT entries (volcanics only) for Sierra Nevada, Basin and Range study area (continued)

Sample ID	Sample Num	Calc Age	Latitude	Longitude	GeoRef	Composition	Rock Name
D85-166	386137	5.7	38.3167	-118.6	1989-079451	intermediate	hawaiite
D85-167	386138	14.55	38.4167	-118.4833	1989-079451	intermediate	trachyandesite
D85-168	386139	14.55	38.4833	-118.35	1989-079451	mafic	basalt
D85-169	386140	14.55	38.4667	-118.4	1989-079451	mafic	basalt
D85-170	386141	14.55	38.2833	-118.6833	1989-079451	intermediate	trachyandesite
D85-172	386142	3.55	38.2667	-119.2	1989-079451	intermediate	basaltic-andesite
D85-174	386144	3.55	38.1	-119.25	1989-079451	intermediate	basaltic-andesite
D85-175A	386146	11.3	38.0833	-119.1667	1989-079451	intermediate	trachyandesite
D85-175B	386147	11.3	38.0833	-119.1667	1989-079451	intermediate	trachyandesite
D85-177	386149	13.3	38.0833	-119.1	1989-079451	intermediate	trachyandesite
D85-180	386151	3.55	38.15	-118.6333	1989-079451	mafic	basalt
D85-181	386152	3.55	38.1667	-118.7167	1989-079451	intermediate	basaltic-andesite
D85-185	386154	3.55	38.15	-118.8167	1989-079451	mafic	basalt
D85-187A	386155	0.3	38.3	-118.9167	1989-079451	intermediate	trachyandesite
D85-190	386157	3.1	37.55	-119.1	1989-079451	mafic	basalt
D85-192	386159	0.3	37.6667	-119.0333	1989-079451	mafic	basalt
D85-193	386160	0.8	37.5667	-119.0167	1989-079451	mafic	basalt
D85-198	386162	3.55	37.7	-118.6333	1989-079451	intermediate	trachyandesite
D85-201A	386164	3.55	37.7833	-118.8333	1989-079451	mafic	basalt
D85-202	386165	3.55	37.7833	-118.8	1989-079451	mafic	basalt
D85-215	386175	3.55	37.9167	-118.4333	1989-079451	intermediate	trachyandesite
D85-219	386177	3.55	38.0167	-118.2833	1989-079451	intermediate	hawaiite
D85-222	386178	2.8	38.15	-118.1167	1989-079451	intermediate	trachyandesite
D85-226	386180	3.55	37.9167	-118.1167	1989-079451	intermediate	trachyandesite

Table B.1 NAVDAT entries (volcanics only) for Sierra Nevada, Basin and Range study area (continued)

Sample ID	Sample Num	Calc Age	Latitude	Longitude	GeoRef	Composition	Rock Name
D85-228	386182	1.3	37.0594	-118.2326	1989-079451	mafic	basalt
D85-229	386183	0.9	37.0283	-118.1763	1989-079451	mafic	basalt
D85-235	386185	2.6	37.5667	-118.8667	1989-079451	mafic	basalt
MC72-1	388591	0.0006	38	-119	1991-010933	felsic	rhyolite
DP78-3	388592	0.0006	38	-119	1991-010933	felsic	rhyolite
DP78-1	388593	0.0006	38	-119	1991-010933	felsic	rhyolite
83083-1	388594	0.0006	38	-119	1991-010933	intermediate	andesite
LV87-1	388595	0.0006	38	-119	1991-010933	intermediate	andesite
VGC-1	388596	0.0006	38	-119	1991-010933	intermediate	andesite
M72-7	388597	0.0006	38	-119	1991-010933	mafic	basalt
DP73-12	388598	0.0006	38	-119	1991-010933	mafic	basalt
148	390625	0.05	37.9077	-119.0355	1992-049812	felsic	rhyolite
147	390626	0.05	37.9313	-119.0412	1992-049812	felsic	rhyolite
M72-8	390628	2.25	37.6667	-118	1992-049812	felsic	rhyolite
M72-21	390629	2.25	37.6833	-118.8833	1992-049812	felsic	rhyolite
M72-62	390630	2.25	37.6333	-118.8333	1992-049812	felsic	rhyolite
9	390631	0.6	37.0563	-118.2978	1992-049812	felsic	rhyolite
No Sample Name	390682	0.01	37.7699	-118.7237	1992-049812	felsic	rhyolite
No Sample Name	390683	0.01	37.7699	-118.7237	1992-049812	felsic	rhyolite
No Sample Name	390684	0.05	37.8642	-119.0067	1992-049812	felsic	rhyolite
No Sample Name	390685	0.05	37.8642	-119.0067	1992-049812	felsic	rhyolite
No Sample Name	390686	0.05	37.8642	-119.0067	1992-049812	felsic	rhyolite
No Sample Name	390687	0.05	37.8642	-119.0067	1992-049812	felsic	rhyolite
No Sample Name	390688	0.01	37.7699	-118.7237	1992-049812	felsic	rhyolite

Table B.1 NAVDAT entries (volcanics only) for Sierra Nevada, Basin and Range study area (continued)

Sample ID	Sample Num	Calc Age	Latitude	Longitude	GeoRef	Composition	Rock Name
No Sample Name	390689	0.01	37.7765	-118.7326	1992-049812	felsic	rhyolite
No Sample Name	390690	5	37.75	-117.8333	1992-049812	felsic	rhyolite
245	397993	1.74	37.775	-118.708	1993-001953	felsic	rhyolite
68	397994	1.92	37.775	-118.708	1993-001953	felsic	rhyolite
262	397996	1.41	37.775	-118.708	1993-001953	felsic	rhyolite
200	397998	2.13	37.775	-118.708	1993-001953	felsic	rhyolite
205	398000	1.6	37.775	-118.708	1993-001953	felsic	rhyolite
203	398001	1.89	37.775	-118.708	1993-001953	felsic	rhyolite
57	398003	1.77	37.775	-118.708	1993-001953	felsic	rhyolite
56	398005	1.82	37.775	-118.708	1993-001953	felsic	rhyolite
230	398007	1.75	37.775	-118.708	1993-001953	felsic	rhyolite
220	398008	1.65	37.775	-118.708	1993-001953	felsic	rhyolite
225	398010	1.65	37.775	-118.708	1993-001953	felsic	rhyolite
16	398012	1	37.775	-118.708	1993-001953	felsic	rhyolite
147	398014	0.9	37.775	-118.708	1993-001953	felsic	rhyolite
52	398015	0.94	37.775	-118.708	1993-001953	felsic	rhyolite
47	398017	1	37.775	-118.708	1993-001953	felsic	rhyolite
38	398019	1	37.775	-118.708	1993-001953	felsic	rhyolite
31	398021	0.98	37.775	-118.708	1993-001953	felsic	rhyolite
30	398022	1	37.775	-118.708	1993-001953	felsic	rhyolite
126	398024	0.81	37.775	-118.708	1993-001953	felsic	rhyolite
206	398026	0.92	37.775	-118.708	1993-001953	felsic	rhyolite
214	398028	1	37.775	-118.708	1993-001953	felsic	rhyolite
212	398029	1.1	37.775	-118.708	1993-001953	felsic	rhyolite

Table B.1 NAVDAT entries (volcanics only) for Sierra Nevada, Basin and Range study area (continued)

Sample ID	Sample Num	Calc Age	Latitude	Longitude	GeoRef	Composition	Rock Name
221	398031	1.06	37.775	-118.708	1993-001953	felsic	rhyolite
KA-5	398181	3.55	37.7667	-118.1767	1993-005802	intermediate	andesite
KA-6	398182	0.003	37.7733	-118.1817	1993-005802	intermediate	andesite
KA-7	398183	3.55	37.775	-118.1783	1993-005802	intermediate	andesite
KA-8	398184	0.003	37.7933	-118.1867	1993-005802	intermediate	andesite
KA-9	398185	0.0032	37.825	-118.2183	1993-005802	intermediate	andesite
KA-18	398186	3.55	37.8017	-118.2033	1993-005802	intermediate	andesite
KA-19	398187	3.55	37.8017	-118.205	1993-005802	intermediate	andesite
KA-20	398188	3.55	37.8017	-118.2083	1993-005802	intermediate	andesite
KA-21	398189	3.55	37.8	-118.215	1993-005802	intermediate	andesite
KA-22	398190	3.55	37.8	-118.2183	1993-005802	intermediate	andesite
KA-23	398191	3.55	37.7733	-118.1783	1993-005802	intermediate	andesite
KA-36	398192	0.9	37.8783	-118.175	1993-005802	felsic	rhyolite
KA-48	398193	0.9	37.8817	-118.1733	1993-005802	felsic	rhyolite
KA-49	398194	0.9	37.9217	-118.1267	1993-005802	felsic	rhyolite
D85-24	398267	0.9	37	-118.25	1993-010551	mafic	basalt
D85-28B	398268	0.9	37	-118.25	1993-010551	mafic	basalt
D85-30A	398269	0.9	37	-118.25	1993-010551	mafic	basalt
D85-31	398270	0.9	37	-118.25	1993-010551	mafic	basalt
D85-32	398271	0.9	37	-118.25	1993-010551	mafic	basalt
D85-35	398272	0.9	37	-118.25	1993-010551	mafic	basalt
L67-61	398273	0.9	37	-118.25	1993-010551	mafic	basalt
L82-113	398274	0.9	37	-118.25	1993-010551	mafic	basalt
L82-114	398275	0.9	37	-118.25	1993-010551	mafic	basalt

Table B.1 NAVDAT entries (volcanics only) for Sierra Nevada, Basin and Range study area (continued)

Sample ID	Sample Num	Calc Age	Latitude	Longitude	GeoRef	Composition	Rock Name
L82-115	398276	0.9	37	-118.25	1993-010551	mafic	basalt
23	398602	2.6	38.1553	-118.859	1993-038104		not-given
90	398603	3.32	37.7392	-118.6548	1993-038104		not-given
129	398605	2.96	37.9912	-118.659	1993-038104		not-given
160	398607	0.47	38.3553	-118.896	1993-038104		not-given
5G203	399295	0.0128	37.8619	-119.0061	1994-037732	felsic	rhyolite
5G204	399296	0.0108	37.8253	-119.015	1994-037732	felsic	rhyolite
6G007	399297	0.0144	37.8244	-119.0186	1994-037732	felsic	rhyolite
75M005	399298	0.0112	37.8139	-119.0297	1994-037732	felsic	rhyolite
5G201	399299	0.0131	37.8131	-119.0325	1994-037732	felsic	rhyolite
WS-908	400896	1.5	37.0636	-117.7319	1995-044484	mafic	basalt
WS980	400897	5.5	37.205	-117.5961	1995-044484	mafic	basalt
YR-240B	400204	6.17	38.9979	-119.3789	1995-029811	felsic	pyroclastic-fall
93-87-S6	400206	9.23	38.8397	-118.8047	1995-029811	intermediate	basaltic-andesite
110JD91	400207	8.86	38.9047	-119.0075	1995-029811	felsic	pyroclastic-fall
74JD91	400209	11.88	38.885	-118.9036	1995-029811	felsic	pyroclastic-fall
108JD89B	400212	13.03	38.985	-119.3783	1995-029811	felsic	dacite
FL-KA-1	402853	3.2	37.8356	-118.3266	1997-034538		
FL-KA-4	402855	11.5	37.3415	-117.7618	1997-034538		
FL-KA-8	402857	3	37.8356	-118.3266	1997-034538		
FL-KA-10	402859	9.8	37.3446	-117.7534	1997-034538		
FL-KA-35	402861	9.8	37.704	-118.29	1997-034538		
FL-KA-43	402863	6.7	37.3804	-117.8751	1997-034538		
FL-KA-52B	402865	5.3	37.3651	-117.8264	1997-034538		

Table B.1 NAVDAT entries (volcanics only) for Sierra Nevada, Basin and Range study area (continued)

Sample ID	Sample Num	Calc Age	Latitude	Longitude	GeoRef	Composition	Rock Name
W-1	404453	0.19	37.0148	-118.1737	1999-027986	mafic	basalt
W-2	404454	0.19	37.0095	-118.1625	1999-027986	mafic	basalt
W-5	404455	0.19	37.0147	-118.1662	1999-027986	mafic	basalt
W-7	404456	0.19	37.015	-118.1646	1999-027986	mafic	basalt
W-20	404457	0.19	37.0143	-118.1692	1999-027986	mafic	basalt
W-21A	404458	0.19	37.0143	-118.1692	1999-027986	mafic	basalt
W-21D	404459	0.19	37.0143	-118.1692	1999-027986	mafic	basalt
W-26	404460	0.19	37.0109	-118.166	1999-027986	mafic	basalt
W-28	404461	0.19	37.0142	-118.1655	1999-027986	mafic	basalt
W-33	404462	0.19	37.0143	-118.1631	1999-027986	mafic	basalt
W-35	404463	0.19	37.0143	-118.1631	1999-027986	mafic	basalt
W-37	404464	0.19	37.0143	-118.1631	1999-027986	mafic	basalt
W-4C	404465	0.74	37.0159	-118.1711	1999-027986	mafic	basalt
W-4G	404466	0.74	37.0159	-118.1711	1999-027986	mafic	basalt
W13	404467	0.41	37.0052	-118.1992	1999-027986	mafic	basalt
W-14	404468	0.41	37.0104	-118.194	1999-027986	mafic	basalt
W-16	404469	0.41	37.0188	-118.1828	1999-027986	mafic	basalt
W17	404470	0.74	37.0209	-118.1805	1999-027986	mafic	basalt
sv92-94a	403794	13.783	38.6653	-117.9817	1998-025813	felsic	pyroclastic-fall
sv93-404	403795	15.342	38.5405	-117.9508	1998-025813	felsic	pyroclastic-fall
DS92-1	404851	2.6	37.3533	-118.0562	1999-055339		not-given
DS93-1	404852	2.6	37.3528	-118.0569	1999-055339		not-given
DS93-7	404853	2.6	37.3576	-118.0554	1999-055339		not-given
DS93-6	404854	2.6	37.3552	-118.0556	1999-055339		not-given

Table B.1 NAVDAT entries (volcanics only) for Sierra Nevada, Basin and Range study area (continued)

Sample ID	Sample Num	Calc Age	Latitude	Longitude	GeoRef	Composition	Rock Name
DS92-2	404855	2.6	37.3532	-118.0565	1999-055339		not-given
DS93-3	404856	2.6	37.3528	-118.0569	1999-055339		not-given
DS93-2	404857	2.6	37.3528	-118.0569	1999-055339		not-given
DS93-4	404858	2.6	37.353	-118.0564	1999-055339		not-given
91-54	406391	0.5	37.8167	-117.66	2000-066389	mafic	basalt
91-55	406392	6.4	37.835	-117.6667	2000-066389	mafic	basalt
91-56	406393	3.5	37.925	-118.13	2000-066389	mafic	basalt
91-57	406394	5.8	37.96	-118.3467	2000-066389	mafic	basalt
91-58	406395	5.5	38.28	-119.1567	2000-066389	mafic	basalt
91-59	406396	10.8	38.2683	-119.1983	2000-066389	mafic	basalt
91-60	406397	9.3	38.1667	-119.1217	2000-066389	mafic	basalt
91-61	406398	9.2	38.1467	-119.2	2000-066389	mafic	basalt
91-62	406399	0.12	37.6317	-118.8633	2000-066389	mafic	basalt
91-63	406400	0.5	37.0933	-118.265	2000-066389	mafic	basalt
91-64	406401	0.5	37.02	-118.2317	2000-066389	mafic	basalt
SL97-19	406469	9.81	37.1192	-119.393	2000-073550		
KP97-25B	406474	3.84	37.3991	-119.2317	2000-073550		
BK111	406476	7.76	37.5481	-119.3167	2000-073550		
SL 97-19	408748	9.81	37.1192	-119.393	2002-043002	intermediate	basaltic-andesite
HL 97-27	408749	9.9	37.2172	-119.1568	2002-043002	mafic	trachybasalt
BK-003	408754	8.62	37.5593	-119.3194	2002-043002	intermediate	basaltic-andesite
MP 97-18	408756	3.6	37.5048	-119.2936	2002-043002	mafic	trachybasalt
SP 97-23	408758	3.6	37.4332	-119.286	2002-043002	mafic	absarokite
KP 97-24	408759	3.6	37.3366	-119.2374	2002-043002	mafic	absarokite

Table B.1 NAVDAT entries (volcanics only) for Sierra Nevada, Basin and Range study area (continued)

Sample ID	Sample Num	Calc Age	Latitude	Longitude	GeoRef	Composition	Rock Name
KP 97-25B	408760	3.84	37.3991	-119.2317	2002-043002	mafic	shoshonite
98-CA-WC-1	408775	3.6	37.0191	-118.8992	2002-043002	exotic	leucitite
98-CA-WC-2	408776	3.6	37.0196	-118.8971	2002-043002	exotic	leucitite
98-CA-WC-3	408777	3.6	37.0265	-118.8832	2002-043002	intermediate	basaltic-andesite
98-CA-WC-4	408778	3.6	37.0235	-118.8715	2002-043002	intermediate	basaltic-andesite
97WM024	410321	12.28	37.7883	-118.2114	2003-048086	mafic	basalt
97WM030	410322	4.13	37.7761	-118.2175	2003-048086	mafic	basalt
97WM032	410323	3.55	37.7831	-118.2056	2003-048086	intermediate	andesite
97WM033	410324	3.98	37.7858	-118.2061	2003-048086	felsic	rhyolite
97WM041	410325	4.24	37.7928	-118.2092	2003-048086	intermediate	andesite
97WM046	410326	5.36	37.7919	-118.2075	2003-048086	intermediate	andesite
97WM048	410327	4.18	37.7942	-118.2125	2003-048086	intermediate	andesite
97WM051	410328	4.47	37.7928	-118.2075	2003-048086	intermediate	andesite
97WM052	410329	4.16	37.7933	-118.2114	2003-048086	intermediate	andesite
97WM054	410330	4.17	37.7956	-118.2092	2003-048086	felsic	rhyolite
97WM056	410331	3.85	37.7972	-118.2067	2003-048086	felsic	rhyolite
97WM059	410332	3.88	37.7975	-118.2072	2003-048086	mafic	basalt
96WM008	410334	4.23	37.8214	-118.24	2003-048086	intermediate	andesite
96WM009	410335	5.05	37.8214	-118.2408	2003-048086	intermediate	andesite
97WM008	410337	5.7	37.8219	-118.2675	2003-048086	intermediate	andesite
97WM014	410338	4.6	37.8253	-118.2333	2003-048086	intermediate	andesite
CV-517	412325	6.93	38.7963	-119.2137	2004-900009	felsic	tuff
CV-427	412326	7	38.7955	-119.2155	2004-900009	felsic	tuff
cDP83-90	412552	3.15	37.7417	-119.1467	2005-004738	mafic	basalt

Table B.1 NAVDAT entries (volcanics only) for Sierra Nevada, Basin and Range study area (continued)

Sample ID	Sample Num	Calc Age	Latitude	Longitude	GeoRef	Composition	Rock Name
cDP83-100	412554	3.15	37.735	-119.135	2005-004738	mafic	basalt
cDP83-75	412555	3.15	37.7233	-119.1233	2005-004738	mafic	basalt
cDP83-93	412557	3.15	37.735	-119.135	2005-004738	mafic	basalt
DP72-10	412559	3.15	37.6767	-119.065	2005-004738	intermediate	andesite
DP81-20	412561	0.1	37.5683	-119.0633	2005-004738	intermediate	andesite
M72-19	412562	3.15	37.7467	-118.9983	2005-004738	intermediate	andesite
DP78-33A	412564	2.9	37.7083	-119.1083	2005-004738	felsic	dacite
DP78-19	412566	2.9	37.725	-119.0483	2005-004738	felsic	dacite
DP78-14	412568	2.9	37.7417	-119.075	2005-004738	felsic	dacite
CT72-3	412570	3.15	37.7617	-118.9917	2005-004738	mafic	basalt
CD73-8	412571	3.15	37.6867	-118.6767	2005-004738	mafic	basalt
CT72-1	412573	3.15	37.7617	-118.875	2005-004738	mafic	basalt
GM85-4	412575	3.15	37.7917	-118.6767	2005-004738	mafic	basalt
CT85-6	412577	3.15	37.8067	-118.8733	2005-004738	intermediate	andesite
CT85-30	412579	3.15	37.7683	-118.915	2005-004738	intermediate	andesite
GM85-3	412580	3.15	37.81	-118.6867	2005-004738	intermediate	andesite
CT78-8	412582	3.15	37.9817	-118.81	2005-004738	intermediate	andesite
M92-1	412588	0.68	37.6767	-118.89	2005-004738	mafic	basalt
M72-90	412589	0.5	37.7233	-118.8917	2005-004738	mafic	basalt
M72-7	412591	0.25	37.645	-118.9317	2005-004738	mafic	basalt
DP73-1	412593	0.1	37.665	-119.0217	2005-004738	mafic	basalt
DP73-12	412595	0.25	37.6783	-119.0083	2005-004738	mafic	basalt
M72-5	412597	0.25	37.6583	-118.9267	2005-004738	intermediate	andesite
DP72-13	412598	0.25	37.6917	-119.01	2005-004738	intermediate	andesite

Table B.1 NAVDAT entries (volcanics only) for Sierra Nevada, Basin and Range study area (continued)

Sample ID	Sample Num	Calc Age	Latitude	Longitude	GeoRef	Composition	Rock Name
DP72-1A	412600	0.15	37.7367	-119.0083	2005-004738	felsic	dacite
DP73-3	412602	0.1	37.665	-119.0217	2005-004738	felsic	dacite
CT72-14	412604	0.7	37.7533	-118.7833	2005-004738	felsic	dacite
BO81-1	412606	0.013	38.025	-119.1	2005-004738	mafic	basalt
DP86-3	412607	0.25	37.6983	-119.055	2005-004738	mafic	basalt
MC74-7	412609	0.25	37.885	-119.0567	2005-004738	mafic	basalt
BO74-4	412611	0.0002	38.0117	-119.025	2005-004738	intermediate	andesite
MC74-13	412613	0.0002	37.995	-119.02	2005-004738	felsic	dacite
BO74-2	412615	0	38.0067	-119.025	2005-004738	felsic	rhyolite
BO74-1	412616	0	38.0067	-119.025	2005-004738	felsic	rhyolite
G-1	437162	2.14	37.6117	-118.4433	1982-017260	mafic	basalt
G-2	437163	2.14	37.6	-119.4333	1982-017260	mafic	basalt
G-3	437164	2.14	37.61	-119.25	1982-017260	intermediate	andesite
G-4	437165	2.14	37.5933	-119.2667	1982-017260	mafic	basalt
G-5	437166	2.14	37.585	-119.2567	1982-017260	mafic	basalt
G-6	437167	2.14	37.585	-119.335	1982-017260	mafic	basalt
G-7	437168	2.14	37.5833	-119.3367	1982-017260	mafic	basalt
G-8	437169	2.14	37.56	-119.3183	1982-017260	mafic	basalt
G-9	437170	2.14	37.53	-119.4667	1982-017260	mafic	basalt
G-10	437171	2.14	37.52	-119.2717	1982-017260	mafic	basalt
G-11	437172	2.14	37.515	-119.3883	1982-017260	mafic	basalt
H-1	437173	2.14	37.7383	-119.125	1982-017260	mafic	basalt
H-2	437174	2.14	37.7317	-119.0033	1982-017260	felsic	dacite
H-3	437175	2.14	37.7117	-119.0983	1982-017260	felsic	rhyolite

Table B.1 NAVDAT entries (volcanics only) for Sierra Nevada, Basin and Range study area (continued)

Sample ID	Sample Num	Calc Age	Latitude	Longitude	GeoRef	Composition	Rock Name
H-4	437176	2.14	37.6817	-119.05	1982-017260	mafic	basalt
H-6	437177	2.14	37.6783	-119.07	1982-017260	intermediate	andesite
H-7	437178	2.14	37.6367	-119.0383	1982-017260	felsic	rhyolite
H-8	437179	2.14	37.6133	-119.09	1982-017260	mafic	basalt
H-10	437180	2.14	37.61	-119.055	1982-017260	intermediate	andesite
H-11	437181	2.14	37.6083	-119.005	1982-017260	mafic	basalt
H-12	437182	2.14	37.5917	-119.1217	1982-017260	mafic	basalt
H-13	437183	2.14	37.58	-119.2133	1982-017260	mafic	basalt
H-14	437184	2.14	37.5633	-119.2	1982-017260	mafic	basalt
F-120	371804	8.9	38.3637	-119.4648	1977-007325	mafic	basalt
F-272	371807	8.9	38.308	-119.375	1977-007325	mafic	basalt
TML-5	371820	8.9	38.2513	-119.3999	1977-007325	intermediate	latite
177-3	371822	8.9	38.2527	-119.3965	1977-007325	intermediate	latite
177-6	371825	8.9	38.281	-119.365	1977-007325	intermediate	latite
D-148	371827	8.9	38.2907	-119.3662	1977-007325	intermediate	latite
F-259	371829	8.9	38.2797	-119.3809	1977-007325	intermediate	latite
M74B	375498	3.6	37.6067	-119.4417	1981-050018	mafic	basanite
M73	375501	3.5	37.6075	-119.44	1981-050018	mafic	basalt
MP275	375504	3.5	37.59	-119.2683	1981-050018	mafic	basalt
MP71	375507	3.5	37.5567	-119.3183	1981-050018	mafic	basalt
H101D	375510	3.5	37.19	-119.1083	1981-050018		
DS110A	375513	3.5	37.3667	-118.05	1981-050018		
R-1	437208	2	37.355	-118.0533	1982-017260	mafic	basalt
R-2	437209	2	37.355	-118.0533	1982-017260	mafic	basalt

Table B.1 NAVDAT entries (volcanics only) for Sierra Nevada, Basin and Range study area (continued)

Sample ID	Sample Num	Calc Age	Latitude	Longitude	GeoRef	Composition	Rock Name
R-3	437210	2	37.355	-118.0533	1982-017260	mafic	basalt
R-4	437211	2	37.355	-118.0533	1982-017260	mafic	basalt
S-1	437212	11.15	37.5	-117.8533	1982-017260	mafic	basalt
S-3	437213	11.15	37.4133	-117.9667	1982-017260	mafic	basalt
S-4	437214	11.15	37.41	-117.9867	1982-017260	mafic	basalt
BP73-1	374042	2.66	37.0562	-118.3008	1978-010582	felsic	rhyolite
WL-1	374459	3.8	38.0264	-118.7072	1980-010483	mafic	basalt
15-Mar	374471	9.3	37.0142	-119.1394	1980-010483	intermediate	andesite
S17	369053	0.29	37.6305	-118.8171	1966-000404	felsic	rhyolite
5G203	369274	0.007	37.8619	-119.0061	1968-062978	felsic	rhyolite
6G006	369276	0.0112	37.8156	-119.0261	1968-062978	felsic	rhyolite
6G014	369279	0.004	37.7175	-119.0181	1968-062978	felsic	rhyolite
6G017	369281	0.0093	37.8822	-119.0031	1968-062978	felsic	rhyolite
D85-15	383607	9.5	37.45	-117.8667	1988-052744	mafic	basalt
D85-152	383614	6.8	38.7	-119.2167	1988-052744	mafic	basalt
D85-228	383616	1.3	37.0667	-118.1833	1988-052744	mafic	basalt
I-2-2	382933	0	37.751	-119.018	1988-001163	felsic	rhyolite
I-2-16	382935	0	37.751	-119.018	1988-001163	felsic	rhyolite
I-3-3	382937	0	37.751	-119.018	1988-001163	felsic	rhyolite
I-5-2	382940	0	37.751	-119.018	1988-001163	felsic	rhyolite
I-5-20	382942	0	37.751	-119.018	1988-001163	felsic	rhyolite
SS3-3	382944	0	37.751	-119.018	1988-001163	felsic	rhyolite
SS6-1	382947	0	37.751	-119.018	1988-001163	felsic	rhyolite
I-3-2	382949	0	37.751	-119.018	1988-001163	felsic	rhyolite

Table B.1 NAVDAT entries (volcanics only) for Sierra Nevada, Basin and Range study area (continued)

Sample ID	Sample Num	Calc Age	Latitude	Longitude	GeoRef	Composition	Rock Name
I-5-1	382951	0	37.751	-119.018	1988-001163	felsic	rhyolite
LV-9	382954	0	37.751	-119.018	1988-001163	felsic	rhyolite
H-18	437186	2.14	37.5017	-119.1533	1982-017260	mafic	basalt
I-1	437187	3.1	37.6983	-118.9067	1982-017260	felsic	rhyolite
I-2	437188	3.1	37.68	-118.9867	1982-017260	felsic	rhyolite
I-3	437189	3.1	37.6533	-118.9667	1982-017260	intermediate	andesite
I-4	437190	3.1	37.64	-118.8417	1982-017260	mafic	basalt
I-5	437191	3.1	37.6217	-118.99	1982-017260	felsic	dacite
K-1	437192	3.3	37.55	-118.5	1982-017260	felsic	rhyolite
M-1	437195	2.14	37.4667	-119.3033	1982-017260	mafic	basalt
M-2	437196	2.14	37.4667	-119.2667	1982-017260	mafic	basalt
M-3	437197	2.14	37.3967	-119.3733	1982-017260	mafic	basalt
N-1	437198	2.14	37.4317	-119.1483	1982-017260	mafic	basalt
N-2	437199	2.14	37.4067	-119.2317	1982-017260	intermediate	andesite
N-3	437200	2.14	37.42	-119.2317	1982-017260	mafic	basalt
N-4	437201	2.14	37.385	-119.0767	1982-017260	mafic	basalt
N-5	437202	2.14	37.385	-119.01	1982-017260	mafic	basalt
N-7	437203	2.14	37.3717	-119.0817	1982-017260	mafic	basalt
O-1	437204	2.14	37.4967	-118.965	1982-017260	mafic	basalt
O-2	437205	2.14	37.405	-118.89	1982-017260	mafic	basalt
H-16	437185	2.14	37.5517	-119.0083	1982-017260	mafic	basalt
N3015	423221	12.5	38.978	-117.615	1980-024531	intermediate	basaltic-andesite
B-2/UT-283	377268	9.2	38.2458	-119.21	1983-046157	intermediate	andesite
B-23/UT-284	377271	5.55	38.28	-119.1575	1983-046157	mafic	basalt

Table B.1 NAVDAT entries (volcanics only) for Sierra Nevada, Basin and Range study area (continued)

Sample ID	Sample Num	Calc Age	Latitude	Longitude	GeoRef	Composition	Rock Name
C3013	423161	11.1	37.412	-117.964	1980-024531	mafic	basalt
MC73-1A	390627	0.01	37.7667	-119.0167	1992-049812	felsic	rhyolite
66	397995	1.35	37.775	-118.708	1993-001953	felsic	rhyolite
D85-11	386036	3.55	38.1667	-117.7	1989-079451	mafic	basalt
D85-15	386038	9.5	37.4667	-117.8667	1989-079451	mafic	basalt
D85-24	386041	0.9	37.0672	-118.2617	1989-079451	mafic	basalt
D85-36	386047	0.9	37.1064	-118.3142	1989-079451	mafic	basalt
D85-55	386059	3.2	37.5167	-118.55	1989-079451	intermediate	mugearite
D85-57	386061	0.8	37.5833	-119.0167	1989-079451	intermediate	trachyandesite
D85-61	386064	3.1	37.5833	-119	1989-079451	mafic	basalt
D85-173	386143	3.55	38.1333	-119.25	1989-079451	intermediate	trachyandesite
D85-175	386145	11.3	38.0833	-119.1667	1989-079451	intermediate	trachyandesite
D85-176	386148	9.3	38.1333	-119.1	1989-079451	intermediate	trachyandesite
D85-178	386150	3.55	38.25	-118.95	1989-079451	intermediate	trachyandesite
D85-184	386153	3.55	38.1667	-118.7333	1989-079451	intermediate	trachyandesite
D85-189A	386156	0.3	38.35	-118.9167	1989-079451	intermediate	trachyandesite
D85-191	386158	3.1	37.6833	-119.0667	1989-079451	intermediate	hawaiite
D85-195	386161	3.55	37.75	-118.9167	1989-079451	intermediate	trachyandesite
D85-199	386163	3.55	37.8167	-118.6833	1989-079451	intermediate	basaltic-andesite
D85-204	386166	3.55	37.8667	-118.8333	1989-079451	mafic	basalt
D85-213	386174	3.7	37.8833	-118.7833	1989-079451	intermediate	trachyandesite
D85-216	386176	3.55	37.9333	-118.35	1989-079451	intermediate	mugearite
D85-224	386179	2.8	38.1667	-118.0333	1989-079451	intermediate	trachyandesite
D85-227	386181	4.8	37.7333	-118.0333	1989-079451	intermediate	hawaiite

Table B.1 NAVDAT entries (volcanics only) for Sierra Nevada, Basin and Range study area (continued)

Sample ID	Sample Num	Calc Age	Latitude	Longitude	GeoRef	Composition	Rock Name
D85-230B	386184	0.9	37.0224	-118.1742	1989-079451	mafic	basalt
YR-1	400205	7.54	38.9383	-119.2492	1995-029811	intermediate	basaltic-andesite
YR13B	400208	8.91	38.9306	-118.9861	1995-029811	felsic	pyroclastic-fall
YR-6	400213	13.83	38.9864	-119.2556	1995-029811	intermediate	andesite
41JD89	400216	14.95	38.9844	-118.9511	1995-029811	intermediate	andesite
FL-KA-3	402852	11	37.3415	-117.7618	1997-034538		
FL-KA-2	402854	3.9	37.8356	-118.3266	1997-034538		
FL-KA-6	402856	3	37.8356	-118.3266	1997-034538		
FL-KA-9	402858	3.2	37.8356	-118.3266	1997-034538		
FL-KA-16	402860	6.3	37.3432	-117.8359	1997-034538		
FL-KA-39	402862	5.3	37.3804	-117.8751	1997-034538		
FL-KA-49	402864	2.9	37.8892	-118.2451	1997-034538		
CT75-6	397997	1.65	37.775	-118.708	1993-001953	felsic	rhyolite
141	397999	1.44	37.775	-118.708	1993-001953	felsic	rhyolite
165	398002	1.6	37.775	-118.708	1993-001953	felsic	rhyolite
215	398004	1.77	37.775	-118.708	1993-001953	felsic	rhyolite
161	398006	1.65	37.775	-118.708	1993-001953	felsic	rhyolite
158	398009	1.93	37.775	-118.708	1993-001953	felsic	rhyolite
28	398011	0.79	37.775	-118.708	1993-001953	felsic	rhyolite
20	398013	0.96	37.775	-118.708	1993-001953	felsic	rhyolite
155	398016	1	37.775	-118.708	1993-001953	felsic	rhyolite
4	398018	0.92	37.775	-118.708	1993-001953	felsic	rhyolite
48	398020	1.06	37.775	-118.708	1993-001953	felsic	rhyolite
132	398023	0.97	37.775	-118.708	1993-001953	felsic	rhyolite

Table B.1 NAVDAT entries (volcanics only) for Sierra Nevada, Basin and Range study area (continued)

Sample ID	Sample Num	Calc Age	Latitude	Longitude	GeoRef	Composition	Rock Name
55	398025	0.91	37.775	-118.708	1993-001953	felsic	rhyolite
58	398027	0.82	37.775	-118.708	1993-001953	felsic	rhyolite
210	398030	1.2	37.775	-118.708	1993-001953	felsic	rhyolite
96	398604	3.86	37.8015	-118.6838	1993-038104		not-given
158	398606	0.11	38.3677	-118.8098	1993-038104		not-given
97WM060	410333	4.01	37.7972	-118.2061	2003-048086	mafic	basalt
97WM007	410336	5.36	37.8244	-118.2542	2003-048086	intermediate	andesite
97WM016	410339	3.9	37.8264	-118.2342	2003-048086	mafic	basalt
MP97-19	406475	3.43	37.5937	-119.2665	2000-073550		
HL 97-28	408750	10.2	37.2172	-119.1568	2002-043002	intermediate	basaltic-andesite
MP 97-17	408755	3.47	37.5212	-119.4677	2002-043002	mafic	shoshonite
MP 97-19	408757	3.43	37.5937	-119.2665	2002-043002	mafic	trachybasalt
SL 97-26B	408761	3.6	37.2318	-119.2588	2002-043002	mafic	trachybasalt
cDP83-85	412551	3.15	37.7417	-119.1467	2005-004738	mafic	basalt
DP72-7	412553	3.15	37.675	-119.065	2005-004738	mafic	basalt
cDP83-74	412556	3.15	37.7233	-119.1233	2005-004738	mafic	basalt
D-801e	412558	3.15	37.6783	-119.065	2005-004738	intermediate	andesite
DP78-34A	412560	2.9	37.7083	-119.1083	2005-004738	intermediate	andesite
cDP83-68	412563	3.15	37.7183	-119.11	2005-004738	intermediate	andesite
DP78-35	412565	2.9	37.7033	-119.0967	2005-004738	felsic	dacite
D-800	412567	2.9	37.7117	-119.1	2005-004738	felsic	dacite
GM78-1	412569	3.15	37.7667	-118.6633	2005-004738	mafic	basalt
CT85-7	412572	3.15	37.795	-118.8717	2005-004738	mafic	basalt
CD85-6A	412574	3.15	37.5683	-118.6167	2005-004738	mafic	basalt

Table B.1 NAVDAT entries (volcanics only) for Sierra Nevada, Basin and Range study area (continued)

Sample ID	Sample Num	Calc Age	Latitude	Longitude	GeoRef	Composition	Rock Name
CD85-5	412576	3.15	37.715	-118.43	2005-004738	mafic	basalt
CT78-7	412578	3.15	37.965	-118.84	2005-004738	intermediate	andesite
GM72-1	412585	3.15	37.7967	-118.68	2005-004738	felsic	dacite
M72-37	412590	0.4	37.7083	-118.9483	2005-004738	mafic	basalt
CT72-13	412592	0.1	37.7533	-118.8983	2005-004738	mafic	basalt
M72-15	412594	0.25	37.725	-118.9617	2005-004738	mafic	basalt
M72-99	412596	0.1	37.6383	-118.8983	2005-004738	mafic	basalt
M73- 5	412599	0.15	37.6683	-119.0233	2005-004738	intermediate	andesite
M73-4	412601	0.15	37.6667	-118.9917	2005-004738	felsic	dacite
M72- 92	412603	0.15	37.655	-119	2005-004738	felsic	dacite
DP81-2	412605	0.005	37.4233	-119.0583	2005-004738	mafic	basalt
MC74-8	412608	0.25	37.8283	-119.0683	2005-004738	mafic	basalt
BO75-2	412610	0.0002	38.02	-119.05	2005-004738	intermediate	andesite
BO75-4	412612	0.0002	38.025	-119.05	2005-004738	felsic	dacite
BO75-5	412614	0.0002	38.0283	-119.04	2005-004738	felsic	dacite
B-1	447666	0.31	37.0712	-118.255	2007-043967	mafic	basalt
B-3	447668	0.13	37.0661	-118.2619	2007-043967	mafic	basalt
M12-1A	452464	0.02	38	-119	1990-066032	felsic	rhyolite
M12-2A	452465	0.02	38	-119	1990-066032	felsic	rhyolite
Neg-RD2	452466	0	38	-119	1990-066032	felsic	dacite
Pao3	452467	0	38	-119	1990-066032	felsic	rhyolite
M19-1	452468	0.02	38	-119	1990-066032	felsic	rhyolite
BP83-1	452462	0.0138	38	-119	1990-066032	mafic	basalt
M24-1	452469	0.02	38	-119	1990-066032	felsic	rhyolite

Table B.1 NAVDAT entries (volcanics only) for Sierra Nevada, Basin and Range study area (continued)

Sample ID	Sample Num	Calc Age	Latitude	Longitude	GeoRef	Composition	Rock Name
M11-1	452470	0.02	38	-119	1990-066032	felsic	rhyolite
M11-3	452471	0.02	38	-119	1990-066032	felsic	rhyolite
M14-1A	452472	0.02	38	-119	1990-066032	felsic	rhyolite
M18-1A	452473	0.02	38	-119	1990-066032	felsic	rhyolite
M29-2	452474	0.02	38	-119	1990-066032	felsic	rhyolite
M28(m22-1)	452475	0.02	38	-119	1990-066032	felsic	rhyolite
M16-1	452476	0.02	38	-119	1990-066032	felsic	rhyolite
M8-3	452477	0.02	38	-119	1990-066032	felsic	rhyolite
M23-1	452478	0.02	38	-119	1990-066032	felsic	rhyolite
M22-1	452479	0	38	-119	1990-066032	felsic	rhyolite
M3(m1-2)	452480	0	38	-119	1990-066032	felsic	rhyolite
MP-378	453322	3.55	37.6333	-119.4	1983-052545	felsic	rhyodacite
MP-164B	453330	3.55	37.5833	-119.3333	1983-052545	mafic	trachybasalt
MP-37B	453331	3.55	37.5333	-119.2667	1983-052545	mafic	trachybasalt
MP-265C	453334	3.55	37.6	-119.25	1983-052545	intermediate	trachyandesite
MP-164A	453335	3.55	37.5833	-119.3333	1983-052545	intermediate	phonolite
MP-71	453336	3.55	37.5667	-119.3167	1983-052545	intermediate	phonolite
MP-840A	453338	3.55	37.5167	-119.4667	1983-052545	intermediate	phonolite
MP-507A	453339	3.55	37.5167	-119.45	1983-052545	intermediate	phonolite
MP-842A	453340	3.55	37.6167	-119.45	1983-052545	intermediate	phonolite

References for Table B.1

1963-009923 G. Brent Dalrymple
Potassium-argon dates of some Cenozoic volcanic rocks of the Sierra Nevada
GSA Bulletin, Apr 1963; 74: 379 - 390.

1964-007048 J. F. Evernden, D. E. Savage, G. H. Curtis, and G. T. James
Potassium-argon dates and the Cenozoic mammalian chronology of North America
American Journal of Science (February 1964), 262(2):145-198

1964-010952 G. B. Dalrymple
Potassium-argon dates of three Pleistocene interglacial basalt flows from the Sierra Nevada, California
GSA Bulletin, Aug 1964; 75: 753 - 757.

1964-012355 J. F. Evernden and G. T. James
Potassium-argon dates and the Tertiary floras of North America
American Journal of Science (October 1964), 262(8):945-974

1964-013614 G. Brent Dalrymple
Cenozoic chronology of the Sierra Nevada, California
University of California Publications in Geological Sciences (1964), 47 41 *pp.*

1966-000404 Richard R. Doell, G. Brent Dalrymple, and Allan Cox
Geomagnetic polarity epochs; Sierra Nevada data, [Part] 3
Journal of Geophysical Research (1966), 71(2):531-541

1968-058802 C. M. Gilbert, M. N. Christensen, Yehya Al-Rawi, and K. R. Lajoie
Structural and volcanic history of Mono Basin, California-Nevada (*in* Studies in volcanology--A memoir in honor of Howel Williams)
Memoir - Geological Society of America (1968), 275-329

1968-062978 G. Brent Dalrymple
Potassium-argon ages of recent rhyolites of the mono and inyo craters, california
Earth and Planetary Science Letters (1967), 3(4):289-298

1972-010381 Harold W. Krueger and John H. Schilling
Geochron/Nevada Bureau of Mines K/Ar age determinations; list 1
Isochron/West (1971), 1 9-14

1972-022655 Miles L. Silberman and Charles W. Chesterman
K/Ar Age of volcanism and mineralization, Bodie Mining District and Bodie Hills Volcanic Field, Mono County, California
Isochron/West (1972), 3 13-22

1973-004168 Miles L. Silberman and Edwin H. McKee
A summary of radiometric age determinations on Tertiary volcanic rocks from Nevada and eastern California; Part II, Western Nevada
Isochron/West (1972), 4 7-28

1976-029758 M. L. Silberman, H. F. Bonham, L. J. Garside, and D. H. Osborne
New K-Ar ages of volcanic and plutonic rocks and ore deposits in western Nevada

Isochron/West (August 1975), (13):13-21

1977-007325 George R. Priest
Eruptive history and geochemistry of the Little Walker volcanic center, East central California
University of Nevada at Reno, Reno, NV, United States, Master's thesis (1974) 99 *pp.*

1977-900002 Morton, J.L. and Silberman, M.L. (USGS, Menlo Park), Bonham,H.F. and Garside, L.J. (NBMG, Reno) and Nobel, D.C. (Mich. Tech. Univ., Houghton), K-Ar ages of volcanic rocks, plutonic rocks, and ore deposits in Nevada and eastern California – determinations run under the USGS-NBMG cooperative program.

1977-900034 Marvin, R.F. and Mehnert, H. (USGS, Denver), K-Ar ages of Tertiary igneous and sedimentary rocks of the Mina-Candelaria region, Mineral County, Nevada.

1978-010575 Gerald F. Brem
Petrogenesis of late Tertiary potassic volcanic rocks in Sierra Nevada and western Great Basin
University of California at Riverside, Riverside, CA, United States, Doctoral thesis (1977) 361 *pp.*

1978-010582 J. W. Babcock
The late Cenozoic Coso volcanic field, Inyo County, California
University of California at Santa Barbara, Santa Barbara, CA, United States, Doctoral thesis (1977) 257 *pp.*

1978-034495 R. F. Marvin and J. C. Cole
Radiometric ages; Compilation A, U. S. Geological Survey
Isochron/West (August 1978), (22):3-14

1980-010483 Norbert William Larsen
Chronology of late Cenozoic basaltic volcanism; the tectonic implications along a segment of the Sierra Nevada and Basin and Range Province boundary
Brigham Young University, Provo, UT, United States, Doctoral thesis (1979) 95 *pp.*

1980-024531 Joel Earl Everson
Regional variations in the lead isotopic characteristics of late Cenozoic basalts from the southwestern United States
California Institute of Technology, Pasadena, CA, United States, Doctoral thesis (1979) 464 *pp.*

1980-028332 R. F. Marvin and S. W. Dobson
Radiometric ages; compilation B, U. S. Geological Survey
Isochron/West (December 1979), (26):3-30

1980-045824 C. W. Naeser, G. A. Izett, and J. D. Obradovich
Fission-track and K-Ar ages of natural glasses
U. S. Geological Survey Bulletin (1980), B 1489:31 *pp.*

1981-009079 E. C. Bingler, M. L. Silberman, and E. H. McKee
K-Ar ages of volcanic and plutonic rocks in the northern Wassuck Range,

central-western Nevada
Isochron/West (April 1980), (27):13-16

1981-011633 G. Brent Dalrymple
K-Ar ages of the Friant Pumice Member of the Turlock Lake Formation, the Bishop Tuff, and the tuff of Reds Meadow, central California
Isochron/West (August 1980), (28):3-5

1981-050018 Gerald K. Van Kooten
An ultrapotassic basaltic suite from the central Sierra Nevada, California; a study of the mineralogy, petrology, geochemistry and isotopic composition
University of California at Santa Barbara, Santa Barbara, CA, United States, Doctoral thesis (1980) 112 *pp.*

1982-017260 Franklin C. W. Dodge and James G. Moore
Late Cenozoic volcanic rocks of the southern Sierra Nevada, California; II, Geochemistry
Geological Society of America Bulletin (December 1981), 92(12):I 912-I 914, II 1670-II 1761

1983-046157 Chris T. Higgins and Stanley H. Evans
K-Ar dates of volcanic rocks in the western Bodie Hills, California
Isochron/West (April 1983), 36 3-6

1983-052545 D. L. Peck and G. K. Van Kooten
Merced Peak Quadrangle, central Sierra Nevada, California; analytic data
U. S. Geological Survey Professional Paper (1983), P 1170-D:29 *pp.*

1984-019557 Andrei M. Sarna-Wojcicki, H. R. Bowman, C. E. Meyer, P. C. Russell, M. J. Woodward, Gail McCoy, J. J. Rowe, P. A. Baedecker, Frank Asaro, and Helen Michael
Chemical analyses, correlations, and ages of upper Pliocene and Pleistocene ash layers of east-central and Southern California
U. S. Geological Survey Professional Paper (1984), P 1293:40 *pp.*

1985-023627 Edwin H. McKee and Paul R. Klock
K-Ar ages of Cenozoic volcanic rocks; Walker Lake 1X2 degrees Quadrangle, eastern California and western Nevada
Isochron/West (August 1984), 40 9-11

1986-028002 Edward A. Mankinen, C. Sherman Gromme, G. Brent Dalrymple, Marvin A. Lanphere, and Roy A. Bailey
Paleomagnetism and K-Ar ages of volcanic rocks from Long Valley Caldera, California
Journal of Geophysical Research (January 1986), 91(B1):633-652

1988-001163 Daniel E. Sampson and Kenneth L. Cameron
The geochemistry of the Inyo volcanic chain; multiple magma systems in the Long Valley region, eastern California
Journal of Geophysical Research (September 1987), 92(B10):10,403-10,421

1988-052744 David S. Ormerod, Christopher J. Hawkesworth, Nicholas W. Rogers, William P. Leeman, and Martin A. Menzies
Tectonic and magmatic transitions in the western Great Basin, USA
Nature (London) (May 1988), 333(6171):349-353

1988-079677 Glen A. Izett, John D. Obradovich, and Harald H. Mehnert
The Bishop ash bed (middle Pleistocene) and some older (Pliocene and Pleistocene) chemically and mineralogically similar ash beds in California, Nevada, and Utah
U. S. Geological Survey Bulletin (1988), B 1675:37 *pp.*

1989-042953 Richard F. Marvin, Harald H. Mehnert, and Charles W. Naeser
U. S. Geological Survey radiometric ages; Compilation "C", Part three; California and Nevada
Isochron/West (March 1989), 52 3-12

1989-065947 David Burton Slemmons
Geology of the Sonora Pass region
University of California at Berkeley, Berkeley, CA, United States, Doctoral thesis (1953) 222 *pp.*

1989-073447 Edward Wesley Hildreth
The magma chamber of the Bishop Tuff; gradients in temperature, pressure, and composition
University of California at Berkeley, Berkeley, CA, United States, Doctoral thesis (1977) 328 *pp.*

1989-079451 David Stephen Ormerod
Late- to post-subduction magmatic transitions in the western Great Basin, U.S.A.
Open University, Milton Keynes, United Kingdom, Doctoral thesis (1988) 331 *pp.*

1990-066032 Patrick C. Kelleher and Kenneth L. Cameron
The geochemistry of the Mono Craters-Mono Lake islands volcanic complex, eastern California
Journal of Geophysical Research (October 1990), 95(B11):17,643-17,659

1991-010933 Robert J. Varga, Roy A. Bailey, and Gene A. Suemnicht
Evidence for 600 year-old basalt and magma mixing at Inyo Craters volcanic chain, Long Valley Caldera, California
Journal of Geophysical Research (December 1990), 95(B13):21,441-21,450

1992-049812 Ray Macdonald, Robert L. Smith, and John E. Thomas
Chemistry of the subalkalic silicic obsidians
U. S. Geological Survey Professional Paper (1992), P 1523:214 *pp.*

1993-001953 J. M. Metz and G. A. Mahood
Development of the Long Valley, California, magma chamber recorded in precaldera rhyolite lavas of Glass Mountain
Contributions to Mineralogy and Petrology (1991), 106(3):379-397

1993-005802 M. C. Reheis, T. L. Sawyer, J. L. Slate, and A. R. Gillespie
Geologic map of late Cenozoic deposits and faults in the southern part of the Davis Mountain 15' Quadrangle, Esmeralda County, Nevada
Miscellaneous Investigations Series - U. S. Geological Survey (1993) I-2342
Maps: colored geologic map; 1:24,000, 1 sheet

1993-010551 D. S. Ormerod, N. W. Rogers, and C. J. Hawkesworth
Melting in the lithospheric mantle; inverse modelling of alkali-olivine

basalts from the Big Pine volcanic field, California
Contributions to Mineralogy and Petrology (September 1991), 108(3):305-317

1993-038104 Rebecca A. Lange, Ian S. E. Carmichael, and Paul R. Renne
Potassic volcanism near Mono Basin, California; evidence for high water and oxygen fugacities inherited from subduction
Geology, Oct 1993; 21: 949 - 952.

1994-037732 Qiang Hu, Patrick E. Smith, Norman M. Evensen, and Derek York
Lasing in the Holocene; extending the ^{40} Ar- ^{39} Ar laser probe method into the ^{14} C age range
Earth and Planetary Science Letters (May 1994), 123(1-4):331-336

1995-029811 John H. Dilles and Phillip B. Gans
The chronology of Cenozoic volcanism and deformation in the Yerington area, western Basin and Range and Walker Lane
GSA Bulletin, Apr 1995; 107: 474 - 486.

1995-044484 Robert J. Miller and Chester T. Wrucke
Age, chemistry, and geologic implications of Tertiary volcanic rocks in the Last Chance Range and part of the Saline Range, northern Death Valley region, California
Isochron/West (May 1995), 62 30-36

1997-021098 Brian L. Cousens
Magmatic evolution of Quaternary mafic magmas at Long Valley Caldera and the Devils Postpile, California; effects of crustal contamination on lithospheric mantle-derived magmas
Journal of Geophysical Research (December 1996), 101(B12):27,673-27,689

1997-034538 Marith C. Reheis and Thomas L. Sawyer
Late Cenozoic history and slip rates of the Fish Lake Valley, Emigrant Peak, and Deep Springs fault zones, Nevada and California
GSA Bulletin, Mar 1997; 109: 280 - 299.

1998-025813 Michael E. Perkins, Francis H. Brown, William P. Nash, William McIntosh, and S. K. Williams
Sequence, age, and source of silicic fallout tuffs in middle to late Miocene basins of the northern Basin and Range Province
GSA Bulletin, Mar 1998; 110: 344 - 360.

1999-027986 J. R. Waits
Geochemical and isotopic study of peridotite-bearing lavas in eastern California
University of North Carolina at Chapel Hill, Chapel Hill, NC, United States, Master's thesis (1995) 59 *pp*.

1999-055339 Brian L. Beard and Allen F. Glazner
Petrogenesis of isotopically unusual Pliocene olivine leucitites from Deep Springs Valley, California
Contributions to Mineralogy and Petrology (December 1998), 133(4):402-417

2000-066389 Donald J. DePaolo and E. Ellen Daley
Neodymium isotopes in basalts of the Southwest Basin and Range and lithospheric thinning during continental extension (*in*)
Chemical Geology (August 2000), 169(1-2):157-185

2000-073550 Curtis R. Manley, Allen F. Glazner, and G. Lang Farmer
Timing of volcanism in the Sierra Nevada of California: Evidence for Pliocene delamination of the batholithic root?
Geology, Sep 2000; 28: 811 - 814.

2002-043002 GEOCHEMISTRY:
G. Lang Farmer, Allen F. Glazner, and Curtis R. Manley
Did lithospheric delamination trigger late Cenozoic potassic volcanism in the southern Sierra Nevada, California?
GSA Bulletin, Jun 2002; 114: 754 - 768.

2003-048086 Daniel F. Stockli, Trevor A. Dumitru, Michael O. McWilliams, and Kenneth A. Farley
Cenozoic tectonic evolution of the White Mountains, California and Nevada
GSA Bulletin, Jul 2003; 115: 788 - 816.

2004-900009 Kelly, T.S. and Henry, C.D., unpublished data.

2005-004738 Roy A. Bailey
Eruptive history and chemical evolution of the precaldera and postcaldera basalt-dacite sequences, Long Valley, California; implications for magma sources, current seismic unrest, and future volcanism
U. S. Geological Survey Professional Paper (2004), P 1692:75 *pp.*

2007-043967 B. E. Mordick and A. F. Glazner
Clinopyroxene thermobarometry of basalts from the Coso and Big Pine volcanic fields, California
Contributions to Mineralogy and Petrology (July 2006), 152(1):111-124

Table B.2 NAVDAT entries (volcanics only) for Mojave study area

Sample ID	Sample Num	Calc Age	Latitude	Longitude	GeoRef	Composition	Rock Name
YAB 93-96	398608	4.47	36	-114.75	1993-038710	Mafic	Basalt
OAB 57-113	398614	4.95	35.8772	-114.5875	1993-038710	Mafic	Basalt
M-2	398261	2	35.9215	-114.6399	1993-010351	Mafic	Basalt
714-35	406375	12.5	35.6617	-114.6617	2000-066389	Mafic	Basalt
OAB 57-107	398615	4.95	35.8772	-114.5875	1993-038710	Mafic	Basalt
TID-1	406379	4.6	35.94	-114.64	2000-066389	Mafic	Basalt
M-1	398262	5.8	35.8691	-114.6051	1993-010351	Mafic	Basalt
3	439091	10.2	35.088	-115.3615	1989-067667	Mafic	Alkali Basalt
7382	439058	10.6	35	-115.25	1989-024207	Mafic	Not-Given
10	377306	14.5	35.1	-115.3583	1983-046225	Mafic	Basanite
A-22	390219	0.1	34.5459	-115.7908	1992-017921	Mafic	
Ci-10-101	400836	5.9	35.357	-115.6419	1995-043332	Mafic	Basalt
Ci-12	400824	3	35.3385	-115.632	1995-043332	Mafic	Basalt
A-17	390216	0.1	34.5423	-115.7909	1992-017921	Mafic	
Ci-49	400841	7.55	35.2171	-115.7052	1995-043332	Mafic	Basalt
A-28	390223	0.1	34.5517	-115.803	1992-017921	Mafic	
A-3	390206	0.1	34.5458	-115.7906	1992-017921	Mafic	
A-8	390208	0.1	34.5448	-115.7904	1992-017921	Mafic	
MC21	380245	0.63	35.2232	-115.7808	1986-021700	Mafic	Basalt
Ci 9-101	400838	6.2	35.3603	-115.6544	1995-043332	Mafic	Basalt
A-27	390222	0.1	34.5444	-115.8089	1992-017921	Mafic	
TH 60-04	398612	10.15	35.75	-114.6667	1993-038710	Mafic	Basalt
MC43	380256	0.32	35.2998	-115.7149	1986-021700	Mafic	Basalt
A-32	390226	0.1	34.5282	-115.7559	1992-017921	Mafic	

Table B.2 NAVDAT entries (volcanics only) for Mojave study area (continued)

Sample ID	Sample Num	Calc Age	Latitude	Longitude	GeoRef	Composition	Rock Name
MC12	380239	0.58	35.204	-115.8705	1986-021700	Mafic	Basalt
MC29	380250	0.99	35.1908	-115.7381	1986-021700	Mafic	Basalt
TMF-2	406376	4.9	35.9517	-114.6483	2000-066389	Mafic	Basalt
A-25	390221	0.1	34.5419	-115.7963	1992-017921	Mafic	
C4025	423169	0.05	35.288	-115.726	1980-024531	Mafic	Basalt
A-2	390205	0.1	34.5458	-115.7906	1992-017921	Mafic	
A-19	390217	0.1	34.5447	-115.7922	1992-017921	Mafic	
A-21	390218	0.1	34.5453	-115.7913	1992-017921	Mafic	
BC355	372336	12.65	35.825	-114.7833	1978-006456	Mafic	Basalt
MC37	380252	0.25	35.257	-115.7478	1986-021700	Mafic	Basalt
73723	439059	10.6	35	-115.25	1989-024207	Mafic	Not-Given
C-19	404479	0.5	35.2034	-115.7463	1999-027986	Mafic	Basalt
PB34	419882	0.5	35.1667	-115.8667	1989-056727	Mafic	Basalt
PB-34	418998	0.001	35.1667	-115.8167	1986-024128	Mafic	Basalt
MC20	380244	0.46	35.2005	-115.8095	1986-021700	Mafic	Basalt
A-6	390207	0.1	34.5448	-115.7882	1992-017921	Mafic	
Ci-43	400814	0.15	35.1946	-115.8408	1995-043332	Mafic	Basalt
Ci-15	400821	0.85	35.2355	-115.7439	1995-043332	Mafic	Basalt
A-30	390224	0.1	34.565	-115.7976	1992-017921	Mafic	
MC25	380247	0.39	35.245	-115.7875	1986-021700	Mafic	Basalt
Ci-6-1	400815	0.27	35.2766	-115.732	1995-043332	Mafic	Basalt
Ci-9-102	400835	5.5	35.353	-115.6544	1995-043332	Mafic	Basalt
Ci-53	400840	6.92	35.2209	-115.6851	1995-043332	Mafic	Basalt
A-10	390210	0.1	34.5448	-115.7897	1992-017921	Mafic	

Table B.2 NAVDAT entries (volcanics only) for Mojave study area (continued)

Sample ID	Sample Num	Calc Age	Latitude	Longitude	GeoRef	Composition	Rock Name
C-7	404473	0.14	35.2011	-115.7571	1999-027986	Mafic	Basalt
A-12	390212	0.1	34.5454	-115.7899	1992-017921	Mafic	
C-22	404480	0.47	35.2017	-115.7603	1999-027986	Mafic	Basalt
Ci-16	400837	6.08	35.3142	-115.8188	1995-043332	Mafic	Basalt
CD-8	400839	6.5	35.2171	-115.7052	1995-043332	Mafic	Basalt
A-23	390220	0.1	34.5455	-115.7904	1992-017921	Mafic	
C-11	404476	0.5	35.2021	-115.7299	1999-027986	Mafic	Basalt
C-8L	404475	0.5	35.2014	-115.7296	1999-027986	Mafic	Basalt
Ci-20	400816	0.33	35.2541	-115.729	1995-043332	Mafic	Basalt
C-2	404471	0.7	35.2016	-115.7262	1999-027986	Mafic	Basalt
C-17	404478	0.99	35.1994	-115.7398	1999-027986	Mafic	Basalt
A-9	390209	0.1	34.5449	-115.7898	1992-017921	Mafic	
C-5	404472	0.13	35.2008	-115.755	1999-027986	Mafic	Basalt
TP26	372352	15.55	35.7625	-114.8694	1978-006456	Mafic	Basalt
C-8A	404474	0.5	35.2014	-115.7296	1999-027986	Mafic	Basalt
A-16	390215	0.1	34.5393	-115.7924	1992-017921	Mafic	
C8439	404729	10.7	35.32	-115.0289	1999-038369	Mafic	Not-Given
TMF-9	406378	10.5	35.805	-114.635	2000-066389	Mafic	Basalt
A-1	390204	0.1	34.5458	-115.7906	1992-017921	Mafic	
MC-1A	400826	3.85	35.3064	-115.7775	1995-043332	Mafic	Basalt
BC405	372333	5	35.9442	-114.6569	1978-006456	Mafic	Basalt
C-15	404477	0.5	35.2009	-115.7342	1999-027986	Mafic	Basalt
CD-4	400817	0.99	35.1995	-115.7307	1995-043332	Mafic	Basalt
CD-5	400823	0.99	35.1931	-115.7379	1995-043332	Mafic	Basalt

Table B.2 NAVDAT entries (volcanics only) for Mojave study area (continued)

Sample ID	Sample Num	Calc Age	Latitude	Longitude	GeoRef	Composition	Rock Name
TMF-5	406377	10.5	35.805	-114.635	2000-066389	Mafic	Basalt
A-11	390211	0.1	34.5449	-115.7892	1992-017921	Mafic	
A-14	390213	0.1	34.5433	-115.7861	1992-017921	Mafic	
CX-2	404481	0.5	35.2005	-115.7286	1999-027986	Mafic	Basalt
CD-2	400818	0.35	35.1966	-115.782	1995-043332	Mafic	Basalt
MC1a	380234	3.8	35.3078	-115.7755	1986-021700	Mafic	Basalt
1	439089	10.2	35.088	-115.3615	1989-067667	Mafic	Basalt
A-15	390214	0.1	34.5424	-115.7877	1992-017921	Mafic	
CD-3	400813	0.135	35.2196	-115.7548	1995-043332	Mafic	Basalt
CX-3	404482	0.5	35.2022	-115.7286	1999-027986	Mafic	Basalt
A-31	390225	0.1	34.5553	-115.782	1992-017921	Mafic	
CD-7	400822	0.85	35.2092	-115.7159	1995-043332	Mafic	Basalt
MC-1	400827	3.88	35.3064	-115.7775	1995-043332	Mafic	Basalt
Ci-19	400833	4.48	35.4209	-115.8357	1995-043332	Mafic	Basalt
CD-1	400820	0.56	35.1839	-115.7758	1995-043332	Mafic	Basalt
MC3	380210	4.48	35.4198	-115.8409	1986-021700	Mafic	Basalt
MC5a	380213	5.12	35.3891	-115.8615	1986-021700	Mafic	Basalt
C6002	423175	0.91	34.117	-114.845	1980-024531	Mafic	Basaltic-Andesite
CD-6	400819	0.5	35.2062	-115.7397	1995-043332	Mafic	Basalt
Ci-60	400828	3.93	35.478	-115.8295	1995-043332	Mafic	Basalt
BC409B	374116	15	35.5283	-114.625	1978-025983	Mafic	Basalt
TDM-5	406372	13	35.7983	-114.795	2000-066389	Mafic	Basalt
MC-5	400831	4.24	35.3874	-115.8563	1995-043332	Mafic	Basalt

Table B.2 NAVDAT entries (volcanics only) for Mojave study area (continued)

Sample ID	Sample Num	Calc Age	Latitude	Longitude	GeoRef	Composition	Rock Name
Ci-57	400829	4.02	35.4537	-115.8062	1995-043332	Mafic	Basalt
Ci-25	400832	4.46	35.3809	-115.7273	1995-043332	Mafic	Basalt
Ci-18	400834	4.76	35.3435	-115.7413	1995-043332	Mafic	Basalt
TP66	372345	15.55	35.7375	-114.8167	1978-006456	Mafic	Basaltic-Andesite
J863	404722	8	35.2717	-114.9953	1999-038369	Mafic	Not-Given
TDM-2	406371	13	35.7983	-114.795	2000-066389	Mafic	Basalt
91-12	406385	14	35.1133	-114.9667	2000-066389	Mafic	Basalt
TP41	372344	15.55	35.775	-114.8375	1978-006456	Mafic	Basaltic-Andesite
Ci-56	400830	4.03	35.4196	-115.7865	1995-043332	Mafic	Basalt
J84CMP	404735	10.7	35.3125	-115.0625	1999-038369	Mafic	Not-Given
TP57	372338	15.55	35.7722	-114.8056	1978-006456	Mafic	Basaltic-Andesite
BC411	372337	14.2	35.7797	-114.8106	1978-006456	Mafic	Basaltic-Andesite
D-3	398249	12.2	34.9106	-114.7649	1993-010351	Mafic	Basalt
BC356	372335	12.65	35.675	-114.7833	1978-006456	Intermediate	Andesite
TDM-9	406373	13	35.7983	-114.795	2000-066389	Intermediate	Basalt
91-9	406384	14	35.0933	-114.9867	2000-066389	Intermediate	Basalt
D-2	398248	12.2	34.9104	-114.7648	1993-010351	Intermediate	Basalt
TPV-2	406370	15.2	35.7967	-114.7883	2000-066389	Intermediate	Basalt
D-1	398247	12.2	34.9105	-114.765	1993-010351	Intermediate	Basalt
SL-6	398246	10	35.3802	-114.8029	1993-010351	Intermediate	Basalt

Table B.2 NAVDAT entries (volcanics only) for Mojave study area (continued)

Sample ID	Sample Num	Calc Age	Latitude	Longitude	GeoRef	Composition	Rock Name
SL-5	398245	10	35.38	-114.8027	1993-010351	Intermediate	Basalt
MP1	457378	15.5	35.5	-114.5189	2003-042429	Intermediate	Andesite
J866	404718	8	35.0919	-114.9731	1999-038369	Intermediate	Not-Given
2	439090	11.6	35.088	-115.3615	1989-067667	Intermediate	Basaltic-Andesite
11	377307	14.5	35.1	-115.3583	1983-046225	Intermediate	Andesite
73814	439057	10	35	-115.25	1989-024207	Intermediate	Not-Given
J8493	404711	10.7	35.2167	-115.0306	1999-038369	Intermediate	Not-Given
JF-94-64	408296	15.66	35.5442	-114.9694	2002-027711	Intermediate	Trachyandesite
TP46	372342	15.55	35.7653	-114.8069	1978-006456	Intermediate	Andesite
JF-94-63	408297	15.98	35.5364	-114.9692	2002-027711	Intermediate	Trachyandesite
C84101	404723	8	35.1875	-114.9375	1999-038369	Intermediate	Not-Given
TP52	372340	15.55	35.7694	-114.8069	1978-006456	Intermediate	Andesite
TP47	372341	15.55	35.7681	-114.8069	1978-006456	Intermediate	Andesite
C8429	404727	8	35.3125	-115.0625	1999-038369	Intermediate	Not-Given
J8527	404724	8	35.1875	-114.9375	1999-038369	Intermediate	Not-Given
353-T	389484	12.8	35.3247	-115.0781	1991-040849	Intermediate	Andesite
C8470	404716	8	35.2	-115.0183	1999-038369	Intermediate	Not-Given
Tba	377286	13.5	36	-114.89	1983-046190	Intermediate	Andesite
C84107	404715	10.7	35.1875	-114.9375	1999-038369	Intermediate	Not-Given
J8481	404732	8	35.3125	-115.0625	1999-038369	Intermediate	Not-Given
T130	439039	15.8	35	-115.25	1989-024207	Intermediate	Pyroclastic Fall
126T	404707	10.7	35.3125	-115.0625	1999-038369	Intermediate	Not-Given
J8484	404733	10.7	35.3125	-115.0625	1999-038369	Intermediate	Not-Given

Table B.2 NAVDAT entries (volcanics only) for Mojave study area (continued)

Sample ID	Sample Num	Calc Age	Latitude	Longitude	GeoRef	Composition	Rock Name
16	439102	15.8	35.1494	-115.3826	1989-067667	Intermediate	Trachydacite
C8433	404728	8	35.2931	-115.0375	1999-038369	Termediate	Not-Given
J84109a	404734	8	35.3125	-115.0625	1999-038369	Termediate	Not-Given
C8442	404730	8	35.3125	-115.0625	1999-038369	Termediate	Not-Given
MP3	457379	15.5	35.5447	-114.5503	2003-042429	Intermediate	Andesite
TP35	372348	15.55	35.7431	-114.8444	1978-006456	Termediate	Dacite
J8491	404710	10.7	35.1875	-115.0625	1999-038369	Termediate	Not-Given
8	439094	15.8	35.208	-115.3579	1989-067667	Intermediate	Trachyte
6	377302	14.5	35.1833	-115.2	1983-046225	Felsic	Tuff
8	377304	14.5	35.1	-115.225	1983-046225	Intermediate	Trachyte
9	439095	15.8	35.208	-115.3579	1989-067667	Intermediate	Trachyte
TP44	372343	15.55	35.775	-114.8361	1978-006456	Felsic	Dacite
351-T	389483	12.8	35.3247	-115.0781	1991-040849	Intermediate	Andesite
93-79	457380	15.5	35.5339	-114.5544	2003-042429	Felsic	Dacite
J861	404720	8	35.3125	-114.9375	1999-038369	Felsic	Tuff
4	377300	14.5	35.2	-115.2333	1983-046225	Felsic	Rhyolite
J84134	404717	8	35.0625	-114.9375	1999-038369	Felsic	Not-Given
TP64	372346	15.55	35.7367	-114.8175	1978-006456	Felsic	Tuff
L207	372339	15.55	35.7667	-114.8167	1978-006456	Felsic	Rhyolite
TP62	372347	15.55	35.7364	-114.8192	1978-006456	Felsic	Tuff
T205	439053	15.8	35	-115.25	1989-024207	Felsic	Pyroclastic Fall
T208	439054	15.8	35	-115.25	1989-024207	Felsic	Pyroclastic Fall
Tbd	377285	13.5	36	-114.87	1983-046190	Felsic	Dacite
BC397	374117	15.55	35.7667	-114.8333	1978-025983	Felsic	Tuff

Table B.2 NAVDAT entries (volcanics only) for Mojave study area (continued)

Sample ID	Sample Num	Calc Age	Latitude	Longitude	GeoRef	Composition	Rock Name
J8318	404714	10.7	35.0625	-114.9375	1999-038369	Felsic	Not-Given
A160	439042	15.8	35	-115.25	1989-024207	Felsic	Pyroclastic Fall
140-T	389479	12.8	35.3492	-115.0819	1991-040849	Felsic	Rhyolite
J8496	404712	10.7	35.2333	-115.0264	1999-038369	Felsic	Not-Given
5	377301	14.5	35.2333	-115.205	1983-046225	Felsic	Trachyte
R1	439035	15.8	35	-115.25	1989-024207	Felsic	Pyroclastic Flow
9	377305	14.5	35.1333	-115.1833	1983-046225	Felsic	Rhyolite
TP25	372353	15.55	35.7639	-114.8694	1978-006456	Felsic	Rhyolite
R161	439043	15.8	35	-115.25	1989-024207	Felsic	Pyroclastic Flow
1	377297	14.5	35.1167	-115.425	1983-046225	Felsic	Rhyolite
A159	439041	15.8	35	-115.25	1989-024207	Felsic	Pyroclastic Fall
R190	439049	15.8	35	-115.25	1989-024207	Felsic	Pyroclastic Flow
137-T	389478	14.4	35.3575	-115.085	1991-040849	Felsic	Rhyolite
R214	439052	15.8	35	-115.25	1989-024207	Felsic	Pyroclastic Flow
L311	372351	15.55	35.7	-114.8167	1978-006456	Felsic	Rhyolite
93-84	457381	15.5	35.5367	-114.5714	2003-042429	Felsic	Rhyolite
A158	439040	15.8	35	-115.25	1989-024207	Felsic	Pyroclastic Fall
L345	372350	15.55	35.75	-114.75	1978-006456	Felsic	Rhyolite
R167	439045	15.8	35	-115.25	1989-024207	Felsic	Pyroclastic Flow
L350	372349	15.55	35.75	-114.75	1978-006456	Felsic	Rhyolite
R169	439046	15.8	35	-115.25	1989-024207	Felsic	Pyroclastic Flow
15	439101	15.8	35.2025	-115.4036	1989-067667	Felsic	Rhyolite
R164	439044	15.8	35	-115.25	1989-024207	Felsic	Pyroclastic Flow
12	439098	15.8	35.1987	-115.397	1989-067667	Felsic	Rhyolite

Table B.2 NAVDAT entries (volcanics only) for Mojave study area (continued)

Sample ID	Sample Num	Calc Age	Latitude	Longitude	GeoRef	Composition	Rock Name
11	439097	15.8	35.1922	-115.394	1989-067667	Felsic	Rhyolite
R49	439036	15.8	35	-115.25	1989-024207	Felsic	Pyroclastic Flow
7	377303	14.5	35.125	-115.21	1983-046225	Felsic	Rhyolite
R179	439048	15.8	35	-115.25	1989-024207	Felsic	Pyroclastic Flow
10	439096	15.8	35.208	-115.3579	1989-067667	Felsic	Rhyolite
13	439099	15.8	35.1447	-115.3874	1989-067667	Felsic	Rhyolite
R212	439051	15.8	35	-115.25	1989-024207	Felsic	Pyroclastic Flow
R89	439037	15.8	35	-115.25	1989-024207	Felsic	Pyroclastic Flow
24-H	389481	14	35.3247	-115.0781	1991-040849	Felsic	Rhyolite
71-T	389482	14	35.3247	-115.0781	1991-040849	Felsic	Rhyolite
Plugs	439056	15.8	35	-115.25	1989-024207	Felsic	Rhyolite
3	377299	14.5	35.2	-115.3333	1983-046225	Felsic	Rhyolite
R201	439050	15.8	35	-115.25	1989-024207	Felsic	Pyroclastic Flow
2	377298	14.5	35.2	-115.3667	1983-046225	Felsic	Tuff
C8486	404731	12.8	35.3125	-115.0625	1999-038369	Felsic	Not-Given
R170	439047	15.8	35	-115.25	1989-024207	Felsic	Pyroclastic Flow
14	439100	15.8	35.195	-115.4018	1989-067667	Felsic	Rhyolite
Flows	439055	15.8	35	-115.25	1989-024207	Felsic	Rhyolite
R112	439038	15.8	35	-115.25	1989-024207	Felsic	Pyroclastic Flow
93-80	457382	15.5	35.5428	-114.5581	2003-042429	Felsic	Rhyolite
32	370149	14.89	35.7389	-114.825	1972-008224	Felsic	Dacite
36	370151	15.7	35.75	-114.8444	1972-008224	Felsic	Vitrophere
178	370752	14.8	35.7894	-114.8814	1974-002192	Felsic	Pyroclastic-Fall
180	370754	14.9	35.7542	-114.8611	1974-002192	Felsic	Rhyolite

Table B.2 NAVDAT entries (volcanics only) for Mojave study area (continued)

Sample ID	Sample Num	Calc Age	Latitude	Longitude	GeoRef	Composition	Rock Name
181	370755	15.7	35.75	-114.8444	1974-002192	Felsic	Rhyodacite
182	370756	14.9	35.7389	-114.825	1974-002192	Felsic	Dacite
red sandstone-silver tuff unit	374417	11.25	35.75	-114.5	1979-026763	Felsic	Pyroclastic Fall
BSW-1	399204	8.99	35.0094	-115.9917	1994-028537	Felsic	Rhyolite
Ca84PR-33a	399208	8	35.2931	-115.0375	1994-028542	Felsic	Dacite
JF-96-45	408288	15.21	35.6161	-114.9994	2002-027711	Felsic	Tuff
JF-96-42	408294	15.26	35.5714	-114.9853	2002-027711	Felsic	Tuff
JF-96-44	408295	15.22	35.5744	-114.9814	2002-027711	Felsic	Tuff
22	369454	12.94	35.6944	-115.45	1970-000478	Felsic	Rhyolite
34	370150	14.89	35.7894	-114.8814	1972-008224	Felsic	Rhyolite
40	370153	15.91	35.7542	-114.8611	1972-008224	Felsic	Vitrophere
35	370167	14.78	35.7894	-114.8814	1972-008224	Felsic	Rhyolite
39	370169	14.89	35.7542	-114.8611	1972-008224	Felsic	Vitrophere
47	370183	12.94	35.6944	-115.45	1972-008224	Felsic	Rhyolite
JP84PR-96	399207	13.3	35.2333	-115.0264	1994-028542	Felsic	Rhyolite
JF-94-82	408287	15	35.6172	-114.9992	2002-027711	Felsic	Tuff
JF-96-41	408293	14.98	35.57	-114.9858	2002-027711	Felsic	Tuff
JF92-25	457392	15.74	35.6569	-114.5844	2003-042429	Felsic	Rhyolite
JF92-35	457405	14.97	35.5478	-114.6339	2003-042429	Felsic	Rhyolite
JF92-37	457406	15.21	35.5478	-114.6317	2003-042429	Felsic	Rhyolite
88-067	457735	15.92	35.7168	-114.5928	1993-024880	Felsic	Tuff
124	370698	12.3	35.8117	-115.4733	1974-002192	Intermediate	Andesite
CA84PR-70a	399213	12.7	35.2	-115.0183	1994-028542	Intermediate	Andesite

Table B.2 NAVDAT entries (volcanics only) for Mojave study area (continued)

Sample ID	Sample Num	Calc Age	Latitude	Longitude	GeoRef	Composition	Rock Name
JP83TM-127	399229	16	34.4083	-114.8458	1994-028552	Intermediate	Andesite
JF-94-70	408291	15.81	35.5681	-115.0336	2002-027711	Intermediate	Trachyandesite
JN86-PR-3	399209	10.2	35.2716	-114.9708	1994-028542	Intermediate	Andesite
JN86PR-2	399212	12.4	35.2717	-114.9953	1994-028542	Intermediate	Andesite
S18	369054	1.17	35.3984	-114.7262	1966-000404	Mafic	Basalt
28	370182	14.17	35.7797	-114.8106	1972-008224	Mafic	Basalt
179	370753	14.2	35.7797	-114.8106	1974-002192	Mafic	Basalt
A5006	423194	5	35.95	-114.646	1980-024531	Mafic	Basalt
C6009	423176	0.91	34.91	-115.057	1980-024531	Mafic	Basalt
1	378448	3.88	35.3398	-115.7589	1984-029708	Mafic	Basalt
1A	378449	3.86	35.3398	-115.7589	1984-029708	Mafic	Basalt
1AR	378450	3.83	35.3398	-115.7589	1984-029708	Mafic	Basalt
2	378451	6.47	35.2301	-115.6822	1984-029708	Mafic	Basalt
3	378453	4.48	35.3398	-115.7589	1984-029708	Mafic	Basalt
5	378454	4.24	35.3398	-115.7589	1984-029708	Mafic	Basalt
6	378455	0.33	35.2567	-115.7185	1984-029708	Mafic	Basalt
11	378456	0.56	35.1774	-115.8264	1984-029708	Mafic	Basalt
12	378457	0.58	35.2045	-115.8709	1984-029708	Mafic	Basalt
13	378458	0.17	35.2069	-115.8709	1984-029708	Mafic	Basalt
14	378459	0.16	35.2071	-115.8686	1984-029708	Mafic	Basalt
14R	378460	0.17	35.2071	-115.8686	1984-029708	Mafic	Basalt
16	378461	0.32	35.2055	-115.8665	1984-029708	Mafic	Basalt
19	378462	0.13	35.2254	-115.7539	1984-029708	Mafic	Basalt
20	378463	0.46	35.222	-115.81	1984-029708	Mafic	Basalt

Table B.2 NAVDAT entries (volcanics only) for Mojave study area (continued)

Sample ID	Sample Num	Calc Age	Latitude	Longitude	GeoRef	Composition	Rock Name
21	378464	0.63	35.2424	-115.7911	1984-029708	Mafic	Basalt
24	378465	0.75	35.2457	-115.7964	1984-029708	Mafic	Basalt
25	378466	0.39	35.2469	-115.7989	1984-029708	Mafic	Basalt
26	378467	0.06	35.2105	-115.8131	1984-029708	Mafic	Basalt
28	378468	0.33	35.2018	-115.7419	1984-029708	Mafic	Basalt
29	378469	0.99	35.1999	-115.7453	1984-029708	Mafic	Basalt
36	378470	0.33	35.2562	-115.7396	1984-029708	Mafic	Basalt
37	378471	0.25	35.2591	-115.748	1984-029708	Mafic	Basalt
40	378472	0.67	35.2572	-115.7219	1984-029708	Mafic	Basalt
41	378473	0.27	35.2543	-115.7207	1984-029708	Mafic	Basalt
41R	378474	0.26	35.2543	-115.7207	1984-029708	Mafic	Basalt
42	378475	0.27	35.2963	-115.7143	1984-029708	Mafic	Basalt
43	378476	0.32	35.3006	-115.7168	1984-029708	Mafic	Basalt
51	378477	0.27	35.2642	-115.8005	1984-029708	Mafic	Basalt
55	378478	0.7	35.2363	-115.7236	1984-029708	Mafic	Basalt
56	378479	0.17	35.2343	-115.7913	1984-029708	Mafic	Basalt
59	378480	3.64	35.3289	-115.8505	1984-029708	Mafic	Basalt
62	378481	0.85	35.2096	-115.7138	1984-029708	Mafic	Basalt
MC4	380211	4.76	35.3449	-115.7435	1986-021700	Mafic	Basalt
MC50	380214	0.7	35.2606	-115.792	1986-021700	Mafic	Basalt
MC58	380215	0.16	35.227	-115.7685	1986-021700	Mafic	Basalt
MC61	380216	0.59	35.2345	-115.7385	1986-021700	Mafic	Basalt
MC70	380217	0.35	35.1905	-115.7815	1986-021700	Mafic	Basalt
MC75	380218	0.22	35.2065	-115.8115	1986-021700	Mafic	Basalt

Table B.2 NAVDAT entries (volcanics only) for Mojave study area (continued)

Sample ID	Sample Num	Calc Age	Latitude	Longitude	GeoRef	Composition	Rock Name
MC76	380219	0.15	35.2535	-115.7932	1986-021700	Mafic	Basalt
MC86	380221	0.13	35.1895	-115.851	1986-021700	Mafic	Basalt
MC87	380222	0.5	35.2025	-115.7315	1986-021700	Mafic	Basalt
MC88	380223	0.33	35.2275	-115.7315	1986-021700	Mafic	Basalt
MC90	380224	0.14	35.2159	-115.7525	1986-021700	Mafic	Basalt
MC91c	380225	6.92	35.2191	-115.6845	1986-021700	Mafic	Basalt
MC100	380226	1.09	35.2438	-115.6745	1986-021700	Mafic	Basalt
MC115	380228	3.27	35.3475	-115.7305	1986-021700	Mafic	Basalt
MC121	380229	0.15	35.1949	-115.8462	1986-021700	Mafic	Basalt
MC122	380230	0.4	35.1939	-115.8479	1986-021700	Mafic	Basalt
MC123	380231	0.51	35.1891	-115.8325	1986-021700	Mafic	Basalt
MC124	380232	1.14	35.198	-115.7049	1986-021700	Mafic	Basalt
MC1	380233	3.88	35.3078	-115.7755	1986-021700	Mafic	Basalt
MC2	380235	6.47	35.2145	-115.7025	1986-021700	Mafic	Basalt
MC2a	380236	7.55	35.2145	-115.7025	1986-021700	Mafic	Basalt
MC6	380237	0.33	35.226	-115.7185	1986-021700	Mafic	Basalt
MC11	380238	0.56	35.1638	-115.8065	1986-021700	Mafic	Basalt
MC13	380240	0.17	35.2065	-115.8735	1986-021700	Mafic	Basalt
MC14	380241	0.2	35.2035	-115.8665	1986-021700	Mafic	Basalt
MC16	380242	0.32	35.2015	-115.868	1986-021700	Mafic	Basalt
MC24	380246	0.75	35.2421	-115.7872	1986-021700	Mafic	Basalt
MC26	380248	0.06	35.1955	-115.8088	1986-021700	Mafic	Basalt
MC28	380249	0.33	35.1915	-115.7372	1986-021700	Mafic	Basalt
MC36	380251	0.33	35.2592	-115.7365	1986-021700	Mafic	Basalt

Table B.2 NAVDAT entries (volcanics only) for Mojave study area (continued)

Sample ID	Sample Num	Calc Age	Latitude	Longitude	GeoRef	Composition	Rock Name
MC40	380253	0.67	35.2588	-115.7185	1986-021700	Mafic	Basalt
MC41	380254	0.3	35.2575	-115.7172	1986-021700	Mafic	Basalt
MC42	380255	0.27	35.2932	-115.7182	1986-021700	Mafic	Basalt
MC51	380257	0.27	35.2635	-115.7965	1986-021700	Mafic	Basalt
MC55	380258	0.7	35.2365	-115.7228	1986-021700	Mafic	Basalt
MC56	380259	0.17	35.2095	-115.7845	1986-021700	Mafic	Basalt
MC59	380260	3.64	35.3281	-115.8495	1986-021700	Mafic	Basalt
MC62	380261	0.85	35.2095	-115.7061	1986-021700	Mafic	Basalt
MC66	380262	0.24	35.1942	-115.8385	1986-021700	Mafic	Basalt
C84-40	381669	0.48	35.2583	-115.7167	1987-055281	Mafic	Basalt
C84-41	381670	0.23	35.2583	-115.7167	1987-055281	Mafic	Basalt
KM87-53	390026	4.74	35.8772	-114.5875	1991-900010	Mafic	Basalt
KM86-72	390027	5.16	35.8739	-114.6017	1991-900010	Mafic	Basalt
CA84PR-39	399210	10.7	35.32	-115.0289	1994-028542	Mafic	Basalt
JP84PR-93	399211	12.2	35.2167	-115.0306	1994-028542	Mafic	Basalt
Ci-75	400825	3.64	35.3284	-115.8438	1995-043332	Mafic	Basalt
CIM8142	419880	1	35.2333	-115.7167	1989-056727	Mafic	Basalt
CIM8143	419881	0.04	35.2	-115.8667	1989-056727	Mafic	Basalt
ODC16-11	419883	0.5	35.1833	-115.7167	1989-056727	Mafic	Basalt
JF-94-79	408286	12.79	35.6517	-115.0136	2002-027711	Mafic	Basalt
CIM-8142	418996	1	35.2333	-115.7167	1986-024128	Mafic	Basalt
CIM-8143	418997	0.04	35.2	-115.8667	1986-024128	Mafic	Basalt
2A	378452	7.55	35.2301	-115.6822	1984-029708	Mafic	Basalt
MC5	380212	4.24	35.3891	-115.8615	1986-021700	Mafic	Basalt

Table B.2 NAVDAT entries (volcanics only) for Mojave study area (continued)

Sample ID	Sample Num	Calc Age	Latitude	Longitude	GeoRef	Composition	Rock Name
MC85	380220	0.09	35.1885	-115.8505	1986-021700	Mafic	Basalt
MC111	380227	0.5	35.2012	-115.7615	1986-021700	Mafic	Basalt
MC19	380243	0.13	35.2175	-115.7522	1986-021700	Mafic	Basalt
JF92-27	457390	14.27	35.6525	-114.5967	2003-042429	Mafic	Basalt
JF92-26	457391	14.5	35.6539	-114.5897	2003-042429	Mafic	Basalt
JF92-44	457402	11.35	35.5792	-114.7611	2003-042429	Mafic	Basalt
JF92-45	457403	12.78	35.5514	-114.75	2003-042429	Mafic	Basalt
JF92-34	457404	14.79	35.5522	-114.6397	2003-042429	Mafic	Basalt
88-177	457728	13.13	35.5783	-114.7039	1993-024880	Mafic	Basalt
88-065	457729	14.32	35.9122	-114.5816	1993-024880	Mafic	Basalt
88-063	457730	14.1	35.9122	-114.5816	1993-024880	Mafic	Basalt
88-176	457734	13.71	35.7168	-114.5928	1993-024880	Mafic	Basalt

References for Table B.2

1966-000404 Richard R. Doell, G. Brent Dalrymple, and Allan Cox
Geomagnetic polarity epochs; Sierra Nevada data, [Part] 3
Journal of Geophysical Research (1966), 71(2):531-541

1970-000478 Richard Lee Armstrong
Geochronology of tertiary igneous rocks, eastern basin and range province, western utah, eastern nevada, and vicinity, u.s.a
Geochimica et Cosmochimica Acta (1970), 34(2):203-232

1972-008224 R. Ernest Anderson, Chester R. Longwell, Richard Lee Armstrong, and Richard F. Marvin
Significance of K-Ar Ages of Tertiary Rocks from the Lake Mead Region, Nevada-Arizona
GSA Bulletin, Feb 1972; 83: 273 - 287.

1974-002192 Richard F. Marvin, Harald H. Mehnert, and Edwin H. Mckee
A summary of radiometric ages of Tertiary volcanic rocks in Nevada and eastern California; Part 3; southeastern Nevada
Isochron/West (1973), 6 1-30

1978-006456 R. E. Anderson
Composite stratigraphic section of Tertiary volcanic rocks in the Eldorado Mountains, Nevada
Open-File Report - U. S. Geological Survey (1977), OF 77-0483:6 *pp.*

1978-025983 R. E. Anderson
Chemistry of Tertiary volcanic rocks in the Eldorado Mountains, Clark County, Nevada, and comparisons with rocks from some nearby areas
Journal of Research of the U. S. Geological Survey (June 1978), 6(3):409-424

1979-026763 R. G. Bohannon
Fission track ages from the Miocene continental deposits of eastern Clark County, Nevada
Abstracts with Programs - Geological Society of America (February 1979), 11(3):70

1980-024531 Joel Earl Everson
Regional variations in the lead isotopic characteristics of late Cenozoic basalts from the southwestern United States
California Institute of Technology, Pasadena, CA, United States, Doctoral thesis (1979) 464 *pp.*

1983-046190 Eugene I. Smith
Geology and geochemistry of the volcanic rocks in the River Mountains, Clark County, Nevada and comparisons with volcanic rocks in nearby areas (*in* Mesozoic-Cenozoic tectonic evolution of the Colorado River region, California, Arizona, and Nevada)
Cordilleran Publ., San Diego, CA, United States (1982) 41-54

1983-046225 Michael McCurry
The geology of a late Miocene silicic volcanic center in the Woods and Hackberry mountains area of the eastern Mojave Desert, San Bernardino

County, California (*in* Mesozoic-Cenozoic tectonic evolution of the Colorado River region, California, Arizona, and Nevada)
Cordilleran Publ., San Diego, CA, United States (1982) 433-439

1984-029708 John C. Dohrenwend, Leslie D. McFadden, Brent D. Turrin, and Stephen G. Wells
K-Ar dating of the Cima volcanic field, eastern Mojave Desert, California; late Cenozoic volcanic history and landscape evolution
Geology, Mar 1984; 12: 163 - 167.

1986-021700 Brent D. Turrin, John C. Dohrenwend, Robert E. Drake, and Garniss H. Curtis
K-Ar ages from the Cima volcanic field, eastern Mojave Desert, California
Isochron/West (December 1985), 44 9-16

1986-024128 Steven Christian Semken
A neodymium and strontium isotopic study of late Cenozoic basaltic volcanism in the southwestern Basin and Range Province
University of California at Los Angeles, Los Angeles, CA, United States, Master's thesis (1984) 68 *pp.*

1987-055281 B. D. Leavy and M. Shafiqullah
New K-Ar analyses of basalts from Southern California and central New Mexico
Isochron/West (April 1987), 48 19-20

1989-024207 Michael McCurry
Geology and petrology of the Woods Mountains volcanic center, southeastern California; implications for the genesis of peralkaline rhyolite ash flow tuffs (*in* Special section on How volcanoes work; Part 3, Tilling,)
Journal of Geophysical Research (December 1988), 93(B12):14,835-14,855

1989-056727 G. L. Farmer, F. V. Perry, S. Semken, B. Crowe, D. Curtis, and D. J. DePaolo
Isotopic evidence on the structure and origin of subcontinental lithospheric mantle in southern Nevada (*in*)
Journal of Geophysical Research (June 1989), 94(B6):7885-7898

1989-067667 D. S. Musselwhite, D. J. DePaolo, and M. McCurry
The evolution of a silicic magma system; isotopic and chemical evidence from the Woods Mountains Volcanic Center, eastern California
Contributions to Mineralogy and Petrology (1989), 101(1):19-29

1991-040849 Ryan D. Turner and Allen F. Glazner
Miocene volcanism, folding, and faulting in the Castle Mountains, southern Nevada and eastern California (*in* Basin and Range extensional tectonics near the latitude of Las Vegas, Nevada, Wernicke,)
Memoir - Geological Society of America (1990), 176 23-35

1991-900010 Mallin, K. and W.K. Hart
New K-Ar ages of mafic lavas from the basin and range-Cascade transition zone in northeastern California and southern Oregon: Isochron/West (1991)

1992-017921 G. Lang Farmer, Allen F. Glazner, William T. Hughes, Joseph L. Wooden, and William J. Pickthorn

Mixing of basaltic magma with mafic crust at Amboy and Pisgah craters, Mojave Desert, California (*in* AGU 1990 fall meeting, Anonymous,)
Eos, Transactions, American Geophysical Union (October 1990), 71(43):1682

1993-010351 T. K. Bradshaw, C. J. Hawkesworth, and K. Gallagher
Basaltic volcanism in the southern Basin and Range; no role for a mantle plume
Earth and Planetary Science Letters (April 1993), 116(1-4):45-62

1993-024880 James E. Faulds, John W. Geissman, and Muhammad Shafiqullah
Implications of paleomagnetic data on Miocene extension near a major accommodation zone in the Basin and Range Province, northwestern Arizona and southern Nevada
Tectonics (April 1992), 11(2):204-227

1993-038710 Dan L. Feuerbach, Eugene I. Smith, J. D. Walker, and J. A. Tangeman
The role of the mantle during crustal extension; constraints from geochemistry of volcanic rocks in the Lake Mead area, Nevada and Arizona
GSA Bulletin, Dec 1993; 105: 1561 - 1575.

1994-028537 Roland H. Brady
Cenozoic stratigraphy and structure of the northern Bristol Mountains, Calif. (*in* Tertiary stratigraphy of highly extended terranes, California, Arizona, and Nevada)
U. S. Geological Survey Bulletin (1993), 25-28

1994-028542 Jane E. Nielson and John K. Nakata
Tertiary stratigraphy and structure of the Piute Range, Calif. and Nev. (*in* Tertiary stratigraphy of highly extended terranes, California, Arizona, and Nevada)
U. S. Geological Survey Bulletin (1993), 51-53

1994-028552 Jane E. Nielson and John K. Nakata
Tertiary stratigraphy and structure of the northern Turtle Mountains, Calif. (*in* Tertiary stratigraphy of highly extended terranes, California, Arizona, and Nevada)
U. S. Geological Survey Bulletin (1993), 127-129

1995-043332 G. L. Farmer, A. F. Glazner, H. G. Wilshire, J. L. Wooden, W. J. Pickthorn, and M. Katz
Origin of late Cenozoic basalts at the Cima volcanic field, Mojave Desert, California
Journal of Geophysical Research (May 1995), 100(B5):8399-8415

1999-027986 J. R. Waits
Geochemical and isotopic study of peridotite-bearing lavas in eastern California
University of North Carolina at Chapel Hill, Chapel Hill, NC, United States, Master's thesis (1995) 59 *pp*.

1999-038369 Jane E. Nielson and Ryan D. Turner
Geologic map of the Hart Peak Quadrangle, California and Nevada
Open-File Report - U. S. Geological Survey (1998) OF 98-0470 Maps: colored geologic map; 1:24,000, 1 sheet

2000-066389 Donald J. DePaolo and E. Ellen Daley
Neodymium isotopes in basalts of the Southwest Basin and Range and lithospheric thinning during continental extension (*in*)
Chemical Geology (August 2000), 169(1-2):157-185

2002-027711 James E. Faulds, Eric L. Olson, Stephen S. Harlan, and William C. McIntosh
Miocene extension and fault-related folding in the Highland Range, southern Nevada; a three-dimensional perspective (*in* Fault-related folds; the transition from 2-D to 3-D)
Journal of Structural Geology (2002), 24(4):861-886

2003-042429 James E. Faulds, Daniel L. Feuerbach, Mark K. Reagan, Rodney V. Metcalf, Phil Gans, and J. D. Walker
The Mount Perkins Block, northwestern Arizona; an exposed cross section of an evolving, preextensional to synextensional magmatic system
Journal of Geophysical Research (August 1995), 100(B8):15,249-15,266

Table B.3 NAVDAT entries (volcanics only) for Central Nevada study area

Sample ID	Sample Num	Calc Age	Latitude	Longitude	GeoRef	Composition	Rock Name
R8-1-11	459019	3.8	38.075	-116.1467	1996-073164	Mafic	Basalt
R8-1-30	459020	3.8	38.0867	-116.14	1996-073164	Mafic	Basalt
R8-1-23	459016	3.8	38.0567	-116.155	1996-073164	Mafic	Basalt
R8-1-27	459015	3	38.0533	-116.1567	1996-073164	Mafic	Basalt
R9-1-47	459021	3.8	38.1733	-116.1067	1996-073164	Mafic	Basalt
R8-1-22	459018	3.8	38.0583	-116.155	1996-073164	Mafic	Basalt
R8-1-26	459017	3.8	38.0533	-116.1617	1996-073164	Mafic	Basalt
NV10	385026	4.65	38.2	-116.1	1989-056726	Mafic	Basalt
LC-48	385017	4.65	38.2	-116.1	1989-056726	Mafic	Basalt
1ESh	447164	2.86	38.4861	-116.0042	1983-013966	Mafic	Basalt
RS-2	447168	2.86	38.485	-115.9381	1983-013966	Mafic	Basalt
N5024	423229	0.1	38.48	-116.012	1980-024531	Mafic	Basanitoid
2BB3	447166	2.86	38.4953	-115.9903	1983-013966	Mafic	Basalt
BRSF3	385014	4.65	38.2	-116.1	1989-056726	Mafic	Basalt
BRSF3	447175	2.86	38.5508	-115.9283	1983-013966	Mafic	Basalt
R8-1-6	459029	3.8	38.0783	-116.1267	1996-073164	Mafic	Basalt
CCB	385013	4.65	38.2	-116.1	1989-056726	Mafic	Basalt
CCB	447163	2.86	38.4869	-115.9769	1983-013966	Mafic	Basalt
NV8	385024	4.65	38.2	-116.1	1989-056726	Mafic	Basalt
BSS-2	447172	2.86	38.3953	-115.9953	1983-013966	Mafic	Basalt
PC-1	447178	2.86	38.425	-116.0144	1983-013966	Mafic	Basalt
BCB3	447167	2.86	38.4489	-116.0286	1983-013966	Mafic	Basalt
NV9	385025	4.65	38.2	-116.1	1989-056726	Mafic	Basalt
NV12	385028	4.65	38.2	-116.1	1989-056726	Mafic	Basalt

Table B.3 NAVDAT entries (volcanics only) for Central Nevada study area (continued)

Sample ID	Sample Num	Calc Age	Latitude	Longitude	GeoRef	Composition	Rock Name
LL-2	447170	2.86	38.4028	-116.0122	1983-013966	Mafic	Basalt
R8-1-1	459031	3.8	38.06	-116.1333	1996-073164	Mafic	Basalt
R8-1-19	459028	4.15	38.04	-116.12	1996-073164	Mafic	Basalt
NV83-55	385016	4.65	38.2	-116.1	1989-056726	Mafic	Basalt
SKB-1	447174	2.86	38.3733	-116.0333	1983-013966	Mafic	Basalt
2AB13	447165	2.86	38.4806	-116.0144	1983-013966	Mafic	Basalt
NV7	385023	4.65	38.2	-116.1	1989-056726	Mafic	Basalt
R9-2-59	459008	5.5	37.955	-116.1	1996-073164	Mafic	Basalt
R8-1-14	459009	5.5	38.0667	-116.1133	1996-073164	Mafic	Basalt
R8-1-18	459030	3.99	38.0733	-116.1233	1996-073164	Mafic	Basalt
LLQ-1	447180	2.86	38.3972	-116.0953	1983-013966	Mafic	Basalt
R8-1-25	459007	5.5	38.0517	-116.1433	1996-073164	Mafic	Basalt
NV83-11	385015	4.65	38.2	-116.1	1989-056726	Mafic	Basalt
R8-1-4	459001	5.5	38.0667	-116.1283	1996-073164	Mafic	Basalt
R8-1-7	459006	5.5	38.0617	-116.1317	1996-073164	Mafic	Basalt
R8-1-32	459025	3.8	38.0367	-116.1167	1996-073164	Mafic	Basalt
BJ-1	447189	2.86	38.2889	-116.1694	1983-013966	Mafic	Basalt
RS-1	447169	2.86	38.4711	-115.9844	1983-013966	Mafic	Basalt
R9-1-46	459024	3.76	38.175	-116.11	1996-073164	Mafic	Basalt
NV4	385020	4.65	38.2	-116.1	1989-056726	Mafic	Basalt
R0-1-77	459010	5.5	37.845	-116.215	1996-073164	Mafic	Basalt
BRSF1	447176	2.86	38.5089	-115.8833	1983-013966	Mafic	Basalt
WC-1	447177	2.86	38.3461	-116.0294	1983-013966	Mafic	Basalt
R9-1-44	459026	3.8	38.1183	-116.1	1996-073164	Mafic	Basalt

Table B.3 NAVDAT entries (volcanics only) for Central Nevada study area (continued)

Sample ID	Sample Num	Calc Age	Latitude	Longitude	GeoRef	Composition	Rock Name
NV5	385021	4.65	38.2	-116.1	1989-056726	Mafic	Basalt
R0-1-73	459004	5.5	38.0783	-116.2183	1996-073164	Mafic	Basalt
R8-1-17	459002	5.13	38.0717	-116.125	1996-073164	Mafic	Basalt
NV3	385019	4.65	38.2	-116.1	1989-056726	Mafic	Basalt
R8-1-39	459012	5.5	38.115	-116.1267	1996-073164	Mafic	Basalt
R9-1-55	459022	3.8	38.1367	-116.1283	1996-073164	Mafic	Basalt
C-3	447186	2.86	38.3814	-116.0706	1983-013966	Mafic	Basalt
LC-109	385018	4.65	38.2	-116.1	1989-056726	Mafic	Basalt
R9-3-60	458999	5.5	37.9083	-116.12	1996-073164	Mafic	Basalt
R9-1-48	458998	5.8	38.1633	-116.1017	1996-073164	Mafic	Basalt
R9-4-61	459000	5.5	37.985	-116.115	1996-073164	Mafic	Basalt
C-1	447184	2.86	38.3814	-116.0706	1983-013966	Mafic	Basalt
R8-1-12	459027	3.8	38.0708	-116.1167	1996-073164	Mafic	Basalt
C-2	447185	2.86	38.3814	-116.0706	1983-013966	Mafic	Basalt
D-3	447181	2.86	38.38	-116.0681	1983-013966	Mafic	Basalt
R8-1-28	459013	5.74	38.095	-116.135	1996-073164	Mafic	Basalt
C-4	447187	2.86	38.3814	-116.0706	1983-013966	Mafic	Basalt
C-5	447188	2.86	38.3814	-116.0706	1983-013966	Mafic	Basalt
D-1	447183	2.86	38.3806	-116.0703	1983-013966	Mafic	Basalt
WBP-1	447173	2.86	38.3486	-116.0211	1983-013966	Mafic	Basalt
NV11	385027	4.65	38.2	-116.1	1989-056726	Mafic	Basalt
PR7-12-31V	419865	10.2	38.6333	-116.0667	1989-056727	Mafic	Basalt
PR-7.12.31V	418981	10.2	38.6333	-116.0667	1986-024128	Intermediate	Hawaiite
R8-1-37	459005	5.5	38.1033	-116.1367	1996-073164	Mafic	Basalt

Table B.3 NAVDAT entries (volcanics only) for Central Nevada study area (continued)

Sample ID	Sample Num	Calc Age	Latitude	Longitude	GeoRef	Composition	Rock Name
NV6	385022	4.65	38.2	-116.1	1989-056726	Mafic	Basalt
QTV-1	447190	2.86	38.15	-116.1	1983-013966	Mafic	Basalt
NV13	385029	4.65	38.2	-116.1	1989-056726	Mafic	Basalt
LCU-1	447179	2.86	38.4	-116.0833	1983-013966	Mafic	Basalt
TS6-15-2	419867	8.8	37.3667	-116.3667	1989-056727	Mafic	Basalt
D-2	447182	2.86	38.3803	-116.0697	1983-013966	Mafic	Basalt
R9-1-66	459014	5.5	38.16	-116.195	1996-073164	Mafic	Basalt
LL-8	447171	2.86	38.3931	-116.0119	1983-013966	Mafic	Basalt
R8-1-40	459033	4.3	38.1283	-116.1017	1996-073164	Intermediate	Andesite
R9-1-43	459034	4.24	38.1292	-116.0883	1996-073164	Intermediate	Trachyte
R9-1-62	459035	4.3	38.1267	-116.1017	1996-073164	Intermediate	Andesite
R8-1-41	459036	4.3	38.1317	-116.095	1996-073164	Intermediate	Andesite
R8-1-42	459037	4.3	38.1267	-116.1017	1996-073164	Intermediate	Andesite
5	369270	13.45	37.4	-116.35	1968-059422	Intermediate	Trachyte
4	369269	13.45	37.4	-116.35	1968-059422	Felsic	Rhyolite
2	369267	14.17	37.3417	-116.0166	1968-059422	Felsic	Tuff
3	369268	14.17	37.3417	-116.0166	1968-059422	Felsic	Tuff
1	369266	13.45	37.4	-116.35	1968-059422	Felsic	Rhyolite
No Sample Name	390692	9	37.3111	-116.8444	1992-049812	Felsic	Rhyolite
N6035	423232	3.55	37.729	-115.885	1980-024531	Intermediate	Andesite
84-259	399260	8.8	37.305	-116.8717	1994-032750	Intermediate	Andesite
22	370597	10.5	38.6544	-116.0722	1974-002192	Mafic	Basalt
34	370609	5.9	38.1167	-116.2333	1974-002192	Mafic	Basalt
USGSDLC12-11-20v	384794	4.2	38.3833	-116	1989-042953	Mafic	Basalt

Table B.3 NAVDAT entries (volcanics only) for Central Nevada study area (continued)

Sample ID	Sample Num	Calc Age	Latitude	Longitude	GeoRef	Composition	Rock Name
USGSDVH-1-126	384805	3.6	38.7833	-116.55	1989-042953	Mafic	Basalt
USGSDLC12-8-2	384806	0.57	38.4833	-115.9667	1989-042953	Mafic	Basalt
USGSDRE9-28-2	384807	5.3	38.1667	-116.1167	1989-042953	Mafic	Basalt
79-R-A	399244	5.44	38.055	-116.1478	1994-032750	Mafic	Basalt
79-R-B	399245	5.74	38.0944	-116.1347	1994-032750	Mafic	Basalt
RE10-2-53V	419866	5	38.0833	-116.1167	1989-056727	Mafic	Basalt
79-S-3	399243	5.13	38.0708	-116.1233	1994-032750	Intermediate	Basaltic-Andesite
M678	399248	5.94	38.1758	-116.0917	1994-032750	Felsic	Dacite
M678	399249	5.76	38.1208	-116.0958	1994-032750	Felsic	Dacite
M718	399250	4.03	38.0583	-116.1389	1994-032750	Felsic	Dacite
83-602	399251	4.64	38.0731	-116.1217	1994-032750	Felsic	Dacite
83-602	399252	3.99	38.0722	-116.1233	1994-032750	Felsic	Dacite
RE-10.2.53V	418982	5	38.0833	-116.1167	1986-024128	Intermediate	Hawaiite
TS-6.15.2	418983	8.8	37.3667	-116.3667	1986-024128	Intermediate	Hawaiite
27	370602	14.7	38.6333	-116.35	1974-002192	Felsic	Pyroclastic Flow
52	370626	8	37.3383	-116.6617	1974-002192	Felsic	Pyroclastic Flow
89	370662	14.2	37.3417	-116.0167	1974-002192	Felsic	Pyroclastic Flow
7	369784	15.19	37.3533	-116.0167	1970-027213	Felsic	Rhyolite
65	370639	11.6	37.95	-116.6833	1974-002192	Felsic	Rhyolite
90	370663	15.2	37.3533	-116.0167	1974-002192	Felsic	Rhyolite
BH86N33	388566	7.54	37.4833	-117	1991-007027	Felsic	Rhyolite
BH86N9	388567	7.61	37.5	-116.9167	1991-007027	Felsic	Rhyolite
LABCAN081	388569	7.69	37.295	-116.6733	1991-007027	Felsic	Rhyolite

Table B.3 NAVDAT entries (volcanics only) for Central Nevada study area (continued)

Sample ID	Sample Num	Calc Age	Latitude	Longitude	GeoRef	Composition	Rock Name
89USA2A	399253	4.15	38.0375	-116.1194	1994-032750	Felsic	Rhyolite
89USA1A	399254	3	38.0528	-116.1564	1994-032750	Felsic	Rhyolite
89USA1A	399255	3.76	38.175	-116.1083	1994-032750	Felsic	Rhyolite
78-1288	399257	4.39	38.055	-116.1478	1994-032750	Felsic	Rhyolite
M739	399258	4.24	38.1292	-116.0889	1994-032750	Intermediate	Trachyte
N80A-S	369254	6.36	37.3038	-116.6024	1968-059410	Felsic	Tuff
6	369797	14.17	37.3417	-116.0167	1970-027213	Felsic	Tuff
53	370627	6.4	37.3	-116.5833	1974-002192	Felsic	Tuff
Tcc-7	383791	6.1	37.5283	-116.9417	1988-073166	Felsic	Tuff
1	369795	9.8	37.3383	-116.6617	1970-027213	Felsic	Vitrophere
5	369796	13.45	37.4	-116.35	1970-027213	Felsic	Vitrophere
50	370624	13.4	37.4	-116.35	1974-002192	Felsic	Vitrophyre

References for Table B.3

1968-059410 Ronald W. Kistler
Potassium-argon ages of volcanic rocks in Nye and Esmeralda counties, Nevada (*in* Nevada Test Site)
Memoir - Geological Society of America (1968), 251-262

1968-059422 Donald C. Noble, K. A. Sargent, H. H. Mehnert, E. B. Ekren, and F. M. Byers
Silent Canyon volcanic center, Nye County, Nevada (*in* Nevada Test Site)
Memoir - Geological Society of America (1968), 65-75

1970-027213 Richard F. Marvin, F. M. Byers, Harald H. Mehnert, Paul P. Orkild, and T. W. Stern
Radiometric ages and stratigraphic sequence of volcanic and plutonic rocks, southern Nye and western Lincoln counties, Nevada
GSA Bulletin, Sep 1970; 81: 2657 - 2676.

1974-002192 Richard F. Marvin, Harald H. Mehnert, and Edwin H. Mckee
A summary of radiometric ages of Tertiary volcanic rocks in Nevada and eastern California; Part 3; southeastern Nevada
Isochron/West (1973), 6 1-30

1980-024531 Joel Earl Everson
Regional variations in the lead isotopic characteristics of late Cenozoic basalts from the southwestern United States
California Institute of Technology, Pasadena, CA, United States, Doctoral thesis (1979) 464 *pp.*

1983-013966 Steven Clark Bergman
Petrogenetic aspects of the alkali basaltic lavas and included megacrysts and nodules from the Lunar Crater volcanic field, Nevada, USA
Princeton University, Princeton, NJ, United States, Doctoral thesis (1982) 447 *pp.*

1986-024128 Steven Christian Semken
A neodymium and strontium isotopic study of late Cenozoic basaltic volcanism in the southwestern Basin and Range Province
University of California at Los Angeles, Los Angeles, CA, United States, Master's thesis (1984) 68 *pp.*

1988-073166 Donald C. Noble, Edwin H. McKee, and Steven I. Weiss
Nature and timing of pyroclastic and hydrothermal activity and mineralization at the Stonewall Mountain volcanic center, southwestern Nevada
Isochron/West (July 1988), 51 25-28

1989-042953 Richard F. Marvin, Harald H. Mehnert, and Charles W. Naeser
U. S. Geological Survey radiometric ages; Compilation "C", Part three; California and Nevada
Isochron/West (March 1989), 52 3-12

1989-056726 Clinton C. L. Lum, William P. Leeman, Kenneth A. Foland, Jeff A. Kargel, and J. Godfrey Fitton
Isotopic variations in continental basaltic lavas as indicators of mantle

heterogeneity; examples from the Western U.S. Cordillera (*in*)
Journal of Geophysical Research (June 1989), 94(B6):7871-7884

1989-056727 G. L. Farmer, F. V. Perry, S. Semken, B. Crowe, D. Curtis, and D. J. DePaolo
Isotopic evidence on the structure and origin of subcontinental lithospheric mantle in southern Nevada (*in*)
Journal of Geophysical Research (June 1989), 94(B6):7885-7898

1991-007027 Brian P. Hausback, Alan L. Deino, Brent D. Turrin, Edwin H. McKee, Virgil A. Frizzell, Donald C. Noble, and Steven I. Weiss
New Ar-40/Ar-39 ages for the Spearhead and Civet Cat Canyon members of the Stonewall Flat Tuff, Nye County, Nevada; evidence for systematic errors in standard K-Ar age determinations on sanidine
Isochron/West (December 1990), 56 3-7

1992-049812 Ray Macdonald, Robert L. Smith, and John E. Thomas
Chemistry of the subalkalic silicic obsidians
U. S. Geological Survey Professional Paper (1992), P 1523:214 *pp.*

1994-032750 Peter D. Rowley, Harald H. Mehnert, Charles W. Naeser, Lawrence W. Snee, Charles G. Cunningham, Thomas A. Steven, John J. Anderson, Edward G. Sable, and R. Ernest Anderson
Isotopic ages and stratigraphy of Cenozoic rocks of the Marysvale volcanic field and adjacent areas, west-central Utah
U. S. Geological Survey Bulletin (1994), B 2071:35 *pp.*

1996-073164 G. M. Yogodzinski, T. R. Naumann, E. I. Smith, T. K. Bradshaw, and J. D. Walker
Evolution of a mafic volcanic field in the central Great Basin, south central Nevada
Journal of Geophysical Research (August 1996), 101(B8):17,425-17,445